Aspects of strong and new CP violation

Shain Poruvelil, S.

Publication date
2023
Document Version
Final published version

Aspects of strong and new CP violation

Sachin Shain Poruvelil

Aspects of strong and new CP violation

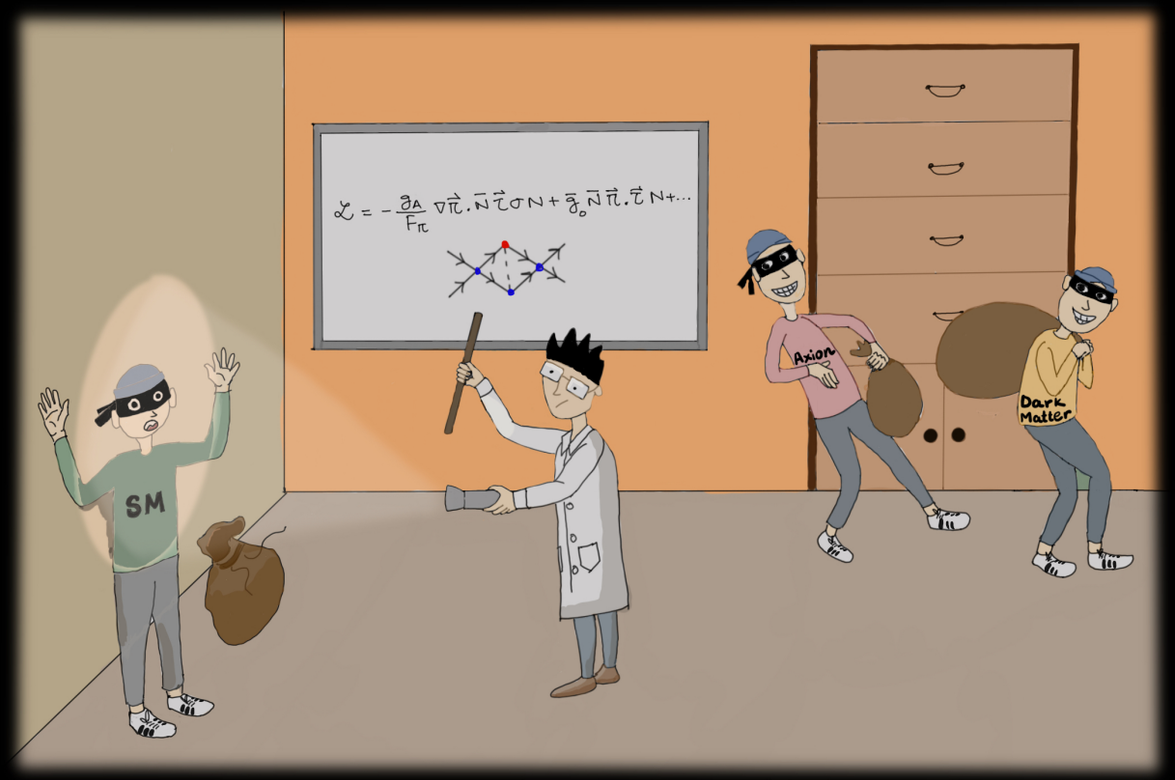

Sachin Shain Poruvelil

Aspects of strong and new CP violation

Sachin Shain Poruvelil

Title: Aspects of strong and new *CP* violation
Printed by: Proefschriftspecialist

University of Amsterdam

Nikhef

Aspects of strong and new CP violation

ACADEMISCH PROEFSCHRIFT

ter verkrijging van de graad van doctor
aan de Universiteit van Amsterdam
op gezag van de Rector Magnificus
prof. dr. ir. P.P.C.C. Verbeek
ten overstaan van een door het
College voor Promoties ingestelde commissie,
in het openbaar te verdedigen in de Agnietenkapel
op maandag 3 april 2023, te 14.00 uur

door

Sachin Shain Poruvelil

geboren te Ernakulam, Kerala

Promotiecommissie

Promotor:	dr. W.J. Waalewijn	Universiteit van Amsterdam
Copromotor:	dr. J. de Vries	Universiteit van Amsterdam
Overige leden:	prof. dr. A.P. Colijn	Universiteit van Amsterdam
	dr. C. Weniger	Universiteit van Amsterdam
	dr. A. Safavi Naini	Universiteit van Amsterdam
	prof. dr. E.L.M.P. Laenen	Universiteit van Amsterdam
	dr. S. Westhoff	Radboud Universiteit
	prof. dr. R.G.E. Timmermans	Rijksuniversiteit Groningen

Faculteit der Natuurwetenschappen, Wiskunde en Informatica

This thesis is based on the following publications.

[1] J. de Vries, A. Gnech, and S. Shain, "Renormalization of CP-violating nuclear forces," *Phys. Rev. C* **103** no. 1, (2021) L012501, [arXiv:2007.04927].

[2] W. Dekens, J. de Vries, and S. Shain, "CP-violating axion interactions in effective field theory," *JHEP* **07** (2022) 014, [arXiv:2203.11230].

[3] J. de Vries, C. Körber, A. Nogga, and S. Shain, "Dark Matter scattering off ^{4}He through scalar interactions." *(to be submitted).*

Author contributions:

- In Ref. [1], I did all calculations for this project, both numerical and analytical. I wrote all Python code from scratch in order to compute the CP-even and CP-odd phase shifts and mixing angles for various channels and to determine the contact LECs.

- In Ref. [2], I developed the framework, based on the LEFT operators and the matching to χPT, to compute the axion-hadron CP-violating couplings. I wrote most parts of the paper, in particular the section on the experimental searches for long-range axion-induced forces.

- In Ref. [3], I calculated the LO and NLO DM-nucleon scattering currents in the partial wave basis. Then I used this result to analytically calculate the cross sections using a test nuclear wave functions. This results was used to check the validity of the numerical computations. I helped to implement the density formalism into the nuclear computations and did the analysis of the results.

Contents

Chapter 1

Introduction

1.1 Beyond the Standard Model physics

The Standard Model (SM) [1–6] of particle physics summarizes our current understanding of the fundamental nature of our Universe. It describes the weak, electromagnetic, and strong interactions between elementary particles, apart from gravity. The SM puzzle was filled by decades of complementary efforts of both theorists and experimentalists. The final piece, the Higgs boson, was found by ATLAS [7] and CMS [8] collaboration in 2012.

Even with the most successful agreement between predictions and experiments in the history of physics, the SM is still lacking in answering some key features of the Universe, such as the matter-antimatter asymmetry, neutrino masses and mixing angles, the existence and nature of dark matter (DM) [9]. All these observations provide clear indications of the existence of beyond-the-Standard Model (BSM) physics.

Particle physicists are constantly on the lookout for more pieces of the puzzle. The experimental searches happen on three fronts. The first front is associated with the High-Energy collider experiments [10, 11], such as the CERN Large Hadron Collider (LHC). The second one is the cosmological and astrophysical frontier, which studies the Cosmic Microwave Background (CMB), neutrino production at the sun and supernovae, exploring the role of neutrinos in cosmological processes, and so on [12]. The third is relatively low-energy high-precision measurements [13], which includes atomic and nuclear physics experiments, rare and forbidden processes like electric dipole moment experiments, neutrinoless double β-decays, etc. The Fermilab Muon g-2 collaboration, one of the high-precision experiments, reported a muon magnetic momentum value different from the SM prediction [14]. However, the recent lattice QCD results reduced the discrepancy to 1.5 σ [15, 16]. The Fermilab Muon g-2 result was from their Run 1 data, and they have already finished collecting data up to Run 5. They are currently analyz-

ing this data, and it is expected that the Run 2 data will reduce the uncertainty by a factor of two. Currently, the community is waiting for this improved result.

On the other side, particle theorists work on two fronts. The first one is the "model-dependent" approach in which the SM is extended with some specific new particles motivated by theoretical arguments. Some famous examples of these BSM models are the left-right symmetric models (LRSMs) [17–21], leptoquark models [22, 23], composite Higgs model [24, 25], and so on. The second one is the "model-independent" approach in which effective field theories (EFTs) are used to study BSM physics. The EFTs are tailor-made to study physics at a specific range of energies. Some popular EFTs are Standard Model effective field theory (SMEFT) [26–28], Low-Energy EFT (LEFT) [29], chiral perturbation theory (χPT) [30, 31], pionless-EFT [32, 33], and so on. Since a general EFT contains all possible BSM interactions, we can always translate the result of EFT to any particular BSM model. Chapter 4 demonstrates this feature of some BSM models discussed above. This feedback helps to improve the designs of these BSM models.

The next big goal of particle physicists is to establish a new Standard Model which overcomes the failures of SM; this model may be one of the BSM models discussed before, a combination of those, or something yet to be considered. Unfortunately, the lack of direct experimental evidence of BSM physics makes it impossible to make any significant progress in identifying this new Standard Model. However, we were able to narrow down the parameter space of many BSM models based on the negative results. In this thesis, I have taken the EFT approach to study BSM physics.

1.2 Effective field theories

The EFTs are effective because of the fascinating feature of nature called *decoupling*, which states that most (but not all) of the details of small-distance phenomena tend to be largely irrelevant for the description of much larger systems. This is why natural phenomena can be explained using simple laws without knowing the underlying physics. EFTs are based on the idea that physics at one energy scale does not depend on the physics at another energy scale, and each EFT comes with its degrees of freedom [34] (see Ref. [35] for review on EFTs).

There are two approaches to constructing an EFT. They are the top-down and the bottom-up approach. In the top-down approach, we know the fundamental (UV complete) theory at an energy scale Λ. We construct the EFT at a lower energy scale by *integrating out* the heavy degrees of freedom. Thus, we end up with a more straightforward theory with degrees of freedom and interactions relevant to the problem we are trying to solve. The parameters of EFTs, the Wilson coefficients, are fixed by the parameters of the UV complete theory. For example, if one considers the electroweak theory as the full theory, then by *integrating out* W and Z bosons, we arrive at the EFT: Fermi's theory of weak interaction in

terms of local four-fermion operators. The Fermi constant

$$G_F = \frac{\sqrt{2}g^2}{8m_W^2}\,, \tag{1.1}$$

is given by the parameters of electroweak theory: the weak coupling constant g and W boson mass m_W.

In the bottom-up approach, we construct the Lagrangian with a set of symmetries, which are motivated by some partial understanding of the UV complete theory at the energy scale Λ. In this case, the Wilson coefficients are independent parameters of the EFT, and a power counting rule gives the relative relevance of the operators. An example of this approach is the SMEFT, where we assumed Lorentz and gauge invariance

$$\mathcal{L}_{\text{SMEFT}} = \mathcal{L}_{\text{SM}} + \sum_{\forall i, n\geq 5} \frac{C_i \mathcal{O}_i^{(n)}}{\Lambda^{n-4}}\,, \tag{1.2}$$

where $\mathcal{O}_i^{(n)}$ are all possible operators in SM fields of mass dimension n which are invariant under $SU(3)_c \times SU(2)_L \times U(1)_Y$ and C_i are called Wilson coefficients.

A part of this thesis is focused on providing a theoretical understanding of various nuclear physics experiments. This requires understanding the interaction of nucleons with external probes (such as DM, axion, etc.); it would have been ideal if we could use quantum chromodynamics (QCD) to achieve this, but the non-perturbative nature of QCD at the nuclear scale makes it impractical.

An alternative approach is to apply QCD numerically; this is achieved by the lattice QCD (LQCD) [36–38]. LQCD is a set of advanced numerical techniques to compute the QCD interactions between quarks and gluons. In LQCD, we implement the quantum field theory (QFT) in a grid or lattice of space-time points. In the continuum limit, i.e., when the lattice space is reduced to zero and the lattice size is increased to infinity, we recover QCD. LQCD has made significant progress in recent years but has yet to reach the desired accuracy. Since we are interested in a specific energy scale, the nuclear scale, this is an ideal scenario to use an EFT. It is best to construct an EFT using a top-down approach since we know the UV complete theory, i.e., QCD. The EFT developed this way is called chiral EFT (χPT). Moreover, to accommodate BSM physics, we can expand on this by using this top-down approach on the SMEFT operators. Because we use χPT throughout this thesis, we will discuss it in detail in Chapter 2.

1.3 *CP* violation

Symmetries and conservation laws are very important in physics. Noether's theorem states that every continuous symmetry of the Lagrangian leads to a conservation law [39]. For example, rotational and time translation invariance leads to

angular momentum and energy conservation, respectively. Apart from these continuous symmetries, discrete symmetries are very interesting in particle physics. There are three space-time discrete symmetries. The parity (P) transformation flips the space coordinates with respect to origin $\boldsymbol{r} \xrightarrow{P} -\boldsymbol{r}$. This transformation changes the sign of momentum and position, but the spin angular momentum remains unaffected. The charge conjugation (C) transformation flips matter to antimatter and vice versa. This transformation changes the charge of particles, but the momentum and spin angular momentum remains unchanged. Finally, the time reversal (T) transformation flips the time coordinate $t \xrightarrow{T} -t$. This transformation changes the sign of momentum and spin, but position and energy remain unaffected. Some fundamental interactions respect some of these symmetries, and others do not. For example, weak interaction violates parity, whereas strong and electromagnetic interactions respect parity.

The CP symmetry is the product of parity and charge conjugation symmetries. Under CP transformation, an electron travel with momentum $\boldsymbol{p}$ becomes a positron with opposite momentum $-\boldsymbol{p}$ and opposite spin. In short, CP transformation changes matter to mirrored antimatter. The CPT theorem state that natures always respect the CPT symmetry. This implies CP symmetry is equivalent to time-reversal symmetry, which was believed to be a proper symmetry of nature until the experimental discovery of CP-violation from β-decay of Cobalt 60 [40]. Why should we bother about CP-violation? Because it is one of the Sakharov conditions [41]. Sakharov conditions are the three necessary conditions required in a baryon-generating interaction to produce matter and antimatter at different rates. The three conditions are i) baryon number violation, ii) C and CP violation, and iii) interactions out of thermal equilibrium.

The Standard Model has two sources of CP-violation. The first one arises in the weak sector, specifically from the Cabibbo-Kobayashi-Maskawa (CKM) matrix [42, 43], which describes the mixing of quark generations. The second one arises from the strong sector in the form of flavor-conserving strong interaction. This thesis focuses on the CP violation from the strong sector of the SM and on potential new sources of CP violation from BSM physics.

1.4 Strong CP problem and the axion solution

Quantum chromodynamics is the theory of strong interactions. The QCD Lagrangian contains CP-conserving and CP-violating interactions. However, various experiments concluded that the CP-violating interactions in QCD are minimal. This is called the strong CP problem. This is not a problem in the strict sense, but it seems improbable that nature just chose the CP-violating QCD parameter $\bar{\theta}$ to be extremely small. However, if we treat it as a problem, one solution is the BSM particle called the axion, which occurs naturally in many BSM models. This section explores the strong CP problem and the axion solution. The strong CP problem is related to the $U(1)_A$ problem of quantum chromodynamics, which

is briefly discussed below.

1.4.1 $U(1)_A$ problem of QCD

Let us consider the QCD Lagrangian with two *massless* flavors u and d

$$\mathcal{L}_{\rm QCD} = -\frac{1}{4} G^A_{\mu\nu} G^{A,\mu\nu} + \bar{q} i \gamma^\mu \partial_\mu q + g_s \bar{q} \gamma^\mu G^A_\mu T^A q \,, \tag{1.3}$$

where $q = (u, d)^T, G^A_{\mu\nu}$ is gluon tensor, T^A are the Gell-Mann matrices, γ^μ are the Dirac matrices, and g_s is the coupling constant of strong interaction. In this limit the Lagrangian has the global symmetry $SU(2)_R \times SU(2)_L \times U(1)_R \times U(1)_L$. This can be rewritten as the vector $(R + L)$ and axial-vector $(R - L)$ form, and their corresponding transformations are given by

$$SU(2)_V : \begin{pmatrix} u \\ d \end{pmatrix} \to \exp\left(i \alpha^a_V \frac{\tau^a}{2} \right) \begin{pmatrix} u \\ d \end{pmatrix} , \tag{1.4}$$

$$SU(2)_A : \begin{pmatrix} u \\ d \end{pmatrix} \to \exp\left(i \gamma_5 \alpha^a_A \frac{\tau^a}{2} \right) \begin{pmatrix} u \\ d \end{pmatrix} , \tag{1.5}$$

$$U(1)_V : \begin{pmatrix} u \\ d \end{pmatrix} \to \exp\left(i \beta_V \right) \begin{pmatrix} u \\ d \end{pmatrix} , \tag{1.6}$$

$$U(1)_A : \begin{pmatrix} u \\ d \end{pmatrix} \to \exp\left(i \gamma_5 \beta_A \right) \begin{pmatrix} u \\ d \end{pmatrix} , \tag{1.7}$$

where τ^a are Pauli matrices. The $SU(2)_V$ and $U(1)_V$ symmetries are readily recognized in the QCD spectrum; the former leads to isospin conservation, and the latter manifests as the baryon number conservation.

The $SU(2)_A$ symmetry is spontaneously broken due to the non-zero quark condensates

$$\langle 0 | \bar{u} u | 0 \rangle \approx \langle 0 | \bar{d} d | 0 \rangle \neq 0 \,. \tag{1.8}$$

This leads to three Goldstone bosons, which appear as the pion triplet ($\pi^{0,\pm}$). The pions are massive because of the non-zero quark masses, which we have neglected.

The $U(1)_A$ transformation connects states of opposite parity but the same flavor and spin. This means that if $U(1)_A$ is a symmetry observed by nature, we should observe degenerate hadrons of opposite parity. However, this is not observed. The quark condensate also breaks $U(1)_A$ symmetry, and the Goldstone boson associated with this is called the η' boson. Weinberg has shown that such a boson should have mass m_L comparable to the pion [44]

$$m_L \leq \sqrt{3} m_\pi \,. \tag{1.9}$$

However, no such particle is observed. The particle with the right quantum numbers (zero-isospin pseudoscalar) is the η' boson, but it is much more massive than

the pions

$$\frac{m_{\eta'}}{m_\pi} \simeq 4\,. \tag{1.10}$$

This is called the missing meson or $U(1)_A$ problem of QCD. If we consider the QCD Lagrangian with the light quarks (u, d, and s), we will get a spontaneously broken $SU(3)_A$ symmetry; this will lead to eight Goldstone bosons: three pions ($\pi^{0,\pm}$), four kaons ($\bar{K}^0, K^{0,\pm}$), and the η meson. If $U(1)_A$ symmetry was spontaneously broken, we should see a ninth Goldstone boson with masses similar to these eight Goldstone bosons, which is not observed, leading to the $U(1)_A$ problem.

One interesting feature of $U(1)_A$ transformation is, it has an anomaly

$$\partial_\mu j^\mu_A = \frac{N\alpha_s}{8\pi}\tilde{G}^A_{\mu\nu}G^{A,\mu\nu}\,, \tag{1.11}$$

where $\alpha_s = \frac{g_s^2}{4\pi}$, $N = 2$ is the number of quarks, and $\tilde{G}^A_{\mu\nu} = \frac{1}{2}\epsilon_{\mu\nu\rho\sigma}G^{A,\mu\nu}$. The anomaly originated from the Jacobian in the integration measure ($\mathcal{D}q\mathcal{D}\bar{q} \xrightarrow{U(1)_A} J^{-2}\mathcal{D}q\mathcal{D}\bar{q}$) [45, 46]. It is easy to show that the right side of the above equation is a total derivative

$$\tilde{G}^A_{\mu\nu}G^{A,\mu\nu} = \partial_\mu K^\mu\,, \quad K^\mu = \epsilon^{\mu\nu\rho\sigma}G^A_\nu\left(G^A_{\rho\sigma} - \frac{g_s}{3}f^{ABC}G^B_\rho G^C_\sigma\right)\,, \tag{1.12}$$

where G^A_ν are the gluons and f^{ABC} are the $SU(3)$ structure constants. We would think that during the space-time integration, this will become a surface term and would vanish, provided the gauge fields go to zero at infinity. 't Hooft realized that if we could describe QCD by the semi-classical approximation of the path integral, then the $U(1)_A$ problem can be solved by a kind of configuration called an instanton [47, 48].

In the semi-classical approximation, the gauge fields at the boundary can be of different configurations, categorized by a parameter called winding number n, and the weight of the functional integral can be represented by adding the following term to the Lagrangian

$$\mathcal{L}_\theta = \sum_{n=-\infty}^{\infty} e^{in\theta'}\frac{\alpha_s}{8\pi}\tilde{G}^A_{\mu\nu}G^{A,\mu\nu} \equiv \theta\frac{\alpha_s}{8\pi}\tilde{G}^A_{\mu\nu}G^{A,\mu\nu}\,. \tag{1.13}$$

where θ' is a free phase parameter. In the semi-classical approximation, instantons provide a non-zero contribution in the path integral, and therefore we need to add this term to the QCD Lagrangian. Since this term explicitly breaks the $U(1)_A$ symmetry, this explains the higher mass of η' meson, thereby solving the $U(1)_A$ problem.

1.4.2 Strong CP problem

The QCD Lagrangian with the quark mass term and the θ-term is

$$\mathcal{L}_{QCD} = -\frac{1}{4}G^A_{\mu\nu}G^{A,\mu\nu} + \bar{q}i\gamma^\mu\partial_\mu q + g_s\bar{q}\gamma^\mu G^A_\mu T^A q - \bar{q}Mq - \theta\frac{\alpha_s}{8\pi}\tilde{G}^A_{\mu\nu}G^{A,\mu\nu}\,, \tag{1.14}$$

where $q = (u, d, s)^T$ and $M = \mathrm{Diag}(m_f e^{\theta_f})$. It is convenient to make the quark mass matrix real; this can be done by $U(1)_A$ transformations on the quark flavor basis

$$q_f \to e^{i\gamma_5\beta_{A_f}}q_f\,, \tag{1.15}$$

$$\Rightarrow \bar{q}_f m_f e^{\theta_f} q_f \to \bar{q}_f m_f e^{i(\theta_f + 2\beta_{A_f})} q_f\,. \tag{1.16}$$

We can make the quark mass real by assigning $\beta_{A_f} = -\theta_f/2$, but since $U(1)_A$ is an anomalous symmetry

$$\mathcal{L}_\theta \to \mathcal{L}_\theta + 2\theta_f\frac{\alpha_s}{8\pi}\tilde{G}^A_{\mu\nu}G^{A,\mu\nu}\,, \tag{1.17}$$

$$\Rightarrow \mathcal{L}_{\mathrm{QCD}} \to -\frac{1}{4}G^A_{\mu\nu}G^{A,\mu\nu} + \bar{q}i\gamma^\mu\partial_\mu q + g_s\bar{q}\gamma^\mu G^A_\mu T^A q - \bar{q}M_0 q - \bar{\theta}\frac{\alpha_s}{8\pi}\tilde{G}^A_{\mu\nu}G^{A,\mu\nu}\,, \tag{1.18}$$

where $M_0 = \mathrm{Diag}(m_u, m_d, m_s)$ and $\bar{\theta} = \theta + \mathrm{Arg}(\mathrm{Det}(M))$. Thus, the only physical parameter in QCD that violates CP is $\bar{\theta}$. Now that we have established that CP-violation is a theoretical feature of SM (CKM matrix and $\bar{\theta}$ term), we pass the baton to experimentalists to measure the CP-violating observables to fix these parameters.

The most sought-out CP-violating observables induced by the $\bar{\theta}$ term are the permanent electric dipole moments (EDMs) of nucleons, atoms, and molecules. The EDM (d) is defined through

$$\mathcal{H} = -\mu\frac{\boldsymbol{\sigma}}{|\boldsymbol{\sigma}|}\cdot\boldsymbol{B} - d\frac{\boldsymbol{\sigma}}{|\boldsymbol{\sigma}|}\cdot\boldsymbol{E} \xrightarrow{CP} -\mu\frac{\boldsymbol{\sigma}}{|\boldsymbol{\sigma}|}\cdot\boldsymbol{B} + d\frac{\boldsymbol{\sigma}}{|\boldsymbol{\sigma}|}\cdot\boldsymbol{E}\,, \tag{1.19}$$

where μ is the magnetic dipole moment, $\boldsymbol{E}$ and $\boldsymbol{B}$ are electric and magnetic field respectively.

As we have discussed, the SM contribution to neutron-EDM (d_n) can be attributed to only two sources: the $\bar{\theta}$ term and CKM contribution. The most precise calculation of $\bar{\theta}$ term contribution to d_n comes from the lattice QCD calculation [49], and the CKM contribution is calculated in Ref. [50, 51]; and by comparing both with the most precise experimental result [52]

$$|d_n|_{\mathrm{exp}} = (0.0 \pm 1.1_{stat} \pm 0.2_{sys}) \cdot 10^{-26}\,\mathrm{e\,cm}\,, \tag{1.20}$$

$$|d_n|_{\bar{\theta}} = (-1.52 \pm 0.71) \cdot 10^{-16}\,\bar{\theta}\,\mathrm{e\,cm}\,, \tag{1.21}$$

$$|d_n|_{CKM} \sim 10^{-31}\,\mathrm{e\,cm}\,. \tag{1.22}$$

Since the most accurate EDM searches are orders of magnitude away from the CKM contribution to the EDMs, the SM contribution to any non-zero EDM measurement comes purely from the QCD $\bar{\theta}$ term. This leads to the limit

$$\bar{\theta} \lesssim 10^{-10}\,, \tag{1.23}$$

which is commonly known as the strong *CP* problem.

One could argue that this is not a problem; nature chose a very small value of $\bar{\theta}$ to mess with particle physicists. However, this could also hint at something we have failed to consider. Therefore, the best approach is to treat it like a problem we need to solve. There are three main solutions.

Massless quark solution: If one of the quarks is massless, for example, the up quark u, QCD will acquire a global $U(1)_u$ symmetry. This can be used to do an axial transformation and rotate the $\bar{\theta}$ to zero. For a given quark masses, we can calculate the hadron masses using LQCD. Similarly, we can reverse calculate the quark masses from the experimental data on hadron masses. This method gives a non-zero up-quark mass $m_u^{\overline{\text{MS}}}(2\,\text{GeV}) = 2.16^{+0.49}_{-0.26}\,\text{MeV}$ [53]. An independent method was proposed in Refs. [54, 55] to analyze the massless quark solution by avoiding any quark mass fitting procedures, and was implemented on the lattice, which ended up further confirming the non-zero quark masses [56].

Soft P(CP) Breaking: If P or CP are good symmetries of the high-energy theory (UV regime) and SM is an effective field theory of this theory at a lower (energy) scale, then we can fix $\bar{\theta} = 0$ in the UV. This will result in a small value of $\bar{\theta}$ at a lower scale. This is because if $\bar{\theta}$ is small on some high-energy scale, it is still small on a lower-energy scale. After all, the renormalization group running of $\bar{\theta}$ occurs at 7-loops [57]. The first class of such models had CP as a good symmetry, which gets broken at the electroweak scale [58, 59], and the second class was proposed based on grand-unified models [60, 61]. In these models, CP gets broken at a lower scale to account for the SM chiral structure and CKM phase. In this approach, the $\bar{\theta}$ term becomes calculable. The downside is that some tuning is required to keep $\bar{\theta} \lesssim 10^{-10}$ while maintaining a relatively large CKM phase.

Peccei-Quinn solution: The most popular solution to the strong CP problem was proposed by Peccei and Quinn (PQ) in 1977 [62, 63]. They proposed that if there is a global chiral symmetry $U(1)_{\text{PQ}}$ in which quarks and Higgs transform non-trivially, the $\bar{\theta}$ becomes a dynamic variable and can be set to zero. It was later pointed out by Weinberg [64] and Wilczek [65] that the $U(1)_{\text{PQ}}$ symmetry gets spontaneously broken by the vacuum at low energies and leads to the existence of a Goldstone boson, commonly called the axion. Though we have yet to observe any particle that fits the axion, this is the most promising solution to the strong CP problem.

1.5 *CP*-violating axion interactions

For part of this thesis, we choose the axion solution to the strong *CP* problem. The axion modifies the *CP*-violating gluonic interaction as $\mathcal{L}_{\bar{\theta}} \to (\bar{\theta} + \frac{a}{f_a})G\tilde{G}$, where f_a is the axion decay constant. Once we expand around the minimum of the axion field: $a = \langle a \rangle + a_{\rm ph}$, the pure gauge $\bar{\theta}$ term $\bar{\theta}G\tilde{G}$ disappears, and we are left with only the $a_{\rm ph}G\tilde{G}$ interactions. We can use the $U(1)_{\rm PQ}$ symmetry to translate the axion field to its minimum, and we relabel $a_{\rm ph} \to a$ for notational convenience

$$\begin{gathered} a \xrightarrow{U(1)_{\rm PQ}} a + \langle a \rangle \\ \left(\bar{\theta} + \frac{a}{f_a}\right) G\tilde{G} \xrightarrow{U(1)_{\rm PQ}} \left(\bar{\theta}_{\rm ind} + \frac{a}{f_a}\right) G\tilde{G} \xrightarrow{\rm SM} \frac{a}{f_a} G\tilde{G}\,, \end{gathered} \tag{1.24}$$

thereby solving the strong *CP* problem.

However, we have already established that SM does not account for the observed matter-antimatter asymmetry. Therefore, there should be *CP*-violating sources from new physics. These sources will lead to a contribution to $\bar{\theta}_{\rm ind}$, and the PQ mechanism can not offset all these contributions; therefore, in general, $\bar{\theta}_{\rm ind} \neq 0$. Thus the axion-hadron interaction contributes to the new physics via $\bar{\theta}_{\rm ind}$. Thus it will be worthwhile to study the *CP*-odd axion-nucleon interaction to glimpse into the nature of new physics.

Chapter 4 is part of my thesis that details my research on the *CP*-odd axion-nucleon interaction from the SM and the BSM physics. We have used dimension-six SMEFT operators for the BSM interactions and finally used χPT to extract the meson and hadron interactions with the axion. We also explored the limits imposed on the *CP*-odd couplings by the various experiments. Finally, we connected our EFT results to the leptoquark and LRSM BSM models.

1.6 *CP*-violating nuclear forces

QCD describes the strong interactions. It is mediated by vector bosons called gluons, which come in eight flavors. An interesting feature of QCD is the asymptotic freedom, discovered by Gross, Wilczek, and Politzer [4, 5] in 1973. Asymptotic freedom is the property that the strong interaction becomes weaker for higher energies and becomes stronger for lower energies; see Fig. 1.1. This strong coupling at the lower energy scale is the reason for the existence of hadrons, the quark-bound states. Only a few percent of nucleon mass is attributed to its constituent quarks; the rest comes from the non-perturbative QCD effects. Because of this non-perturbative nature of QCD at low energies, we can not use it directly to predict nuclear observables such as nucleon binding energy or nucleon scattering cross-section. However, with the use of EFTs, we can circumvent this problem to a great extent.

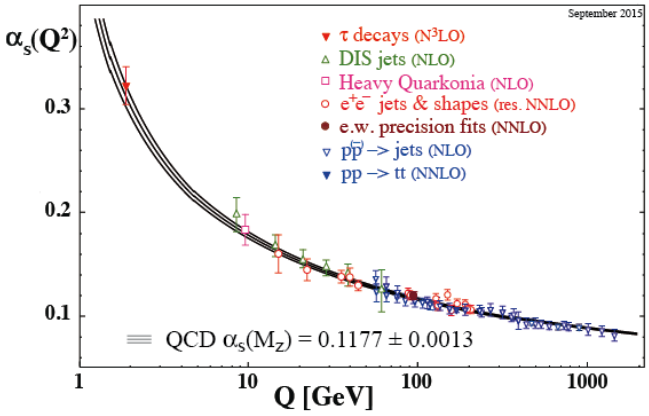

Figure 1.1: The summary of α_s from various experiments and LQCD as a function of energy. This figure is taken from Ref. [66].

It is convenient to have an EFT with hadrons as the degrees of freedom to describe nuclear interactions. Since we do not want phenomenological models, the EFT should be based on QCD and respects its symmetries. χPT is constructed to satisfy all these requirements. It is based on the $SU(3)_L \times SU(3)_R$ chiral symmetry of QCD, which is spontaneously broken in the ground state of the nucleons. χPT follows the Weinberg power counting scheme, which allows us to calculate hadronic observables as a perturbative expansion in powers of Q/Λ_χ, where Q is momentum associated with the system under consideration and $\Lambda_\chi \sim 1\,\text{GeV}$ is the chiral symmetry breaking scale. Therefore, by including all contributions up to $(Q/\Lambda_\chi)^\nu$, we can predict observables with accuracy of $\mathcal{O}\left((Q/\Lambda_\chi)^{\nu+1}\right)$. χPT is described in detail in Section 2.3.

In recent years, considerable progress has been made in applying χPT to describe nuclear forces. We have seen in the previous sections that QCD conserves *CP* to extremely high accuracy, apart from the small $\bar{\theta}$ term. Since the nuclear force originates from QCD interactions, the nuclear forces are approximately *CP* conserving. The *CP* conserving *NN* nuclear force has been calculated up to N^4LO using χPT [67–69] and has very successfully described various observed nuclear phenomena. The top panel of Fig. 1.2 shows the full LO and N^2LO short-distance diagrams for calculating the *CP* conserving *NN* nuclear force.

As we have seen in the previous section, molecular, atomic, and nuclear EDMs are excellent probes for BSM physics. However, it is a non-trivial task to connect the *CP*-violating sources of SM and from BSM to complex objects like nuclear EDMs. In recent years, there has been theoretical advancement in calculating the EDMs in a model-independent approach using first-principle calculations by combing the results of lattice QCD [49, 70, 71], χPT [72–74], and nuclear calculations [75–79]. The strategy is to start with dimension-four ($\bar{\theta}$ term) and

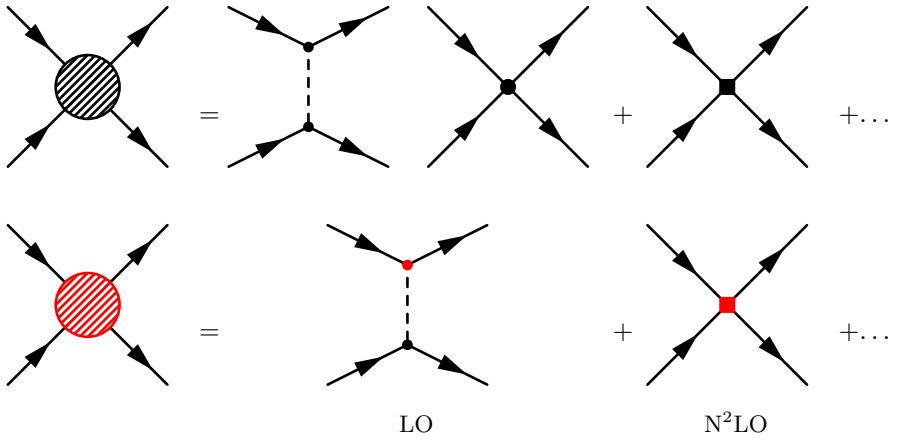

Figure 1.2: The top (bottom) panel shows LO and N^{2}LO chiral contributions of the *CP*-even (odd) nuclear force in χPT. The black (red) vertices represent the *CP*-even (odd) interactions. The solid and dashed lines represent nucleons and pions, respectively.

dimension-six (BSM physics) *CP*-violating operators in the SMEFT framework and evolve the theory to hadronic scale and match to the *CP*-violating operators in χPT. A key component in the EDM calculations is the *CP*-odd nuclear force. Therefore, understanding the *CP*-odd nuclear force is essential.

The χPT follows the Weinberg power counting to determine the relative relevance of diagrams contributing to observables. The Weinberg power counting is based on naive dimensional analysis (NDA). The LO diagrams and N^{2}LO contact diagrams for *CP*-even and *CP*-odd *NN* nuclear force are shown in Fig. 1.2. All physical quantum field theories should be renormalized. Renormalization is the procedure of removing nonphysical infinities that arises while calculating any observables. We achieve this by redefining the contact interactions to absorb these infinities. Since EFT calculations are done order by order, there should be enough contact interactions for any given order to cancel all infinities. If there are not enough contact interactions to achieve this, then the theory is not properly renormalized, and the power counting fails. The NDA is known to fail in some *CP*-even *NN* scattering channels, and we had to promote some higher-order terms to lower order to renormalize the theory. However, no one has investigated the renormalization of the *CP*-odd nuclear force. A part of this thesis is focused on this investigation.

1.7 Dark matter direct detection

Evidence is abundant for the existence of dark matter (DM) from various astrophysical and cosmological observations, spanning scales from galaxies to the observable Universe. The current understanding of DM is that it is massive (interacts gravitationally), dark (almost no electromagnetic interactions in comparison with ordinary matter), non-baryonic in nature, cold (leading to observed large-scale DM structures), and stable on cosmological time scales (leading to the observed DM density) (see Ref. [9] for a review). The current understanding of the standard cosmological model predicts, based on the various cosmic microwave background radiation experiments [80–83], about 23% of the Universe is made up of DM and 72% of the Universe consists of Dark Energy (anti-gravity); the baryonic matter (ordinary matter) only accounts to 5% of the Universe.

Since SM fails to account for the existence of DM, it should be made up of one or more BSM particles that are massive, uncolored, electrically chargeless, weakly interacting, and stable.

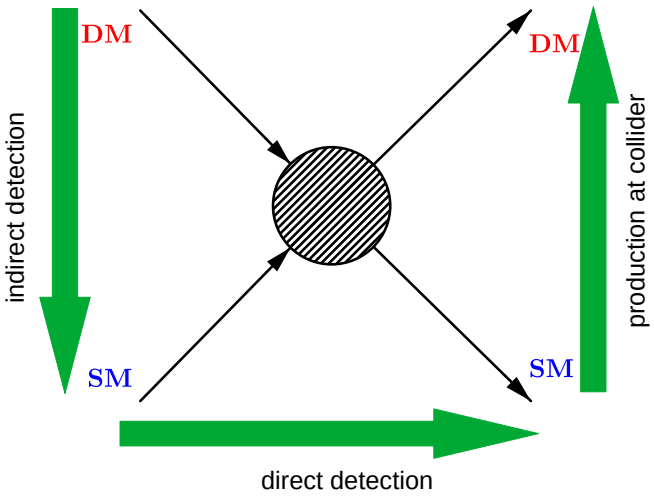

Figure 1.3: Illustration of direct, indirect, and collider dark matter searches. The hashed circle represents the SM-DM interaction.

One possible class of candidates that fit these descriptions are the weakly interacting massive particles (WIMPs), which have masses from $1\,\text{GeV} - 100\,\text{TeV}$; WIMPs are also motivated by predictions of some BSM models. The current DM searches can be divided into three categories: direct detection, indirect detection, and production at colliders, see Fig. 1.3.

- *Direct detection*: This class of experiments looks for DM by identifying the nuclear recoils produced by the DM and target nuclei: $\text{DM} + N \to \text{DM} + N$.

These experiments target WIMPs with masses $(10-1000)$ GeV, which would results in nuclear recoils in the range $(1-100)$ keV [84]. The signature of dark matter in a direct detection experiment consists of a recoil spectrum of single scattering events. Given the low interaction strength expected for the dark matter particle, the probability of multiple collisions within a detector is negligible. In the case of a WIMP, a nuclear recoil is expected [85]. Some of the experiments that use direct detection methods are DAMIC [86], CRESST [87], EDELWEISS [88], SuperCDMS [89], LUX [90], and XENON100 [91].

- *Indirect detection*: This class of experiments looks for DM by observing the radiation produced by DM when they annihilate or decay: $\mathrm{DM}+\mathrm{DM}\rightarrow e^+e^-, \bar{p}p, \ldots$. This experiment focuses on the regions with high DM concentrations. This method takes advantage of long-running *experiments* run by the Universe and can probe higher energies, longer decay lengths, and weaker couplings. All the best limits of DM come from these astrophysical and cosmological observations. These experiments are looking for DM signatures from the high-energy neutrinos from the Sun's core and Galactic Centre, gamma-rays from the Galactic Centre and dwarf spheroidal galaxies, and positrons, antiprotons, and antideuterons from the galactic halo. The drawback is that a thorough understanding of these processes is required to interpret the observations, and thus the results often come with large error bars. Some of the experiments that use this method are PAMELA [92], AMS [93], Fermi-LAT [94], HESS [95], and MAGIC [96].

- *Production at colliders*: In this search, they look for DM production at the LHC: $\bar{p}p\rightarrow \mathrm{DM}+\mathrm{DM}$. The DM production can affect the energy momenta of the SM particles detected in the LHC. One signature is the recoil on the SM particles colliding with *invisible particles* within the detector or the sudden appearance of SM particles with appropriate energy-momentum from the decay of DM. The processes like $pp\rightarrow \bar{\chi}\chi + X$, where the so-called mono-object X is a photon, a jet, or Z boson, etc., produces a signature of missing transverse energy accompanied by a so-called mono-object. So far, no results have been produced using mono-jets or mono-photons accompanied by missing transverse energy [97–99].

In this thesis, we focus on DM direct detection searches using light nuclei. We choose light nuclei because they are sensitive to low-massive DM and provide *cleaner* theoretical calculations. Our goal is to provide a theoretical interpretation of the DM direct detection results (or lack of results) by starting from the fundamental DM-SM interactions. First, we focus on the scalar interaction of the DM with the quarks and gluons, then we evolve it to the hadronic scale and match it up with χPT to get the DM-hadron interactions.

To understand the DM-nucleus scattering, we will study the leading order one-nucleon current and the subleading two-nucleon current in the framework of χPT.

It has been known that the two-nucleon currents introduce distinct dependence of the DM-nucleus cross-section on A (the atomic mass number) and Z (the number of protons). Moreover, DM-quark/gluon interactions will lead to similar χPT operators in the one-nucleon current but produce different interactions for two-nucleon currents. Thus, if the experimental data from various nuclei are available, it is potentially possible to understand the difference in the interaction between DM and quark/gluons [100]. We can calculate the nuclear wave function by solving the Schrödinger equation for the nuclear potential. To be consistent, we will calculate the nuclear potential using the χPT framework. This allows for a first-principle calculation, i.e., starting from an assumed (set of) DM-SM interaction(s) of the DM-nucleus cross sections.

We will implement a new way of calculating the matrix elements of one, and two-nucleon currents. This method, called density formalism, reduces the computation time by a factor of ten [101]. In the "traditional method", to calculate the matrix element we have to do the following integration

$$\langle \Psi' | O | \Psi \rangle_{\text{traditional}} = \int \{\mathrm{d}p_i\} \Psi'^{\dagger}(\{p_i\}) \Psi(\{p_i\}) O(\{p_i\}) \,, \tag{1.25}$$

where $\{p_i\}$ are the internal momentum, and quantum numbers of the scattering particles are suppressed for simplicity. Every time we need to calculate a matrix element, we have to use this nuclear wave function, a large data file and multiply it by the operator at each moment. This requires the aid of a supercomputer.

In the density matrix formalism, the above matrix element can be separated into two parts

$$\langle \Psi' | O | \Psi \rangle_{\text{density formalism}} = \sum_{\{n_i\}} \rho(\{n_i\}) \otimes O(\{n_i\}) \,, \tag{1.26}$$

where $\{n_i\}$ are the quantum number of the internal nucleons, and the energy-momenta and quantum numbers of the scattering particles are suppressed for simplicity. The density function (ρ) contains all the nuclear wave function information. Therefore, we only need to compute the density function once, which can be stored for future computation. This drastically reduces matrix elements' computation time because we bypass the redundant wave function calculation. By 'reading' the stored ρ file, we can calculate the matrix element using a personal computer instead of a supercomputer. Finally, the DM-nuclei cross section is calculated using the matrix element of the one, two-nucleon currents for ^{2}H, ^{3}He, and ^{4}He nuclei. Our calculation of ^{4}He is further motivated by the upcoming DM search using a liquid ^{4}He detector [102].

1.8 Outline

The basic structure of this thesis is that the first chapter covers the introductory material, and the second chapter focuses on EFTs, which is the primary theoretical

tool used for this thesis. The original research is described in the remaining chapters, and the conclusion and the thesis summary are given at the end of the thesis.

Chapter 1 gives the introduction for this thesis and the motivation behind my research. The initial sections demonstrate the existence of BSM physics, the relevance of EFTs, and motivate the relevance of *CP*-violating phenomena as a window to new physics. The later sections introduce BSM particle axions as a possible solution to the strong *CP* problem and the importance of studying *CP* violating axion interactions and nuclear forces to understand BSM physics. The last section discusses the direct detection of DM using light nuclei.

Chapter 2 describes the EFTs and introduces various EFTs generally used in particle physics. In the initial sections, we describe the key feature of the EFTs and the advantages they provide and briefly describes a few popular EFTs. Then we provide a recipe for building a general EFT. Finally, in the last section, we use this recipe to construct the EFT known as χPT, which is the critical tool used in this thesis.

In Chapter 3, we present our research results in the renormalization of *CP*-violating nuclear forces. The initial sections are spent on describing the relevance of studying the renormalization of *CP*-violating nuclear forces and the approach we took to achieve this objective. The third section describes the basic structure of the Python algorithm used to calculate our results. We presented our results in the fourth section and demonstrated that *CP*-odd nuclear forces are not properly renormalized in the LO. In the following sections, we fix this renormalization by introducing a counter term. We proposed a novel strategy to overcome the problem of lack of data to calculate this counter term and presented our conclusion and outlook in the last section.

In Chapter 4, we studied the complete set of dimension six *CP*-odd LEFT operators and connected them to various axion and other BSM experimental searches. The initial sections lay out the structure of *CP*-odd axion-SM interactions; then, we connect it to the axion-hadron interactions using χPT. We list the experiments looking for *CP*-violating interactions in detail in the fifth and sixth sections. In the next section, we presented the results of our calculations on the constraints on the BSM interactions from the experiments discussed in the previous section. Then, we used these EFT results and applied them to a few BSM models. Finally, the chapter concludes by providing an outlook into the future and ongoing work.

In Chapter 5, we explored the scalar DM interactions relevant to DM direct searches involving light nuclei. The first few sections are used to lay out the theoretical foundation for calculating the cross-section relevant to the direct searches. We started with the DM-SM scalar interactions and used χPT to bridge this to the DM-nuclei scalar interactions. Next, we discussed how we calculated the cross-section and density matrix formalism in the following section. In the following section, we presented our results and argued the existence of a renormalization problem for two-body scalar DM current. In the last section, we concluded our results and discussed the future prospects.

In Chapter 6, we concluded and summarized this thesis and outlined the plan for future works.

Chapter 2

Effective field theories

2.1 Introduction

We have been trying to understand the natural phenomena around us for a long time. We have made phenomenal advancements in this goal over the past century. For example, we can explain how leptons and quarks, particles around the length scale of 10^{-28} m, interact. We can also understand the expansion of the Universe, which is around the scale of 10^{26} m. All of these were possible because of the remarkable feature of nature called *decoupling*, which states that physics at a higher energy scale is largely irrelevant to describing physics at a lower energy scale. This property is why we can design and build bridges and dams without knowing anything about atoms or quantum gravity.

The decoupling feature of nature helps to explain the physics at a given energy scale with an *effective theory* containing some relevant parameters. For example, in the case of building bridges, the effective theory is classical mechanics, and one of the relevant parameters is the bulk modulus of the steel. We design and implement experiments based on the current understanding of physics. The experimental results provide feedback to theoretical advancement, leading to better experimental design and precise measurement. These feedback loops result in going from one energy scale to another. This is how we started from understanding how an apple falls and planets moves to how quarks and leptons interact to make atoms.

The basic strategy to develop a theory for an energy scale E is to create a first-order approximation and set all scales to infinity (zero) which are larger (smaller) than energy E for the interested physical processes. Then, we can add the neglected energy scales as a perturbation to the first-order approximation if needed. For example, we can describe a hydrogen atom as a system of electrons and an infinitely massive nucleus. The relevant parameters are electron mass, m_e, and the fine structure constant, α_{em}. We can implement the finite mass of the

nucleus by using reduced mass (m_{reduced}), which is a perturbative correction to electron mass m_e in terms of proton mass m_p: $m_{\text{reduced}} \simeq m_e \left(1 - \frac{m_p}{m_e}\right)$.

Effective field theories (EFTs) are theoretical tools used to implement the strategy described above in a precise and quantitative framework. Different energy scales separate the EFTs associated with particle physics. Nevertheless, these scales can generally be any dimensionful quantities like lengths, times, velocities, momenta, angular momenta, etc., in which physics gets separated. We can make a general claim that when adequately formulated,

all physical theories are effective theories.

The chapter is structured as follows. Section 2.2 provide the recipe for a general EFT, how to formulate them, and their advantages, and briefly discuss some of the popular EFTS used by particle physicists, like Standard Model EFT (SMEFT), low-energy EFT (LEFT), and chiral perturbation EFT (χPT). Section 2.3 focuses on chiral perturbation theory and elaborates on the various steps involving the formulation of χPT, like associated symmetry, the chiral Lagrangian, and the power counting rule, and also demonstrates how to apply the power counting rule on some of the operators relevant to this thesis.

2.2 Effective field theories

EFTs are theoretical tools appropriate for describing *low-energy* physics at a relevant energy scale (E) using just the relevant parameters and interactions; here, low-energy is with respect to some higher energy scale Λ. EFTs are complete quantum field theories in their own right, described in terms of relevant degrees of freedom.

A general feature of an EFT Lagrangian is that it consists of an infinite number of terms with couplings proportional power of $\frac{\text{energy/momenta}}{\Lambda}$. This feature results from our lack of knowledge regarding the "true" theory at the relevant energy scale. The solution for this problem is another feature of EFT, namely the power counting rule. The power counting rule will determine each term's relevance and the relevance of operators calculated from the Lagrangian in terms of an expansion parameter δ. In general, there can be multiple expansion parameters depending on the EFT. Even though there are infinite terms in the Lagrangian, renormalization is achieved order-by-order since there are only a finite number of terms for a given order of δ.

The theoretical basis of effective field theory can be formulated from the theorem [103, 104]: *For a given set of asymptotic states, perturbation theory with the most general Lagrangian containing all terms allowed by the assumed symmetries will yield the most general S-matrix elements consistent with analyticity, perturbative unitarity, cluster decomposition and the assumed symmetries.*

There are two ways to construct an EFT: the top-down and the bottom-up approaches. In the top-down approach, we know the ultraviolet (UV) complete

theory, but it contains fields heavier than the interested energy scale. In this case, the EFT calculations become more straightforward for the observables in the low-energy regime. The EFT Lagrangian will have the same symmetries as the UV theory, but the degrees of freedom do not always follow the UV theory. For example, Fermi theory and its UV complete theory (weak interaction) share the same degrees of freedom, the quarks. However, in the case of χPT, the degrees of freedom are hadrons, compared to quarks and gluons in the UV theory (QCD).

The EFT Lagrangian follows the symmetries of the UV theory and is obtained from the UV theory by 'integrating out' the heavy degrees of freedom (Φ_{heavy}). The effects of these heavy fields hide in the coefficients of operators allowed by the symmetries. Wilson and others first pioneered this approach in the 1960s (see Ref. [105] for a review)

$$e^{iS_{\text{EFT}}(\phi_{\text{light}})} \equiv \int \mathcal{D}\Phi_{\text{heavy}} e^{iS(\phi_{\text{light}},\Phi_{\text{heavy}})}\,, \tag{2.1}$$

$$\mathcal{L}_{\text{EFT}} = \sum_d \sum_{i=1}^{n_d} \frac{c_i^{(d)}}{\Lambda^{d-4}} \mathcal{O}_i^{(d)}\,, \tag{2.2}$$

where the dimensionless couplings c_is are Wilson's coefficient corresponding to the operator $\mathcal{O}_i^{(d)}$ of mass dimension d. These coefficients are obtained from the UV theory by a *matching* procedure.

In the bottom-up approach, we do not know the UV complete theory or the matching to the EFT is too difficult. The EFT is constructed by accommodating all the interested symmetries of the UV limit. The EFT Lagrangian will consist of operators that respect these symmetries, and each operator is accompanied by a coupling constant. One example of this approach is SMEFT

$$\mathcal{L}_{\text{SMEFT}} = \mathcal{L}_{\text{SM}} + \sum_{d=5}^{\infty} \sum_{i=1}^{n_d} \frac{c_i^{(d)}}{\Lambda^{d-4}} \mathcal{O}_i^{(d)}\,, \tag{2.3}$$

where the dimensionless couplings $c_i^{(d)}$ are called Wilson coefficients and $\mathcal{O}_i^{(d)}$ are the operators of mass dimension d. These coupling constants are unknown but are fitted from the experimental data with the help of the power counting rule. These types of EFTs are mainly used when trying to understand new physics. Once enough Wilson's coefficients are known, we can make predictions for experiments and can extract some features of the new physics. One famous example is the Fermi theory, which was constructed before SM was known.

2.2.1 Main ingredients of EFTs

Once we identify a problem we want to solve and the relevant energy scale, we can start constructing the EFT. There are three main ingredients for any EFT, which are listed below.

1. *Degrees of freedom.* The first step in building an EFT is identifying the degrees of freedom relevant to describing the interested system. Sometimes the degrees of freedom will come naturally from the symmetries or based on the problem we try to solve. For example, to extend the SM to an EFT (i.e., SMEFT), it is straightforward to use SM fields as the degrees of freedom. On the other hand, if one wants to design an EFT to explain nuclear physics, it is better to use protons and neutrons as degrees of freedom. There is no unique way to select the degrees of freedom; as long as it is simple enough to describe the problem we are trying to solve and implement the theory's symmetries, they are 'good' degrees of freedom.

2. *Symmetries.* The next step in the EFT building process is to identify the relevant symmetries of the system that we are trying to describe. All the terms of the Lagrangian should respect these symmetries, and thereby symmetries dictate the dynamics of our theory. If one knows the underlying high energy theory (top-down approach), those symmetries manifest in our EFT. Symmetries can come in multiple forms: global, gauged, accidental, spontaneously broken, anomalous, approximated, etc. For example, χPT is the low-energy EFT of QCD, which respects the P, CP, and C symmetries because QCD respects these symmetries.

3. *Expansion parameters.* Any operator that respects the symmetry should be added to the Lagrangian, this will lead to an infinite number of terms, and any meaningful calculation would be impossible. The expansion parameters and power counting rule handle this problem. They are the effects of the high-energy degrees of freedom we integrated-out from the action (top-down approach). For particle physics, these are usually the ratios of energy or momenta associated with the physical processes, $\frac{p}{\Lambda}, \frac{m}{\Lambda}$. All the physical observables calculated will be in a series of these expansion parameters. The power counting rule will determine the relevance of these terms. For a given order, only a finite number of terms, defined by the power counting rule, will contribute to the calculation. For example, in an EFT with one expansion parameter δ, an order n calculation of an observable will have contributions from Feynman diagrams proportional to $\delta^{i\leq n}$, and the error will be in the order of δ^{n+1}. The power counting rule will determine the power of δ associated with Feynman diagrams.

Even though it is relatively easy to state these concepts, implementing this to an EFT can be challenging, depending on the problem we are trying to solve. Therefore, in Section 2.3, we will implement these concepts and use the following recipe to construct χPT.

> **Step 1.** Identify the energy scale of the low-energy system (E) and the scale of the underlying physics Λ where the EFT breaks down. Choose appropriate degrees of freedom to describe the system.

Step 2. Identify the symmetries of the system. Then, investigate if they are broken; if yes, then how they are broken.

Step 3. Construct the most general Lagrangian, which respects these symmetries and symmetry breakings.

Step 4. Design a power counting scheme that can distinguish the relative relevance of the terms which are in the series of expansion parameters.

Step 5. Using this power counting scheme, calculate the relevant Feynman diagrams to obtain the Wilson coefficients. A top-down approach uses the matching procedure to get the Wilson coefficients. In the case of a bottom-up approach, the coefficients are fitted to experimental data.

> *Matching procedure:* In the top-down approach, we integrate out heavy fields (see Eq. (2.1)), and this will lead to higher dimensional operators suppressed by inverse powers of heavy field masses (m_Φ). At heavy field mass scale, $E \sim m_\Phi$, the observable calculated from the EFT and the UV complete theory should be identical. Using this 'matching condition', we can obtain the values of the Wilson coefficients.

Step 6. Calculate the relevant Feynman diagrams for the interested problem up to the desired accuracy.

2.2.2 Advantages of EFTs

Even if we know the underlying theory, often time EFTs become more convenient to use. This situation can arise because the UV theory becomes strongly coupled and non-perturbative in the interested energy scale to perform any meaningful calculation. QCD demonstrates this scenario in the nuclear energy scale. This problem led to the chiral perturbation theory, which is a low-energy EFT of QCD. In this section, we will list other advantages provided by the EFTs.

- EFTs allow us to focus on the degrees of freedom and operators relevant to the problem we are trying to solve and simplify the calculations. We can ignore all other fields that are unimportant to the energy scale and all other complications arising from them.
- New symmetries can manifest when we *zoom in* on the relevant energy scale. Moreover, these symmetries will lead to conservation laws (Noether's theorem) which will further simplify our calculations.
- The EFT calculations can be factorized into two parts. The one related to the light degrees of freedom (the actual EFT calculations) and the other associated with the heavy-scale physics that we have neglected. Since the heavy-scale physics remains the same relative to the EFT calculations, we can do it once and avoid repeated calculations.

- The EFTs have a built-in mechanism to systematically account for the neglected UV theory using expansion parameters and power counting rule. This feature allows for a model-independent calculation when the underlying theory is unknown or poorly understood. Furthermore, the constraints on the Wilson coefficients arising from the experimental data can signal the symmetries of the UV theory and guide the model building of the UV theory.

- The EFTs allows the calculation of any observable in as a series expansion of expansion parameters guided by the power counting rule. This structure provides a means to associate a theoretical error with any calculations. By including higher-order terms of the series, one can make more precise predictions.

- The EFT calculations are only meaningful when done on the EFT energy scale. Whenever someone crosses this relevant energy scale, the EFT always notifies us by making the expansion parameters of $\mathcal{O}(1)$, and the perturbation expansion is no longer meaningful. If we still want to do the calculation, we must construct a new EFT following the recipe outlined in the previous section.

- EFT solves the problem of summing logs of the ratios of scales. For example, consider a one-loop diagram with two scalar fields ϕ and Φ, and loop four-momentum k. The field ϕ (Φ) of mass m (M) is a low-energy (high-energy) field, i.e., $m \ll \Lambda$ ($M \gg \Lambda$). In UV theory, the loop diagrams contribute as

$$\begin{aligned} I_{\rm UV} &= g^2 \mu^{2\epsilon} \int \frac{\mathrm{d}^d k}{(2\pi)^d} \frac{1}{k^2 - m^2} \frac{1}{k^2 - M^2} \,, \\ &= \frac{i g^2}{16\pi^2} \left[\frac{1}{\epsilon} - \log \frac{M^2}{\bar{\mu}^2} - \frac{m^2}{M^2 - m^2} \log \frac{M^2}{m^2} + 1 \right] , \end{aligned} \tag{2.4}$$

  where $d = 4 - 2\epsilon$, $\mu = \bar{\mu}^2 e^{\gamma}/4\pi$ is the renormalization scale, ϵ and γ are constants associated with the $\overline{\rm MS}$ renormalization scheme. The renormalization is the procedure of removing infinities from the S-matrix and making it finite, see Ref. [106]. In general, the ratio of M/m is such that $\mathcal{O}(g^2 \log M^2/m^2) > 1$, and the perturbative theory can break down. However, in the EFT framework, Φ is integrated out, and the loop integral

becomes

$$
\begin{aligned}
I_{\text{EFT}} &= g^2\mu^{2\epsilon}\int \frac{\mathrm{d}^d k}{(2\pi)^d}\frac{1}{k^2-m^2}\left(-\frac{1}{M^2}-\frac{k^2}{M^4}-\frac{k^4}{M^6}+\dots\right), \\
&= \frac{ig^2}{16\pi^2M^2}\left[-\frac{m^2}{\epsilon}+m^2\log\frac{m^2}{\bar{\mu}^2}-m^2\right] \\
&\quad+\frac{ig^2}{16\pi^2M^4}\left[-\frac{m^4}{\epsilon}+m^4\log\frac{m^2}{\bar{\mu}^2}-m^4\right] \\
&\quad+\frac{ig^2}{16\pi^2M^6}\left[-\frac{m^6}{\epsilon}+m^6\log\frac{m^2}{\bar{\mu}^2}-m^6\right]+\dots,
\end{aligned}
\tag{2.5}
$$

and all the problematic $g^2\log M^2/m^2$ are traded for $g^2\log m^2/\bar{\mu}^2$, which can be summed using perturbation theory.

- Using EFT, we can convert infrared (IR) logs in the full theory to UV logs in EFT. The renormalization group equations can sum up these UV logs. We are not demonstrating this feature of the EFT in this thesis; instead, we refer to Ref. [107].

2.2.3 Examples of EFTs

We will discuss some examples of EFTs used by particle physicists, see Table 2.1.

Effective Field Theory	**Relevant energy scale**	**Degrees of Freedom**	
SMEFT	$\Lambda_{\text{LEFT}} \lesssim E \lesssim \Lambda_{\text{SMEFT}} \gtrsim 1$ TeV	Standard Model fields	
LEFT	$E \lesssim \Lambda_{\text{LEFT}} = v = 256$ GeV	quarks	u, d, s, c, b
		bosons	γ
		leptons	e, μ, τ
		neutrinos	ν_e, ν_μ, ν_τ
χPT	$E \lesssim \Lambda_\chi = 1$ GeV	mesons	$\pi^{0,\pm}, K^{0,\pm}, \bar{K}^0, \eta$
		baryons	$p, n, \Sigma^{0,\pm}, \Xi^\pm, \Lambda$

Table 2.1: The most common effective field theories used in particle physics, their relevant energy scales, and their degrees of freedom.

Fermi theory of weak interactions

The Fermi theory of weak interactions [108] is an EFT of weak interactions for the energy scale below the mass of W and Z bosons ($\Lambda \sim M_W \sim 80\,\text{GeV}$). SM

was invented after the proposal of the Fermi theory. However, like any other EFT, calculations and predictions do not require the knowledge of UV complete theory (SM). The 'new physics' at that time was the W, Z bosons, t quark, and the Higgs boson. The weak interactions were studied using Fermi theory, and the expansion parameters were $\delta = p/\Lambda$, where p is momentum associated with the weak interactions. Fermi was motivated by electromagnetic interaction. The Fermi Lagrangian consists of two weak currents, the $\bar{p}n$ and $\bar{e}\nu_e$, which interact vector-like, mimicking the vector form of the electromagnetic interaction. The relevant Fermi Lagrangian for the beta decay is

$$\mathcal{L}_{\rm F} = \frac{G_F}{\sqrt{2}}(\bar{p}n\bar{e}\nu + \bar{n}p\bar{\nu}e)\,, \tag{2.6}$$

where G_F is the associated low-energy constant (Fermi constant), and p, n, e, ν represents standard particles.

The Fermi theory was very successful for a time in which EFTs were not adequately studied. Since the original Fermi Lagrangian only had one particular (vector) form, it could not completely explain all the experimental results. To solve this problem, the Fermi Lagrangian was expanded to include a general combination of scalar (s), pseudo scalar (p), vector (v), axial vector (a), and tensor(t) interactions. The experimental evidence of the parity violation nature of weak interaction discovered by T.D. Lee, C. N. Yang, and C. S. Wu [40, 109] was the final clue to the true form of the weak interaction $v - a$, which Fermi almost got it right in his first guess. The modern form of Fermi Lagrangian in terms of SM fields is

$$\mathcal{L}_{\rm Fermi} = -\frac{G_F}{\sqrt{2}}\mathcal{J}_\mu\mathcal{J}^{\mu\dagger} + \mathcal{O}\left(\frac{1}{M_W^4}\right)\,, \tag{2.7}$$

where

$$\mathcal{J}_\mu = \sum_{\substack{i=1,2\\ j=1,2,3}} \bar{u}_i\gamma_\mu(1-\gamma_5)V_{ij}d_j + \sum_{l=e,\mu,\tau}\bar{\nu}_l\gamma_\mu(1-\gamma_5)l\,, \tag{2.8}$$

with V_{ij} as the Cabibbo–Kobayashi–Maskawa mixing matrix and the i, j indices represents the generation of quarks. The Fermi constant expressed in terms of SM parameters as

$$\frac{G_F}{\sqrt{2}} \equiv \frac{g^2}{8M_W^2} = \frac{1}{2v^2}\,, \tag{2.9}$$

where $v \sim 246\,\text{GeV}$ is the electroweak symmetry breaking scale.

Low-energy effective field theory

The low-energy effective field theory (LEFT) [29] can be considered a systematic extension of Fermi's theory to describe flavor conserving and violating contact

interactions. LEFT describes physics below the electroweak scale ($\Lambda = v = 256\,\text{GeV}$), and SMEFT is used to study physics above the electroweak scale. The degrees of freedom of LEFT are the photons and SM fermions except for the top quark. Therefore, the LEFT can be considered the top-down EFT approach of SMEFT by integrating the heavy fields: $t, W^{\pm}, Z$, and h.

The symmetries of the LEFT are the Lorentz symmetry and the gauge symmetry ($SU(3)_c \times U(1)_{\text{em}}$), which allows accommodating various BSM contributions. The LEFT Lagrangian contains 70 Hermitian operators of dimension five and 3631 Hermitian operators of dimension six that do not violate baryon ($\Delta B = 0$) or lepton number ($\Delta L = 0$), as well as baryon- and lepton-number-violating operators. In addition, LEFT contains $\Delta L = \pm 2$ Majorana-neutrino mass operators in dimension three, and in dimension five, it includes $\Delta L = \pm 2$ Majorana-neutrino dipole operators. In dimension six, numerous additional LEFT operators have $\Delta L = \pm 4, \Delta L = \pm 2, \Delta B = \Delta L = \pm 1$, and $\Delta B = -\Delta L = \pm 1$. In Chapter 4, we discuss *CP*-violating dimension six operators in detail.

Standard Model EFT

The first run of the Large Hadron Collider (LHC) started over a decade ago. It has further reinforced the success of the Standard Model and detected the Higgs boson. Since LHC explored energies that have never been reached before, the expectations were high that it would reveal new physics and be able to narrow down the landscape of the BSM models. However, the new physics seems beyond the reach of LHC. Thus the model-independent EFT approach became popular.

Standard Model effective field theory is a bottom-up EFT extension of the Standard Model. It assumes the SM symmetries and the new physics scale is well beyond the LHC limit, $\Lambda \gg E_{\text{LHC}}$. SMEFT has the same degrees of freedom and the exact local $SU(3) \times SU(2) \times U(1)$ symmetry as the SM, with the vacuum expectation value (vev) of the Higgs field breaking the gauge symmetry down to $SU(3) \times U(1)$. The SMEFT Lagrangian is constructed from gauge-invariant operators involving the SM fermion, gauge, and Higgs fields. The SMEFT Lagrangian is given by

$$\mathcal{L}_{\text{SMEFT}} = \mathcal{L}_{\text{SM}} + \sum_{d=5}^{\infty} \sum_{i=1}^{n_d} \frac{c_i^{(d)}}{\Lambda^{d-4}} \mathcal{O}_i^{(d)} \,, \tag{2.10}$$

where $\mathcal{L}_{\text{SM}}$ is the SM Lagrangian, $c_i^{(d)}$ are called the Wilson coefficients, and $\mathcal{O}_i^{(d)}$ are all possible operators in mass dimension d.

The only possible dimension five ($d = 5$) operator is the famous Weinberg operator [110], which violates the lepton number. Nevertheless, the number of operators for higher dimensions ($n_{d>5}$) increases quickly, and it becomes a challenging task to calculate them while avoiding redundancy. Buchmüller and Wyler [26] calculated the first list of dimension six operators, but it contained redundant

operators. To avoid these redundancies, theorists use equations of motion, integration by parts, and Fierz identities. A complete set of dimension six, seven, and eight operators was calculated in Refs. [111–113], Refs. [114, 115], and Ref. [116] respectively.

The EFT used for most of this thesis is the χPT, which will be discussed in the following section.

2.3 Chiral perturbation theory

QCD has successfully predicted all strong interactions observed in the LHC and other collider experiments. It has already been established as the theory of strong interactions. Unfortunately, due to the asymptotic freedom of QCD, calculations become impractical at lower energies. It would have been more convenient to have a QFT based on QCD but with hadrons as degrees of freedom to analyze various nuclear and sub-nuclear phenomena. This inconvenience motivated the invention of chiral perturbation effective field theory (χPT). This section briefly covers the critical aspects of χPT; see Ref. [30] for a detailed review.

2.3.1 Degrees of freedom

We have discovered more than hundreds of hadrons in the past century, especially with the help of LHC. It would have been adequate to have an EFT to describe all the hadrons, but given its richness, it is impossible. However, if we narrow it down to the lighter hadrons, a significant simplification occurs.

The eight lightest pseudoscalar mesons ($\pi^{0,\pm}, K^{0,\pm}, \bar{K}^0$, and η) have smaller masses compared to the typical hadrons like ρ-meson ($M_\rho = 770\,\text{MeV}$) or proton ($m_p = 938\,\text{MeV}$). Especially the mass gap between isospin pion triplets ($m_\pi = 139\,\text{MeV}$) and the ρ meson is 630 MeV, where the mass gap between the isospin multiplets of the meson octet containing the s-quark being significant but comparatively smaller. All these observations indicate that these pseudoscalar mesons are the manifest of some underlying global symmetry. This underlying symmetry is the chiral symmetry of the QCD, which will be discussed in detail in the next section. It would be more convenient to incorporate the baryon octet ($p, n, \Sigma^{0,\pm}, \Xi^{0,-}$, and Λ) along with meson octet to describe nuclear physics phenomena. The chiral perturbation theory is the low-energy EFT of QCD which describes the meson octet and baryon octet below the chiral symmetry breaking scale ($\Lambda_\chi = M_\rho \approx 1\,\text{GeV}$) [103].

The one-loop contributions to any physical observable calculated using chiral perturbation theory will be proportional to (m_{meson} or momentum)$/\Lambda_\chi$. This calculation is another way to obtain the chiral symmetry-breaking scale once we know the χPT Lagrangian. The pion mass and pion decay constant calculated

up to one-loop order is [117]

$$m_{\pi\,(1-\text{loop})} = m_\pi \left[1 + \frac{1}{2}\left(\frac{m_\pi}{4\pi F_\pi}\right)^2 \ln m_\pi^2 + \dots\right], \tag{2.11}$$

$$F_{\pi\,(1-\text{loop})} = F_\pi \left[1 - \left(\frac{m_\pi}{4\pi F_\pi}\right)^2 \ln m_\pi^2 + \dots\right], \tag{2.12}$$

where F_π is the pion decay constant. From this we can conclude $\Lambda_\chi = 4\pi F_\pi \sim M_\rho \sim 1\,\text{GeV}$.

Step 1. The χPT describes the physics below the chiral symmetry breaking scale ($1\,\text{MeV} \lesssim E < \Lambda_\chi = 4\pi F_\pi \sim M_\rho \sim 1\,\text{GeV}$). It is constructed with degrees of freedom as the meson octet $(\pi^{\pm,0}, K^{\pm,0}, \bar{K}^0, \eta)$ and the baryon octet $(p, n, \Sigma^{\pm,0}, \Xi^{-,0}, \Lambda)$.

2.3.2 Chiral symmetry of QCD

The QCD Lagrangian is given by

$$\mathcal{L}_{\text{QCD}} = -\frac{1}{4} G^A_{\mu\nu} G^{A,\mu\nu} + \sum_{f=\substack{u,d,s,\\c,b,t}} \bar{q}_f (i\gamma^\mu D_\mu - m_f) q_f \,. \tag{2.13}$$

Each quark flavor q is composed to three colors (c) namely r (red), g (green), and b (blue): $q_f \equiv q_{f,c}$, and m_f is the quark mass. The covariant derivative and gluon field strength are given by

$$D_\mu = \partial_\mu - i g_s G^A_\mu T^A, \qquad A = 1, 2, \dots, 8\,, \tag{2.14}$$

$$G^A_{\mu\nu} = \partial_\mu G^A_\nu - \partial_\mu G^A_\mu + g_s f^{ABC} G^B_\mu G^C_\nu \,, \tag{2.15}$$

where g_s is the strong coupling constant, G^A_ν are the gluon fields, T^A are the Gell-Mann matrices, and f^{ABC} are the $SU(3)$ structure constants. The quark fields transform according to the fundamental representation of $SU(3)_c$ as

$$q_f \to q'_f = \exp\left(-i \sum_A \Theta_A(x) T^A\right) q_f \,. \tag{2.16}$$

Note that the QCD interaction 'sees' only the color of quarks, not their flavors. Along with local $SU(3)$ gauge symmetry, QCD also has $U(1)$ global symmetry since the Lagrangian is invariant under: $q_f(x) \to e^{i\theta} q_f(x)$. The latter leads to the Baryon number conservation. The QCD also has anomalous $U(1)_A$ symmetry, as discussed in Chapter 1. The anomalous $U(1)_A$ symmetry will not be considered for the remainder of this chapter. Now we will focus on some accidental symmetries of QCD, which help construct the low-energy QCD EFT.

Chiral symmetry

Six quark flavors can be categorized into light quarks (u, d, s) and heavy quarks(c, b, t). Among them, the heavy quark's masses lie above the Λ_χ, and the light quark's masses lie deep below Λ_χ ($m_u = 2.2\,\text{MeV}, m_d = 4.7\,\text{MeV}, m_s = 96\,\text{MeV} \ll \Lambda_\chi \sim 1\,\text{GeV}$). Since we are interested in the physics below the Λ_χ, a good first step is to start with the QCD with only light quarks in the chiral limit: $m_u, m_d, m_s \to 0$. This low-energy QCD Lagrangian is given by

$$\mathcal{L}^0_{\text{QCD}} = -\frac{1}{4} G^A_{\mu\nu} G^{A,\mu\nu} + \sum_{l=u,d,s} \bar{q}_l i \not{D} q_l \,, \tag{2.17}$$

where $\not{D} = \gamma^\mu D_\mu$. In this limit, QCD acquires a new global symmetry. It is more evident once we introduce the left and right quark fields

$$q_L = \frac{1}{2}(1+\gamma_5) q \,, \qquad\qquad q_R = \frac{1}{2}(1-\gamma_5) q \,. \tag{2.18}$$

The QCD Lagrangian rewritten in these field definitions is

$$\mathcal{L}^0_{\text{QCD}} = -\frac{1}{4} G^A_{\mu\nu} G^{A,\mu\nu} + \sum_{l=u,d,s} \bar{q}_{L,l} i \not{D} q_{L,l} + \bar{q}_{R,l} i \not{D} q_{R,l} \,. \tag{2.19}$$

Since the covariant derivative (D_μ) is flavor insensitive, the Lagrangian is invariant under the following global transformations

$$\begin{pmatrix} u_L \\ d_L \\ s_L \end{pmatrix} \to \exp\left(-i \sum_A \Theta^L_A T^A\right) \begin{pmatrix} u_L \\ d_L \\ s_L \end{pmatrix} \,, \tag{2.20}$$

$$\begin{pmatrix} u_R \\ d_R \\ s_R \end{pmatrix} \to \exp\left(-i \sum_A \Theta^R_A T^A\right) \begin{pmatrix} u_R \\ d_R \\ s_R \end{pmatrix} \,. \tag{2.21}$$

Thus, the $\mathcal{L}^0_{\text{QCD}}$ has a global $SU(3)_R \times SU(3)_L$ symmetry, also known as the *chiral symmetry*; and also the $U(1)_V$, which leads to the conservation of baryon number. The Lagrangian is invariant under global $SU(3)_R \times SU(3)_L \times U(1)_V$ symmetry.

Noether's theorem states that every continuous global symmetry of the action will give rise to a conserved current, which in turn provides a conserved charge [39]. The global $SU(3)_R \times SU(3)_L \times U(1)_V$ symmetry gives the following conserved currents

$$L^{\mu,A} = \bar{q}_L \gamma^\mu T^A q_L \,, \qquad \text{with } \partial_\mu L^{\mu,A} = 0 \,, \tag{2.22}$$

$$R^{\mu,A} = \bar{q}_R \gamma^\mu T^A q_R \,, \qquad \text{with } \partial_\mu R^{\mu,A} = 0 \,, \tag{2.23}$$

$$V^\mu = \bar{q}_L \gamma^\mu q_L + \bar{q}_R \gamma^\mu q_R \,, \qquad \text{with } \partial_\mu V^\mu = 0 \,. \tag{2.24}$$

And the associated charges are

$$Q_L^A(t) = \int \mathrm{d}^3x \; q_L^\dagger(\boldsymbol{x},t) T^A q_L(\boldsymbol{x},t)\,, \tag{2.25}$$

$$Q_R^A(t) = \int \mathrm{d}^3x \; q_R^\dagger(\boldsymbol{x},t) T^A q_R(\boldsymbol{x},t)\,, \tag{2.26}$$

$$Q_V(t) = \int \mathrm{d}^3x \; (q_L^\dagger(\boldsymbol{x},t) q_L(\boldsymbol{x},t) + q_R^\dagger(\boldsymbol{x},t) q_R(\boldsymbol{x},t))\,. \tag{2.27}$$

It is straightforward to show that these charge operators satisfy the Lie algebra of $SU(3)_R \times SU(3)_L \times U(1)_V$

$$[Q_L^A, Q_L^B] = i f_{ABC} Q_L^C\,, \tag{2.28}$$

$$[Q_R^A, Q_R^B] = i f_{ABC} Q_r^C\,, \tag{2.29}$$

$$[Q_L^A, Q_R^B] = 0\,, \tag{2.30}$$

$$[Q_L^A, Q_V] = [Q_R^A, Q_V] = 0\,. \tag{2.31}$$

If the symmetry associated with these charges is conserved, then by the Noether theorem, these charges will become time-independent and commute with the Hamiltonian. This will lead to degeneracies in the particle spectrum. In the next section, we will see how the non-zero mass of quarks affects these degeneracies.

Explicit symmetry breaking

We have explored the chiral limit of the QCD Lagrangian. However, it has been observed that the light quarks have small masses. To reflect this, we need to reintroduce the quark mass term to $\mathcal{L}^0_{\mathrm{QCD}}$. It is more convenient to write left and right currents in terms of vector ($V^{\mu,A} = R^{\mu,A} + L^{\mu,A}$) and axial-vector ($A^{\mu,A} = R^{\mu,A} - L^{\mu,A}$) currents. The quark masses modifies the conserved current as follows.

$$\partial_\mu V^{\mu,A} = i\bar{q}[MT^A - T^A M]q\,, \tag{2.32}$$

$$\partial_\mu A^{\mu,A} = i\bar{q}(MT^A + T^A M)q\,, \tag{2.33}$$

$$\partial_\mu V^\mu = 0\,, \tag{2.34}$$

Since $M = \mathrm{Diag}(m_u, m_d, m_s) \neq 0$, this clearly shows that the quark masses break the chiral symmetry explicitly. If the quarks had equal masses, we would get a conserved vector current, but the axial current would not the conserved. Considering only the $u-$ and $d-$quarks and assuming $m_u = m_d$ leads to a $SU(2)_V$ symmetry and conserved vector current. This is the isospin symmetry. Since $m_u \simeq m_d$, we have an approximate isospin symmetry. We can extend this to s-quark, and we will get the famous flavor $SU(3)$ symmetry [118], but it is significantly broken due to the large s-quark mass.

The QCD Lagrangian extended with external currents is [117]

$$\mathcal{L} = \mathcal{L}_{\rm QCD} + \bar{q}\gamma_\mu \left(v^\mu + \frac{1}{3} v^\mu_{(s)} + \gamma_5 a^\mu \right) q - \bar{q}(s - i\gamma_5 p) q \,. \tag{2.35}$$

The regular QCD is recovered when $v^\mu = v^\mu_{(s)} = a^\mu = p = 0$ and $s = M$. This Lagrangian is invariant under local $SU(3)_R \times SU(3)_L \times U(1)_V$ transformations, provided the external fields transform appropriately. The χPT is constructed from this underlying Lagrangian, which will be discussed later in this section.

Spontaneous symmetry breaking and Goldstone bosons

A continuous symmetry of a Lagrangian is defined as spontaneously broken or hidden when the ground state of the Lagrangian is no longer invariant under the said symmetry. In the case of explicit symmetry breaking, both the Lagrangian and the ground state are no longer invariant under the symmetry. The spontaneous symmetry breaking and the associated Goldstone bosons are discussed in detail in Appendix A. In the following, we will use the results from Appendix A.

We have seen that the QCD Lagrangian in the chiral limit is invariant under $SU(3)_L \times SU(3)_R \times U(1)_V$. The hadron spectrum should exhibit specific properties if this symmetry is "good" in the low-energy limit. For example, the $U(1)_V$ symmetry manifest as the conservation of baryon number (B). All the low-energy experiments verified the baryon number conservation; the hadrons categorize into two types: baryons ($B = 1$) and mesons ($B = 0$).

It is convenient to rewrite the left and right charges corresponding to the chiral symmetry as vector ($Q^A_V = Q^A_R + Q^A_L$) and axial vector ($Q^A_V = Q^A_R - Q^A_L$)

$$Q^A_V(t) = \int \mathrm{d}^3x \; q^\dagger(\boldsymbol{x}, t) T^A q(\boldsymbol{x}, t) \,, \tag{2.36}$$

$$Q^A_A(t) = \int \mathrm{d}^3x \; q^\dagger(\boldsymbol{x}, t) \gamma_5 T^A q(\boldsymbol{x}, t) \,. \tag{2.37}$$

One can easily see that these charges have opposite parity. Since these are conserved charges (i.e., time-independent), they commute with the Hamiltonian ($H^0_{\rm QCD}$). Suppose there exists a positive parity eigenstate $|i, +\rangle$ of the Hamiltonian with energy E_i

$$H^0_{\rm QCD} \, |i, +\rangle = E_i \, |i, +\rangle \,, \tag{2.38}$$

$$P \, |i, +\rangle = + \, |i, +\rangle \,. \tag{2.39}$$

This state could be a member of the baryon octet in the chiral limit. Because the axial charge commute with the Hamiltonian, there should exist a degenerate eigenstate $|\phi\rangle = Q^A_A \, |i, +\rangle$ with opposite parity

$$H^0_{\rm QCD} \, |\phi\rangle = H^0_{\rm QCD} Q^A_A \, |i, +\rangle = Q^A_A H^0_{\rm QCD} \, |i, +\rangle = E_i \, |\phi\rangle \,, \tag{2.40}$$

$$P \, |\phi\rangle = P Q^A_A \, |i, +\rangle = (P Q^A_A P^\dagger)(P \, |i, +\rangle) = (-Q^A_A)(+ \, |i, +\rangle) = - \, |\phi\rangle \,. \tag{2.41}$$

However, there are no degenerate baryons in the baryon octet with opposite parity. This means that the ground state is not invariant under the $SU(3)_A$ [30]

$$Q_A^A |0\rangle \neq 0 \,. \tag{2.42}$$

This result indicates that the axial symmetry spontaneously breaks in the low-energy limit. Ref. [30] shows that a non-zero value for a scalar quark condensate ($\langle \bar{q}q \rangle \neq 0$) in the chiral limit is a sufficient condition for spontaneous symmetry breaking in QCD. We will not show this here and recommend Ref. [30] for the details.

The Goldstone theorem predicts the existence of eight light pseudoscalar bosons because of the spontaneous symmetry breaking of axial transformations and the explicit symmetry breaking caused by small quark masses. These are nothing but the pseudoscalar meson octet. The relative heavier mass of the s-quark explains why the meson octet members ($m_K \sim 500\,\text{MeV}, m_\eta \sim 550\,\text{MeV}$) with s-quarks are heavier than the members without s-quark ($m_\pi \sim 140\,\text{MeV}$).

The hadron spectrum exhibit an approximate flavor $SU(3)_V$ symmetry. This observation means that $SU(3)_L \times SU(3)_R \times U(1)_V$ is spontaneously broken to $SU(3)_V \times U(1)_V$. If this was exact, the decay constant of pions and kaons should have been the same ($\frac{F_K}{F_\pi} = 1.2$). However, because s-quark is relatively more massive than the u and d quark ($\frac{m_s}{m_u} = 44$, $\frac{m_s}{m_d} = 20$), flavor $SU(3)_V$ is heavily broken. However, a considerable simplification happens if we consider only the u and d quark, which are almost the same mass ($\frac{m_d}{m_u} = 2$). In this case, we observe a nearly exact $SU(2)_V$ isospin symmetry.

> **Step 2.** The Lagrangian has a $SU(3)_L \times SU(3)_R \times U(1)_V$ symmetry, which is spontaneously broken to $SU(3)_V \times U(1)_V$. The Lagrangian is also invariant under the Lorentz, parity, charge conjugation, and time-reversal symmetries. In Chapter 4, we incorporate the axial anomaly of QCD as an additional operator to the χPT Lagrangian.

2.3.3 Chiral effective Lagrangians

We have seen all the symmetries of the low-energy QCD. Now we have to create an effective field theory that respects these symmetries. Callan, Coleman, Wess, and Zumino (CCWZ) [119] developed a formal way to achieve this using non-linear realization of chiral symmetry using group theory. They have shown that a spacetime derivative always accompanies all the Goldstone fields (pions) in the Lagrangian. Now we will use the CCWZ formalism to derive the chiral Lagrangian.

The most general Lagrangian can be written as

$$\mathcal{L}_\chi = \mathcal{L}_{\pi\pi} + \mathcal{L}_{\pi N} + \mathcal{L}_{NN} + \dots \,, \tag{2.43}$$

where $\mathcal{L}_{\pi\pi}, \mathcal{L}_{\pi N}$, and $\mathcal{L}_{NN}$ govern meson-meson dynamics, meson-baryon interactions, and baryon-baryon dynamics (including nuclear force), respectively. The

ellipsis stands for the Lagrangian which describes the interactions with mesons and more than two baryons. The Lagrangian above can be further arranged as

$$\mathcal{L}_{\pi\pi} = \mathcal{L}^{(2)}_{\pi\pi} + \mathcal{L}^{(4)}_{\pi\pi} + \dots \,, \tag{2.44}$$

$$\mathcal{L}_{\pi N} = \mathcal{L}^{(1)}_{\pi N} + \mathcal{L}^{(2)}_{\pi N} + \mathcal{L}^{(3)}_{\pi N} + \dots \,, \tag{2.45}$$

$$\mathcal{L}_{NN} = \mathcal{L}^{(1)}_{NN} + \mathcal{L}^{(2)}_{NN} + \mathcal{L}^{(3)}_{NN} + \dots \,, \tag{2.46}$$

where the superscripts indicate the number of meson mass or derivative insertions (chiral dimension).

We start by collecting the meson (baryon) octet in the $SU(3)$ matrix $U(x)[\Psi(x)]$

$$U(x) = \exp\left(i\frac{\phi(x)}{F_\pi}\right) \equiv u(x)^2 \,, \tag{2.47}$$

$$\phi(x) = \sum_{A=1}^{8} 2T^A\phi_A(x) \equiv \begin{pmatrix} \pi^0 + \frac{1}{\sqrt{3}}\eta & \sqrt{2}\pi^+ & \sqrt{2}K^+ \\ \sqrt{2}\pi^- & -\pi^0 + \frac{1}{\sqrt{3}}\eta & \sqrt{2}K^0 \\ \sqrt{2}K^- & \sqrt{2}\bar{K}^0 & -\frac{2}{\sqrt{3}}\eta \end{pmatrix} , \tag{2.48}$$

$$\Psi(x) = \sum_{A=1}^{8} 2T^A\Psi_A(x) \equiv \begin{pmatrix} \frac{1}{\sqrt{2}}\Sigma^0 & \Sigma^+ & p \\ \Sigma^- & -\frac{1}{\sqrt{2}}\Sigma^0 + \frac{1}{\sqrt{6}}\Lambda & n \\ \Xi^- & \Xi^0 & -\frac{2}{\sqrt{3}}\Lambda \end{pmatrix} . \tag{2.49}$$

It is convenient to define the following fields for the construction of the Lagrangian

$$\begin{aligned} u_\mu &= i\left\{ u^\dagger(\partial_\mu - ir_\mu)u - u(\partial_\mu - il_\mu)u^\dagger \right\} , \\ \chi_\pm &= u^\dagger\chi u^\dagger \pm u\chi^\dagger u \,, \\ F^\pm_{\mu\nu} &= u^\dagger F^R_{\mu\nu} u \pm u F^L_{\mu\nu} u^\dagger \,, \\ \mathcal{M} &= \begin{pmatrix} m_u & 0 & 0 \\ 0 & m_d & 0 \\ 0 & 0 & m_s \end{pmatrix} , \end{aligned} \tag{2.50}$$

where

$$\begin{aligned} \chi &= 2B(\mathcal{M} + s + ip) \,, \\ F^\pm_{\mu\nu} &= u^\dagger F^R_{\mu\nu} u \pm u F^L_{\mu\nu} u^\dagger \,, \\ F^{\mu\nu}_R &= \partial^\mu r^\nu - \partial^\nu r^\mu - i[r^\mu, r^\nu] \,, \qquad r_\mu = v_\mu + v_{(s),\mu} + a_\mu \,, \\ F^{\mu\nu}_L &= \partial^\mu l^\nu - \partial^\nu l^\mu - i[l^\mu, l^\nu] \,, \qquad l_\mu = v_\mu + v_{(s),\mu} - a_\mu \,. \end{aligned} \tag{2.51}$$

The external fields $v^\mu, v^\mu_{(s)}, a^\mu, s$ and p are the same external fields as in Eq. (2.35). These fields are convenient because they all have the same transformation under the chiral group $SU(3)_L \times SU(3)_R$

$$X \xrightarrow{g} h(g,\Phi) X h^{-1}(g,\phi) \tag{2.52}$$

	u_μ	χ_+	χ_-	$F^+_{\mu\nu}$	$F^-_{\mu\nu}$	D_μ
chiral dimension	1	2	2	2	2	1
parity	$-(-1)^\mu$	$+$	$-$	$(-1)^\mu(-1)^\nu$	$-(-1)^\mu(-1)^\nu$	$(-1)^\mu$
time reversal	$(-1)^\mu$	$+$	$-$	$-(-1)^\mu(-1)^\nu$	$(-1)^\mu(-1)^\nu$	$-(-1)^\mu$
charge conjugation	$+$	$+$	$+$	$-$	$+$	$+$
hermitian conjugation	$+$	$+$	$-$	$+$	$+$	$+$

Table 2.2: The chiral dimension and discrete transformation properties of various chiral fields and the covariant derivative acting on mesons/external fields. Here charge conjugation means $\pm$transposed, and hermitian conjugation indicates $\pm$itself. The notation used is $(-1)^\mu = 1$ for $\mu = 0$ and $(-1)^\mu = -1$ for $\mu = 1, 2, 3$.

where $g \in SU(2)_L \times SU(2)_R$ and the compensator $h(g, \phi)$ defines a non-linear realization of the chiral symmetry. Since the baryon fields transform as

$$\Psi \xrightarrow{g} h(g, \Phi)\Psi\,, \qquad\qquad \bar{\Psi} \xrightarrow{g} \bar{\Psi}h^{-1}(g, \Phi)\,, \tag{2.53}$$

we can construct the Lagrangian using the invariants in the form

$$\bar{\Psi}X\Psi \xrightarrow{g} \bar{\Psi}X\Psi\,. \tag{2.54}$$

Now we can define covariant derivative as

$$D_\mu = \partial_\mu + \Gamma_\mu\,, \qquad \Gamma_\mu = \frac{1}{2}\left\{\, u^\dagger(\partial_\mu - ir_\mu)u + u(\partial_\mu - il_\mu)u^\dagger \,\right\}\,. \tag{2.55}$$

Using this we can show that $[D_\mu, X], [D_\mu, [D_\nu, X]], \ldots$ transforms as Eq. (2.52) and $D_\mu\Psi, D_\mu D_\nu\Psi, \ldots$ transforms as Eq. (2.53). Sometimes separating the isosinglet and isotriplet terms of the external currents is useful. To achieve this, the following fields are used in the χPT Lagrangian

$$\widetilde{X} = X - \frac{1}{2}\langle X\rangle\,, \tag{2.56}$$

where $\langle\cdot\rangle$ is trace over flavor space.

Since χPT is also invariant under discrete symmetries, we want the individual terms of the Lagrangian to be invariant under chiral symmetry, these discrete symmetries, and be Lorentz scalar. Table 2.2 shows how some fields and covariant derivatives acting on mesons/external fields transform under the discrete transformations, and Table 2.3 has the transformation properties of the Clifford algebra, metric, Levi-Civita tenser, and the covariant derivative acting on baryons. The discussion on the negative sign for the charge and hermitian conjugation of $D_\mu\Psi$ and the chiral dimension of γ_5 is not included in this thesis, and we refer to Ref. [120] for the explanation.

We have assembled all the ingredients to make the χPT Lagrangian. The χPT Lagrangian is constructed by writing down all possible operators that satisfy the

	γ_5	γ^μ	$\gamma^\mu\gamma_5$	$\sigma_{\mu\nu}$	$g_{\mu\nu}$	$\epsilon_{\mu\nu\alpha\beta}$	$D_\mu\Psi$
chiral dimension	0	0	0	0	0	0	1
parity	-1	$(-1)^\mu$	$-(-1)^\mu$	$(-1)^\mu(-1)^\nu$	$(-1)^\mu(-1)^\nu$	$(-1)^\mu(-1)^\nu$ $(-1)^\alpha(-1)^\beta$	$(-1)^\mu$
time reversal	-1	$(-1)^\mu$	$(-1)^\mu$	$-(-1)^\mu(-1)^\nu$	$(-1)^\mu(-1)^\nu$	$(-1)^\mu(-1)^\nu$ $(-1)^\alpha(-1)^\beta$	$(-1)^\mu$
charge conjugation	$+$	$-$	$+$	$-$	$+$	$+$	$-$
hermitian conjugation	$-$	$+$	$+$	$+$	$+$	$+$	$-$

Table 2.3: The chiral dimension and discrete transformation properties of elements of Clifford algebra, metric, Levi-Civita tensor, and the covariant derivative on baryon. The notation used is $(-1)^\mu = 1 for \mu = 0$ and $(-1)^\mu = -1$ for $\mu = 1, 2, 3$. Here hermitian conjugate equals $\pm\gamma_0$(itself)γ_0 and charge conjugation corresponds to $\pm$transposed.

chiral symmetry, Lorentz invariance, the charge conjugation symmetry, hermitian conjugation, and parity symmetry. This process will lead to redundant operators, which should be eliminated. This objective is achieved using equations of motions (or equivalently field re-definitions), integration by parts, Fierz identities, the Bianchi identity, cyclic property of trace, specific operator identities such as commutator relations of covariant derivatives, Schouten's identity, Cayley-Hamilton theorem, and so on. We refer to Refs. [30, 121] for the detailed construction of Chiral Lagrangian. The chiral Lagrangians with the smallest chiral dimension are

$$\begin{aligned}
\mathcal{L}^{(2)}_{\pi\pi} &= \frac{F_\pi^2}{4}\mathrm{Tr}\left(D_\mu U (D^\mu U)^\dagger\right) + \frac{F_\pi^2}{4}\mathrm{Tr}\left(\chi U^\dagger + U\chi^\dagger\right), \\
\mathcal{L}^{(1)}_{\pi N} &= \bar\Psi\left(i\not{D} - m_N + \frac{g_A}{2}\gamma^\mu\gamma_5 u_\mu\right)\Psi, \\
\mathcal{L}^{(0)}_{NN} &= -\frac{1}{2}C_s\bar\Psi\gamma^\mu\Psi\bar\Psi\gamma_\mu\Psi - \frac{1}{2}C_t(\bar\Psi\gamma^\mu\gamma_5\Psi)(\bar\Psi\gamma_\mu\gamma_5\Psi).
\end{aligned} \tag{2.57}$$

The chiral dimension is the number of derivatives or meson/baryon mass insertions, which is indicated as a superscript in the above Lagrangians.

Heavy baryon formalism

The large mass of baryons causes problems in χPT. For example, the baryon derivative terms are expected to give a small contribution at the low-energy limit. Even though the space derivative ($\boldsymbol{\nabla}\Psi \sim \boldsymbol{p}\Psi$) is well below the Λ_χ, the time derivative ($\partial_t\Psi = E_N\Psi \sim m_N\Psi$) is comparable or greater than Λ_χ ($m_N/\Lambda_\chi \sim 1$). Jenkins and Manohar [122] solve this problem using the effective field theory techniques developed by Georgi [123]. The idea is to consider baryons as heavy

static fields so that the transfer momentum is small compared to baryon mass. Then expand the theory around this small transfer momentum; this is called heavy baryon chiral perturbation theory (HBχPT).

We write the momentum in terms of small residual momentum as $p^\mu = m_N v^\mu + l^\mu$, where $v^2 = 1$ and $v \cdot l \ll m_N$. Now we define projection operators $P_v^\pm = \frac{1 \pm \not{v}}{2}$ and rewrite Dirac spinor fields of baryons as

$$\Psi = e^{i m_N v.x}(N_v + h_v)\,, \tag{2.58}$$

where we defined $N = e^{i m_N v.x} P_v^+ \Psi$, and $h = e^{i m_N v.x} P_v^- \Psi$.

If we identify Ψ with positive energy plane wave solution of the Dirac equation with three-momentum $\boldsymbol{p}$

$$\begin{aligned} \psi_{\boldsymbol{p}}^{(+)}(x) &= e^{-ip\cdot x} u^{(\alpha)}(\boldsymbol{p})\,, \\ u^{(\alpha)}(\boldsymbol{p}) &= \sqrt{E(\boldsymbol{p}) + m_N} \begin{pmatrix} \chi^{(\alpha)} \\ \frac{\boldsymbol{\sigma}\cdot\boldsymbol{p}}{E(\boldsymbol{p})+m_N}\chi^{(\alpha)} \end{pmatrix}, \end{aligned} \tag{2.59}$$

where $E(\boldsymbol{p}) = \sqrt{m_N^2 + \boldsymbol{p}^2}$

$$\chi^{(1)} = \begin{pmatrix} 1 \\ 0 \end{pmatrix}, \qquad \chi^{(2)} = \begin{pmatrix} 0 \\ 1 \end{pmatrix}, \tag{2.60}$$

are the two-component Pauli spinors, and by assuming $v^\mu = (1,0,0,0)$ we get

$$N_v^{(\alpha)} = \sqrt{E(\boldsymbol{p}) + m_N} \begin{pmatrix} \chi^{(\alpha)} \\ 0 \end{pmatrix} \exp^{-i(E(\boldsymbol{p})-m_N)t + i\boldsymbol{p}\cdot\boldsymbol{x}}\,, \tag{2.61}$$

$$h_v^{(\alpha)} = \sqrt{E(\boldsymbol{p}) + m_N} \begin{pmatrix} 0 \\ \frac{\boldsymbol{\sigma}\cdot\boldsymbol{p}}{E(\boldsymbol{p})+m_N}\chi^{(\alpha)} \end{pmatrix} \exp^{-i(E(\boldsymbol{p})-m_N)t + i\boldsymbol{p}\cdot\boldsymbol{x}}\,. \tag{2.62}$$

This achieves our goal to make the time-derivative of the baryon field below the Λ_χ, $i\partial_t N_v^{(\alpha)} = (E(\boldsymbol{p}) - m_N) N_v^{(\alpha)} \simeq \frac{\boldsymbol{p}^2}{2m_N} N_v^{(\alpha)}$. The h_v fields can be expressed in terms of N_v fields using equations of motion; this comes as $1/m_N$ corrections. The last step is to write $\mathcal{L}_{\pi N}$ and $\mathcal{L}_{NN}$ in N_v fields using the above re-definitions to get the HBχPT

$$\begin{aligned} \mathcal{L}_{\pi N}^{(1)} &= \bar{N}_v \left(i D_0 + g_A \frac{\boldsymbol{\sigma}\cdot\boldsymbol{u}}{2} \right) N_v\,, \\ \mathcal{L}_{NN}^{(0)} &= -\frac{1}{2} C_s \bar{N}_v N_v \bar{N}_v N_v - \frac{1}{2} C_t (\bar{N}_v \boldsymbol{\sigma}^i N_v)(\bar{N}_v \boldsymbol{\sigma}^i N_v)\,, \end{aligned} \tag{2.63}$$

where the Clifford algebras are written as

$$\begin{aligned}
\bar{N}_v \mathcal{I} N_v &= \bar{N}_v \mathcal{I} N_v \,, \\
\bar{N}_v \gamma_5 N_v &= 0 \,, \\
\bar{N}_v \gamma^\mu N_v &= v^\mu \bar{N}_v N_v \,, \\
\bar{N}_v \gamma^\mu \gamma_5 N_v &= 2 \bar{N}_v S^\mu N_v \,, \\
\bar{N}_v \sigma^{\mu\nu} N_v &= 2 \epsilon^{\mu\nu\alpha\beta} v_\alpha \bar{N}_v S_\beta N_v \,, \\
\bar{N}_v \sigma^{\mu\nu} \gamma_5 N_v &= 2i (v^\mu \bar{N}_v S^\nu N_v - v^\nu \bar{N}_v S^\mu N_v) \,,
\end{aligned} \tag{2.64}$$

with the definition $S^\mu \equiv \frac{i}{2} \gamma_5 \sigma^{\mu\nu} v_\nu = (0, \boldsymbol{\sigma}/2)$.

Step 3. We have constructed the most general χPT Lagrangian which respects the symmetries listed in Step 2.

2.3.4 Chiral power counting

In the previous section, we demonstrated how to construct the chiral Lagrangian. In principle, the chiral Lagrangian consists of infinite terms, a general feature for any EFT. The next step is to determine the relative relevance of these terms for the process under consideration. Since each term is proportional to some power of the expansion parameter, we can 'order' the terms based on this exponent. In χPT, the expansion parameter is Q/Λ_χ, where Q is the momentum (or transfer momentum) associated with the particle, nuclear binding momentum, or meson mass. Then, each term in χPT is proportional to $(Q/\Lambda_\chi)^\nu$ for some chiral order ν. The chiral power counting is the process that determines the chiral order ν. Since most of this thesis focuses on nucleons and pions, we are considering the two flavors $SU(2)$ χPT instead of the general $SU(3)$ χPT. It is straightforward to extend the power counting rule to the general $SU(3)_L \times SU(3)_R \times U(1)_V$ χPT.

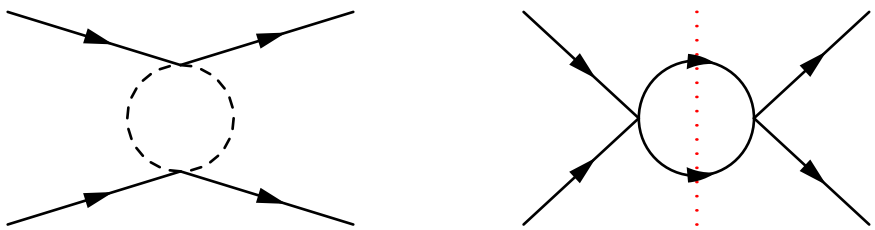

Figure 2.1: Some of the diagrams contributing to $NN \to NN$ scattering, the solid lines are nucleons, and the dashed lines are pions. The left and right panels represent irreducible and reducible diagrams, respectively. The red dotted lines split the reducible diagram by cutting through the intermediate state containing only nucleon propagators.

We can divide any Feynman diagrams into two parts: reducible parts and irreducible subdiagrams. The reducible parts contain intermediate states purely made up of nucleon propagators, and the irreducible subdiagrams do not contain such states, diagram 2.1a is an example of an irreducible diagram. In other words, if we can split a diagram into two by cutting across only the intermediate nucleon propagators, it is reducible. This cut is shown as a red dotted line for the reducible diagram 2.1b.

We will first focus on irreducible diagrams. By following the Feynman rules of covariant perturbation theory, the pion propagator is of the order Q^{-2}, any derivative is of the order Q, the nucleon propagator in heavy-baryon formalism is of the order Q^{-1} (from heavy baryon formalism), and each loop is of the order $Q^4/(2\pi)^2$. The chiral order ν for a general diagram involving A nucleons, C disconnected diagrams, L loops, and containing vertices v_i is [124–126]

$$\nu_W = 4 - A - 2C + 2L + \sum_i \Delta_i \,, \tag{2.65}$$

with

$$\Delta_i = d_i + \frac{n_i}{2} - 2 \,, \tag{2.66}$$

where d_i is the number of pion mass or derivatives for vertex i and n_i is number of nucleon legs coming from vertex i.

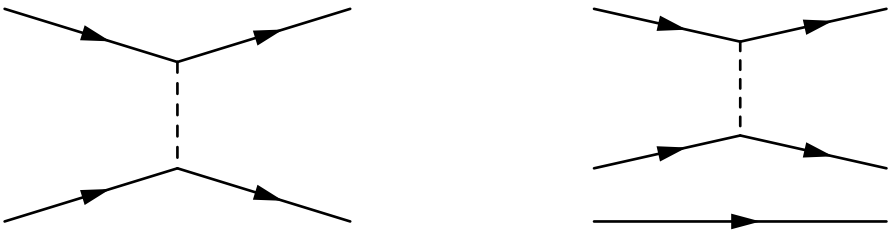

Figure 2.2: One pion exchange diagrams of $NN \to NN$ scattering in the absence (left panel) and presence (right panel) of a background nucleon, the solid lines are nucleons, and the dashed lines are pions.

The Weinberg chiral order formula in Eq. (2.65) fails for $A > 2$. Consider the case of one pion exchange diagram for $NN \to NN$ scattering in Fig. 2.2a. The Weinberg formula for this diagram ($A = 2, C = 0, L = 0$, and $\Delta_i = 1 + 2/2 = 2 = 0$ gives $\nu_W = 0$, see Eq. (2.65). However, for the same interaction in a $A = 3$ environment, see Fig. 2.2b, the Weinberg formula gives $\nu_W = -3$. This discrepancy is the result of the particle normalization convention

$$\langle p'|p\rangle = \delta^{(3)}(\boldsymbol{p} - \boldsymbol{p}') \,, \tag{2.67}$$

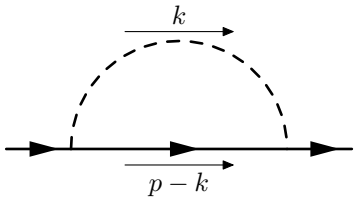

(a) nucleon self energy

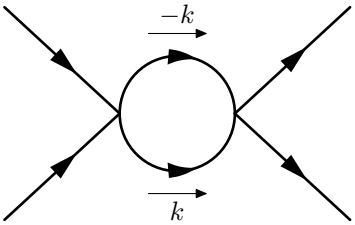

(b) $NN \to NN$

Figure 2.3: One loop Feynman diagrams for nucleon self-energy and NN scattering.

which is of the order Q^{-3}. The disconnected nucleon line in diagram 2.2b contributes as a momentum-conserving delta function, which results in the discrepancy in ν_W.

By modifying Eq. (2.65) for $A > 2$, we can solve this problem. First, we negate the -3 contribution from the nucleon lines by adding a factor of $3A$, and to make the $\nu_W = 0$ for diagram 2.2b, we have to subtract a factor of 6. The modified Weinberg formula for chiral order is $\nu = \nu_W + 3A - 6$

$$\nu = -2 + 2A - 2C + 2L + \sum_i \Delta_i \,, \qquad A > 2 \,. \tag{2.68}$$

We will now implement the power counting rules for irreducible and reducible diagrams. Let us first consider the power counting rules for loops and nucleon propagators. The Fig. 2.3 represented a typical one loop irreducible (diagram 2.3a) and reducible (diagram 2.3b) diagrams. Neglecting the vertex factors, the irreducible diagram 2.3a scales as

$$\int \frac{\mathrm{d}^4 k}{(2\pi)^4} \frac{i}{v \cdot (p-k) + i\epsilon} \frac{i}{k^2 - m_\pi^2 + i\epsilon} + \mathcal{O}\left(\frac{p}{m_N}\right) , \tag{2.69}$$

where p is the on-shell four-momentum of the nucleon and k is loop momentum. Since $v \cdot p = \mathcal{O}(p^2/m_N)$ and $v \cdot k = k_0$, we have

$$\int \frac{\mathrm{d}^4 k}{(2\pi)^4} \frac{i}{-k_0 + i\epsilon} \frac{i}{k_0^2 - (\boldsymbol{k}^2 + m_\pi^2) + i\epsilon} + \mathcal{O}\left(\frac{p}{m_N}\right) . \tag{2.70}$$

Since there is at most one nucleon propagator for irreducible loops, the contour integral of the time component of the momentum can be done by avoiding the nucleon pole. Therefore, for irreducible diagrams, the nucleon propagator is of the order $k_0 = \sqrt{\boldsymbol{k}^2 + m_\pi^2} = \mathcal{O}(Q)$. Including the characteristic loop factor of $1/(2\pi)^2$, an irreducible loop is proportional to $\mathcal{O}(Q^4/(2\pi)^2)$.

Let us now consider a typical one-loop reducible diagram of NN scattering in the center of mass frame, shown in Fig. 2.3b. The incoming nucleons have the

nucleon propagator	$\mathcal{O}(Q^{-1})$	: irreducible
	$\mathcal{O}\left(\frac{m_N}{Q^2}\right)$	: reducible
loop integral	$\mathcal{O}\left(\frac{Q^4}{(2\pi)^2}\right)$	: irreducible
	$\mathcal{O}\left(\frac{Q^5}{4\pi m_N}\right)$	: reducible
pion propagator	$\mathcal{O}(Q^{-2})$	
LEC	NDA estimate	

Table 2.4: Weinberg power counting for χPT.

one-shell four-momenta $p_1 = (v \cdot p, p)$ and $p_2 = (v \cdot p, -p)$, and the loop with momentum k scales as

$$\int \frac{\mathrm{d}^4 k}{(2\pi)^4} \frac{i}{v \cdot k + i\epsilon} \frac{i}{v \cdot (-k) + i\epsilon} + \mathcal{O}\left(\frac{p}{m_N}\right). \tag{2.71}$$

In this case, we can avoid only one of the nucleon poles while doing the contour integral of the time component of the loop momentum, which results in an infrared divergence [124]. However, this nonphysical divergence disappears after we add the kinetic energy of the nucleon

$$\int \frac{\mathrm{d}^4 k}{(2\pi)^4} \frac{i}{v \cdot (p+k) - \frac{(\boldsymbol{p}+\boldsymbol{k})^2}{2m_N} + i\epsilon} \frac{i}{v \cdot (p-k) - \frac{(\boldsymbol{p}-\boldsymbol{k})^2}{2m_N} + i\epsilon} \sim \int \frac{\mathrm{d}^3 k}{(2\pi)^3} \frac{i}{\boldsymbol{k}^2/2m_N}.$$

Therefore, for reducible diagrams, the nucleon propagator scales as $\mathcal{O}(m_N/Q^2)$, and by including the additional loop factor of 4π, the reducible loops scales as $\mathcal{O}(Q^5/4\pi m_N)$. For all diagrams, the pion propagator is $\mathcal{O}(Q^{-2})$, and the LECs scaling is determined by naive dimensional analysis (NDA). The Weinberg power counting is summarized in Table 2.4.

Naive dimensional analysis

Georgi and Manohar first proposed the naive dimensional analysis technique for the chiral quark model [127]. Here, we will adapt NDA for χPT. To demonstrate the idea behind this technique, consider the one loop $\pi - \pi$ scattering amplitude diagram 2.4 in the center of mass frame, with loop four-momentum k. To simplify, let us assume that the quarks are massless. Then the relevant Lagrangian for this diagram is

$$\mathcal{L} = \frac{1}{2}(D_\mu \vec{\pi})^2 = \frac{1}{2}(\partial_\mu \vec{\pi})^2 - \frac{4}{F_\pi^2}\vec{\pi}^2(\partial_\mu \vec{\pi})^2 + \mathcal{O}(\vec{\pi}^6). \tag{2.72}$$

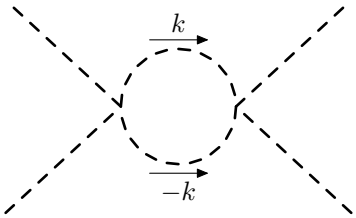

Figure 2.4: One loop diagram of $\pi - \pi$ scattering. The dashed lines denote the pions.

We focus on the loop diagram where all the derivatives act on the external pions with four-momentum p. The scattering amplitude is proportional to

$$\frac{p^4}{F_\pi^4} \int \frac{\mathrm{d}^4 k}{(2\pi)^4} \left(\frac{1}{k^2}\right)^2 \simeq \frac{p^4}{F_\pi^4} \frac{1}{(4\pi)^2} \log \frac{\Lambda}{\mu} \,, \tag{2.73}$$

where Λ is the cut-off [1] and μ is the renormalization scale. A counter term should absorb this log divergence. Since the amplitude is proportional to four power of pion momentum, we need a contact term with derivative acting on all four pions

$$\mathcal{L}_{\text{c.t.}} = \frac{c}{F_\pi^2} (D_\mu \vec{\pi})^2 (D_\nu \vec{\pi})^2 \,, \tag{2.74}$$

with some LEC c. The total scattering amplitude with the counterterm is

$$\frac{p^4}{F_\pi^2} \left(\frac{1}{(4\pi F_\pi)^2} \log \frac{\Lambda}{\mu} + c \right) . \tag{2.75}$$

The total amplitude should be renormalization scale μ independent, i.e., any shift in μ is compensated by a corresponding shift in c. For a shift in μ such that there is an $\mathcal{O}(1)$ shift in log should produce an change in c with $\delta c \sim (4\pi F_\pi)^{-2} \simeq \Lambda_\chi^{-2}$. In general, c should be at least as big as δc, which gives

$$|c| \gtrsim |\delta c| = \mathcal{O}\left(\frac{1}{\Lambda_\chi^2}\right) . \tag{2.76}$$

The above-discussed NDA estimate is summarized by "reduced" coupling constants [128]. A coupling constant c of an interaction of dimension D involving N fields has a reduced coupling

$$c^R = c \, \Lambda_\chi^{D-4} (4\pi)^{2-N} \,. \tag{2.77}$$

Using this formula, we will list NDA rules for some low-energy constants (LECs) relevant to this thesis and compare them with the experimental LQCD results.

[1] see Section 3.2.1 for a discussion on cut-off

- g_A
  The chiral Lagrangian with coupling g_A is given by

$$\mathcal{L}_\chi = -\frac{g_A}{F_\pi}\bar{N}\boldsymbol{S}\cdot\boldsymbol{\nabla}\vec{\pi}^a\tau^a N\,, \tag{2.78}$$

  which have $D=5, N=3$ and Eq. (2.77) gives

$$\left(\frac{g_A}{F_\pi}\right)^R = \frac{g_A}{F_\pi}\frac{\Lambda_\chi}{4\pi} \sim \frac{g_A}{2}\,,$$
$$\Rightarrow g_A = \mathcal{O}(1)\,, \tag{2.79}$$

  This result agrees with the experiment $g_A \simeq 1.27$.

- m_π
  The chiral Lagrangian with pion mass is given by

$$\mathcal{L}_\chi = -\frac{1}{2}m_\pi^2\boldsymbol{\pi}\cdot\boldsymbol{\pi}\,, \tag{2.80}$$

  which have $D=2, N=2$ and Eq. (2.77) gives

$$(m_\pi^2)^R = \frac{m_\pi^2}{\Lambda_\chi^2}\,. \tag{2.81}$$

  The masses of Goldstone bosons pions result from the explicit symmetry breaking by the quark masses. Then the reduced pion mass should be in the same order as the reduced quark mass. The reduced quark mass $(\bar{m})^R$ is

$$\mathcal{L} = -\bar{m}\bar{q}q\,, \qquad D=3, N=2\,, \tag{2.82}$$
$$(\bar{m})^R = \frac{\bar{m}}{\Lambda_\chi}\,. \tag{2.83}$$

  Then $(m_\pi^2)^R = (\bar{m})^R$ recovers the well-known result $m_\pi^2 = \mathcal{O}(\bar{m}\Lambda_\chi)$.

- $\bar{g}_0$
  The chiral Lagrangian with coupling $\bar{g}_0$, relevant for Chapter 3 and Chapter 4, is given by

$$\mathcal{L}_\chi = \bar{g}_0\bar{N}\vec{\pi}\cdot\vec{\tau}N \tag{2.84}$$

  which have $D=4, N=3$ and Eq. (2.77) gives

$$\bar{g}_0^R = \frac{\bar{g}_0}{4\pi} = \bar{g}_0\frac{F_\pi}{\Lambda_\chi}\,,$$
$$\Rightarrow \bar{g}_0 = \mathcal{O}\left(\frac{\Lambda_\chi}{F_\pi}\right)\,, \tag{2.85}$$

where we have used $4\pi F_\pi = \Lambda_\chi$.

After removing CP-violating $\bar{\theta}$ term by chiral rotations as discussed in Section 4.2.2, the CP-violating SM term is

$$\mathcal{L}_{\bar{\theta}} = m_* \bar{\theta} \bar{q} i\gamma_5 q \,, \tag{2.86}$$

where $m_* = (\frac{1}{m_u} + \frac{1}{m_d} + \frac{1}{m_s})^{-1}$. From Eq. (2.77) we have

$$\begin{aligned} (m_* \bar{\theta})^R &= \frac{m_* \bar{\theta}}{\Lambda_\chi} \\ \Rightarrow m_* \bar{\theta} &= \mathcal{O}(\Lambda_\chi) \,, \qquad (2.87) \\ \Rightarrow \bar{g}_0 &= \mathcal{O}\left(\frac{m_* \bar{\theta}}{F_\pi}\right) . \qquad (2.88) \end{aligned}$$

This is expected since the $\bar{\theta}$ can induce the $\bar{g}_0$ by itself. The $\bar{g}_0$ should be in the same order as the CP-violating SM coupling $m_* \bar{\theta}$.

- c_1

  The chiral Lagrangian with coupling c_1, relevant for Chapter 5, is

$$\mathcal{L}_\chi = -2c_1 \frac{m_\pi^2}{F_\pi^2} \bar{N} \boldsymbol{\pi} \cdot \boldsymbol{\pi} N \,, \tag{2.89}$$

  which have $D = 5, N = 4$ and Eq. (2.77) gives

$$\begin{aligned} \left(c_1 \frac{m_\pi^2}{F_\pi^2}\right)^R &= \frac{c_1 m_\pi^2 \Lambda_\chi}{(4\pi F_\pi)^2} \,, \\ \Rightarrow c_1 &= \mathcal{O}(\Lambda_\chi^{-1}) \,, \qquad (2.90) \end{aligned}$$

  which agrees with the experimental result $c_1 = (0.9 \pm 0.1)\,\mathrm{GeV}^{-1}$ [129].

- C_0

  The chiral Lagrangian with coupling C_0, relevant for Chapter 3, is given by

$$\mathcal{L}_\chi = C_0 \bar{N} N \bar{N} N \,, \tag{2.91}$$

  which have $D = 6, N = 4$ and Eq. (2.77) gives

$$\begin{aligned} C_0^R &= C_0 F_\pi^2 \,, \\ \Rightarrow C_0 &= \mathcal{O}\left(Q^{-2}\right) . \end{aligned} \tag{2.92}$$

  As demonstrated in Chapter 4, C_0 can take wide range of values and our NDA estimate $C_0 = \mathcal{O}\left(Q^{-2}\right)$ does not hold, see Fig. 3.10. NDA is a simple and powerful tool to build EFTs, and it works well in most cases as we have seen, but it could fail in some cases because of the complex nature of the UV complete theory.

Step 4. The χPT follows the power counting rule based on naive dimensional analysis.

Now we have everything to perform the **Step 5**, i.e., to calculate relevant Feynman diagrams. This is demonstrated in the following chapters.

Chapter 3

Renormalization of CP-violating nuclear force

J. de Vries, A. Gnech, and S. Shain,
"Renormalization of CP-violating nuclear forces,"
Phys. Rev. C 103 no. 1, (2021) L012501, [arXiv:2007.04927].

3.1 Introduction

As we discussed in Chapter 1, electric dipole moments (EDMs) are ideal experimental probes to measure CP-violation [130, 131]. The SM has two primary sources of CP-violation, the fermion mixing CKM matrix and QCD $\bar{\theta}$ term. Since EDMs do not involve flavor-changing interactions, the EDM contribution from the CKM comes through multiple electroweak loops, which lead to immeasurably small values [51, 132]. Therefore, if we detect any EDM signals, they originated from new CP-violating BSM sources or the not-yet-discovered QCD $\bar{\theta}$ term. In addition to this minimal SM background, EDMs have the benefits of having high sensitivity and low experimental costs. Furthermore, EDM measurements in multiple systems such as neutron, proton, electron, atoms, molecules, and muon provide independent limits on different BSM sources.

Two leading sources induce the nuclear EDMs: the intrinsic EDM of the constituent nucleons and the P-odd, CP-odd NN interactions (nuclear force) that polarize the nucleus. In this chapter, we will be focusing on the CP-odd nuclear force. The Fig. 3.1 shows the progress made in the neutron EDM (nEDM) limits over time, along with the most recent results [52], the expected limit from the n2EDM experiment [133], and the SM electroweak contribution. The nEDM limits impose severe constraints on the BSM model with additional CP-violation such as supersymmetry, left-right symmetric model, multi-Higgs, leptoquarks, and scenarios of electroweak baryogenesis [134]. In model-independent SMEFT,

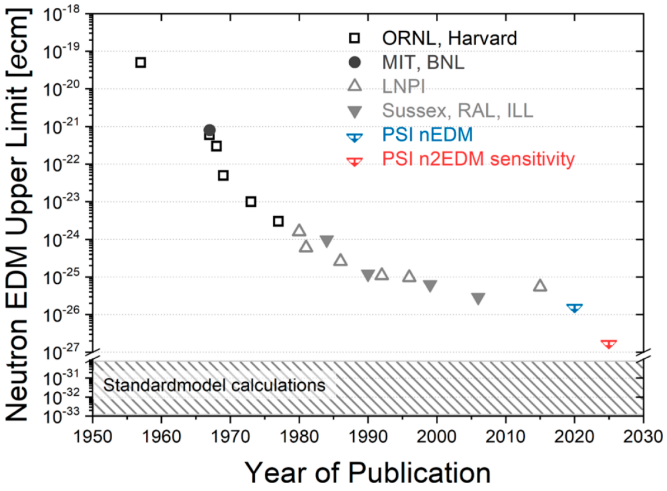

Figure 3.1: The neutron EDM limits published over past decades by various experiments. The data points in blue and red colors represent the most recent EDM limit [52] and expected n2EDM limit [133] (in the absence of any signals), respectively. The different symbols indicate different experimental groups. The shaded region represents the CKM contribution to the EDM. The figure is taken from Ref. [136]

the EDM limits constraints a large set of *CP*-odd dimension-six operators at the multi-TeV scale, well above the limits from the collider experiments [135].

Translating the EDM limits from complex systems like nuclei to the underlying *CP*-violating source at the quark level is a non-trivial task. However, in recent years significant theoretical improvements have been made towards model-independent first-principle calculations of EDMs from a combination of LQCD [49, 70, 71], χPT [72–74], and nuclear calculations [75–79]. We can split this procedure into three parts. We use the SMEFT framework in the first part and derive a general set of dimension-four (the $\bar{\theta}$ term) and -six *CP*-violating operators involving light quarks, gluons, and photons. The second part is translating these interactions in SM fields to hadronic fields using the χPT framework. In Chapter 2, we have seen a subset of this part, where we connected dimension-four SM operators to hadronic interactions. Then the corresponding LECs are ideally calculated using LQCD. However, sometimes the vast uncertainty associated with LQCD results does not make this feasible. The last part is to calculate the EDMs using the chiral Lagrangian.

The EDM form factors are calculated up to next-to-next-to-leading order ($\mathrm{N^2LO}$) in χPT [137–140]. The *CP*-violating nuclear forces and currents are necessary ingredients to compute EDMs and EDM form factors. The *CP*-violating nucleon-nucleon (*NN*) potential is calculated up to $\mathrm{N^2LO}$ [79, 141] and used to calculate nuclear and atomic EDMs [75–79].

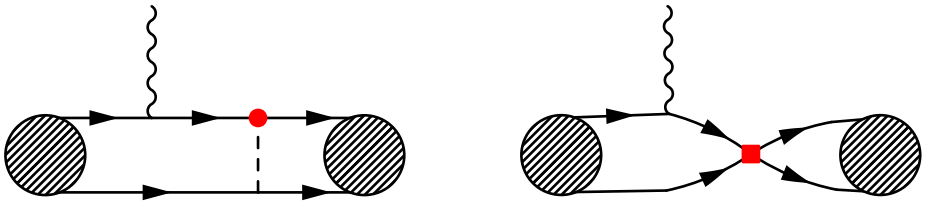

(a) LO **(b)** N^2LO

Figure 3.2: The diagrams contributing to nuclear EDMs at LO and N^2LO. The red circle and square represent the *CP*-odd OPE and short-distance vertices. The striped circle represents the nucleon wave function. The solid, dashed, and wavy lines correspond to nucleons, pions, and photons.

The *CP*-violating *NN* potential of Refs. [79, 141] is derived using Weinberg's power-counting scheme outlined in Section 2.3.4 [124]. In this scheme, the *CP*-violating potential arises from the one-pion-exchange (OPE) diagrams, and the corresponding LECs are fixed using processes involving nucleons and pions. However, this is only in principle, as πN scattering experiments are not sufficiently accurate to extract *CP*-violating couplings. In the case of *CP*-conserving potential, the leading order (LO) consists of OPE diagrams and two non-derivative contact interactions in $^1S_0$ and $^3S_1$ waves. In the *CP*-violating case, *NN* interactions require at least one space-time derivative, and Weinberg's power-counting scheme predicts that the short-distance operators enter only at N^2LO, see Fig. 3.2. This works in our favor because it implies that we only need a few LECS to calculate nuclear EDMs, and we can pinpoint the underlying *CP*-violating source using the ratios of EDMs [142].

Weinberg's power counting scheme is based on naive dimensional analysis (NDA) (see Section 2.3.4) of the *NN* LECs [127], which is not always reliable in nuclear physics. Sometimes, it fails to provide order-by-order renormalized nuclear amplitudes [143, 144]. This feature is particularly evident in the case of partial waves, where OPE potential is attractive and non-perturbative. Ref. [145] studied this case in detail. They demonstrated the failure of NDA for the $^3P_0$ channel where phase shift shows oscillatory limit-cycle-like cut-off dependence for the LO nuclear potential. The same problem affects external currents inserted in *NN* scattering states [146, 147]. In this part of the thesis, we investigate *CP*-violating OPE potentials and use cut-off dependence of observables as a diagnostic tool to demonstrate that a LO shot-distance operator for $^1S_0$-$^1P_0$ transition is required. This result directly affects the interpretation of EDM experiments and other time-reversal-odd observables, such as magnetic quadrupole moments or neutron-nucleus scattering.

An axion dark matter (DM) field can induce oscillating EDMs. Many axion DM experiments utilize these oscillating EDMs as probes for their searches [148]. Such DM axions act as a coherently oscillating classical scalar field, $a = a_0 \cos m_a t$,

where m_a and a_0 are the mass and the constant amplitude of the axion, respectively [149, 150]. This is one of the future projects we plan to explore; see Section 4.9 for the current progress. The hadronic and nuclear matrix elements that connect static EDMs to the $\bar{\theta}$ term are identical to those that relate oscillating EDMs to the axion field. Here we focus on the former, but all expressions below apply to DM searches for axions by replacing $\bar{\theta}$ by $(a_0/f_a)\cos m_a t$, where f_a is the axion decay constant.

We organize the chapter as follows. We introduce the relevant chiral Lagrangian and how to obtain the *CP*-even and *CP*-odd physical observables like phase shift and mixing angles for nucleon-nucleon scattering in Section 3.2. In Section 3.3, we demonstrate how to implement this procedure numerically. We study the regulator dependence of our results in Section 3.4, and we reproduce the known failure of Weinberg's power counting to renormalize *CP*-even nuclear force in LO. We observed that Weinberg's power counting fails to renormalize the *CP*-odd nuclear force in the LO. We demonstrated that promoting N^{2}LO short-distance term to LO restores the renormalization of the *CP*-odd nuclear forces in the LO. In Section 3.6, we propose two methods to obtain the LEC for the promoted N^{2}LO term. We briefly explore other *CP*-odd operators and *P*-odd operators in Section 3.7 and we conclude in Section 3.8. Finally, in Section 3.9 we discuss the future and ongoing projects.

3.2 Chiral Lagrangian and the phase shifts

In this part of the thesis, we focus on the *CP*-violation from the QCD $\bar{\theta}$ term. Since we are only interested in nucleon-nucleon scattering, we will limit to u and d quarks. This will lead to $SU(2)_L \times SU(2)_R$ chiral symmetry, and the Goldstone bosons resulting from its spontaneous breaking is the pion triplets ($\pi^{0,\pm}$) [117]. The relevant QCD Lagrangian is [151, 152]

$$\mathcal{L} = \bar{q} i \not{D} q - \bar{q}\left(M_0 - i\gamma_5 m_\star \bar{\theta}\right) q\,, \tag{3.1}$$

where $q = (u\,d)^T$ denotes the quark field, D_μ the color and electromagnetic covariant derivative, $M_0 = \mathrm{Diag}(m_u, m_d)$ the quark mass matrix, and $m_\star = m_u m_d/(m_u + m_d)$. The chiral Lagrangian is constructed by following well-known methods [153], and the leading *CP*-even and *CP*-odd nucleon-pion interactions are

$$\mathcal{L}_{\pi N} = -\frac{g_A}{F_\pi} \boldsymbol{\nabla}\vec{\pi}\cdot\bar{N}\vec{\tau}\boldsymbol{\sigma}N + \bar{g}_0 \bar{N}\vec{\pi}\cdot\vec{\tau}N + \ldots\,, \tag{3.2}$$

where $N = (p\,n)^T$, $g_A \simeq 1.27$, $\vec{\pi}$, $\boldsymbol{\sigma}$, and $\vec{\tau}$ denotes the non-relativistic nucleon doublet, the nucleon axial coupling, pion triplet, and the nuclear spin, and nuclear isospin operators respectively. The *CP*-odd LEC is represented by

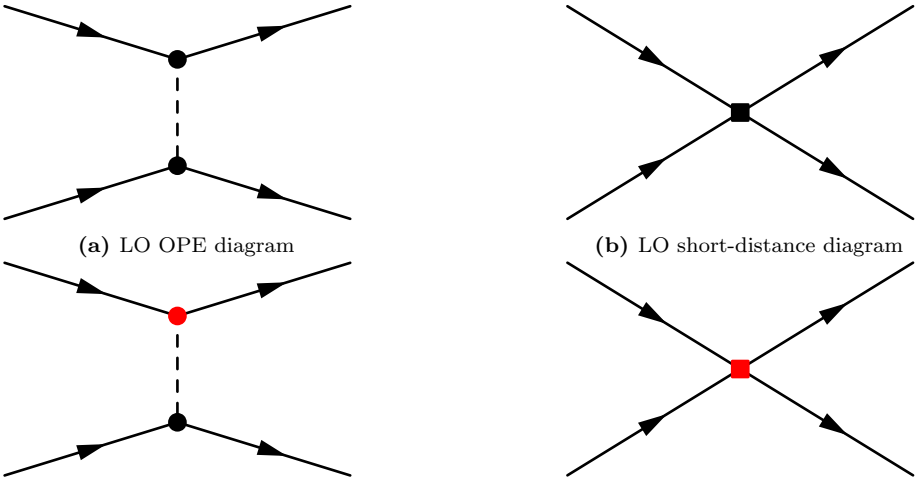

(a) LO OPE diagram **(b)** LO short-distance diagram

(c) LO OPE diagram **(d)** N^{2}LO short-distance diagram

Figure 3.3: The OPE and short-distance diagrams for *NN* nuclear force. The diagrams in the top (bottom) row contribute to the *CP*-even (*CP*-odd) nuclear force. The black (red) circle and the black (red) square represents the *CP*-even (*CP*-odd) OPE and short-distance vertices, respectively. The solid lines represent nucleons, and the dashed lines represent pions.

$\bar{g}_0 = \mathcal{O}\left(m_*\bar{\theta}/F_\pi\right)$, see Eq. (2.88). The ellipsis denotes the higher-order terms involving multiple pions.

A chiral rotation relates the QCD $\bar{\theta}$ term and an isospin-breaking component of quark masses [137]. Using this, we can get the exact expression of $\bar{g}_0$ in terms of $\bar{\theta}$ as [154]

$$\bar{g}_0 = \frac{\delta m_N^{\rm str}(1-\varepsilon^2)}{4F_\pi\varepsilon}\bar{\theta} = -(14.7 \pm 2.3)\cdot 10^{-3}\,\bar{\theta}\,, \tag{3.3}$$

where $\delta m_N^{\rm str}$ is the quark-mass induced part of the proton-neutron mass splitting that has been calculated with LQCD [155] and $\varepsilon = (m_u - m_d)/(m_u + m_d)$. The value of $\bar{g}_0$ agrees with the LQCD results [49].

The OPE *NN* potentials calculated using the chiral Lagrangian in Eq. (3.2) and the power counting rule are

$$V_{{\rm str},\pi} = -\frac{1}{(2\pi)^3}\left(\frac{g_A}{2F_\pi}\right)^2 \vec{\tau}_1\cdot\vec{\tau}_2\frac{(\boldsymbol{\sigma}_1\cdot\boldsymbol{q})(\boldsymbol{\sigma}_2\cdot\boldsymbol{q})}{\boldsymbol{q}^2+m_\pi^2}\,, \tag{3.4}$$

$$V_{\bar{g}_0} = -\frac{1}{(2\pi)^3}\frac{g_A\bar{g}_0}{2F_\pi}\vec{\tau}_1\cdot\vec{\tau}_2\frac{i(\boldsymbol{\sigma}_1-\boldsymbol{\sigma}_2)\cdot\boldsymbol{q}}{\boldsymbol{q}^2+m_\pi^2}\,, \tag{3.5}$$

where $\boldsymbol{q} = \boldsymbol{p} - \boldsymbol{p}'$ is the momentum transfer between in- and outgoing nucleon pairs with relative momenta $\boldsymbol{p}$ and $\boldsymbol{p}'$ respectively ($|\boldsymbol{p}| = p$ and $|\boldsymbol{p}'| = p'$), and m_π

denotes the pion mass. The subscript 'str' stand for strong (*CP*-even) interaction. These OPE diagrams are shown in the left panel of Fig. 3.3. We include the strong contact/short-distant (sd) *NN* interactions

$$V_{\rm str,sd} = \frac{1}{(2\pi)^3}\left(C_s P_s + C_t P_t + \frac{1}{4} pp' C_p P_p\right) , \tag{3.6}$$

where $P_{s,t,p}$ project respectively on the ^{1}S$_0$, ^{3}S$_1$, and ^{3}P$_0$ waves. In Weinberg's power counting, the S-wave contact terms appear at LO while the P-wave contact term enters at N^{2}LO. The *CP*-odd short-distance interactions (Eq. (3.26)) contributes at N^{2}LO according to Weinberg's power counting rule. The short-distance diagrams are shown in the right panel of Fig. 3.3.

3.2.1 Phase shift calculation

We consider the *NN* scattering in the center-of-mass (CM) frame. We denote the reduced mass of the system by μ, which is twice the nucleon mass (m_N), and the energy by E. By following the standard normalization for the plane wave, the Lippmann-Schwinger (LS) equation[1]

$$T(\boldsymbol{p}', \boldsymbol{p}, E) = V(\boldsymbol{p}', \boldsymbol{p}) + \int \mathrm{d}^3 p'' V(\boldsymbol{p}', \boldsymbol{p}'') \frac{1}{E - \frac{\boldsymbol{p}''^2}{2\mu} + i\varepsilon} T(\boldsymbol{p}'', \boldsymbol{p}, E) , \tag{3.7}$$

where V is potential. To solve the LS equation numerically, we need to introduce a regulator function $f_\Lambda(p', p)$ to the potential $V(p', p) \to V(p', p) f^\Lambda(p', p)$; this is a convenient way to introduce a momentum space cut-off Λ. The regularization procedure modifies the observable with singularities by introducing the parameter regulator (or cut-off), which makes them finite. The cut-off reflects our lack of knowledge of physics outside the relevant energy scale of our EFT. After renormalization, the low-energy results should be independent of the choice of the regulator (renormalization-group invariance), provided $\Lambda > \Lambda_\chi$. In partial wave decomposition, it is convenient to implement regularization using momentum cut-off functions that depend on $\boldsymbol{p}$ and $\boldsymbol{p}'$ rather than on $\boldsymbol{q}$. We chose

$$f_\Lambda(p, p') = e^{-(p/\Lambda)^4} e^{-\left(p'/\Lambda\right)^4} . \tag{3.8}$$

To obtain the *CP*-even/strong *NN* scattering wave functions we solve the LS equation in Eq. (3.7) using the strong potential $V_{\rm str} = (V_{{\rm str},\pi} + V_{\rm str,sd}) f_\Lambda(p, p')$. For convenience, we adopt the following notation to represent Eq. (3.7) from now on

$$T = V + V G_0 T , \qquad G_0 = (E - p^2/m_N + i\varepsilon)^{-1} . \tag{3.9}$$

[1]The Feynman's $i\varepsilon$ prescription used here should not be confused with the ε in Eq. (3.3), the former always appears as $i\varepsilon$.

Once we solve the LS equation and obtain the T-matrix, the S-matrix for nucleon-nucleon scattering for the $\alpha' - \alpha$ scattering is

$$S^{\alpha',\alpha}(E_{\rm CM}) = \delta^{\alpha',\alpha} - i\pi m_N^{3/2} E_{\rm CM}^{1/2} T^{\alpha',\alpha}(p = p' = \sqrt{E_{\rm CM} m_N}) \,. \tag{3.10}$$

where $\alpha \equiv \{(ls)j; tm_t\}$ represent the partial waves. The partial wave analysis of nucleon-nucleon scattering is described in Appendix B. Using the parameterization from Eq. (B.28), for uncoupled channel $\{\alpha\}$

$$S^{\alpha,\alpha} = e^{2i\delta_\alpha} \,, \tag{3.11}$$

and using Eq. (B.29) for coupled channels $\{\alpha_1, \alpha_2\}$

$$S^{\{\alpha_1,\alpha_2\}} = \begin{pmatrix} \cos 2\epsilon \; e^{2i\delta_{\alpha_1}} & i \sin 2\epsilon \; e^{i(\delta_{\alpha_1}+\delta_{\alpha_2})} \\ i \sin 2\epsilon \; e^{i(\delta_{\alpha_1}+\delta_{\alpha_2})} & \cos 2\epsilon \; e^{2i\delta_{\alpha_2}} \end{pmatrix} . \tag{3.12}$$

where δ_α and ϵ are phase shifts and mixing angles, respectively.

The nucleon-nucleon scattering experiments were done using beam and fixed target experiments. The beam and target can be polarized or unpolarized. For different energies, the experimentalists measured various observables like angular distribution, scattered particle polarization, recoil particle polarization, spin correlation of the final state, etc. We can express these observables using phase shifts, mixing angles, and four-momenta. The phase shifts and mixing angles are extracted from the nucleon-nucleon scattering data by fitting it to various energies[2].

We now consider the CP-odd potential $V_{\bar{g}_0}$ which causes ^{1}S$_0$-^{3}P$_0$ and ^{3}S$_1$-^{1}P$_1$ transitions. We treat $V_{\bar{g}_0}$ to excellent accuracy in perturbation theory and write

$$T_{\bar{g}_0} = V_{\bar{g}_0} + V_{\bar{g}_0} G_0 T_{\rm str} + T_{\rm str} G_0 V_{\bar{g}_0} + T_{\rm str} G_0 V_{\bar{g}_0} G_0 T_{\rm str} \,. \tag{3.13}$$

The S-matrix is obtained from the on-shell T-matrix $T = T_{\rm str} + T_{\bar{g}_0}$ using Eq. (3.10). For $j = 0$, we parametrize the S matrix by

$$S_{j=0} = \begin{pmatrix} e^{2i\delta_{1S_0}} & \epsilon^0_{\rm SP} e^{i\left[\delta_{1S_0}+\delta_{3P_0}\right]} \\ -\epsilon^0_{\rm SP} e^{i\left[\delta_{1S_0}+\delta_{3P_0}\right]} & e^{2i\delta_{3P_0}} \end{pmatrix} , \tag{3.14}$$

where $\epsilon^0_{\rm SP} \sim \bar{\theta}$ denotes the small ^{1}S$_0$-^{3}P$_0$ mixing angle. The $j = 1$ channel is more complicated because of strong ^{3}S$_1$-^{3}D$_1$ mixing, and for simplicity, we expand in the small S-D mixing angle ϵ. Up to $\mathcal{O}(\epsilon^3)$

$$\begin{aligned} S_{j=1} &= \begin{pmatrix} e^{2i\delta_{3S_1}} \cos 2\epsilon & ie^{i\left[\delta_{3S_1}+\delta_{3D_1}\right]} \sin 2\epsilon & x_{SP} \\ ie^{i\left[\delta_{3S_1}+\delta_{3D_1}\right]} \sin 2\epsilon & e^{2i\delta_{3D_1}} \cos 2\epsilon & x_{DP} \\ -x_{SP} & -x_{DP} & e^{2i\delta_{1P_1}} \end{pmatrix} , \\ x_{SP} &= \left[\epsilon^1_{\rm SP} + i\epsilon \; \epsilon_{\rm DP}\right] e^{i\left[\delta_{3S_1}+\delta_{1P_1}\right]} , \\ x_{DP} &= \left[\epsilon_{\rm DP} + i\epsilon \; \epsilon^1_{\rm SP}\right] e^{i\left[\delta_{3D_1}+\delta_{1P_1}\right]} , \end{aligned} \tag{3.15}$$

[2] the scattering data is available through https://nn-online.org.

in terms of two CP-odd mixing angles $\epsilon^1_{\rm SP}$ and $\epsilon_{\rm DP}$. S is antisymmetric in the S-P and P-D elements due to time-reversal violation. The CP-odd mixing angles $\epsilon^{0,1}_{\rm SP}$ and $\epsilon_{\rm DP}$ are observable in, for example, spin rotation of polarized ultracold neutrons on a polarized hydrogen target [156]. Still, it is unlikely that these experiments can reach a competitive sensitivity with EDM experiments, although neutron transmission experiments using heavy target nuclei might be up to the task [157, 158]. We can express the nuclear EDMs as linear combinations of the mixing angles and contributions from CP-odd electromagnetic currents such as constituent nucleon EDMs.

3.3 Numerical computation

3.3.1 Numerical solution of LS equation

We consider the general case of coupled partial waves $\{\alpha_1, \alpha_2, \ldots, \alpha_M\}$ nucleon-nucleon scattering. First, we calculate the T-matrix for $\alpha' - \alpha$ transition. The LS equation for T-matrix in the partial wave basis is given by

$$T^{\alpha',\alpha}(p',p,E) = V^{\alpha',\alpha}(p',p) + \sum_{\alpha''} \int {\rm d}p'' V^{\alpha',\alpha''}(p',p'') \frac{1}{\frac{q_0^2 - p''^2}{2\mu} + i\varepsilon} T^{\alpha'',\alpha}(p'',p,E)\,, \tag{3.16}$$

here we defined $q_0 = \sqrt{2E_{\rm CM}\mu}$ and α'' is summed over $\{\alpha_i\}$. The pole in the integrand is isolated using the contour integral method

$$\frac{2\mu}{(q_0 - p'' + i\epsilon)(q_0 + p'' + i\varepsilon)} = \frac{2\mu}{q_0^2 - p''^2}\mathcal{P} - i\pi \frac{2\mu}{q_0 + p''}\delta(p'' - q_0)\,,$$

where $\mathcal{P}$ is the principle value. Using this result in Eq. (3.16) gives

$$\begin{aligned} T^{\alpha'\alpha}(p',p,E) = V^{\alpha'\alpha}(p',p,E) + 2\mu \sum_{\alpha''} \fint dp'' V^{\alpha'\alpha''}(p',p'',E) \frac{p''^2}{q_0^2 - p''^2} T^{\alpha''\alpha}(p'',p,E) \\ - i\pi\mu q_0 \sum_{\alpha''} V^{\alpha'\alpha''}(p',q_0,E) T^{\alpha''\alpha}(q_0,p,E)\,, \end{aligned} \tag{3.17}$$

where $\fint$ denote the principal valued integral ($p'' \neq q_0$), which is further expanded

$$\begin{aligned} &\fint dp'' V^{\alpha'\alpha''}(p',p'',E) \frac{p''^2}{q_0^2 - p''^2} T^{\alpha''\alpha}(p'',p,E) \\ &= \int dp'' \left(\frac{V^{\alpha'\alpha''}(p',p'',E) p''^2 T^{\alpha''\alpha}(p'',p,E) - V^{\alpha'\alpha''}(p',p'',E) q_0^2 T^{\alpha''\alpha}(p'',p,E)}{q_0^2 - p''^2} \right. \\ &\qquad \left. \times T^{\alpha''\alpha}(p'',p,E) \right) \\ &\quad + V^{\alpha'\alpha''}(p',q_0,E) q_0^2 T^{\alpha''\alpha}(q_0,p,E) I_0\,, \end{aligned} \tag{3.18}$$

where we defined $I_0 = \oint dp'' \frac{1}{q_0^2 - p''^2}$. Since our EFT is only valid below the Λ_χ, we can perform the momentum integral by introducing a momentum cut-off $\tilde{\Lambda}$ well above Λ_χ. The I_0 integral evaluated using momentum cut-off gives

$$I_{\tilde{\Lambda}} \equiv I_0(\tilde{\Lambda}) = \int_0^{\tilde{\Lambda}} dp'' \frac{1}{q_0^2 - p''^2} = \frac{1}{2q_0} \log \frac{q_0 + \tilde{\Lambda}}{\tilde{\Lambda} - q_0} \,. \tag{3.19}$$

At this point, we will introduce numerical techniques. The momentum integration is expressed as summing over the momentum mesh: $\{(p_1, \omega_1), (p_2, \omega_2), \ldots, (p_{N_p}, \omega_{N_p})\}$, with $\sum_i \omega_i = \tilde{\Lambda}$. We designed the grid to include more grid points near m_π, which is the most interesting scale for nuclear physics. For notational convenience we are defining $p_{N_p+1} \equiv q_0$ and $V_{ij} \equiv V(p_i, p_j, E)$. The LS equation in (3.17) becomes

$$\begin{aligned} T_{ji}^{\alpha'\alpha} = V_{ji}^{\alpha'\alpha} &+ 2\mu \sum_{\alpha''} \sum_{k=1}^{N_p} \frac{V_{jk}^{\alpha'\alpha''} p_k^2 T_{ki}^{\alpha''\alpha} \omega_k}{q_0^2 - p_k^2} - 2\mu \sum_{\alpha''} \sum_{k=1}^{N_p} q_0^2 \frac{V_{j,N_p+1}^{\alpha'\alpha''} T_{,N_p+1i}^{\alpha''\alpha} \omega_k}{q_0^2 - p_k^2} \\ &- i\pi\mu q_0 \sum_{\alpha''} V_{j,N_p+1}^{\alpha'\alpha''} T_{N_p+1,i}^{\alpha''\alpha} + i\pi\mu q_0^2 I_{\tilde{\Lambda}} \sum_{\alpha''} V_{j,N_p+1}^{\alpha'\alpha''} T_{N_p+1,i}^{\alpha''\alpha} \end{aligned} \tag{3.20}$$

We can arrange the above equation as a matrix equation

$$\sum_{\alpha''} \sum_{k=1}^{N_p} A_{jk}^{\alpha'\alpha''} T_{ki}^{\alpha''\alpha} = V_{ji}^{\alpha'\alpha}. \tag{3.21}$$

where we identify matrix A as

- $j, k \in [1, N_p]$: $A_{jk}^{\alpha'\alpha''} = \delta^{jk}\delta^{\alpha'\alpha''} - \frac{2\mu V_{jk}^{\alpha'\alpha''} p_k^2 \omega_k}{q_0^2 - p_k^2}$.
- $j \in [1, N_p]$: $A_{j,N_p+1}^{\alpha'\alpha''} = 2\mu q_0^2 \sum_{k'=1}^{N_p} \left(\frac{\omega_{k'}}{q_0^2 - p_{k'}^2} \right) V_{j,N_p+1}^{\alpha'\alpha''} + (i\pi\mu q_0 - 2\mu q_0^2 I_{\tilde{\Lambda}}) V_{j,N_p+1}^{\alpha'\alpha''}$.
- $k \in [1, N_p]$: $A_{N_p+1,k}^{\alpha'\alpha''} = -2\mu \frac{\omega_k p_k^2}{q_0^2 - p_k^2} V_{N_p+1,k}^{\alpha'\alpha''}$.
- $A_{N_p+1,N_p+1}^{\alpha'\alpha''} = \delta^{\alpha'\alpha''} + 2\mu q_0^2 \sum_{k'=1}^{N_p} \left(\frac{\omega_{k'}}{q_0^2 - p_{k'}^2} \right) V_{N_p+1,N_p+1}^{\alpha'\alpha''}$
  $+ (i\pi\mu q_0 - 2\mu q_0^2 I_{\tilde{\Lambda}}) V_{N_p+1,N_p+1}^{\alpha'\alpha''}$.

For uncoupled channel, Eq. (3.21) becomes a simple matrix equation $AT = V$ (where matrix dimensions are $N_p+1 \times N_p+1$) and can be solved easily. For coupled channel ($\{\alpha_1, \alpha_2, \ldots, \alpha_M\}$), we can still write it as a simple matrix equation if we replace the matrices A, T, V by bigger matrices given by

$$A \to \begin{pmatrix} A^{\alpha_1\alpha_1} & A^{\alpha_1\alpha_2} & \ldots & A^{\alpha_1\alpha_M} \\ A^{\alpha_2\alpha_1} & A^{\alpha_2\alpha_2} & \ldots & A^{\alpha_2\alpha_M} \\ \vdots & \vdots & \ddots & \vdots \\ A^{\alpha_M\alpha_1} & A^{\alpha_M\alpha_2} & \ldots & A^{\alpha_M\alpha_M} \end{pmatrix}_{M\cdot(N_p+1)\times M\cdot(N_p+1)} , \tag{3.22}$$

and the S-matrix is given by

$$S_{ij} = \delta^{\alpha_i\alpha_j} - 2i\pi\mu q_0 T^{\alpha_i\alpha_j}_{N_p+1,N_p+1}. \tag{3.23}$$

The phase shifts and mixing angles are extracted from the S-matrix using Eqs. (3.11), (3.12), (3.14), and (3.15) for *CP*-even uncoupled channels, *CP*-even coupled channels, *CP*-odd $j = 0$ channels, and *CP*-odd $j = 1$ channels, respectively.

3.3.2 Python program to extract phase shift and mixing angles

A Python program was used to implement the above prescription to solve the LS equation and extract the phase shift and mixing angles as a function of cut-off Λ. The program generates $C_{s,t,p}$ as function of cut-off Λ, by fitting to Nijmegen PWA data for $\delta_{1S0,3S1,3P0}$ at $E_{\rm CM} = 5\,\text{MeV}$. For *CP*-odd potential, the program generates $\bar{C}_0$ as function of cut-off Λ, by fitting $\epsilon^0_{\rm SP} = \epsilon^0_{\rm SP,fit}, \epsilon^0_{\rm SP,fit} + 0.1\,\bar{g}_0, \epsilon^0_{\rm SP,fit} - 0.1\,\bar{g}_0$ at $E_{\rm CM} = 5\,\text{MeV}$, with $\epsilon^0_{\rm SP,fit} = 0.01\,\bar{g}_0$ (these fit choices are explained in Section 3.5). The program's basic structure is briefly demonstrated in this section. The program is divided mainly into two parts: *CP*-even and *CP*-odd. The python code is available at https://github.com/sachin-shain/CP-odd_nn-scattering.

CP-even sub-program

The *CP*-even part calculate the phase shift and mixing angles for $\Lambda = (2-52)\,\text{fm}^{-1}$ and $E_{\rm CM} = (1-100)\,\text{MeV}$, using *CP*-even potential. After fitting to experimental data, it also generates the *CP*-even LECs $C_{s,t,p}$. The main routines and sub-routines of this part of the program are *CP-even phase shift calculator* and C_0^{even} *calculator*.

- **CP-even phase shift calculator:** This routine calculates the phase shift and mixing angles for a given channel, $E_{\rm CM}$, Λ, and C_0. The C_0 is the coupling of the contact terms that contribute to the channel. The short distance contributions are 'turned off' by calling the routine with $C_0 = 0$.

  For renormalizing the potential, $C_0(\Lambda)$ must be fitted for the appropriate channels. The C_0^{even} *calculator* sub-routine achieve this objective. Once the $C_0(\Lambda)$ data file is created, the *CP-even phase shift calculator* will read the $C_0(\Lambda)$ for appropriate channels automatically, and C_0 input is no longer necessary. The routine treats the absence of $C_0(\Lambda)$ file as the absence of short-distance interactions. The flowchart diagram for this routine after creating $C_0(\Lambda)$ data files is given in Fig. 3.4. The data generated by this routine are used to generate plots in Section 3.4.1.

- **$C_0^{\rm even}$ calculator:** For a given channel α (in which short distance interaction contributes), interval (a, b), and experimental phase shift value at $\delta^\alpha_{\rm exp}$ ($E_{\rm CM} = 5\,\text{MeV}$), this sub-routine calculates $C_0(\Lambda)$ for $\Lambda \in (2, 52)\,\text{fm}^{-1}$ such

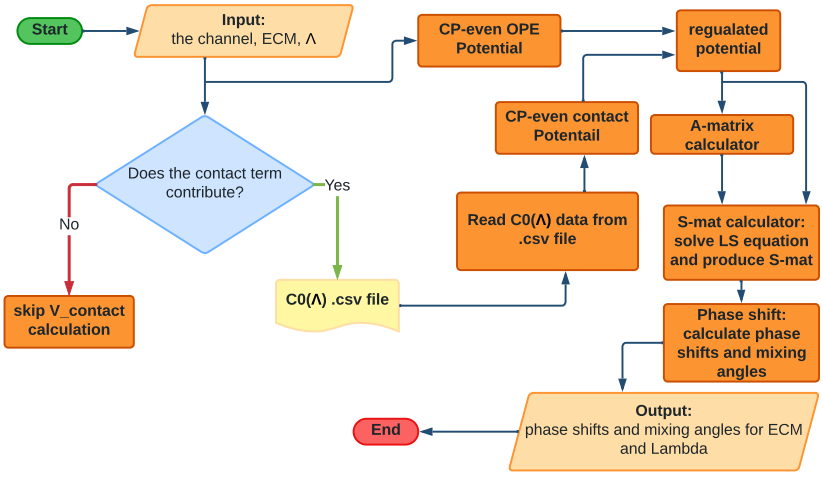

Figure 3.4: The flow chart of the *CP-even phase shift calculator* routine after implementing C_0^{even} *calculator*.

that $\delta^{\alpha}_{C_0} - \delta^{\alpha}_{\text{exp}}$ $(a < \delta^{\alpha}_{C_0} < b)$ lies below a certain tolerance value, the fit is done for $E_{\text{CM}} = 5\,\text{MeV}$.

For each Λ, the function

$$F_c(C_0) = \delta^{\alpha}_{C_0} - \delta^{\alpha}_{\text{exp}}\,, \tag{3.24}$$

is evaluated for $C_0 \in (a, b)$, and $\delta^{\alpha}_{C_0}$ is calculated using *CP-even phase shift calculator*. In general, F_c need not be continuous in the given interval (a, b). We observed that the nature of F_c falls into six types, as shown in Fig. 3.5. The main part of the sub-routine is to identify the interval $(\tilde{a}, \tilde{b})$ in which F_c is continuous and satisfies $F_c(\tilde{a})F_c(\tilde{b}) < 0$, once the sub-routine identifies this interval, it uses Brent's method root-finding algorithm to calculate the root of F_c $C_0(\Lambda)$.

Type	Maximum	Minimum	Sign$(F_c(a))$	Sign$(F_c(b))$	$(\tilde{a}, \tilde{b})$
Type 3	c_-	c_+	$+$	$+$	(c_+, b)
Type 4	c_+	c_-	$+$	$+$	(a, c_-)
Type 5	c_+	c_-	$-$	$-$	(c_+, b)
Type 6	c_-	c_+	$-$	$-$	(a, c_-)

Table 3.1: The conditions to identify the type of the graph.

For the initial plot, five values of $C_0 \in \{a, a + \Delta_c, \ldots, b\}$ ($\Delta_c = \frac{b-a}{5}$) are used. For type-1 and type-2, we can easily identify $\tilde{a} = a, \tilde{b} = b$. For other

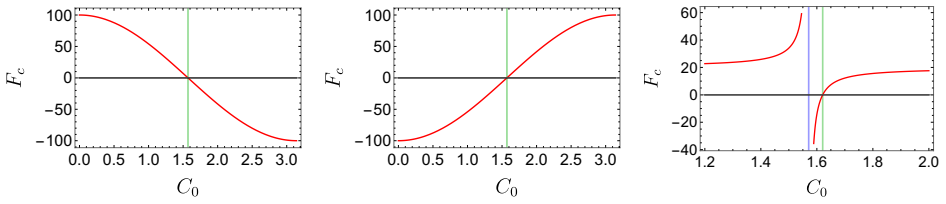

(a) Type 1 **(b)** Type 2 **(c)** Type 3

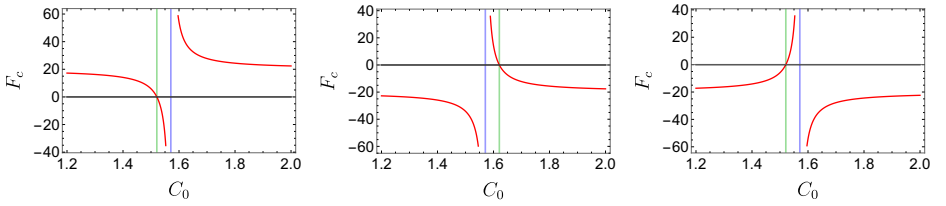

(d) Type 4 **(e)** Type 5 **(f)** Type 6

Figure 3.5: The six types of F_c vs C_0 graphs. The black, green, and blue lines indicate the x-axis, the root $C_0(\Lambda)$, and the discontinuity $c = C_0^{\text{discont}}$, respectively.

types, first, we need to locate the interval containing the discontinuity point c. This interval is identified when F_c obtains maximum (minimum) at c_+ and minimum (maximum) at c_-, with $c_+ = c_- + \Delta_c$. However, we can have $F_c(c_-)F_c(c_+) > 0$, as shown in the left panel of Fig. 3.6. In this case, we repeat the process with the new intervals until $F_c(c_-)F_c(c_+) < 0$. For type-3 graph, this interval is (c_-, c_+) as demonstrated in Fig. 3.6. Now we can identify the type of the graph and interval $\tilde{a}, \tilde{b}$ using Table 3.1. The program store the calculated $C_0(\Lambda)$ in a .csv file for future access. The flowchart for this routine is given in Fig. 3.7.

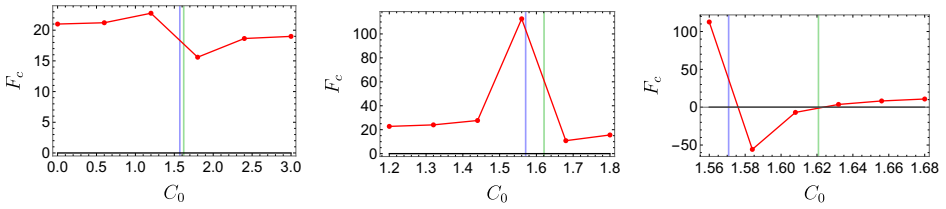

(a) $(a,b) = (0,3), c_- = 1.2, c_+ = 1.8$ **(b)** $(a,b) = (1.2,1.8), c_- = 1.56, c_+ = 1.68$ **(c)** $(a,b) = (1.56,1.68), c_- = 1.56, c_+ = 1.584$

Figure 3.6: Three stages of 'zooming-in' around the discontinuity of a type-3 graph. The discontinuity c and root $C_0(\Lambda)$ of F_c are shown by blue and green lines, respectively.

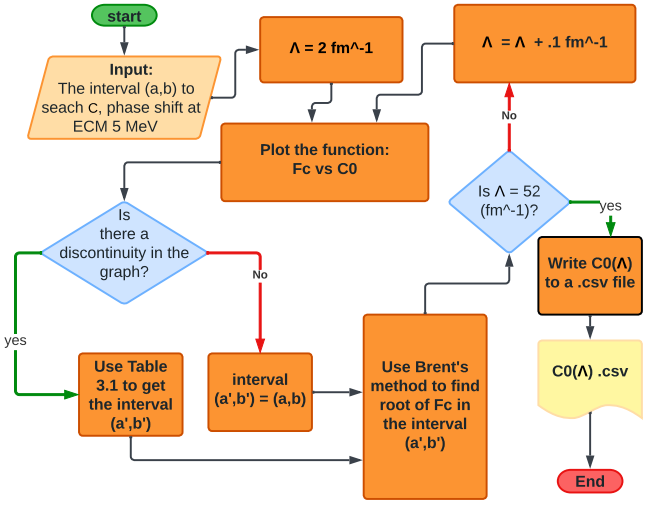

Figure 3.7: The flow chart of the C_0^{even} *calculator* sub-routine.

CP-odd sub-program

The *CP*-odd part of the program is similar to the *CP*-even part. It uses the $C_{s,t,p}(\Lambda)$ generated by the *CP*-even part to calculate the full LO *CP*-even potentials along with *CP*-odd potentials. It calculate the phase shifts and *CP*-odd mixing angles for $\Lambda = (2-52)\,\text{fm}^{-1}$ and $E_{\text{CM}} = (5, 25, 50, 95)\,\text{MeV}$. For a given value of $\epsilon^0_{\text{SP,fit}}$ at $E_{\text{CM}} = 5\,\text{MeV}$, the program calculate $\bar{C}_0(\Lambda)$ by fitting ϵ^0_{SP} to this fit value.

This program evaluate $\epsilon^{0,1}_{\text{SP}}$, and ϵ_{DP} as a function of cut-off and calculates $\bar{C}_0$ and $\epsilon^0_{\text{SP}}(\Lambda)$ after fitting $\epsilon^0_{\text{SP,fit}} = (0.01, 1.10, -0.09)\bar{g}_0$. The program achieves this by using *method 1* and *method 2*, which take advantage of *CP*-odd being perturbative to *CP*-even potential. The *method 1* uses Eq. (3.13) to calculate the T matrix. *Method 2* utilizes the fact that we can express the total *CP*-odd mixing angle as a sum of the *CP*-odd mixing angle from the *CP*-odd OPE and short-distance potentials because *CP*-odd potential can be treat as a perturbative correction to *CP*-even potential

$$\epsilon^{\text{LO}}_{\text{SP}} = \epsilon^{\text{OPE}}_{\text{SP}} + \bar{C}_0 \epsilon^{\text{sd}}_{\text{SP}}\,, \tag{3.25}$$

where we calculated $\epsilon^{\text{sd}}_{\text{SP}}$ without the LEC $\bar{C}_0$. The $\bar{C}_0$ is calculated by fitting $\epsilon^{\text{LO}}_{\text{SP}}$ with $\epsilon^{\text{LO}}_{\text{SP}}$ to $\epsilon^0_{\text{SP,fit}}$. We implement the perturbation nature of *CP*-odd potential numerically by introducing a small factor $\Delta = 10^{-4}$ to all *CP*-odd potentials; this will make sure that *CP*-odd contributions are always smaller by a factor of Δ compared to *CP*-even contributions (see Table 3.2). The *CP*-odd observables are divided by Δ in the end to make them Δ independent. We have checked that

both *method 1* and *method 2* produce the same results. However, we observed that the *method 2* is significantly faster and we used this method for fitting. The data generated by this routine are used to generate plots in Section 3.4.2. The following are the main routines and sub-routines of this part of the program.

- **CP-odd phase shift calculator:** It has almost the same structure as the *CP-even phase shift calculator*, except for the *regulated potential* and *CP-odd phase shift* sub-routines. The *regulated potential* is modified to calculate different types of potentials based on the *index* (internal parameter of the *CP*-odd program) values. The potential corresponding to different index values and their purpose is given in Table 3.2.

- $\boldsymbol{C_0^{\text{even}}}$ **calculator:** This sub-routine calculate $\bar{C}_0(\Lambda)$ by fitting ϵ_{SP}^0 with $\epsilon_{\text{SP,fit}}^0 = 0.01\bar{g}_0$ at $E_{\text{CM}} = 5\,\text{MeV}$ for $\Lambda = (2-52)\,\text{fm}^{-1}$. We do the fitting using *method 2*. To study the effect of different values of ϵ_{SP}^0 (including $\epsilon_{\text{SP}}^0 < 0$), we also fitted for $\epsilon_{\text{SP}}^0 = \epsilon_{\text{SP,fit}}^0 + 0.1\bar{g}_0 = 0.11\bar{g}_0$ and $\epsilon_{\text{SP}}^0 = \epsilon_{\text{SP,fit}}^0 - 0.1\bar{g}_0 = -0.09\bar{g}_0$. The calculated $\bar{C}_0(\Lambda)$ are stored in a .csv file for future access.

Index	$V(p', p)$	Purpose
0	V^{strong}	Evaluate T^{strong}
1	$\Delta V_{\text{OPE}}^{\text{CP-odd}}$	Evaluate $V_{\bar{g}_0}$
2	$V^{\text{strong}} + \Delta V_{\text{OPE}}^{\text{CP-odd}}$	Evaluate $\epsilon_{\text{SP}}^{\text{OPE}}$
3	$V^{\text{strong}} + \Delta V_{\text{sd}}^{\text{CP-odd}}$	Evaluate $\epsilon_{\text{SP}}^{\text{sd}}$
4	$V^{\text{strong}} + \Delta(V_{\text{OPE}}^{\text{CP-odd}} + V_{\text{sd}}^{\text{CP-odd}})$	Evaluate ϵ_{SP}^0, after fitting C_0.

Table 3.2: The potentials that are 'called' by the *regulated potential* for the different index values.

3.4 Nucleon-nucleon phase shifts

In this section, we studied the dependence of *CP*-even and *CP*-odd observables on the cut-off Λ. We did a partial-wave decomposition for the interactions discussed in Section 3.2 and numerically solved the LS equation, as described in the above section, and extracted the phase shifts and mixing angles. One advantage of using partial waves is the total spin quantum number j, z-component of the spin m_j are conserved during the scattering process, see Appendix B. Another advantage is that the nuclear potentials are short-distance, and the wave function of higher partial waves has a lesser probability near the scattering point and becomes less relevant. We also checked whether these observables agreed with the experimental results. We analyzed the dependence of the LO contribution

of the observables, which are determined by the Weinberg's power counting rule based on NDA, on the cut-off Λ. If NDA holds, the observables are expected to show cut-off independence within NLO corrections. We have considered a wide range of cut-off $\Lambda = (2 - 52)\,\mathrm{fm}^{-1}$ and four different center of mass energies $E_{\mathrm{CM}} = (5, 25, 50, 95)\,\mathrm{MeV}$. We present the results for waves with total angular momentum $j = 0, 1$ below.

3.4.1 *CP*-even

Considering only the strong OPE potential leads to phase shifts and mixing angles that are cut-off dependent for the $^1\mathrm{S}_0$ and $^3\mathrm{S}_1$-$^3\mathrm{D}_1$ channels. These cut-off dependence of the phase shift δ_{1S0} for $^1\mathrm{S}_0$ and the phase shift δ_{3S1} for $^3\mathrm{S}_1$-$^3\mathrm{D}_1$ are shown in the top-left panel of Fig. 3.8 and Fig. 3.10, respectively. However, this is resolved in Weinberg's power counting by including the short-distance counter terms C_s and C_t acting in $^1\mathrm{S}_0$ and $^3\mathrm{S}_1$ waves. We fitted the $C_{s,t}$ with Nijmegen energy-dependent partial-wave analysis (PWA) of NN scattering data [3] [159] at $E_{\mathrm{CM}} = 5\,\mathrm{MeV}$. The phase shifts and mixing angles from the full LO strong potential exhibit the expected regulator independence.

We present cut-off dependence of the full LO phase shift of $^1\mathrm{S}_0$ for various energies in the top-right panel of Fig. 3.8. The bottom-left panel of Fig. 3.8 shows the cut-off dependence of LEC C_s after fitting to data at $E_{\mathrm{CM}} = 5\,\mathrm{MeV}$. In the bottom-right panel of Fig. 3.8, we compared the LO phase shift for $\Lambda = 52\,\mathrm{fm}^{-1}$ with the Nijmegen PWA data and observed the known discrepancy. This deviation is an effect of the relatively-large effective range parameter in the $^1\mathrm{S}_0$ wave; without the two-derivative contact term, we can not capture this sufficiently. Once we include the subleading term to the potential, the discrepancy disappears.

We present the cut-off independence of $^3\mathrm{S}_1$-$^3\mathrm{D}_1$ channel phase shift δ_{3S1}, ϵ_1, and δ_{3D1} in the top-right panel of Fig. 3.10, left and right panel of Fig. 3.9, respectively. The contact term LEC C_t of this channel, is shown in the bottom-left panel of Fig. 3.10 as a function of cut-off Λ. The $C_t(\Lambda)$ shows a limit-cycle behavior and appears to be discontinuous at some cut-offs. This behavior is not a cause for concern because C_t is not observable. In the bottom-right panel of Fig. 3.10, we compare the LO results of δ_{3S1} with the experimental data. We are in good agreement at lower energies, which is remarkable because we only use the LO contribution.

In the $^1\mathrm{P}_1$ and $^3\mathrm{P}_1$ waves, the strong OPE potential leads to cut-off independent phase shifts. The cut-off independence of $^1\mathrm{P}_1$ channel phase shift is shown in the left panel of Fig. 3.11. We also observe a good agreement with the experimental data at lower energies; see the right panel of Fig. 3.11.

In the $^3\mathrm{P}_0$ channel, however, the phase shifts arising from OPE are strongly cut-off dependent. They undergo a dramatic limit-cycle-like behavior; see the top-left panel of Fig. 3.12. Following Weinberg's power counting, there is no

[3] the scattering data is available through https://nn-online.org.

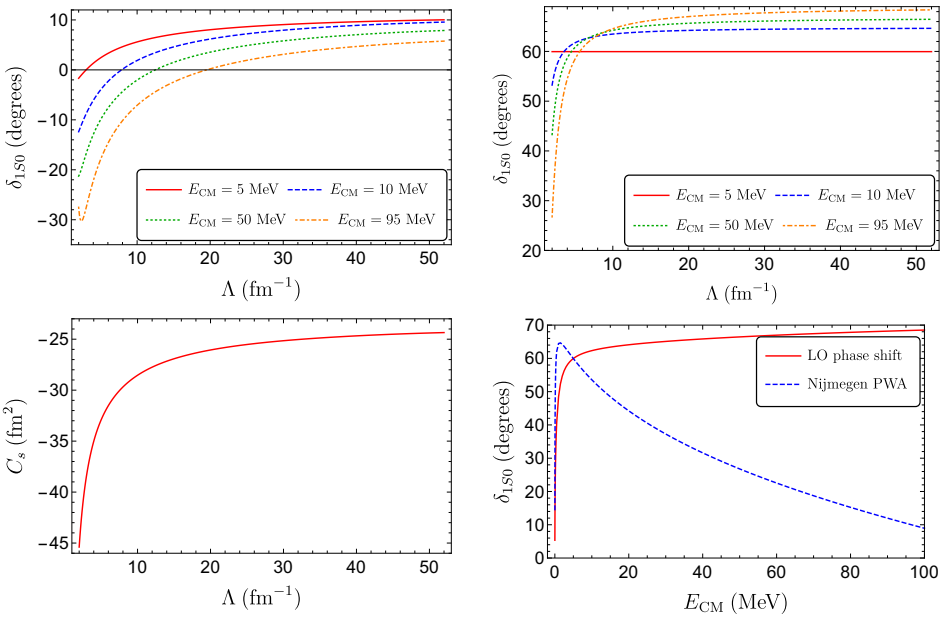

Figure 3.8: The $^1S_0$ channel phase shift from the LO OPE (LO OPE and short distance) *CP*-even diagram, for multiple center of mass energies, as a function of cut-off Λ, is presented in the top-left (top-right) panel. The bottom-left panel shows the dependence of the LEC C_s, fitted for $E_{CM} = 5\,\text{MeV}$, as a function of cut-off Λ, and the bottom-right panel shows the comparison of the LO phase shift δ_{1S0} at cut-off $\Lambda = 52\,\text{fm}^{-1}$ (solid line) to the Nijmegen PWA (dashed line) for a wide range of center of mass energies.

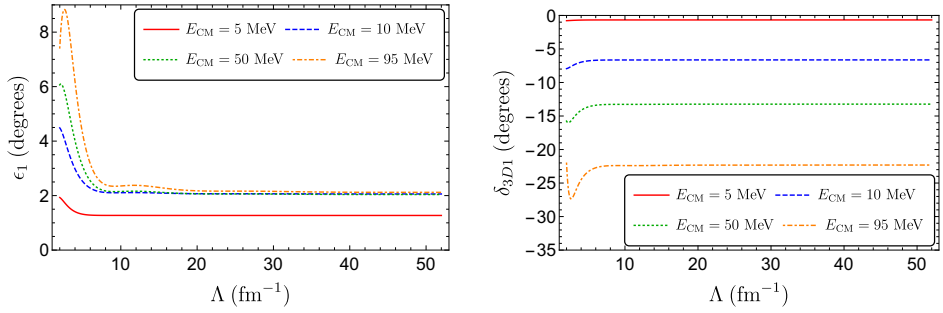

Figure 3.9: The $^3S_1$-$^3D_1$ channel mixing angle ϵ_1 and phase shift δ_{3D1} from the full LO *CP*-even diagram, for multiple center of mass energies, as a function of cut-off Λ is presented in the left and right panels, respectively.

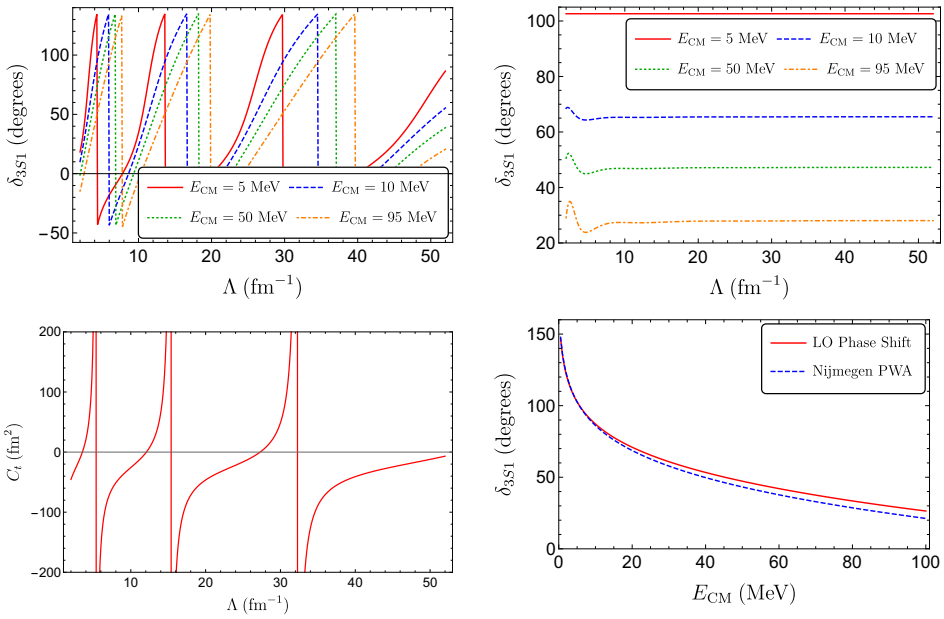

Figure 3.10: The $^3S_1$-$^3D_1$ channel phase shift δ_{3S1} from the LO OPE (LO OPE and LO short distance) *CP*-even diagram, for multiple center of mass energies, as a function of cut-off Λ is presented in the top-left (top-right) panel. The bottom-left panel shows the dependence of the LEC C_t, fitted for $E_{\rm CM} = 5\,$MeV, as a function of cut-off Λ and the bottom-right panel shows the comparison of the LO phase shift δ_{3S1} at cut-off $\Lambda = 52\,\text{fm}^{-1}$ (solid line) to the Nijmegen PWA (dashed line) for a wide range of center of mass energies.

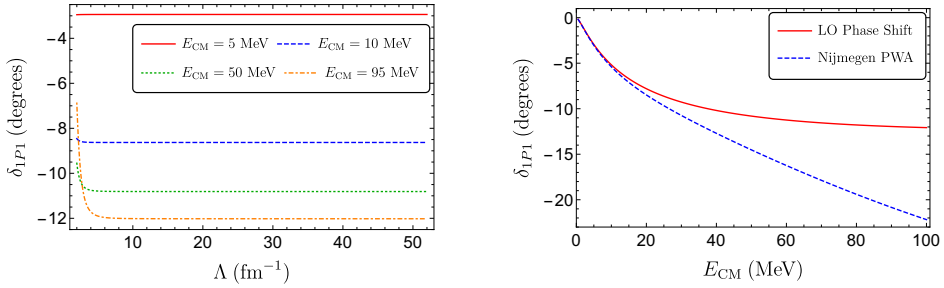

Figure 3.11: The $^1P_1$ channel phase shift from the LO OPE *CP*-even diagram, for multiple center of mass energies, as a function of cut-off Λ is presented in the left panel. In the right panel, we compare the LO $^1P_1$ phase shift at cut-off $\Lambda = 52\,\text{fm}^{-1}$ (solid line) to the Nijmegen PWA (dashed line) for a wide range of center of mass energies.

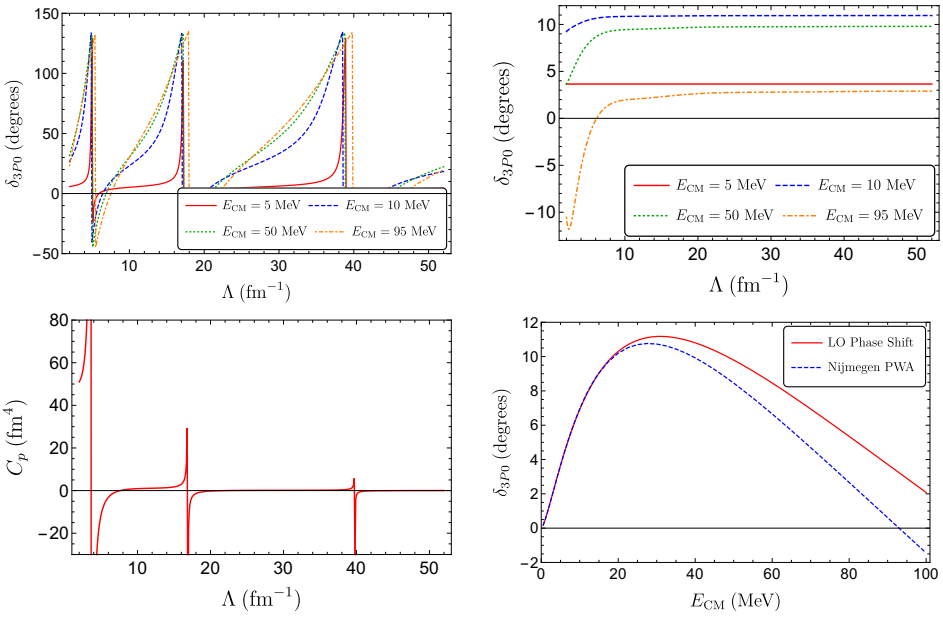

Figure 3.12: The ^{3}P$_0$ channel phase shift $\delta_{^3P0}$ from the LO OPE (LO OPE and LO short distance) *CP*-even diagram, for multiple center of mass energies, as a function of cut-off Λ is presented in the top-left (top-right) panel. The bottom-left panel shows the dependence of the C_p LEC, fitted for $E_{\rm CM} = 5\,$MeV, as a function of cut-off Λ and the bottom-right panel shows the comparison of the LO phase shift $\delta_{^3P0}$ at cut-off $\Lambda = 52\,\text{fm}^{-1}$ (solid line) to the Nijmegen PWA (dashed line) for a wide range of center of mass energies.

counter-term that can absorb this regulator dependence. Following Ref. [145], we promote the ^{3}P$_0$ counter term with LEC C_p in Eq. (3.6) to LO and fit C_p to the ^{3}P$_0$ phase shift at $E_{\rm CM} = 5\,$MeV. With this modified power counting, the phase shifts become cut-off independent; see the top-right panel of Fig. 3.12. The regulator dependence of C_p is given in the bottom-left panel of Fig. 3.12. The LECs C_p show significant Λ dependence, which is of no concern as they are not observable. In the bottom-right panel of Fig. 3.12, we compare the phase shift from the modified LO with the experimental data and agree at lower energies. All results agree with Refs. [145, 160].

3.4.2 *CP*-odd

The *CP*-odd mixing angles are observable and should be cut off independent of NLO corrections. We observed this in the case of $\epsilon^1_{\rm SP}$ and $\epsilon_{\rm DP}$, as shown in Fig. 3.13. We have checked that no regulator dependence appears for any $j = 2$ transition after renormalizing the strong $j = 2$ scattering states.

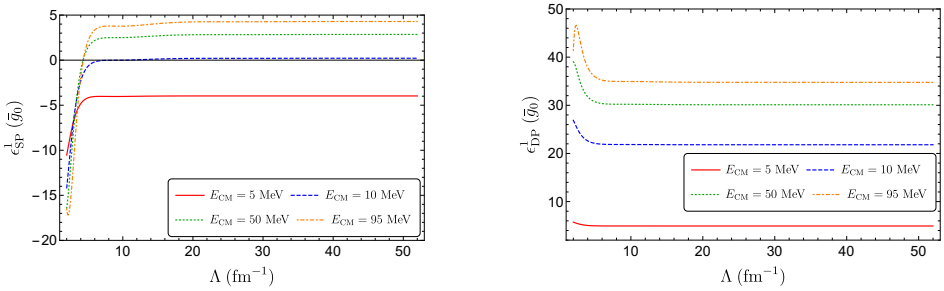

Figure 3.13: The $\epsilon^1_{\rm SP}$ ($\epsilon^1_{\rm DP}$) mixing angle from ^{3}S,D$_1$-^{1}P$_1$ channel for *CP*-odd LO OPE diagrams for various $E_{\rm CM}$ energies as a function of cut-off Λ are shown in the left (right) panel.

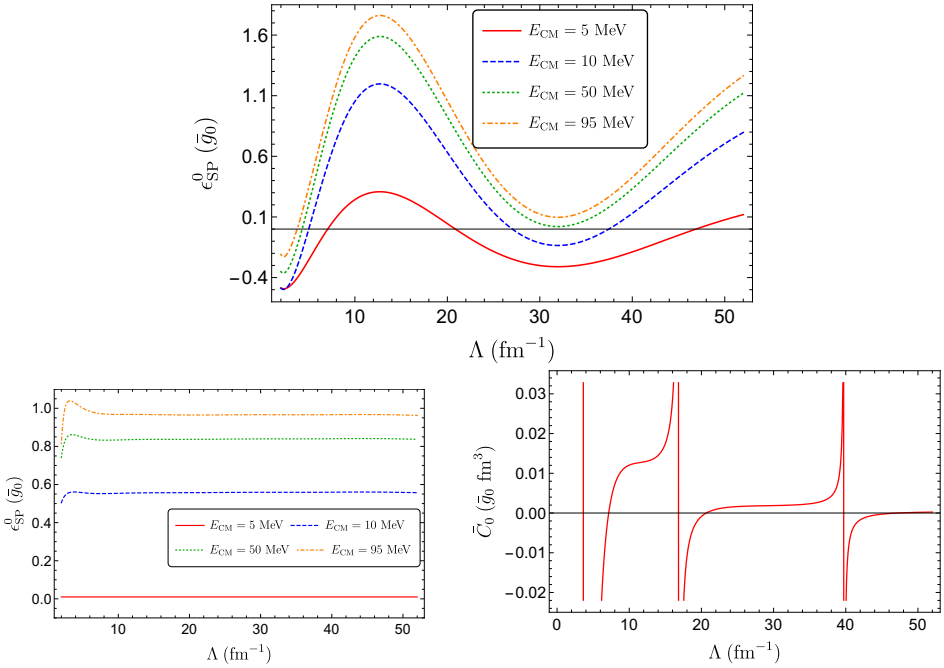

Figure 3.14: The $\epsilon^0_{\rm SP}$ mixing angle, in units of $\bar{g}_0$, for ^{1}S$_0$-^{3}P$_0$ channel from the LO OPE *CP*-odd potential, for multiple center of mass energies, as a function of cut-off Λ is presented in the top panel. In the bottom-left panel, we show the $\epsilon^0_{\rm SP}$ mixing angle from LO OPE and contact diagrams after fitting the LEC $\bar{C}_0$ to $\epsilon^0_{\rm SP,fit} = 0.01\bar{g}_0$ at $E_{\rm CM} = 5\,$MeV for various $E_{\rm CM}$ energies as a function of cut-off Λ. The bottom-right panel shows the cut-off Λ dependence of *CP*-odd LEC $\bar{C}_0$, after fitting $\epsilon^0_{\rm SP}$ to $\epsilon^0_{\rm SP,fit} = 0.01\bar{g}_0$ at $E_{\rm CM} = 5\,$MeV.

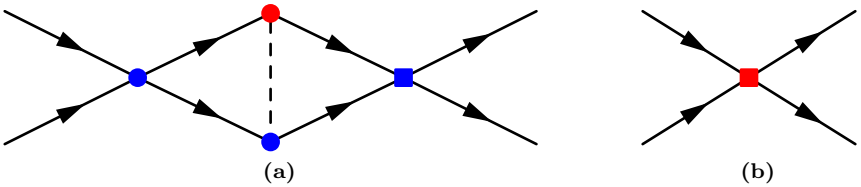

Figure 3.15: Left: Diagram contributing to the regulator dependence of $\epsilon^0_{\rm SP}$. Solid (dashed) lines denote nucleons (pions). The red circle denotes $\bar{g}_0$ while the blue circles denote the g_A or C_s vertices. The blue square denotes C_p. Right: short-distance contribution proportional to $\bar{C}_0$. The red square denote the $\bar{C}_0$ vertex.

In the case of $j = 0$, the *CP*-odd mixing angle $\epsilon^0_{\rm SP}$ shows an oscillatory behavior and even changes sign as a function of Λ. We observed it varies from -0.5 to 1.8 in units of $\bar{g}_0$ for the range of $\Lambda = (2 - 52)\,\mathrm{fm}^{-1}$, as shown in the top panel of Fig. 3.14. We concluded that the regulator dependence arises from divergences in diagrams contributing to $T_{\bar{g}_0}$ with the topology of the diagram 3.15a, where $V_{\bar{g}_0}$ is dressed on both sides by a strong short-distance interaction (an infinite number of LO diagrams are generated by adding additional strong interactions on either side). The absence of LO short-distance ^{1}P$_1$ term prohibits diagrams of the form 3.15a and lead to cut-off independence for *CP*-odd mixing angles in the ^{3}S,D$_1$-^{1}P$_1$ channels. However, because of the LO short-distance ^{3}P$_0$ term, such diagrams are no longer restricted and cause strong regulator dependence.

In χPT calculations using Weinberg's power counting, *P*-wave counter terms appear at N^{2}LO but are iterated to all orders in the solution of the LS equation [161]. As a result, divergent diagrams with the topology of Fig. 3.15 reappear, and the *CP*-odd transitions become regulator dependent. However, this dependence might be hard to see in numerical calculations as regulators are varied in a small window around $\Lambda = 500\,\mathrm{MeV}$ [77, 79].

3.5 Counter term and renormalizaiton of *CP*-odd nuclear forces

Our result established that the $\epsilon^0_{\rm SP}$ is cut-off dependent, which implies that the *CP*-odd observables that depend on ^{1}S$_0$-^{3}P$_0$ can not be directly calculated from $\bar{g}_0$, and thus $\bar{\theta}$ via Eq. (3.3). From an EFT point of view, this indicates that the *CP*-odd nuclear forces are not properly renormalized. A counter term is required to encapsulate missing short-distance physics and absorb the divergence. In χPT, such counter terms are provided by short-range *CP*-odd *NN* interactions, see diagram 3.15b, of the form [73, 74]

$$\mathcal{L}_{NN} = \bar{C}_0 \left[\bar{N}\boldsymbol{\sigma} N \cdot \boldsymbol{\nabla}(\bar{N}\, N) + \frac{1}{3}\bar{N}\vec{\tau}\boldsymbol{\sigma} N \cdot \boldsymbol{\nabla}(\bar{N}\vec{\tau} N) \right] , \tag{3.26}$$

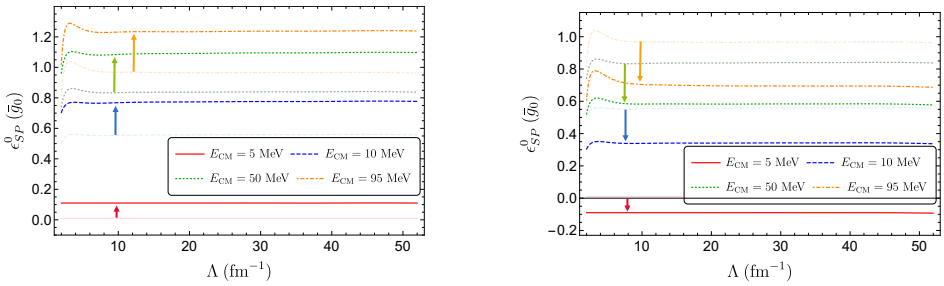

Figure 3.16: The $\epsilon^0_{\rm SP}$ mixing angle from LO OPE and contact diagrams after fitting the LEC $\bar{C}_0$ to $\epsilon^0_{\rm SP,fit} = 0.11\bar{g}_0$ and $\epsilon^0_{\rm SP,fit} = -0.09\bar{g}_0$ at $E_{\rm CM} = 5\,$MeV for various $E_{\rm CM}$ energies as a function of cut-off Λ is shown in the left and right panel, respectively. The $\epsilon^0_{\rm SP}$ mixing angle for $\epsilon^0_{\rm SP,fit} = 0.01\bar{g}_0$ is shown in the lighter shade, and the arrows indicate how the $\epsilon^0_{\rm SP}$ shifted in comparison with the $\epsilon^0_{\rm SP,fit} = 0.01\bar{g}_0$ fit.

which projects on ${}^1\mathrm{S}_0$-${}^3\mathrm{P}_0$. The $\bar{C}_0$ is a LEC that depends on Λ, which needs to be fitted similarly to the *CP*-even case to make $\epsilon^0_{\rm SP}$ cut-off independent. NDA suggests that $\bar{C}_0 = \mathcal{O}(m_\star\bar{\theta}/(F_\pi^2\Lambda_\chi^2))$ and a N^{2}LO contribution, but renormalization enhances $\bar{C}_0$ to LO.

We repeated our calculation for $\epsilon^0_{\rm SP}$ after promoting $\bar{C}_0$ to LO, and indeed this renormalized the ${}^1\mathrm{S}_0$-${}^3\mathrm{P}_0$ transition. We fit $\bar{C}_0$ at a specific kinematical point to a fictitious measurement of $\epsilon^0_{\rm SP}$, picking $\epsilon^0_{\rm SP,fit} = 0.01\,\bar{g}_0$ at $E_{\rm CM} = 5$ MeV for concreteness. The regulator dependence of $\bar{C}_0$ is shown in the bottom-right panel of Fig. 3.14 and shows a limit-cycle-like behavior driven by C_p. The resulting $\epsilon^0_{\rm SP}$ is regulator independent for a wide range of energies as depicted in the bottom-left panel of Fig. 3.14.

While this method accounts for the regulator-dependent part of short-distance contributions and renormalizes the *CP*-odd amplitude, it cannot account for possible finite contributions from $\bar{C}_0$. We also investigated the effect of choosing a different value for $\epsilon^0_{\rm SP,fit}$. We recalculate the $\epsilon^0_{\rm SP}$ dependence on Λ at different energies for fit values $\epsilon^0_{\rm SP} = \epsilon^0_{\rm SP,fit} + 0.10\,\bar{g}_0, \epsilon^0_{\rm SP,fit} - 0.10\,\bar{g}_0 = 0.11\,\bar{g}_0, -0.09\,\bar{g}_0$, at $E_{\rm CM} = 5\,$MeV. We concluded that the results in the bottom-left panel of Fig. 3.14 will remain flat but can shift up (down) if we were to pick a higher (lower) values for $\epsilon^0_{\rm SP,fit}$, see Fig. 3.16. The best way to obtain the total short-distance contribution is by fitting it to a measurement of $\epsilon^0_{\rm SP}$. This is currently not possible, and even if there were data, it would not be satisfactory. We want to use such data to extract a value of $\bar{\theta}$.

3.6 Fixing the value of the short-distance LEC

We discuss two possible methods to obtain a value for $\bar{C}_0$ in the absence of data. The first one is to perform the LQCD calculation of $NN \to NN$ scattering in the presence of nonzero $\bar{\theta}$ background. There have been significant developments in calculations of nucleon EDMs arising from the $\bar{\theta}$ term by applications of the gradient flow [49, 162]. We can adopt the same techniques to study four-point functions in a $\bar{\theta}$ vacuum. A significant challenge for this method will be to control the signal-to-noise ratio. Already for *CP*-conserving $NN \to NN$ processes, signal-to-noise considerations demand pion masses well above the physical point [163]. Going to smaller pion masses is even more daunting for the $\bar{\theta}$ term, as the signal scales as $\sim \bar{\theta} m_\pi^2$. If such LQCD calculations are possible, we can obtain $\bar{C}_0$ from a matching calculation of χEFT to lattice data after taking the appropriate continuum and infinite-volume limits.

Our second method is more achievable on a shorter time scale. This approach is motivated by the striking similarity between the $\bar{\theta}$ term and the quark masses, and $\bar{g}_0$ and $\delta m_N^{\rm str}$ in Eq. (3.3). Using $SU(2)_L \times SU(2)_R$ χPT the operators in Eq. (3.26) arise from

$$\mathcal{L}_{NN} = -\frac{iC_0}{8}\mathrm{Tr}[\chi_-]\left[\bar{N}\boldsymbol{\sigma}N\cdot\boldsymbol{\nabla}(\bar{N}N) + \frac{1}{3}\bar{N}\vec{\tau}\boldsymbol{\sigma}N\cdot\boldsymbol{\nabla}(\bar{N}\vec{\tau}N)\right], \tag{3.27}$$

where $\chi_- = u^\dagger\chi u^\dagger - u\chi^\dagger u$, $u = \exp(i\vec{\tau}\cdot\vec{\pi}/(2F_\pi))$, $\chi = 2B(\mathcal{M} + im_\star\bar{\theta})$, and $B = -\langle\bar{q}q\rangle/F_\pi^2$. Expanding the trace gives $\bar{C}_0 = (Bm_\star\bar{\theta})C_0$ and a relation to the *CP*-conserving, isospin-breaking $NN\pi$ operators [141]

$$\mathcal{L}_{NN,\pi} = \frac{C_0 B(m_d - m_u)}{2}\frac{\pi_0}{F_\pi}\left[\bar{N}\boldsymbol{\sigma}N\cdot\boldsymbol{\nabla}(\bar{N}\,N) + \frac{1}{3}\bar{N}\vec{\tau}\boldsymbol{\sigma}N\cdot\boldsymbol{\nabla}(\bar{N}\vec{\tau}N)\right]. \tag{3.28}$$

These operators contribute to charge-symmetry-breaking (CSB) in $NN \to NN\pi$ processes [164–167]. A LO contribution to this CSB process arises from the $N\pi\pi$ vertex related to $\delta m_N^{\rm str}$ by chiral symmetry

$$\mathcal{L}_{\rm CSB} = -\frac{\delta m_N^{\rm str}}{4F_\pi^2}\bar{N}\vec{\tau}\cdot\vec{\pi}\,\pi_0 N\,. \tag{3.29}$$

According to Weinberg's power counting, the contact operator in Eq. (3.28) contributes at N^{2}LO. At the pion threshold, the transition operator for the process ^{1}S$_0$-^{3}P$_0$+π due to Eq. (3.29) is of the same form as $V_{\bar{g}_0}$. This one-to-one correspondence will lead to the exact regulator dependence seen in the top panel of Fig. 3.14. Following the same arguments in the previous section, we must promote the C_0 to LO for renormalization. Unfortunately, the simplest process where CSB data is available, $pn \to d\pi^0$, is not sensitive to C_0 due to the isosinglet nature of the deuteron. This motivates an investigation of $dd \to \alpha\pi^0$ using renormalized χEFT to fit C_0 to CSB data [168], to directly obtain $\bar{C}_0 = (Bm_\star\bar{\theta})C_0$.

3.7 Other sources of CP or P violation

At the dimension-six level, other CP-odd sources appear. For the present discussion, the most relevant operators are quark chromo-EDMs and chiral-breaking four-quark operators, which are induced in a wide range of BSM models [142,169]. In addition to the isoscalar $\bar{g}_0$ term in Eq. (3.2), the LO CP-odd chiral Lagrangian contains an isovector term

$$\mathcal{L}_{\pi N} = \bar{g}_1 \bar{N} \pi_0 N \,, \tag{3.30}$$

along with a potential subleading isotensor term [73]. In combination with the strong g_A vertex, an OPE diagrams involving $\bar{g}_1$ causes ^{1}S$_0$-^{3}P$_0$ and ^{3}S$_1$-^{3}P$_1$ transitions. The Strong ^{3}P$_1$ interactions arise solely from OPE diagrams, and the divergent diagrams in Fig. 3.15a do not appear. Thereby, we do not expect no regulator dependence for ^{3}S$_1$-^{3}P$_1$ transitions, which we confirmed by explicit calculations.

In $j = 0$ transition, we observe the same regulator dependence as the $\bar{g}_0$ case, up to an isospin factor, and thus, LO isospin-breaking counter term is needed. The associated operator takes the form

$$\mathcal{L}_{NN} = \bar{C}_1 \left[\bar{N} \tau^3 \boldsymbol{\sigma} N \cdot \boldsymbol{\nabla} (\bar{N}\, N) + \bar{N} \boldsymbol{\sigma} N \cdot \boldsymbol{\nabla} (\bar{N} \tau^3 N) \right] \,, \tag{3.31}$$

which projects unto ^{1}S$_0$-^{3}P$_0$ channels, but only for the neutron-neutron and proton-proton case. The simplest EDM that depends on $\bar{g}_1$ is the deuteron EDM [170], which is targeted in storage-ring experiments [171]. Due to the isosinglet nature of the deuteron, its EDM only depends on ^{3}S$_1$-^{3}P$_1$ transitions which do not require a counter term. However, there is no such selection rule for more complex EDMs such as ^{3}He, ^{199}Hg, or ^{225}Ra [76–79, 172, 173], and $\bar{C}_1$ must be included at LO.

The finiteness of ^{3}S$_1$-^{3}P$_1$ transitions is relevant for the field of hadronic parity (P) violation [174]. The LO P-odd, but CP-even, chiral Lagrangian induced by P-odd four-quark operators contains a single πN term [175], usually parametrized as $(h_\pi/\sqrt{2})\bar{N}(\vec{\pi}\times\vec{\tau})^3 N$ that in combination with g_A leads to $^3S_1$-$^3P_1$ transitions [176, 177]. We have checked explicitly that no regulator dependence appears, and no counter terms are needed. The value of h_π recently determined from P-violating asymmetries in $\vec{n}p \to d\gamma$ [178], can thus be directly applied in calculations of other P-odd observables.

3.8 Conclusion

We investigated the regulator dependence of various CP-even and CP-odd nucleon-nucleon scattering phase shifts and mixing angles and demonstrated the need for renormalization of the CP-odd nuclear forces in the ^{1}S$_0$-^{3}P$_0$ channel. We argued the need for a leading-order short-range CP-violating counter term in ^{1}S$_0$-^{3}P$_0$ transitions to recover the regulator independence of observables and thereby

renormalizing the *CP*-odd nuclear forces. This LO counter term affects calculations of EDMs and *CP* violation in nucleon-nucleon and neutron-nucleus scattering at the $\mathcal{O}(1)$ level. This directly affects the interpretation of experimental limits. Hopefully, future signals, in terms of the QCD $\bar{\theta}$ term and other *CP*-odd sources, and the interpretation of axion DM searches via oscillating EDMs. For *CP* violation from the $\bar{\theta}$ term, we have proposed strategies to obtain the value of the associated low-energy constant, $\bar{C}_0$, from existing data on charge-symmetry-breaking in few-body systems. We hope our results stimulate determinations of $\bar{C}_0$ using lattice QCD and analyses of CSB data, and calculations of the impact of the short-range operator on observables of experimental interest such as (oscillating) EDMs, magnetic quadrupole moments, and time-reversal-odd scattering observables.

3.9 Outlook

Much work remains to be done. It would be of great relevance for the experimental program to compute the effects of our new findings in EDMs of light nuclei and Schiff moments of heavier systems. This is not straightforward, as it requires a systemic treatment of the *CP*-even and *CP*-odd forces. Such computations are possible with ab initio quantum Monte Carlo methods, see for instance the related computations for neutrinoless double beta decay [179] where similar regulator dependence was observed. We have started such a computation for the ^{3}He EDM but were not able to satisfactorily test the regulator independence due to technical problems with varying the regulator Λ in a broad range. Therefore, the results are not in a state ready to be included in this thesis. Another important open problem is to determine the value of the short-distance counter term. It would be very interesting, but highly non-trivial, to perform an ab initio computation of CSB effects in $dd \to \alpha\pi^0$ reactions to determine the unknown LEC from data.

Chapter 4

CP-violating axion interactions in effective field theory

W. Dekens, J. de Vries, and S. Shain,
"CP-violating axion interactions in effective field theory,"
JHEP 07 (2022) 014, [arXiv:2203.11230].

4.1 Introduction

In the previous chapters, we discuss that the main CP-violating sources of SM are the QCD $\bar{\theta}$-term $\mathcal{L}_{\bar{\theta}} \sim \bar{\theta} G\tilde{G}$ and CKM matrix. The most recent EDM results from neutron [52] and ^{199}Hg [180] atom impose severe constrain on the CP-violating vacuum angle $\bar{\theta} \lesssim 10^{-10}$ [49]. This strict tuning of $\bar{\theta}$ is the strong CP problem that we investigated in Chapter 1; where we introduced the QCD axion, associated with the Peccei-Quinn (PQ) mechanism, as a possible solution [62–65]. The additional advantage of the axion solution is that the axion could be dark matter in our Universe under certain scenarios [181–183]. For these reasons, the axion searches have grown into a massive endeavor on both the experimental and theoretical fronts; see Refs. [184, 185] for recent reviews. Since its initial proposal, the last 45 years of axion searches have not yielded any success.

If the only source of CP-violation is the QCD $\bar{\theta}$ term, then the PQ mechanism removes all CP-violation from the theory after the axion field takes its vev $\langle a \rangle = (\bar{\theta}_{\rm ind} - \bar{\theta}) f_a$ (see Eq. (1.24)). As shown in Fig. 4.1, in this case the axion potential $V(\frac{a}{f_a} + \bar{\theta})$ has minima at $\frac{a}{f_a} + \bar{\theta} = \bar{\theta}_{\rm ind} = 0$. However, in the presence of additional CP-odd interactions, the minimum of the axion potential is shifted as shown in Fig. 4.1, which leaves a remnant of CP-violation behind in the form of an induced

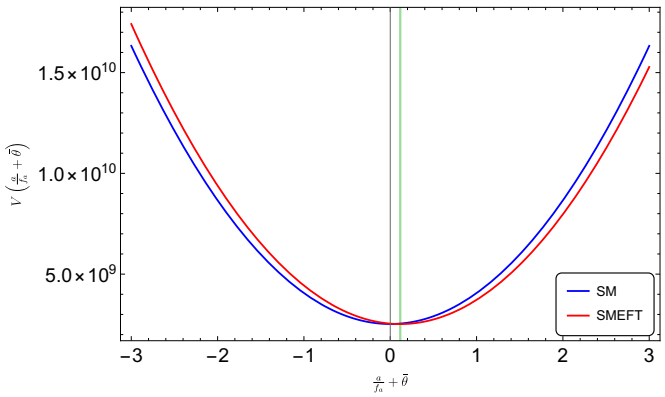

Figure 4.1: The axion potential as a function of $\frac{a}{f_a} + \bar{\theta}$, in SM and the presence of dimension-six *CP*-violating SMEFT operators is shown in blue and red, respectively. The green line indicates the minimum of the latter potential. For illustrative purposes, the only nonzero dimension-six LEC is $L_{\substack{uG \\ uu}} = -2i$ and we choose $\bar{B} = B$.

$\bar{\theta}$ term ($\bar{\theta}_{\text{ind}} \neq 0$) and higher-dimensional operators. The additional sources of *CP*-violation may arise from beyond-the-SM (BSM) physics at a scale Λ well above the electroweak scale. Generic extensions of the SM have additional *CP* phases that cannot be rotated away, something which is reflected by the large number of *CP* invariants in the SM effective field theory (SMEFT) [186]. The number of *CP* invariants is sizable even if one only considers the operators resulting from a minimal seesaw scenario [187,188]. In addition, generating the matter-antimatter asymmetry of the Universe requires additional sources of *CP*-violation.

An interesting property of the SM is that once we choose a small $\bar{\theta}$ at some scale, it remains small in all scales. This happens because the radiative corrections to $\bar{\theta}$ start only at high loop order [57] and lie well below the experimental limit. However, this is only true in the absence of *CP*-violating BSM physics. For example, in certain supersymmetric scenarios, the phases of the soft parameters induce large threshold corrections to $\bar{\theta}$ [189]. In left-right symmetric models (LRSMs) [17, 18, 20, 21, 190] parity can be conserved in the UV so that $\bar{\theta} = 0$ by symmetry. However, after electroweak symmetry breaking, a new $\bar{\theta}$ is induced by phases in the scalar sector of the model [191]. Even models specifically constructed to solve the strong *CP* problem in the UV [192] have severe trouble keeping $\bar{\theta}$ small enough after electroweak symmetry breaking [193]. From an EFT point of view, we can argue that in the presence of higher dimensional *CP*-violating BSM sources, the observed small value of $\bar{\theta}$ is hard to understand [194] without the PQ mechanism.

A natural question is then what the presence of additional sources of *CP*-violation implies for the interactions of the axion. The main consequence is that the pseudoscalar axion field will obtain *CP*-violating scalar couplings to leptons

and quarks (and thus nucleons and atoms) as was already proposed in Ref. [195]. Moreover, the scalar axion-fermion couplings lead to an axion-mediated scalar-scalar (monopole-monopole) potential between atoms. At the same time, they induce a scalar-pseudoscalar (monopole-dipole) potential when combined with the conventional *CP*-conserving pseudoscalar axion-fermion interactions. Experimentalists look for these resulting forces in dedicated experiments; see Refs. [196, 197] for an overview.

As the PQ mechanism acts in the infrared, we can parameterize BSM sources of *CP*-violation in terms of effective higher-dimensional operators. Various studies have computed the scalar axion-nucleon interactions for specific *CP*-odd dimension-six operators such as the quark electric and chromo-electric dipole moments [198, 199] and, more recently, certain four-quark operators [200–202]. The main goal for this part of the thesis is to generalize, extend, and systemize these results. Our starting point is the general set of *CP*-violating effective operators among light SM fields (light quarks, electrons and muons, and photons and gluons). We then compute the axion vev by minimizing the axion potential, align the vacuum to eliminate mesonic tadpoles, and use chiral perturbation theory (χPT), described in Section 2.3, to compute the resulting *CP*-odd axion couplings to mesons, baryons, and leptons.

The second goal for this part of the thesis is to determine the prospects of measuring the resulting *CP*-odd axion interactions. We, therefore, compare the experimental limits on the original *CP*-odd EFT interactions (mainly coming from EDM experiments) to limits on *CP*-odd axion interactions. The latter arise, for instance, from fifth-force searches, violations of the weak equivalence principle, monopole-dipole searches, rare decays, and various astrophysical processes. We find that EDM experiments set very stringent constraints and the prospects of detecting *CP*-violating axion interactions are slim, especially when a single SMEFT operator sources the *CP*-violation. A nonzero signal of *CP*-odd axion couplings would then imply significant cancellations between the contributions to EDMs of multiple operators or a scenario not captured by the EFT involving new light degrees of freedom. We also consider several projected experiments and show that the proposed ARIADNE experiment could detect signs of *CP*-odd axion couplings in parts of parameter space without conflicting with current EDM limits.

Here we do not assume that axions make up dark matter, but note that this assumption would lead to additional interesting signatures, including oscillating EDMs [149, 150, 203–206], which can be searched for in a wide range of experiments [207–210].

This Chapter is organized as follows. First, we introduce the relevant axion interactions and higher-dimensional operators, derive the chiral rotations needed to align the vacuum, and minimize the axion potential in Section 4.2. The resulting Lagrangian is subsequently matched onto chiral perturbation theory in Section 4.3, where the induced *CP*-odd lepton-nucleon and pion-nucleon interactions, as well as the axion-nucleon and axion-lepton couplings, are derived. The contributions of the former to EDM experiments are discussed in Section 4.4,

while Sections 4.5 and 4.6 are dedicated to the effects of the latter in fifth-force, monopole-dipole, and astrophysical searches. We subsequently apply the derived framework to several specific BSM scenarios involving *CP*-violating interactions and a PQ mechanism in Section 4.7. Finally, we conclude in Section 4.8, while several technical details are relegated to several appendices.

4.2 The effective Lagrangian

In this section, we introduce the interactions that can arise from BSM scenarios in which additional sources of *CP*-violation originate at a scale Λ while a PQ mechanism is active at the same time. Assuming that the BSM scale lies well above the electroweak scale, $\Lambda \gg v \simeq 246$ GeV, any new heavy fields can be integrated out, leading to higher-dimensional operators made up of SM fields and the axion. Just below the scale Λ, the resulting interactions between SM fields can be described by the SMEFT [26,27], while the possible axion interactions are given by its coupling to the SM fermions and the $SU(3)_c$, $SU(2)_L$, and $U(1)_Y$ theta terms.

We need to evolve these interactions to the QCD scale, $\mu \simeq 2$ GeV, to describe their effects on EDM experiments and searches for axion-mediated forces. After which, we match them to the chiral perturbation theory (χPT) in terms of leptons, nucleons, and pions instead of leptons, quarks, and gluons. This would require the evolution of the $SU(3)_c \times SU(2)_L \times U(1)_Y$-invariant SMEFT to the electroweak scale and its subsequent matching onto an $SU(3)_c \times U(1)_{\text{em}}$-invariant EFT, sometimes called LEFT [29], see Section 2.2.3. We evolve the resulting LEFT interactions to the QCD scale, where they can finally match onto χPT. In principle, many of the ingredients needed to perform the steps above the QCD scale are available at the one-loop level. For example, the running and matching of the SMEFT and LEFT operators was computed in [111–113, 211, 212], while the renormalization of the axion couplings [213, 214] and the running due to axion loops [215] were discussed more recently. However, we will mainly be concerned with low-energy measurements. In this section, we start directly with the $SU(3)_c \times U(1)_{\text{em}}$-invariant effective theory involving three flavors of quarks (u, d, and s), at a scale of $\mu \sim 2$ GeV. We will briefly comment on the connection to $SU(3)_c \times SU(2)_L \times U(1)_Y$-invariant operators. Nevertheless, the assumption that the EFT below the electroweak scale originates from an $SU(2)_L$-invariant theory will prove useful as it provides additional information about the scaling of certain operators with respect to Λ, as we discuss below.

4.2.1 The interactions

We split the quark-level interactions of the axion-like particle (ALP), a, and the higher-dimensional *CP*-odd sources that we consider into three parts: the SM,

the ALP, and the EFT operators

$$\mathcal{L} = \mathcal{L}_{\text{SM}} + \mathcal{L}_{\text{axion}} + \mathcal{L}_{\text{LEFT}} \,. \tag{4.1}$$

The Standard Model terms

The SM terms that will be relevant for our discussion are

$$\mathcal{L}_{\text{SM}} = \bar{q} i \not{D} q - \bar{q}_L M_0 q_R - \bar{q}_R M_0^\dagger q_L - \bar{\theta} \frac{\alpha_s}{8\pi} \tilde{G}^A_{\mu\nu} G^{A\,\mu\nu} + \dots \,, \tag{4.2}$$

where the dots stand for the lepton sector and the kinetic terms of the gauge fields, while $q = (u, d, s)^T$, $D_\mu = \partial_\mu + i g_s T^A G^A_\mu + ieQA_\mu$, and we work in the quark mass basis $M_0 = \text{Diag}(m_u, m_d, m_s)$. Furthermore, $Q = \text{Diag}(2/3, -1/3, -1/3)$ is the matrix of electromagnetic quark charges, $e = |e|$ is the charge of the proton, and $\tilde{G}^A_{\mu\nu} = \frac{1}{2}\varepsilon_{\mu\nu\alpha\beta} G^{A\,\alpha\beta}$ with $\varepsilon^{0123} = +1$, the Gell-Mann matrices T^A, and color index A.

The axion Lagrangian

The second term in Eq. (4.1) consists of all possible ALP interactions up to dimension-five that are invariant under a shift symmetry, $a \to a + c$, up to total derivatives. These can be written as

$$\begin{aligned} \mathcal{L}_{\text{axion}} \;=\; & \frac{1}{2}\partial_\mu a \partial^\mu a - \frac{\alpha_s}{8\pi}\frac{a}{f_a}\tilde{G}^A_{\mu\nu} G^{A\,\mu\nu} - \frac{1}{4} g^{(0)}_{a\gamma} \frac{a}{f_a} \tilde{F}_{\mu\nu} F^{\mu\nu} \\ & + \sum_{f=\nu,e,q} \frac{\partial_\mu a}{2 f_a} \left[\bar{f}_L c^f_L \gamma^\mu f_L + \bar{f}_R c^f_R \gamma^\mu f_R \right] \,, \end{aligned} \tag{4.3}$$

where $c^f_{L,R}$ are hermitian matrices in flavor space and f_a is the ALP decay constant, indicating the scale related to the PQ mechanism, $\Lambda_a \sim 4\pi f_a$, which we will assume to be above the scale at which the EFT operators are generated, $\Lambda_a \gg \Lambda$. We do not consider the possibility of light right-handed neutrinos [1], so that the term $\sim c^\nu_R$ vanishes.

The interactions in Eq. (4.3) respect a PQ symmetry, $a \to a + c$, at the classical level. The terms involving derivatives are manifestly invariant, while the shifts of the $a\tilde{F}F$ and $a\tilde{G}G$ terms lead to total derivatives, which, in the case of the $\tilde{G}G$ coupling, gives rise to non-perturbative effects that break the PQ symmetry at the quantum level. The Lagrangian of Eq. (4.3) describes all the interactions that are generally induced when the axion arises as the phase of a complex scalar field. However, note that the form of axion-fermion interactions is not unique. Through a redefinition of the fermion fields, one can trade the $c^f_{L,R}$ couplings

[1] The effective theory that systematically includes light right-handed neutrinos is called the νSMEFT [216, 217].

for non-derivative interactions of the form $a\bar{f}_L f_R$ along with a shift of the $a\tilde{F}F$ and/or $a\tilde{G}G$ terms [2].

Finally, as alluded to above, these interactions arise from an $SU(2)_L$-invariant Lagrangian, such as the one discussed in [213]. At the tree level, the matching of the above axion couplings to $F\tilde{F}$ and $G\tilde{G}$ and the fermions are given by

$$\begin{aligned}
&\frac{1}{f_a} = -2\frac{c_{GG}}{f}\,, && && \frac{g_{a\gamma}^{(0)}}{f_a} = -\frac{\alpha}{\pi f}\left(c_{WW}+c_{BB}\right)\,,\\
&\frac{c_L^{(e)}}{f_a} = 2\frac{\boldsymbol{c}_L}{f}\,, && \frac{c_R^{(e)}}{f_a} = 2\frac{\boldsymbol{c}_e}{f}\,, && c_L^{(\nu)} = U_{\text{PMNS}}^\dagger c_L^{(e)} U_{\text{PMNS}}\,,\\
&\frac{c_L^{(q)}}{f_a} = \frac{2}{f}\begin{pmatrix}[\boldsymbol{c}_Q]_{1\times1} & \boldsymbol{0}_{1\times2}\\ \boldsymbol{0}_{2\times1} & \left[V_{\text{CKM}}^\dagger \boldsymbol{c}_Q V_{\text{CKM}}\right]_{2\times2}\end{pmatrix}\,, && \frac{c_R^{(q)}}{f_a} = \frac{2}{f}\begin{pmatrix}[\boldsymbol{c}_u]_{1\times1} & \boldsymbol{0}_{1\times2}\\ \boldsymbol{0}_{2\times1} & [\boldsymbol{c}_d]_{2\times2}\end{pmatrix}\,,
\end{aligned} \tag{4.4}$$

where the right-hand sides correspond to the $SU(2)_L$-invariant couplings in the notation of [213], while U_{PMNS} and V_{CKM} are the PMNS and CKM matrices.

The higher-dimensional operators

Finally, the third term in Eq. (4.1) involves operators of up to dimension-six consisting of SM fields. At energies above the electroweak scale, such operators are described by the SMEFT [26,27]. In contrast, for processes at energies below $\mu \sim m_W$, where the $SU(2)_L$ gauge group of the SM has been broken, these interactions make up the so-called LEFT. The operators in this EFT are invariant under $SU(3)_c \times U(1)_{\text{em}}$ and a complete basis up to dimension-six has been derived in Ref. [29], its Lagrangian can be written as

$$\mathcal{L}_{\text{LEFT}} = \sum_i L_i \mathcal{O}_i\,, \tag{4.5}$$

where the sum extends over all operators in Table 4.1, their flavor indices and hermitian conjugates, when applicable.

Here we do not consider the complete set of operators derived in Ref. [29], as we are only interested in the *CP*-violating ones. Instead, we focus on purely hadronic operators that give unsuppressed contributions to the chiral Lagrangian, i.e., their chiral representations come without derivatives. We also consider LEFT operators that couple the photon or lepton fields to quark currents, which can straightforwardly be included as source terms in the chiral Lagrangian. The hadronic operators give rise to *CP*-odd interactions between nucleons and pions, while the semi-leptonic operators induce couplings of nucleons to leptons. EDM measurements probe both types of interactions. Moreover, as we will see in the

[2] Such terms do not lead to additional independent operators as long as we assume (classical) invariance under the PQ shift symmetry.

upcoming sections, in the presence of a PQ mechanism, the same operators also induce *CP*-odd couplings of the axion to hadrons and leptons, which searches for axion-mediated forces can constrain. The operators that satisfy the above conditions are collected in Table 4.1, while the derivation of this list is discussed in more detail in Appendix C.1.

One possible complication arises due to the fact that Table 4.1 involves both dimension-five and -six operators. For our purposes, the relevant dimension-five operators are the dipole interactions in the $(\bar{\boldsymbol{L}}\boldsymbol{R})\boldsymbol{X}$ class, which, within the LEFT, scale as Λ^{-1}. As we include operators up to dimension-six, scaling as Λ^{-2}, we need to consider terms such as $L_{q\gamma}^2$, L_{qG}^2, or $L_{q\gamma}L_{qG}$ as well since they enter at the same order. However, whenever the LEFT operators originate from an $SU(2)_L$-invariant EFT, the dipole operators are generated by dimension-six operators and scale as $L_{q\gamma,qG} \sim \frac{m_q}{\Lambda^2}$. This is what we will assume in what follows, such that all the operators in Table 4.1 scale as Λ^{-2}. The complete tree-level matching of the LEFT interactions to the SMEFT is given in [212].

Chiral representations

In order to build the chiral Lagrangian in the upcoming section, it is convenient to group the above-described interactions by their transformation properties under the chiral symmetry group $SU(3)_L \times SU(3)_R$. The kinetic terms for the quarks and the axion remain unchanged,

$$\begin{aligned}\mathcal{L} \;=\; & \bar{q}(i\partial\!\!\!/ - g_s\gamma^\mu G_\mu^A T^A)q - \bar{\theta}\frac{\alpha_s}{8\pi}\tilde{G}_{\mu\nu}^A G^{A\,\mu\nu} \\ & + \frac{1}{2}\partial_\mu a \partial^\mu a - \frac{\alpha_s}{8\pi}\frac{a}{f_a}\tilde{G}_{\mu\nu}^A G^{A\,\mu\nu} - \frac{1}{4}g_{a\gamma}^{(0)}\frac{a}{f_a}\tilde{F}_{\mu\nu}F^{\mu\nu} \\ & + \mathcal{L}_{\text{sources}} + \mathcal{L}_6 + \dots\,, \end{aligned} \tag{4.6}$$

while we collect the couplings of quark bilinears to leptons, axions, or photons to quark in $\mathcal{L}_{\text{sources}}$,

$$\mathcal{L}_{\text{sources}} = \bar{q}\Big[\gamma^\mu l_\mu P_L + \gamma^\mu r_\mu P_R - M P_R - M^\dagger P_L + t_R^{\mu\nu}\sigma_{\mu\nu}P_R + t_L^{\mu\nu}\sigma_{\mu\nu}P_L\Big]q\,. \tag{4.7}$$

The electromagnetic gauge couplings, the $c_{L,R}^q$ derivative axion couplings, and semi-leptonic vector operators are now contained in the l_μ and r_μ currents. The quark masses, as well as the scalar and pseudoscalar sources s and p, which contain semi-leptonic scalar interactions, are collected in $M = M_0 + s - ip$, while the tensor sources are denoted by $t_{L,R}^{\mu\nu}$ and capture semi-leptonic tensor interactions as well as the quark EDMs. All of these sources form 3×3 matrices in flavor space and depend on the axion, photon, and lepton fields. Their explicit expressions are given in Appendix C.2.

$(\bar{L}R)X + \text{H.c.}$	
$\mathcal{O}_{u\gamma}$	$\bar{u}_{Lp}\sigma^{\mu\nu}u_{Rr}\,F_{\mu\nu}$
$\mathcal{O}_{d\gamma}$	$\bar{d}_{Lp}\sigma^{\mu\nu}d_{Rr}\,F_{\mu\nu}$
$\mathcal{O}_{uG}$	$\bar{u}_{Lp}\sigma^{\mu\nu}T^A u_{Rr}\,G^A_{\mu\nu}$
$\mathcal{O}_{dG}$	$\bar{d}_{Lp}\sigma^{\mu\nu}T^A d_{Rr}\,G^A_{\mu\nu}$

X^3	
$\mathcal{O}_{\tilde{G}}$	$f^{ABC}\widetilde{G}^{A\nu}_{\mu}G^{B\rho}_{\nu}G^{C\mu}_{\rho}$

$(\bar{L}L)(\bar{L}L)$	
$\mathcal{O}^{V,LL}_{\nu u}$	$(\bar{\nu}_{Lp}\gamma^\mu\nu_{Lr})(\bar{u}_{Ls}\gamma_\mu u_{Lt})$
$\mathcal{O}^{V,LL}_{\nu d}$	$(\bar{\nu}_{Lp}\gamma^\mu\nu_{Lr})(\bar{d}_{Ls}\gamma_\mu d_{Lt})$
$\mathcal{O}^{V,LL}_{eu}$	$(\bar{e}_{Lp}\gamma^\mu e_{Lr})(\bar{u}_{Ls}\gamma_\mu u_{Lt})$
$\mathcal{O}^{V,LL}_{ed}$	$(\bar{e}_{Lp}\gamma^\mu e_{Lr})(\bar{d}_{Ls}\gamma_\mu d_{Lt})$
$\mathcal{O}^{V,LL}_{\nu edu}$	$(\bar{\nu}_{Lp}\gamma^\mu e_{Lr})(\bar{d}_{Ls}\gamma_\mu u_{Lt}) + \text{H.c.}$

$(\bar{R}R)(\bar{R}R)$	
$\mathcal{O}^{V,RR}_{eu}$	$(\bar{e}_{Rp}\gamma^\mu e_{Rr})(\bar{u}_{Rs}\gamma_\mu u_{Rt})$
$\mathcal{O}^{V,RR}_{ed}$	$(\bar{e}_{Rp}\gamma^\mu e_{Rr})(\bar{d}_{Rs}\gamma_\mu d_{Rt})$

$(\bar{L}L)(\bar{R}R)$	
$\mathcal{O}^{V,LR}_{\nu u}$	$(\bar{\nu}_{Lp}\gamma^\mu\nu_{Lr})(\bar{u}_{Rs}\gamma_\mu u_{Rt})$
$\mathcal{O}^{V,LR}_{\nu d}$	$(\bar{\nu}_{Lp}\gamma^\mu\nu_{Lr})(\bar{d}_{Rs}\gamma_\mu d_{Rt})$
$\mathcal{O}^{V,LR}_{eu}$	$(\bar{e}_{Lp}\gamma^\mu e_{Lr})(\bar{u}_{Rs}\gamma_\mu u_{Rt})$
$\mathcal{O}^{V,LR}_{ed}$	$(\bar{e}_{Lp}\gamma^\mu e_{Lr})(\bar{d}_{Rs}\gamma_\mu d_{Rt})$
$\mathcal{O}^{V,LR}_{ue}$	$(\bar{u}_{Lp}\gamma^\mu u_{Lr})(\bar{e}_{Rs}\gamma_\mu e_{Rt})$
$\mathcal{O}^{V,LR}_{de}$	$(\bar{d}_{Lp}\gamma^\mu d_{Lr})(\bar{e}_{Rs}\gamma_\mu e_{Rt})$
$\mathcal{O}^{V,LR}_{\nu edu}$	$(\bar{\nu}_{Lp}\gamma^\mu e_{Lr})(\bar{d}_{Rs}\gamma_\mu u_{Rt}) + \text{H.c.}$
$\mathcal{O}^{V1,LR}_{uu}$	$(\bar{u}_{Lp}\gamma^\mu u_{Lr})(\bar{u}_{Rs}\gamma_\mu u_{Rt})$
$\mathcal{O}^{V8,LR}_{uu}$	$(\bar{u}_{Lp}\gamma^\mu T^A u_{Lr})(\bar{u}_{Rs}\gamma_\mu T^A u_{Rt})$
$\mathcal{O}^{V1,LR}_{ud}$	$(\bar{u}_{Lp}\gamma^\mu u_{Lr})(\bar{d}_{Rs}\gamma_\mu d_{Rt})$
$\mathcal{O}^{V8,LR}_{ud}$	$(\bar{u}_{Lp}\gamma^\mu T^A u_{Lr})(\bar{d}_{Rs}\gamma_\mu T^A d_{Rt})$
$\mathcal{O}^{V1,LR}_{du}$	$(\bar{d}_{Lp}\gamma^\mu d_{Lr})(\bar{u}_{Rs}\gamma_\mu u_{Rt})$
$\mathcal{O}^{V8,LR}_{du}$	$(\bar{d}_{Lp}\gamma^\mu T^A d_{Lr})(\bar{u}_{Rs}\gamma_\mu T^A u_{Rt})$
$\mathcal{O}^{V1,LR}_{dd}$	$(\bar{d}_{Lp}\gamma^\mu d_{Lr})(\bar{d}_{Rs}\gamma_\mu d_{Rt})$
$\mathcal{O}^{V8,LR}_{dd}$	$(\bar{d}_{Lp}\gamma^\mu T^A d_{Lr})(\bar{d}_{Rs}\gamma_\mu T^A d_{Rt})$
$\mathcal{O}^{V1,LR}_{uddu}$	$(\bar{u}_{Lp}\gamma^\mu d_{Lr})(\bar{d}_{Rs}\gamma_\mu u_{Rt}) + \text{H.c.}$
$\mathcal{O}^{V8,LR}_{uddu}$	$(\bar{u}_{Lp}\gamma^\mu T^A d_{Lr})(\bar{d}_{Rs}\gamma_\mu T^A u_{Rt}) + \text{H.c.}$

$(\bar{L}R)(\bar{L}R) + \text{H.c.}$	
$\mathcal{O}^{S,RR}_{eu}$	$(\bar{e}_{Lp}e_{Rr})(\bar{u}_{Ls}u_{Rt})$
$\mathcal{O}^{T,RR}_{eu}$	$(\bar{e}_{Lp}\sigma^{\mu\nu}e_{Rr})(\bar{u}_{Ls}\sigma_{\mu\nu}u_{Rt})$
$\mathcal{O}^{S,RR}_{ed}$	$(\bar{e}_{Lp}e_{Rr})(\bar{d}_{Ls}d_{Rt})$
$\mathcal{O}^{T,RR}_{ed}$	$(\bar{e}_{Lp}\sigma^{\mu\nu}e_{Rr})(\bar{d}_{Ls}\sigma_{\mu\nu}d_{Rt})$
$\mathcal{O}^{S,RR}_{\nu edu}$	$(\bar{\nu}_{Lp}e_{Rr})(\bar{d}_{Ls}u_{Rt})$
$\mathcal{O}^{T,RR}_{\nu edu}$	$(\bar{\nu}_{Lp}\sigma^{\mu\nu}e_{Rr})(\bar{d}_{Ls}\sigma_{\mu\nu}u_{Rt})$
$\mathcal{O}^{S1,RR}_{uu}$	$(\bar{u}_{Lp}u_{Rr})(\bar{u}_{Ls}u_{Rt})$
$\mathcal{O}^{S8,RR}_{uu}$	$(\bar{u}_{Lp}T^A u_{Rr})(\bar{u}_{Ls}T^A u_{Rt})$
$\mathcal{O}^{S1,RR}_{ud}$	$(\bar{u}_{Lp}u_{Rr})(\bar{d}_{Ls}d_{Rt})$
$\mathcal{O}^{S8,RR}_{ud}$	$(\bar{u}_{Lp}T^A u_{Rr})(\bar{d}_{Ls}T^A d_{Rt})$
$\mathcal{O}^{S1,RR}_{dd}$	$(\bar{d}_{Lp}d_{Rr})(\bar{d}_{Ls}d_{Rt})$
$\mathcal{O}^{S8,RR}_{dd}$	$(\bar{d}_{Lp}T^A d_{Rr})(\bar{d}_{Ls}T^A d_{Rt})$
$\mathcal{O}^{S1,RR}_{uddu}$	$(\bar{u}_{Lp}d_{Rr})(\bar{d}_{Ls}u_{Rt})$
$\mathcal{O}^{S8,RR}_{uddu}$	$(\bar{u}_{Lp}T^A d_{Rr})(\bar{d}_{Ls}T^A u_{Rt})$

$(\bar{L}R)(\bar{R}L) + \text{H.c.}$	
$\mathcal{O}^{S,RL}_{eu}$	$(\bar{e}_{Lp}e_{Rr})(\bar{u}_{Rs}u_{Lt})$
$\mathcal{O}^{S,RL}_{ed}$	$(\bar{e}_{Lp}e_{Rr})(\bar{d}_{Rs}d_{Lt})$
$\mathcal{O}^{S,RL}_{\nu edu}$	$(\bar{\nu}_{Lp}e_{Rr})(\bar{d}_{Rs}u_{Lt})$

Table 4.1: The B- and L-conserving operators of the LEFT of dimension-five and -six that contribute to CP-violating effects in the meson sector at leading order. Only the hadronic operators that contribute to the non-derivative meson interactions and the semi-leptonic operators that can be written as external sources (shown in blue) are listed.

Finally, the remaining LEFT operators, which cannot be written as the couplings of quark bilinears, transform under $SU(3)_L \times SU(3)_R$ in several ways. In particular, the quark color-EDM operators transform as $\bar{\mathbf{3}}_\mathbf{L} \times \mathbf{3}_\mathbf{R}$, while the four-quark operators transform as the irreps $\mathbf{8}_\mathbf{L} \times \mathbf{8}_\mathbf{R}$, $\mathbf{3}_\mathbf{L} \times \bar{\mathbf{3}}_\mathbf{R}$, and $\bar{\mathbf{6}}_\mathbf{L} \times \mathbf{6}_\mathbf{R}$. This allows us to write

$$\begin{aligned}
\mathcal{L}_6 = &\left[\bar{q}_L L_5 T^A G^A_{\mu\nu}\sigma^{\mu\nu} q_R + \text{h.c.}\right] \\
&+ L^{ijkl}_{\mathbf{8}\times\mathbf{8}}(\bar{q}^i_L\gamma^\mu q^j_L)\,(\bar{q}^k_R\gamma_\mu q^l_R) + \bar{L}^{ijkl}_{\mathbf{8}\times\mathbf{8}}(\bar{q}^i_L\gamma^\mu T^A q^j_L)\,(\bar{q}^k_R\gamma_\mu T^A q^l_R) \\
&+ \Big[L^{ijkl}_{\mathbf{3}\times\mathbf{3}}(\bar{q}^i_L q^j_R)\,(\bar{q}^k_L q^l_R) + L^{ijkl}_{\mathbf{6}\times\mathbf{6}}(\bar{q}^i_L q^j_R)\,(\bar{q}^k_L q^l_R) \\
&+ \bar{L}^{ijkl}_{\mathbf{3}\times\mathbf{3}}(\bar{q}^i_L T^A q^j_R)\,(\bar{q}^k_L T^A q^l_R) + \bar{L}^{ijkl}_{\mathbf{6}\times\mathbf{6}}(\bar{q}^i_L T^A q^j_R)\,(\bar{q}^k_L T^A q^l_R) + \text{h.c.}\Big],
\end{aligned} \tag{4.8}$$

where $i, j, k, l \in \{1, 2, 3\}$ are flavor indices which are summed over when repeated. Here $L^{ijkl}_{\mathbf{6}\times\mathbf{6}}$ ($L^{ijkl}_{\mathbf{3}\times\mathbf{3}}$) are (a)symmetric in $i \leftrightarrow k$ and $j \leftrightarrow l$, while the $L^{ijkl}_{\mathbf{8}\times\mathbf{8}}$ couplings are traceless in (i, j) and (k, l) and satisfy $L^{ijkl}_{\mathbf{8}\times\mathbf{8}} = L^{jilk\,*}_{\mathbf{8}\times\mathbf{8}}$, so that they project out their particular representations. The explicit expressions for the L_α couplings in terms of the Wilson coefficients of the LEFT are given in Appendix C.3. After collecting the operators either in the external sources or by their chiral representations, we can use Eq. (4.6) as a starting point to derive the chiral Lagrangian.

4.2.2 Vacuum alignment

As the higher-dimensional operators violate *CP* and chiral symmetry, they generally lead to a misalignment of the vacuum. In this case, the $SU(3)$ subgroup of $SU(3)_L \times SU(3)_R$ that is left unbroken by chiral symmetry breaking does not necessarily correspond to the diagonal subgroup, $SU(3)_V$, under which $q_{L,R}$ transform as $q_{L,R} \to U q_{L,R}$. Diagrammatically this corresponds to the appearance of so-called tadpole vertices that allow for meson-vacuum transitions. It is convenient to remove such tadpole diagrams by a non-anomalous chiral rotation, which, at the same time, aligns the unbroken subgroup with $SU(3)_V$. In addition, we will find it helpful to perform an anomalous $U(1)$ chiral rotation that removes the $\tilde{G}G$ and $a\tilde{G}G$ couplings from the quark-level Lagrangian and trade them for $\bar{q}q$ and $a\bar{q}q$ terms. Here we briefly describe these field redefinitions, as well as how the needed angles of rotation can be determined, before constructing the chiral Lagrangian in the next section.

Chiral rotation

All in all we perform the following unitary basis transformation

$$q_L = A^\dagger q'_L\,, \qquad q_R = A q'_R\,, \qquad A = \exp(i\,[\alpha_0/3 + \alpha \cdot t])\,, \tag{4.9}$$

where t are the Gell-Mann matrices in flavor space, we will allow the α_i to depend on the axion field $a(x)$. Here α_0 is the anomalous chiral rotation that removes the $\tilde{G}G$ and $a\tilde{G}G$ terms, while the α_i are chosen to eliminate the tadpoles. This rotation leads to a transformed Lagrangian

$$\mathcal{L}' = \bar{q}(i\partial\!\!\!/ - g_s \gamma^\mu G^A_\mu T^A) q + \frac{1}{2}\partial_\mu a \partial^\mu a - \frac{1}{4} g_{a\gamma} \frac{a}{f_a} \tilde{F}_{\mu\nu} F^{\mu\nu} + \mathcal{L}'_{\text{sources}} + \mathcal{L}'_6 + \dots\,, \tag{4.10}$$

where the $a\tilde{G}G$ terms have been removed by choosing $2\alpha_0 = \theta_a \equiv \bar{\theta} + \frac{a}{f_a}$ while the $a\tilde{F}F$ coupling is given by

$$g_{a\gamma} = g^{(0)}_{a\gamma} - 2N_c \frac{\alpha_0}{\pi} \mathrm{Tr}\left[H_a Q^2\right]\,, \tag{4.11}$$

and H_a is determined by the axion-dependent part of $A = \exp(iH)$, with $H = H_0 + \frac{a}{f_a} H_a$ where $H_{0,a}$ are a-independent matrices in flavor space. $\mathcal{L}'_{\text{sources}}$ and $\mathcal{L}'_6$ can be obtained from the original Lagrangians by the following replacements

$$\begin{aligned}
l_\mu \to l'_\mu &= A\left[l_\mu + i\partial_\mu\right]A^{-1}\,, & r_\mu \to r'_\mu &= A^{-1}\left[r_\mu + i\partial_\mu\right]A\,,\\
S \to S' &= ASA\,, & S &\in \{M\,, t_R^{\mu\nu}\,, L_5\}\,,\\
L_{ijkl} \to L'_{ijkl} &= A_{ia}A^*_{jb}L_{abcd}A^*_{ck}A_{dl}\,, & L &\in \{L_{\mathbf{8}\times\mathbf{8}}\,, \bar{L}_{\mathbf{8}\times\mathbf{8}}\}\,,\\
L_{ijkl} \to L'_{ijkl} &= A_{ia}A_{bj}L_{abcd}A_{kc}A_{dl}\,, & L &\in \{L_{\mathbf{3}\times\mathbf{3}}\,, \bar{L}_{\mathbf{3}\times\mathbf{3}}\,, L_{\mathbf{6}\times\mathbf{6}}\,, \bar{L}_{\mathbf{6}\times\mathbf{6}}\}\,.
\end{aligned} \tag{4.12}$$

This rotation leads to an effective quark mass term that now depends on the *CP*-violating Wilson coefficients, while the higher-dimensional operators generally obtain a dependence on θ_a.

The angles of rotation in A can be determined by requiring that the unbroken subgroup corresponds to $SU(3)_V$. This can be achieved by demanding that the potential is at a minimum

$$\frac{\partial V}{\partial \alpha_i} = 0\,, \qquad V = -\langle 0|\mathcal{L}'_{int}|0\rangle\,, \tag{4.13}$$

and solving for the α_i. One can show that the above condition on the α_i also ensures that the chiral Lagrangian will not induce any tadpole terms. In our particular case, we have $\alpha_{1,2} = \alpha_{4,5} = 0$, as these angles would allow one to remove tadpole terms for the charged mesons, $\pi^\pm$ and $K^\pm$, which are never induced thanks to $U(1)_{\text{em}}$ invariance. The remaining α_i are generally nonzero and become functions of the Wilson coefficients, L_α and the matrix elements of the higher-dimensional operators, while $\langle\theta_a\rangle = \langle a\rangle/f_a$ enters through the axion dependence of the Lagrangian. In the next section, we will introduce the hadronic matrix elements related to the low-energy constants (LECs); we give the explicit relations in Appendix C.1. The vev of the axion field, $\langle a\rangle$, is similarly obtained through minimization of the axion potential. Explicit expressions for the α_i and $\langle a\rangle$ are discussed in Appendix C.5.

Although the solutions obtained from Eq. (4.13) lead to a chiral Lagrangian without tadpole interactions, it will generally mix the pion and axion fields. We can remove such mass-mixing terms by allowing the α_i to depend on the axion field. We can then obtain the needed modification of these angles by including the physical axion field, $a_{\text{ph}}(x)$, whenever the axion vacuum expectation value (vevs) would otherwise appear in the solutions of Eq. (4.13). i.e., we replace $\langle a\rangle \to a \equiv \langle a\rangle + a_{\text{ph}}(x)$. Finally, the chiral Lagrangian, in principle, allows the kinetic terms of the axions and pions fields to become mixed. We can remove such mixings by a redefinition of the axion and pion fields [185], which only modifies the axion-pion interactions beyond the precision of this part of the thesis.

4.3 Chiral Lagrangian

4.3.1 Mesonic Lagrangian

After performing the basis transformations discussed in the previous section, the mesonic part of the chiral Lagrangian becomes

$$\begin{aligned}\mathcal{L}_\pi \;=\; & \frac{F_\pi^2}{4}\mathrm{Tr}\left(D_\mu U D^\mu U^\dagger\right) + \frac{F_\pi^2}{4}\mathrm{Tr}\left(\chi^\dagger U + \chi U^\dagger\right) - F_\pi^2 \bar{B}\mathrm{Tr}\left(L_5'^\dagger U + L_5' U^\dagger\right) \\ & - \frac{F_\pi^4}{4}\left[\mathcal{A}_{\mathbf{8}\times\mathbf{8}} L'^{ijkl}_{\mathbf{8}\times\mathbf{8}} + \bar{\mathcal{A}}_{\mathbf{8}\times\mathbf{8}} \bar{L}'^{ijkl}_{\mathbf{8}\times\mathbf{8}}\right] U_{jk} U^*_{il} \\ & - \frac{F_\pi^4}{8}\Bigg\{\left[\mathcal{A}_{\mathbf{3}\times\mathbf{3}} L'^{ijkl}_{\mathbf{3}\times\mathbf{3}} + \bar{\mathcal{A}}_{\mathbf{3}\times\mathbf{3}} \bar{L}'^{ijkl}_{\mathbf{3}\times\mathbf{3}}\right]\left(U^*_{ij}U^*_{kl} - U^*_{il}U^*_{kj}\right) \\ & \qquad + \left[\mathcal{A}_{\mathbf{6}\times\mathbf{6}} L'^{ijkl}_{\mathbf{6}\times\mathbf{6}} + \bar{\mathcal{A}}_{\mathbf{6}\times\mathbf{6}} \bar{L}'^{ijkl}_{\mathbf{6}\times\mathbf{6}}\right]\left(U^*_{ij}U^*_{kl} + U^*_{il}U^*_{kj}\right) + \text{h.c.}\Bigg\} \\ & - \frac{1}{4} g_{a\gamma}\frac{a}{f_a}\tilde{F}_{\mu\nu}F^{\mu\nu}\,, \end{aligned} \tag{4.14}$$

where we followed the definitions from Section 2.3.3. Furthermore, B, $\bar{B}$, $\mathcal{A}_i$, and $\bar{\mathcal{A}}_i$ are LECs, which are defined in terms of matrix elements of the corresponding operators in Appendix C.1.

The axion field and $\bar{\theta}$ enter through the couplings M' and L'_α and their dependence on the rotation angles, α_i, which are obtained by solving Eq. (4.13). These solutions ensure that the chiral Lagrangian is free of tadpole terms and that the mass matrices do not mix the pion and axion fields. We checked explicitly that the above Lagrangian, together with our solutions of the α_i, satisfies these conditions. By expanding the first two terms of the above Lagrangian one can obtain the axion and meson interactions induced by dimension-four operators. Apart from the usual χPT Lagrangian, this gives rise to the expression for the axion mass

$$m_a = \frac{\sqrt{m_* \bar{B}} F_\pi}{f_a} = \sqrt{\frac{m_*}{m_u + m_d}}\frac{F_\pi}{f_a} m_\pi \simeq 5.9 \cdot 10^6 \left(\frac{\text{eV}}{f_a}\right)\text{GeV}\,, \tag{4.15}$$

where $m_* = (\frac{1}{m_u} + \frac{1}{m_d} + \frac{1}{m_s})^{-1}$. By taking into account the solutions for the α_i and the remaining terms in the above Lagrangian, we can determine the non-standard axion-meson interactions induced by higher-dimensional operators.

4.3.2 Nucleon-pion sector

We can build the πN Lagrangian from the baryon fields (N_v) defined in Section 2.3.3 and several combinations of the Wilson coefficients and meson fields,

$\chi_+ = 2B(u^\dagger M' u^\dagger + u M'^\dagger u)$, $\bar{\chi}_+ = 2\bar{B}(u^\dagger L_5' u^\dagger + u L_5'^\dagger u)$, and

$$\begin{aligned} l^{ijkl}_{\mathbf{8}\times\mathbf{8}} &= u^*_{ai} u_{bj} L'^{abcd}_{\mathbf{8}\times\mathbf{8}} u_{kc} u^*_{ld}\,, \\ l^{ijkl}_{\mathbf{3}\times\mathbf{3},\mathbf{6}\times\mathbf{6}} &= u^*_{ai} u^*_{jb} L'^{abcd}_{\mathbf{3}\times\mathbf{3},\mathbf{6}\times\mathbf{6}} u^*_{ck} u^*_{ld}\,, \end{aligned} \tag{4.16}$$

with analogous definitions for the color-octet operators with Wilson coefficients, $\bar{L}_\alpha$. The different parts of the Lagrangian then take the form (see Section 2.3.3 for notations and $\langle\cdot\rangle$ denote trace over flavor space)

$$\begin{aligned} \mathcal{L}_M^{\pi N} =& \langle \bar{N}_v iv\cdot D N_v\rangle + F\langle \bar{N}_v S_\mu [\hat{u}^\mu, N_v]\rangle + D\langle \bar{N}_v S_\mu \{\hat{u}^\mu, N_v\}\rangle + g_A\langle u^\mu\rangle\langle \bar{N}_v S_\mu N_v\rangle \\ &+ b_0\langle \bar{N}_v N_v\rangle\langle \chi_+\rangle + b_D\langle \bar{N}_v\{N_v,\, \chi_+\}\rangle + b_F\langle \bar{N}_v[\chi_+,\, N_v]\rangle\,, \end{aligned} \tag{4.17}$$

$$\begin{aligned} \mathcal{L}_{L_5}^{\pi N} =& \bar{b}_0\langle \bar{N}_v N_v\rangle\langle \bar{\chi}_+\rangle + \bar{b}_D\langle \bar{N}_v\{N_v,\, \bar{\chi}_+\}\rangle + \bar{b}_F\langle \bar{N}_v[\bar{\chi}_+,\, N_v]\rangle\,, \\ \mathcal{L}^{\pi N}_{\mathbf{8}\times\mathbf{8}} =& a^{(1)}_{\mathbf{8}\times\mathbf{8}}\langle \bar{N}_v N_v\rangle l^{ijji}_{\mathbf{8}\times\mathbf{8}} + (\bar{N}_v)_{ji}(N_v)_{lk} b^{(27)}_{\mathbf{8}\times\mathbf{8}} \left[l^{ijkl}_{\mathbf{8}\times\mathbf{8}}\right]^{\mathbf{27}} \\ &+ a^{(8)}_{\mathbf{8}\times\mathbf{8}}\left[(\bar{N}_v N_v)_{ij} - \frac{\delta_{ij}}{3}\langle N_v\bar{N}_v\rangle\right]\left[l^{jkki}_{\mathbf{8}\times\mathbf{8}} + l^{kijk}_{\mathbf{8}\times\mathbf{8}}\right] \\ &+ b^{(8)}_{\mathbf{8}\times\mathbf{8}}\left[(N_v\bar{N}_v)_{ij} - \frac{\delta_{ij}}{3}\langle N_v\bar{N}_v\rangle\right]\left[l^{jkki}_{\mathbf{8}\times\mathbf{8}} + l^{kijk}_{\mathbf{8}\times\mathbf{8}}\right]\,, \\ \mathcal{L}^{\pi N}_{\mathbf{3}\times\mathbf{3}} =& b^{(1)}_{\mathbf{3}\times\mathbf{3}}\langle \bar{N}_v N_v\rangle l^{iijj}_{\mathbf{3}\times\mathbf{3}} + a^{(8)}_{\mathbf{3}\times\mathbf{3}}\left[(\bar{N}_v N_v)_{ij} - \frac{\delta_{ij}}{3}\langle \bar{N}_v N_v\rangle\right] l^{kkji}_{\mathbf{3}\times\mathbf{3}} \\ &+ b^{(8)}_{\mathbf{3}\times\mathbf{3}}\left[(N_v\bar{N}_v)_{ij} - \frac{\delta_{ij}}{3}\langle \bar{N}_v N_v\rangle\right] l^{kkji}_{\mathbf{3}\times\mathbf{3}} + \text{h.c.}\,, \\ \mathcal{L}^{\pi N}_{\mathbf{6}\times\mathbf{6}} =& b^{(1)}_{\mathbf{6}\times\mathbf{6}}\langle \bar{N}_v N_v\rangle l^{iijj}_{\mathbf{6}\times\mathbf{6}} + a^{(8)}_{\mathbf{6}\times\mathbf{6}}\left[(\bar{N}_v N_v)_{ij} - \frac{\delta_{ij}}{3}\langle \bar{N}_v N_v\rangle\right] l^{kkji}_{\mathbf{6}\times\mathbf{6}} \\ &+ b^{(8)}_{\mathbf{6}\times\mathbf{6}}\left[(N_v\bar{N}_v)_{ij} - \frac{\delta_{ij}}{3}\langle \bar{N}_v N_v\rangle\right] l^{kkji}_{\mathbf{6}\times\mathbf{6}} + b^{(27)}_{\mathbf{6}\times\mathbf{6}}(\bar{N}_v)_{ji}(N_v)_{lk}\left[l^{ijkl}_{\mathbf{6}\times\mathbf{6}}\right]^{\mathbf{27}} + \text{h.c.}\,, \end{aligned} \tag{4.18}$$

where $\hat{u}_\mu = u_\mu - \langle u_\mu\rangle/3$, and $\left[l^{ijkl}_{\mathbf{r}}\right]^{\mathbf{27}}$ stands for the combination of couplings that is symmetric in both $(i \leftrightarrow k)$ and $(j \leftrightarrow l)$ as well as traceless in (i,j), (k,l). The LECs D, F, g_A, and $b_{0,D,F}$ determine the axial and mass terms of the baryons, while the terms generated by the quark color-EDM terms are proportional to $\bar{b}_{0,D,F}$. Finally, $a^{(r')}_{\mathbf{r}}, b^{(r')}_{\mathbf{r}}$ are LECs whose subscripts denote the chiral representation of the corresponding quark-level operator, while the superscripts indicate the representation the baryon fields appear in. For example, $b^{(1)}_{\mathbf{8}\times\mathbf{8}}$ indicates a singlet and therefore appears with the trace of baryon fields, while $b^{(27)}_{\mathbf{8}\times\mathbf{8},\mathbf{6}\times\mathbf{6}}$ indicates the (symmetric) **27** representation and thus appears with a symmetric combination of baryon fields.

The total πN Lagrangian is then given by

$$\mathcal{L}^{\pi N} = \mathcal{L}_M^{\pi N} + \mathcal{L}_{L_5}^{\pi N} + \left[\mathcal{L}^{\pi N}_{\mathbf{8}\times\mathbf{8}} + \mathcal{L}^{\pi N}_{\mathbf{3}\times\mathbf{3}} + \mathcal{L}^{\pi N}_{\mathbf{6}\times\mathbf{6}} + \begin{pmatrix} l_{\mathbf{r}} & \to & \bar{l}_{\mathbf{r}} \\ a_{\mathbf{r}} & \to & \bar{a}_{\mathbf{r}} \\ b_{\mathbf{r}} & \to & \bar{b}_{\mathbf{r}} \end{pmatrix}\right]\,, \tag{4.19}$$

with $\mathbf{r} = \{\mathbf{8}\times\mathbf{8}, \mathbf{3}\times\mathbf{3}, \mathbf{6}\times\mathbf{6}\}$.

4.3.3 Interactions from semi-leptonic operators

The semi-leptonic operators of Table 4.1 enter the meson and nucleon Lagrangians through the source terms. The most important *CP*-violating axion couplings arise from the scalar operators, which contribute to the sources s and p and enter the chiral Lagrangian through χ. In the nucleon sector, these terms induce $\bar{N}N\bar{e}i\gamma_5 e$ interactions ($N = (p\ n)^T$), while $a\bar{e}e$ and $\pi\bar{e}e$ couplings appear in the mesonic Lagrangian. The latter gives rise to *CP*-odd spin-dependent nucleon-lepton couplings through pion exchange at low energies. The axion-lepton couplings can be probed by searches for axion-mediated forces, while EDMs are sensitive to the *CP*-odd hadron-lepton interactions.

Axion-lepton couplings

The relevant interactions are

$$\begin{aligned}\mathcal{L}_{a\bar{l}l} &= g_S^{(e)} a\bar{e}e\,,\\ g_S^{(e)} &= \frac{m_* B F_\pi^2}{2f_a}\mathrm{Im}\left[\frac{1}{m_u}L^{\mathrm{S,RR}}_{\substack{eu\\eeuu}} + \frac{1}{m_d}L^{\mathrm{S,RR}}_{\substack{ed\\eedd}} + \frac{1}{m_s}L^{\mathrm{S,RR}}_{\substack{ed\\eess}} - (RR\to RL)\right]\,. \end{aligned} \tag{4.20}$$

Here we have focused on couplings to electrons, but by replacing $e \to \{\mu, \tau\}$ in the above expressions, we also obtain scalar couplings to muons and taus. While the experimental limits on these couplings are less stringent than for electron-axion couplings, it should be kept in mind that the indirect limits, arising from the μ and τ EDMs [218, 219], are also weaker. By allowing for lepton flavor-violating dimension-six couplings, e.g. $L^{\mathrm{S,RR}}_{\substack{eu\\e\mu uu}}$, we also induce couplings of the form $a\,\bar{e}\mu$ that can be probed in $\mu \to e + a$ searches. However, the $L^{\mathrm{S,RR}}_{\substack{eu\\e\mu uu}}$ dimension-six operators are stringently constrained by muon-to-electron conversion ($\mu + N \to e + N$) experiments [220, 221], and we leave a detailed study of these couplings to future work.

In principle, the *CP*-violating phase in the CKM matrix, δ_{CKM}, in the SM can also induce $g_S^{(e)}$ although we are not aware of estimates in the literature (the estimates for the coupling to nucleons is discussed in Section 4.3.4). It is clear these couplings must be proportional to m_e due to the scalar nature of $g_S^{(e)}$. Furthermore, at least two insertions of the weak interactions, $\sim G_F^2$, are needed to obtain the *CP*-violating combination of CKM elements, given by the Jarlskog invariant $J_{CP} \simeq 3\cdot 10^{-5}$ [222]. While there are many ways to combine these interactions, using naive dimensional analysis [127, 223] to estimate one of the possibilities leads to,

$$g_S^{(e)}(\delta_{\mathrm{CKM}}) f_a \sim m_e \left(\frac{\alpha}{4\pi}\right)^2 \left(G_F F_\pi^2\right)^2 J_{CP} \sim 10^{-25}\,\mathrm{MeV}\,, \tag{4.21}$$

These contributions can be seen to be induced by a $\Delta S = 1$ Fermi interaction, which, together with electromagnetism, can induce couplings $\sim K^0 F_{\mu\nu} F^{\mu\nu}$ in the chiral Lagrangian. Such terms can subsequently generate a $\sim m_e K^0 \bar{e} e$ coupling through a one-loop diagram. Finally, an additional insertion of a $\Delta S = 1$ Fermi interaction can generate mixing between the kaon and the axion, thereby giving rise to the axion-electron coupling. While it is certainly possible that other contributions are enhanced with respect to the above estimate, Eq. (4.21) should give a rough lower limit on $g_S^{(e)}(\delta_{\rm CKM})$.

Semi-leptonic couplings

The induced nucleon-lepton interactions that contribute to EDMs can be written as,

$$\mathcal{L} = -\frac{G_F}{\sqrt{2}} \left\{ \bar{e} i\gamma_5 e\, \bar{N} \left(C_S^{(0)} + \tau_3 C_S^{(1)} \right) N + \bar{e} e \frac{\partial_\mu}{m_N} \left[\bar{N} \left(C_P^{(0)} + \tau_3 C_P^{(1)} \right) S^\mu N \right] \right\} + \dots , \tag{4.22}$$

where G_F is the Fermi constant and $N = (p\ n)^T$ is the non-relativistic nucleon doublet with mass m_N. The matching coefficients are given by

$$\begin{aligned}
C_S^{(0)} &= -v_H^2 \frac{\sigma_{\pi N}}{m_u + m_d} \mathrm{Im} \left[L^{\mathrm{S,RR}}_{\substack{eu \\ eeuu}} + L^{\mathrm{S,RR}}_{\substack{ed \\ eedd}} \right] - v_H^2 \frac{\sigma_s}{m_s} \mathrm{Im} \left[L^{\mathrm{S,RR}}_{\substack{ed \\ eess}} \right] + (RR \to RL) \,, \\
C_S^{(1)} &= -v_H^2 \frac{1}{2} \frac{\delta m_N}{m_d - m_u} \mathrm{Im} \left[L^{\mathrm{S,RR}}_{\substack{eu \\ eeuu}} - L^{\mathrm{S,RR}}_{\substack{ed \\ eedd}} + (RR \to RL) \right] , \\
C_P^{(0)} &= -v_H^2 \frac{m_N B(D-3F)}{3 m_\eta^2} \mathrm{Im} \left[L^{\mathrm{S,RL}}_{\substack{eu \\ eeuu}} + L^{\mathrm{S,RL}}_{\substack{ed \\ eedd}} - 2 L^{\mathrm{S,RL}}_{\substack{ed \\ eess}} - (RL \to RR) \right] , \\
C_P^{(1)} &= v_H^2 \frac{m_N B g_A}{m_\pi^2} \mathrm{Im} \left[L^{\mathrm{S,RL}}_{\substack{eu \\ eeuu}} - L^{\mathrm{S,RL}}_{\substack{ed \\ eedd}} - (RL \to RR) \right] ,
\end{aligned} \tag{4.23}$$

where v_H is the vev of the Higgs field, at tree level $v_H^2 = \left(\sqrt{2} G_F\right)^{-1} \simeq (246\,\mathrm{GeV})^2$, while $C_P^{(0)}$ and $C_P^{(1)}$ arise from the exchange of an η and π^0, respectively. Here $C_S^{(0,1)}$ induce *CP*-odd effects in ThO and the mercury EDM, while $C_P^{(0,1)}$ only contribute to the latter. Furthermore, $g_A = D + F$ is the axial charge of the nucleon, $\delta m_N = (m_n - m_p)_{QCD}$ is the strong nucleon mass splitting, while the nucleon sigma terms are given by $\sigma_q = m_q \frac{\partial \Delta m_N}{\partial m_q}$, where $\Delta m_N = \frac{m_n + m_p}{2}$, and $\sigma_{\pi N} = \sigma_u + \sigma_d$. The input for these hadronic matrix elements can be summarized as [155, 224–227]

$$\begin{aligned}
\sigma_{\pi N} &= (59.1 \pm 3.5)\,\mathrm{MeV} \,, \qquad \sigma_s = (41.1^{+11.3}_{-10.0})\,\mathrm{MeV} \,, \\
\delta m_N &= (2.32 \pm 0.17)\,\mathrm{MeV} \,, \qquad g_A = 1.27 \pm 0.002 \,.
\end{aligned} \tag{4.24}$$

4.3.4 Interactions from hadronic operators

Axion-meson-meson couplings

Although we will mainly focus on the couplings of the axion to nucleons in what follows, here we briefly discuss the *CP*-odd interactions between axions and mesons that arise from Eq. (4.14). These interactions contribute to the axion-mediated potential between nuclei through the second and third diagrams in Fig. 4.2. However, they are typically subleading with respect to direct axion-nucleon interactions discussed in the following subsection.

Apart from contributing to axion-mediated forces between nucleons, the meson-axion interactions can also give rise to rare decays of kaons and the η. In particular, the strangeness-violating operators induce the decay $K \to \pi a$. For example, the strangeness-changing elements of the $L_{\mathbf{3}\times\mathbf{3}}$ Wilson coefficients induce the vertex

$$\begin{aligned}\mathcal{L}_{aK\pi} &= g_{aK\pi}\, aK^+\pi^- + \text{h.c.} \\ &= im_* F_\pi^2 \mathcal{A}_{\mathbf{3}\times\mathbf{3}} \frac{4m_d m_s(m_d+m_s) + (3m_d+m_s)(m_d+3m_s)m_u}{16 m_d m_u m_s (m_d+m_s)} \\ &\quad \times \left[\left(L^{2311}_{\mathbf{3}\times\mathbf{3}}\right)^* - L^{3211}_{\mathbf{3}\times\mathbf{3}}\right] \frac{a}{f_a} K^+\pi^- + \text{h.c.}\,. \end{aligned} \tag{4.25}$$

The general form of the meson-meson-axion interactions is discussed in Appendix C.6.

For axion masses $m_a < 2m_e$, the only available decay channel is $a \to \gamma\gamma$, which is induced by the model-dependent *CP*-even $g_{a\gamma}$ coupling of Eq. (4.10) [3]. In this case, the axion lifetime is given by [185]

$$\tau = \frac{64\pi}{g_{a\gamma}^2}\frac{f_a^2}{m_a^3} \simeq \frac{5\cdot 10^{18}}{g_{a\gamma}^2}\left(\frac{\text{eV}}{m_a}\right)^5 \text{s}\,. \tag{4.26}$$

Since we focus on the range $m_a < 2m_e$ and $g_{a\gamma} = \mathcal{O}(\alpha/\pi)$ we can treat the axion as stable in meson decays, implying $K^+ \to \pi^+ a$ and $K^+ \to \pi^+ \nu\bar{\nu}$ will have the same experimental signature, i.e., $K^+ \to \pi^+$ with missing energy and momentum. We use the upper limit on $\text{BR}(K^+ \to \pi^+ a)$ set by the NA62 experiment [228–230] to constrain $g_{aK\pi}$

$$\text{BR}(K^+ \to \pi^+ a) \simeq \frac{\tau_K}{16\pi m_K}\frac{m_K^2 - m_\pi^2}{m_K^2}|g_{aK\pi}|^2 < 5\cdot 10^{-11}\,, \tag{4.27}$$

for $m_a \ll m_\pi$. For the couplings of Eq. (4.25), this implies

$$\left(\frac{m_a}{\text{eV}}\right)^2 \left|\left(L^{2311}_{\mathbf{3}\times\mathbf{3}}\right)^* - L^{3211}_{\mathbf{3}\times\mathbf{3}}\right|^2 \text{TeV}^4 \leq 6.4\cdot 10^5\,, \tag{4.28}$$

[3] The derivative axion couplings to fermions, $c_R^{(f)} - c_L^{(f)}$, also contribute to $a \to \gamma\gamma$. However, these contributions can be captured by an effective $g_{a\gamma}^{\text{eff}} \sim g_{a\gamma} + \frac{\alpha}{\pi}(c_R^{(f)} - c_L^{(f)})$, after a chiral rotation.

implying TeV-level constraints on Λ for axion masses in the keV range.

At the same time, the $\Delta S = 1$ *CP*-odd operators induce *CP*-violation in kaon decays, thereby contributing to ε'. Using the expressions and estimates for the LECs in [231], we obtain

$$\left(\frac{\varepsilon'}{\varepsilon}\right)_{\mathbf{3\times3}} \simeq 62\,\text{TeV}^2\,\text{Im}\left(\left(L^{2311}_{\mathbf{3\times3}}\right)^* - L^{3211}_{\mathbf{3\times3}}\right)\,, \tag{4.29}$$

implying that ε' is sensitive to very high scales. The ε' and ε are related to the *CP*-violation induced asymmetries in the kaon to two pion decays [232]. If we conservatively demand that this contribution is smaller than the measured value [4], $\left(\frac{\varepsilon'}{\varepsilon}\right)_{\text{expt.}} = (16.6 \pm 2.3)\cdot 10^{-4}$ [236], we obtain $\Lambda \gtrsim 193$ TeV significantly more stringent than the $K^+ \to \pi^+ + a$ limits, for $m_a \lesssim$ keV.

Axion-nucleon couplings

We can split the axion couplings to the nucleons into an isoscalar and isovector component,

$$\mathcal{L}_{a\bar{N}N} = a\bar{N}\left[g_S^{(0)} + g_S^{(1)}\tau_3\right]N\,, \qquad g_S^{(p,n)} = g_S^{(0)} \pm g_S^{(1)}\,. \tag{4.30}$$

These axion-nucleon couplings receive an 'indirect' contribution from Eq. (4.17), which appears after vacuum alignment, as well as a 'direct' contribution that arises from Eq. (4.18), which we write as $g_\alpha = g_\alpha|_{\text{dir}} + g_\alpha|_{\text{ind}}$. The 'direct' and 'indirect' pieces can be written as

$$g_S^{(0,1)}|_{\text{dir}} = \frac{m_*}{f_a}\sum_i \frac{\partial\alpha_i^{(0,1)}}{\partial \text{Re}\, L_i}\text{Im}\, L_i\,, \tag{4.31}$$

$$g_S^{(0,1)}|_{\text{ind}} = \frac{m_*}{f_a}\sum_i \beta_i^{(0,1)}\text{Im}\, L_i\,. \tag{4.32}$$

where the coefficients $\alpha^{(0,1)}$ and $\beta^{(0,1)}$ are given in Table 4.2. Here the symmetry properties of the L_α^{ijkl}, described below Eq. (4.8), were used to rewrite all couplings in terms of those appearing in the table. The expressions in Table 4.2 employ the following combinations of quark masses

$$\bar{m} = \frac{m_u + m_d}{2}\,, \qquad \bar{m}\epsilon = \frac{m_d - m_u}{2}\,, \tag{4.33}$$

and combination of nucleon masses

$$\Delta m_N = \frac{m_n + m_p}{2}\,, \qquad \delta m_N = m_n - m_p\,. \tag{4.34}$$

[4] See e.g. [233–235] for discussions on recent evaluations of the SM contribution based on lattice QCD, χPT, and dual QCD.

	$\alpha_i^{(0)}$	$\beta_i^{(0)}$	$\alpha_i^{(1)}$	$\beta_i^{(1)}$
L^{dG}_{uu}	$\frac{\Delta m_N}{m_u}$	$2\frac{\bar{B}}{Bm_u}\frac{\partial \Delta m_N}{\partial m_u}$	$-\frac{\delta m_N}{2m_u}$	$-\frac{\bar{B}}{2Bm_d}\frac{\partial \delta m_N}{\partial(\bar{m}\epsilon)}$
L^{dG}_{dd}	$\frac{\Delta m_N}{m_d}$	$2\frac{\bar{B}}{Bm_d}\frac{\partial \Delta m_N}{\partial m_d}$	$-\frac{\delta m_N}{2m_d}$	$\frac{\bar{B}}{2Bm_u}\frac{\partial \delta m_N}{\partial(\bar{m}\epsilon)}$
L^{dG}_{ss}	$\frac{\Delta m_N}{m_s}$	$2\frac{\bar{B}}{Bm_s}\frac{\partial \Delta m_N}{\partial m_s}$	0	0
$L^{2112}_{\mathbf{8}\times\mathbf{8}}$	$\frac{m_u-m_d}{m_d m_u}\Delta m_N$	$\frac{F_\pi^2 \mathcal{A}_{\mathbf{8}\times\mathbf{8}}}{2B}\frac{m_u-m_d}{m_u m_d}\frac{\partial \Delta m_N}{\partial m_u}$	0	$-\frac{F_\pi^2 \mathcal{A}_{\mathbf{8}\times\mathbf{8}}}{8B}\frac{m_u+m_d}{m_u m_d}\frac{\partial \delta m_N}{\partial(\bar{m}\epsilon)}$
$L^{3113}_{\mathbf{8}\times\mathbf{8}}$	$\frac{m_u-m_s}{m_u m_s}\Delta m_N$	$\frac{F_\pi^2 \mathcal{A}_{\mathbf{8}\times\mathbf{8}}}{2B}\left[\frac{1}{m_s}\frac{\partial \Delta m_N}{\partial m_s}-\frac{1}{m_u}\frac{\partial \Delta m_N}{\partial m_u}\right]$	$\frac{m_s-m_u}{2m_u m_s}\delta m_N$	$-\frac{F_\pi^2 \mathcal{A}_{\mathbf{8}\times\mathbf{8}}}{8B}\frac{1}{m_u}\frac{\partial \delta m_N}{\partial(\bar{m}\epsilon)}$
$L^{3223}_{\mathbf{8}\times\mathbf{8}}$	$\frac{m_d-m_s}{m_d m_s}\Delta m_N$	$\frac{F_\pi^2 \mathcal{A}_{\mathbf{8}\times\mathbf{8}}}{2B}\left[\frac{1}{m_s}\frac{\partial \Delta m_N}{\partial m_s}-\frac{1}{m_d}\frac{\partial \Delta m_N}{\partial m_d}\right]$	$\frac{m_s-m_d}{2m_d m_s}\delta m_N$	$\frac{F_\pi^2 \mathcal{A}_{\mathbf{8}\times\mathbf{8}}}{8B}\frac{1}{m_d}\frac{\partial \delta m_N}{\partial(\bar{m}\epsilon)}$
$L^{2211}_{\mathbf{3}\times\mathbf{3}}$	$\frac{m_d+m_u}{m_d m_u}\Delta m_N$	$\frac{F_\pi^2 \mathcal{A}_{\mathbf{3}\times\mathbf{3}}}{B}\frac{m_d+m_u}{m_u m_d}\frac{\partial \Delta m_N}{\partial m_u}$	0	$\frac{F_\pi^2 \mathcal{A}_{\mathbf{3}\times\mathbf{3}}}{4B}\frac{m_d-m_u}{m_u m_d}\frac{\partial \delta m_N}{\partial(\bar{m}\epsilon)}$
$L^{3311}_{\mathbf{3}\times\mathbf{3}}$	$\frac{m_s+m_u}{m_s m_u}\Delta m_N$	$\frac{F_\pi^2 \mathcal{A}_{\mathbf{3}\times\mathbf{3}}}{B}\left[\frac{1}{m_u}\frac{\partial \Delta m_N}{\partial m_u}+\frac{1}{m_s}\frac{\partial \Delta m_N}{\partial m_s}\right]$	$-\frac{m_s+m_u}{2m_s m_u}\delta m_N$	$\frac{F_\pi^2 \mathcal{A}_{\mathbf{3}\times\mathbf{3}}}{4B}\frac{1}{m_u}\frac{\partial \delta m_N}{\partial(\bar{m}\epsilon)}$
$L^{3322}_{\mathbf{3}\times\mathbf{3}}$	$\frac{m_d+m_s}{m_d m_s}\Delta m_N$	$\frac{F_\pi^2 \mathcal{A}_{\mathbf{3}\times\mathbf{3}}}{B}\left[\frac{1}{m_d}\frac{\partial \Delta m_N}{\partial m_d}+\frac{1}{m_s}\frac{\partial \Delta m_N}{\partial m_s}\right]$	$-\frac{m_s+m_d}{2m_s m_d}\delta m_N$	$-\frac{F_\pi^2 \mathcal{A}_{\mathbf{3}\times\mathbf{3}}}{4B}\frac{1}{m_d}\frac{\partial \delta m_N}{\partial(\bar{m}\epsilon)}$
$L^{2211}_{\mathbf{6}\times\mathbf{6}}$	$\frac{m_d+m_u}{m_d m_u}\Delta m_N$	$\frac{F_\pi^2 \mathcal{A}_{\mathbf{6}\times\mathbf{6}}}{B}\frac{m_d+m_u}{m_u m_d}\frac{\partial \Delta m_N}{\partial m_u}$	0	$\frac{F_\pi^2 \mathcal{A}_{\mathbf{6}\times\mathbf{6}}}{4B}\frac{m_d-m_u}{m_u m_d}\frac{\partial \delta m_N}{\partial(\bar{m}\epsilon)}$
$L^{3311}_{\mathbf{6}\times\mathbf{6}}$	$\frac{m_u+m_s}{m_u m_s}\Delta m_N$	$\frac{F_\pi^2 \mathcal{A}_{\mathbf{6}\times\mathbf{6}}}{B}\left[\frac{1}{m_u}\frac{\partial \Delta m_N}{\partial m_d}+\frac{1}{m_s}\frac{\partial \Delta m_N}{\partial m_s}\right]$	$-\frac{m_u+m_s}{2m_u m_s}\delta m_N$	$\frac{F_\pi^2 \mathcal{A}_{\mathbf{6}\times\mathbf{6}}}{4B}\frac{1}{m_u}\frac{\partial \delta m_N}{\partial(\bar{m}\epsilon)}$
$L^{3322}_{\mathbf{6}\times\mathbf{6}}$	$\frac{m_d+m_s}{m_d m_s}\Delta m_N$	$\frac{F_\pi^2 \mathcal{A}_{\mathbf{6}\times\mathbf{6}}}{B}\left[\frac{1}{m_d}\frac{\partial \Delta m_N}{\partial m_d}+\frac{1}{m_s}\frac{\partial \Delta m_N}{\partial m_s}\right]$	$-\frac{m_d+m_s}{2m_d m_s}\delta m_N$	$-\frac{F_\pi^2 \mathcal{A}_{\mathbf{6}\times\mathbf{6}}}{4B}\frac{1}{m_d}\frac{\partial \delta m_N}{\partial(\bar{m}\epsilon)}$
$L^{1111}_{\mathbf{6}\times\mathbf{6}}$	$2\frac{\Delta m_N}{m_u}$	$\frac{F_\pi^2 \mathcal{A}_{\mathbf{6}\times\mathbf{6}}}{B}\frac{1}{m_u}\frac{\partial \Delta m_N}{\partial m_u}$	$-\frac{\delta m_N}{m_u}$	$\frac{F_\pi^2 \mathcal{A}_{\mathbf{6}\times\mathbf{6}}}{4B}\frac{1}{m_u}\frac{\partial \delta m_N}{\partial(\bar{m}\epsilon)}$
$L^{2222}_{\mathbf{6}\times\mathbf{6}}$	$2\frac{\Delta m_N}{m_d}$	$\frac{F_\pi^2 \mathcal{A}_{\mathbf{6}\times\mathbf{6}}}{B}\frac{1}{m_d}\frac{\partial \Delta m_N}{\partial m_d}$	$-\frac{\delta m_N}{m_d}$	$-\frac{F_\pi^2 \mathcal{A}_{\mathbf{6}\times\mathbf{6}}}{4B}\frac{1}{m_d}\frac{\partial \delta m_N}{\partial(\bar{m}\epsilon)}$
$L^{3333}_{\mathbf{6}\times\mathbf{6}}$	$2\frac{\Delta m_N}{m_s}$	$\frac{F_\pi^2 \mathcal{A}_{\mathbf{6}\times\mathbf{6}}}{B}\frac{1}{m_s}\frac{\partial \Delta m_N}{\partial m_s}$	0	0

Table 4.2: Coefficients determining the contributions to the axion-nucleon couplings. $g_S^{(0,1)} = \frac{m_*}{f_a}\sum_i \left[\frac{\partial}{\partial \mathrm{Re}\, L_i}\alpha_i^{(0,1)} + \beta_i^{(0,1)}\right] \mathrm{Im}\, L_i$, where i runs over all the Wilson coefficients in the table. Wilson coefficients that do not appear above have either been rewritten using the symmetry properties described below Eq. (4.8) or do not contribute. Note that, we have the following relations at LO $2\frac{\partial \Delta m_N}{\partial m_{u,d}} = \frac{\Delta m_N(m_q)}{\bar{m}} = \frac{\sigma_{\pi N}}{\bar{m}}$.

Couplings to baryons containing valence strange quarks involve mass combinations of the full baryon octet. The expressions in Eqs. (4.31) and (4.32) involve the derivatives of these baryon-mass combinations with respect to the quark masses, written in terms of $\bar{m}$, $\bar{m}\epsilon$, and m_s, as well as the real parts of Wilson coefficients, Re L_α. The dependence on these quantities arises from contributions to the baryon masses of Eq. (4.17) and Eq. (4.18), respectively.

For comparison, we briefly discuss the expected size of the scalar axion-nucleon coupling in the pure Standard Model. In this case, the *CP*-odd couplings arise

from the CKM phase $\delta_{\rm CKM}$. Ref. [237] estimated

$$g_S^{(0)}(\delta_{\rm CKM}) \simeq m_* J_{CP} G_F^2 F_\pi^4 / f_a \simeq 10^{-18}\,{\rm MeV}/f_a\,, \tag{4.35}$$

with $J_{CP} \simeq 3 \cdot 10^{-5}$ [222]. Similar-sized contributions arise from CKM-induced contributions to the light-quark chromo-EDMs. In that case, the estimate can be enhanced by a power m_c^2/F_π^2 but additional loop suppression lead to a very similar estimate of $g_S^{(0)}(\delta_{\rm CKM})$ [199]. Long-distance contributions involving hyperons also appear to be of similar size [199]. We, therefore, take Eq. (4.35) as a rough indication of the size of *CP*-odd axion-nucleon couplings within the Standard Model.

Pion-nucleon couplings

The *CP*-odd pion-nucleon couplings can be written as

$$\mathcal{L}_{\pi\bar{N}N} = \bar{N}\left[\bar{g}_0 \boldsymbol{\tau}\cdot\boldsymbol{\pi} + \bar{g}_1\pi_0 + \bar{g}_2\left(\tau_3\pi_0 - \frac{1}{3}\boldsymbol{\pi}\cdot\boldsymbol{\tau}\right)\right]N\,, \tag{4.36}$$

where $\bar{g}_{0,1,2}$ denote the isoscalar, isovector, and isotensor terms, respectively. The direct pieces of these couplings are related to the axion-nucleon couplings as follows

$$\begin{aligned}
\bar{g}_0|_{\rm dir} &= \tilde{g}_S^{(1)}|_{\rm dir} - \frac{2}{3}\bar{g}_2|_{\rm dir}\,, \qquad \bar{g}_1|_{\rm dir} = \tilde{g}_S^{(0)}|_{\rm dir}\,,\\
\bar{g}_2|_{\rm dir} &= \frac{1}{F_\pi}\left[{\rm Im}\, L^{2211}_{\mathbf{6}\times\mathbf{6}}\frac{d}{d\,{\rm Re}\, L^{2211}_{\mathbf{6}\times\mathbf{6}}}\left(\Delta m_{\Sigma^0} + \Delta m_{\Sigma^-} - 2\Delta m_{\Xi^-}\right)\right.\\
&\quad \left. + \sum_a t_3^a {\rm Im}\, L^{aaaa}_{\mathbf{6}\times\mathbf{6}}\frac{d}{d\,{\rm Re}\, L^{aaaa}_{\mathbf{6}\times\mathbf{6}}}\delta m_N\right],
\end{aligned} \tag{4.37}$$

where $t_3^a \equiv (t_3)_{aa}$ and $\tilde{g}_S^{(0,1)}|_{\rm dir}$ can be obtained from $g_S^{(0,1)}|_{\rm dir}$ in Eq. (4.31) by using the following replacement rules on the imaginary parts of the appearing Wilson coefficients [5]

$$\begin{aligned}
L_5^{ab} &\to -\frac{2f_a}{m_* F_\pi}\left(t_3^a + t_3^b\right)\left(\frac{1}{m_a} + \frac{1}{m_b}\right)^{-1} L_5^{ab}\,,\\
L_{\mathbf{r}}^{abcd} &\to -\frac{2f_a}{m_* F_\pi}\left(t_3^a + t_3^b + t_3^c + t_3^d\right)\left(\frac{1}{m_a} + \frac{1}{m_b} + \frac{1}{m_c} + \frac{1}{m_d}\right)^{-1} L_{\mathbf{r}}^{abcd}\,,\\
&\qquad\qquad \mathbf{r} \in \{\mathbf{3}\times\mathbf{3}\,, \mathbf{6}\times\mathbf{6}\}\,,\\
L_{\mathbf{r}}^{abcd} &\to -\frac{2f_a}{m_* F_\pi}\left(t_3^a - t_3^b - t_3^c + t_3^d\right)\left(\frac{1}{m_a} - \frac{1}{m_b} - \frac{1}{m_c} + \frac{1}{m_d}\right)^{-1} L_{\mathbf{r}}^{abcd}\,,\\
&\qquad\qquad \mathbf{r} = \mathbf{8}\times\mathbf{8}\,,
\end{aligned} \tag{4.38}$$

[5] The partial derivatives with respect to the real parts of the Wilson coefficients should be left unchanged.

where the repeated indices were not summed over. We can write the indirect contributions as

$$\begin{aligned}
\bar{g}_0|_{\rm ind} &= -\frac{F_\pi}{4B}\sum_{a,b}{\rm Im}\Bigg[\left(|t_3^a|+|t_3^b|\right)\left(\mathcal{A}_{\mathbf{3}\times\mathbf{3}}L^{aabb}_{\mathbf{3}\times\mathbf{3}}+\mathcal{A}_{\mathbf{6}\times\mathbf{6}}L^{aabb}_{\mathbf{6}\times\mathbf{6}}+2\delta^{ab}\frac{\bar{B}}{F_\pi^2}L_5^{aa}\right)\\
&\quad+\frac{1}{2}\left(|t_3^a|-|t_3^b|\right)\mathcal{A}_{\mathbf{8}\times\mathbf{8}}L^{abba}_{\mathbf{8}\times\mathbf{8}}\Bigg]\frac{\partial\delta m_N}{\partial(\bar{m}\epsilon)}\,,\\
\bar{g}_1|_{\rm ind} &= -\frac{F_\pi}{2B}\sum_{a,b}{\rm Im}\Bigg[\left(t_3^a+t_3^b\right)\left(\mathcal{A}_{\mathbf{3}\times\mathbf{3}}L^{aabb}_{\mathbf{3}\times\mathbf{3}}+\mathcal{A}_{\mathbf{6}\times\mathbf{6}}L^{aabb}_{\mathbf{6}\times\mathbf{6}}+2\delta^{ab}\frac{\bar{B}}{F_\pi^2}L_5^{aa}\right)\\
&\quad+\frac{1}{2}\left(t_3^a-t_3^b\right)\mathcal{A}_{\mathbf{8}\times\mathbf{8}}L^{abba}_{\mathbf{8}\times\mathbf{8}}\Bigg]\frac{\partial\Delta m_N}{\partial\bar{m}}\,,\\
\bar{g}_2|_{\rm ind} &= 0\,.
\end{aligned}\tag{4.39}$$

Values for the mesonic LECs are discussed in Appendix C.1.

4.4 Constraints from electric dipole moment experiments

The *CP*-odd electron-nucleon and pion-nucleon interactions in Eqs. (4.22) and (4.36) induce EDMs of various systems. We take the expressions from Ref. [238]. The semi-leptonic Wilson coefficients $C_S^{(0,1)}$ mainly contribute to *CP*-odd effects in polar molecules [239–241]

$$\omega_{\rm YbF} = -(17.6\pm2.0)({\rm mrad/s})\left(\frac{C_S}{10^{-7}}\right)\,,\tag{4.40}$$

$$\omega_{\rm HfF} = +(32.0\pm1.3)({\rm mrad/s})\left(\frac{C_S}{10^{-7}}\right)\,,\tag{4.41}$$

$$\omega_{\rm ThO} = +(181.6\pm7.3)({\rm mrad/s})\left(\frac{C_S}{10^{-7}}\right)\,,\tag{4.42}$$

in terms of $C_S = C_S^{(0)} + \frac{Z-N}{Z+N}C_S^{(1)}$ where Z and N correspond to the number of protons and neutrons, respectively, of the heaviest atom of the molecule. In addition, the combination of *CP*-odd and *CP*-even axion couplings, $\sim g_S^N g_P^{(e)}$ or $\sim g_S^{(e)} g_P^{(e)}$, can give rise to *CP*-odd effects in nuclei, atoms, and molecules. Such contributions were considered in Ref. [242], which showed that the most stringent limits arise from the ThO measurement, giving

$$\omega_{\rm ThO}(g_{S,P}) = \left[0.54\, g_S^{(e)} g_P^{(e)} + 1.4\, g_S^N g_P^{(e)}\right]\cdot 10^{19}\,,\tag{4.43}$$

neutron and atoms (e cm)			Molecules (mrad/s)		
d_n	$d_{\rm Hg}$	$d_{\rm Ra}$	$\omega_{\rm YbF}$	$\omega_{\rm HfF}$	$\omega_{\rm ThO}$
$1.8 \cdot 10^{-26}$	$6.3 \cdot 10^{-30}$	$1.2 \cdot 10^{-23}$	23.5	4.6	1.3

Table 4.3: Current experimental limits (at 90% C.L.) from measurements on the neutron [52], ^{199}Hg [180], ^{225}Ra [243], YbF [244], HfF [245], and ThO [246].

where $g_P^{(f)}$ is connected to the *CP*-even couplings in Eq. (4.3) by $g_P^f = C_P^f m_f/f_a$ and $g_P^N = \frac{A-Z}{A} g_P^n + \frac{Z}{A} g_P^p$.

The operators $C_P^{(0,1)}$ and $\bar{g}_{0,1,2}$ induce EDMs of nucleons, nuclei, and diamagnetic atoms. For the nucleon EDMs we use the results [140]

$$d_n = -\frac{e g_A}{8\pi^2 F_\pi}\left[\left(\bar{g}_0 - \frac{\bar{g}_2}{3}\right)\left(\log\frac{m_\pi^2}{m_N^2} - \frac{\pi m_\pi}{2m_N}\right) + \frac{\bar{g}_1}{4}(\kappa_1 - \kappa_0)\frac{m_\pi^2}{m_N^2}\log\frac{m_\pi^2}{m_N^2}\right], \tag{4.44}$$

$$d_p = \frac{e g_A}{8\pi^2 F_\pi}\left[\left(\bar{g}_0 - \frac{\bar{g}_2}{3}\right)\left(\log\frac{m_\pi^2}{m_N^2} - \frac{2\pi m_\pi}{m_N}\right) - \frac{\bar{g}_1}{4}\left(\frac{2\pi m_\pi}{m_N} + (5/2 + \kappa_1 + \kappa_0)\frac{m_\pi^2}{m_N^2}\log\frac{m_\pi^2}{m_N^2}\right)\right], \tag{4.45}$$

where $g_A \simeq 1.27$ is the nucleon axial charge, and $\kappa_1 = 3.7$ and $\kappa_0 = -0.12$ are related to the nucleon magnetic moments. For $\bar{g}_1$ we kept the next-to-next-to-leading-order corrections as this is the first order where a neutron EDM is induced. We have set the renormalization scale to the nucleon mass m_N in order to estimate the EDMs as function of pion-nucleon couplings.

We should point out that the *CP*-odd LEFT operators induce additional *CP*-violating hadronic interactions that also contribute to the nucleon EDMs. For example, a quark chromo-EDM operator $\sim \bar{q}\sigma^{\mu\nu}\gamma^5 T^A q\, G^A_{\mu\nu}$ leads to direct contributions to the neutron EDM in addition to the pion-nucleon terms. Such direct terms depend on hadronic matrix elements that do not appear in the *CP*-odd axion interactions given above (they would be connected to *CP*-odd axion-photon-nucleon terms instead). We, therefore, do not include these effects here, which leads to conservative limits[6], assuming there are no significant cancellations. Instead, we estimate the EDMs of neutrons (and protons) from their pion-loop contributions proportional to $\bar{g}_{0,1,2}$ in Eqs. (4.44) and (4.45).

[6]For certain LEFT operators such as the Weinberg operator, there are no contributions to $\bar{g}_{0,1,2}$ at the chiral order we work. However, terms appear after a quark mass insertion leading to an additional suppression of m_π^2/Λ_χ^2 [73]. In those cases, the direct contributions to the nucleon EDMs, which come with additional LECs, are a better estimate. To keep the discussion compact, we do not further pursue this here.

The expression for the Hg EDM becomes [130, 172, 247–250]

$$d_{\rm Hg} = -(2.1 \pm 0.5) \cdot 10^{-4} \Big[(1.9 \pm 0.1) d_n + (0.20 \pm 0.06) d_p + \left(0.13^{+0.5}_{-0.07}\, \bar{g}_0 + 0.25^{+0.89}_{-0.63}\, \bar{g}_1 + 0.09^{+0.17}_{-0.04}\, \bar{g}_2 \right) e\,{\rm fm} \Big] - \left[(0.028 \pm 0.006) C_S - \frac{1}{3} (3.6 \pm 0.4) \left(\frac{Z\alpha}{5 m_N R} C_P \right) \right] \cdot 10^{-20}\, e\,{\rm cm}\,, \quad (4.46)$$

in terms of the nuclear radius $R \simeq 1.2\, A^{1/3}$ fm, and $C_{P,T} = (C^{(n)}_{P,T} \langle \boldsymbol{\sigma}_n \rangle + C^{(p)}_{P,T} \langle \boldsymbol{\sigma}_p \rangle)/(\langle \boldsymbol{\sigma}_n \rangle + \langle \boldsymbol{\sigma}_p \rangle)$. Here we defined $C^{(n,p)}_{P,T} = C^{(0)}_{P,T} \mp C^{(1)}_{P,T}$. For ^{199}Hg we use the values [251]

$$\langle \boldsymbol{\sigma}_n \rangle = -0.3249 \pm 0.0515\,, \qquad \langle \boldsymbol{\sigma}_p \rangle = 0.0031 \pm 0.0118\,. \quad (4.47)$$

The expression for the octopole-deformed Ra is simpler as nuclear *CP*-violation dominates the atomic EDM [78, 247]

$$d_{\rm Ra} = (7.7 \cdot 10^{-4}) \cdot [(2.5 \pm 7.5)\, \bar{g}_0 - (65 \pm 40)\, \bar{g}_1 + (14 \pm 6.5) \bar{g}_2]\, e\,{\rm fm}\,. \quad (4.48)$$

Note that the radium and mercury EDMs are dominated by the contributions to the pion-nucleon couplings as long as $\bar{g}_{0,1,2}$ receive contributions at LO (which is the case for the LEFT operators under consideration here). The connection between the contributions to $d_{\rm Ra}$ and $d_{\rm Hg}$ and the axion-nucleon couplings are, therefore, more straightforward than was the case for the nucleon EDMs, where additional direct contributions appear at the same order. The current best limits are collected in Table 4.3.

4.5 Fifth-force experiments

The CPV scalar axion-nucleon and axion-lepton couplings of Eqs. (4.30) and (4.20) lead to monopole-monopole forces, which would act like a 'fifth force', thereby modifying Newton's inverse-square law (ISL) and violating the weak equivalence principle (WEP). The combination of the gravitational and axion potentials between two different bodies I and J then becomes

$$V_{IJ}(r) = -\frac{G m_I m_J}{r_{IJ}} \left(1 + \alpha_I \alpha_J e^{-m_a r_{IJ}} \right), \quad (4.49)$$

where $m_a (= 1/\lambda)$ is the axion mass, r_{IJ} is the distance between I and J, while $m_{I,J}$ and $\alpha_{I,J}$ are the masses and total 'axion charges' of I and J (the latter are normalized to $m_{I,J}\sqrt{4\pi G}$). At leading order in χPT, this total charge is determined by the axion couplings to the electron, proton, and neutron, as well as

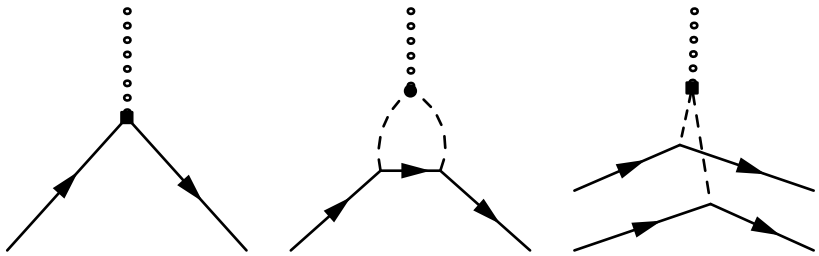

Figure 4.2: Diagrams contributing to the axion-nucleon interactions. The solid lines correspond to nucleons, the dotted lines to axions, and the dashed lines to mesons.

the number of these particles present in the body under consideration. Explicitly, we have

$$\alpha_I = \frac{1}{\sqrt{4\pi G}} \left[g_S^{(n)} \frac{A-Z}{m_A} + g_S^{(p)} \frac{Z}{m_A} + g_S^{(e)} \frac{Z}{m_A} \right] , \tag{4.50}$$

where m_A is the mass of the atom, which in most cases can be approximated by $m_A = A m_{\rm u}$, with $m_{\rm u}$ the atomic mass unit, while Z and $A-Z$ are the number of protons and neutrons of the element that constitute the body I. The leading-order contributions arise from the simple axion-nucleon diagram (left diagram of Fig. 4.2).

Axion-meson-meson couplings modify the axion-nucleon coupling at the one-loop level (middle diagram of Fig. 4.2), in practice part of the one-loop contributions are automatically resummed by using the physical values for $\sigma_{\pi N}$ and δm_N in Eq. (4.24). Graphs such as the one depicted in the right panel of Fig. 4.2 lead to two-nucleon contributions that cannot be captured by Eq. (4.50). In the analogous case of a dilaton (ϕ) coupling to quarks, $\sim \phi \bar{q} q$, such contributions to the potential are related to the binding energy of the nuclei and were considered in Ref. [252]. Within χPT, however, these two-body interactions appear at a higher-order in the power counting. In particular, for scalar axion-quark interactions (e.g. $a\bar{q}q$) axion-nucleon-nucleon currents appear at next-to-leading-order in the power counting and could in principle be relevant [253]. These currents were discussed in detail in light of WIMP scattering off atomic nuclei and were found to be somewhat smaller than power-counting predictions indicate and appear only at the few-percent level [100]. However, this could increase for larger nuclei [254]. We neglect the subleading two-nucleon corrections in this part of the thesis.

Numerous experiments search for the fifth force induced by $\alpha_I \alpha_J$ term in Eq. (4.49). These experiments either look for violations of the WEP, which appear when V_{IJ} is no longer proportional to $m_I m_J$, or departures from the inverse-square law due to deviations from the $1/r_{IJ}$ dependence of the usual gravitational potential. In this section, we summarize several of these experiments and discuss how they limit the axion couplings to nucleons and leptons.

4.5.1 MICROSCOPE mission

The MICROSCOPE mission [255] focuses on constraining the Eötvös parameter, a measure of WEP violations. The Eötvös parameteris the normalized difference between the accelerations of two masses, I and J. In the case of Ref. [255], these masses are made of platinum and titanium and are in free fall aboard the MICROSCOPE satellite

$$\eta = \left(\frac{\Delta a}{a}\right)_{IJ} = 2\frac{|\boldsymbol{a}_I - \boldsymbol{a}_J|}{|\boldsymbol{a}_I + \boldsymbol{a}_J|}\,. \tag{4.51}$$

From Eq. (4.49) one finds that the Eötvös parameterfor two test masses in the external field of Earth (E) can be expressed as

$$\eta = \frac{\alpha_E|\alpha_I - \alpha_J|\,(1+x)\,e^{-x}}{1+\frac{1}{2}(\alpha_J+\alpha_J)\alpha_E\,(1+x)\,e^{-x}} \simeq \alpha_E|\alpha_I - \alpha_J|(1+x)e^{-x}\,, \tag{4.52}$$

where $x = Rm_a$, $R \approx 7000$ km is the distance from the center of the Earth to the satellite, and α_E is the effective 'axion charge' of the Earth. Following [255], we model the Earth as consisting of a core (which is taken to consist of iron) and the mantle (consisting of SiO_2), so that its charge takes the form [7]

$$\alpha_E = \frac{m_C}{m_E}\alpha_{\rm Fe}\Phi\left(R_C m_a\right) + \frac{m_M}{m_E}\alpha_{\rm SiO_2}\frac{R_E^3\Phi(R_E m_a) - R_C^3\Phi(R_C m_a)}{R_E^3 - R_C^3}\,, \tag{4.53}$$

where $R_E \simeq 6371$ km and $R_C \simeq 3500$ km are the radii of the Earth and its core. m_E, m_C, and m_M are, respectively, the masses of the Earth, its core, and its mantle, with $m_C/m_E \simeq 0.33$, while the function $\Phi(x) \equiv 3(x\cosh x - \sinh x)/x^3$ describes the deviation from a simple Yukawa potential due to the finite size of the earth.

Combining these expressions with the experimental limit [255],

$$\eta = (-1 \pm 27) \times 10^{-15}\,, \tag{4.54}$$

allows us to set constraints on $g_S^{(e,n,p)}$ as a function of m_a.

4.5.2 Eöt-Wash (WEP)

The Eöt-Wash experiment [256] constrained deviations from the WEP at distance scales $\gtrsim 0.1$ m. In this case, two test bodies, made of Pb and Cu, were connected to a torsion balance around which a ^{238}U attractor mass rotates. A difference in the accelerations of the two bodies would then show up as a torque, $\vec{\tau} = \frac{1}{2}\vec{d}\times(\vec{F}_{\rm Cu} - \vec{F}_{\rm Pb})$, where $\vec{d}$ is the distance between the two test bodies and $\vec{F}_{\rm Cu,Pb}$ are the forces that work on them, due to the Earth and the attractor. The

[7] This result differs from the expression obtained in Ref. [255].

experiment looks for signals that vary as a function of the angle, ϕ, between $\vec{d}$ and the vector from the test bodies to the attractor. The fact that only accelerations orthogonal to $\vec{d}$ contribute to the torque implies τ is a measure of deviations from the WEP, $\tau \sim \alpha_{\rm Cu} - \alpha_{\rm Pb}$, while looking for ϕ-dependent signals means signals are due to the force (whether gravitational or axionic) exerted by the attractor. In total, the ϕ-dependent part of the z-component of the torque can be written as [8]

$$\begin{aligned}\frac{\tau_z|_{\rm varying}}{g' d m_{\rm Cu}/2} &= \frac{|a_{\rm Pb} - a_{\rm Cu}|}{g'} \sin\phi \\ &\simeq |\alpha_{\rm Pb} - \alpha_{\rm Cu}| \left[\alpha_A I_A(m_a) - \alpha_E (1 + R_E m_a) e^{-R_E m_a}\right] \sin\phi \,, \end{aligned} \tag{4.55}$$

where $g' = 9.2 \cdot 10^{-7}$ m/s^2 and $\alpha_{\rm A}$ are the gravitational acceleration and the axion charge of the element of the attractor, while I_A is a function that captures the geometry of the attractor. The experimental limit

$$|a_{\rm Pb} - a_{\rm Cu}| \leq 5.7 \cdot 10^{-15}\, {\rm m/s}^2 \,, \qquad 95\%\ {\rm C.L.} \,, \tag{4.56}$$

together with I_A, which we obtain from interpolating the numerical values in Table 4.4, again allows us to set constraints on $g_S^{(n,p,e)}$.

λ (m)	0.01	0.014	0.020	0.028	0.05	0.07	0.1	0.2	0.5	1	2	5
$I_A(m_a)$	$1.3{\cdot}10^{-5}$	$1.8 \cdot 10^{-4}$	0.0016	0.0079	0.057	0.13	0.26	0.59	0.89	0.97	0.99	1.0

Table 4.4: Numerical values for the function $I_A(m_a)$ that describes the geometry of the attractor in the Eöt-Wash experiment [256] as a function of $\lambda = 1/m_a$.

Later work suspended the torsion pendulum from a rotating turntable instead of using a rotating attractor and used test bodies made of Be and Ti [257]. The role of source mass was dominated by features in the surrounding environment, local topography, and finally, the Earth, depending on the value of λ. Lacking knowledge of the size, density, and composition of the environmental features, we approximate the effective axion coupling of the source masses by $\alpha_{\rm source} = \alpha_{\rm SiO_2}$. The experimental results are shown in Table 4.5.

λ (m)	1	10	$1 \cdot 10^2$	$1 \cdot 10^3$	$1 \cdot 10^4$	$1 \cdot 10^5$	$1 \cdot 10^6$	$> 1 \cdot 10^7$
$\lvert\alpha_{\rm source}(\alpha_{\rm Be} - \alpha_{\rm Ti})\rvert$	$8 \cdot 10^{-6}$	$1 \cdot 10^{-6}$	$2 \cdot 10^{-7}$	$7 \cdot 10^{-8}$	$4 \cdot 10^{-8}$	$4 \cdot 10^{-8}$	$5 \cdot 10^{-9}$	$2 \cdot 10^{-10}$

Table 4.5: Constraints set by Eöt-Wash experiment [257] as a function of $\lambda = 1/m_a$.

[8] Here we neglect a small correction to the contributions $\sim \alpha_A$ due to the centrifugal force induced by the Earth's rotation.

4.5.3 Irvine

This experiment [258] consists of two sets of measurements, searching for fifth forces at distances between 105-5 cm and 5-2 cm. Both measurements used a torsion balance to constrain the torque that a Yukawa potential would induce. The test and attractor masses used in these set-ups were designed so as to give rise to a net-zero torque if the force between them has a pure $1/r^2$ dependence. The measurements on smaller distance scales searched for fifth forces between a copper test mass and a stainless steel cylinder. In contrast, the test and attractor masses used in the measurements at larger distances were both made from copper. As the elements in these materials all have a similar $Z/A \simeq 0.45$, which determines α in Eq. (4.50), we will approximate the effective axion charges $\alpha_{I,J}$ by $\alpha_{\rm Cu}$. We summarize the constraints on the combination $\alpha_I \alpha_J$ as a function of λ in Table 4.6.

λ (mm)	5	10	50	100	500	$1.0 \cdot 10^3$	$5.0 \cdot 10^3$	$1.0 \cdot 10^4$
$\lvert\alpha_{\rm Cu}\alpha_{\rm Cu}\rvert$	$1.1 \cdot 10^{-3}$	$2.1 \cdot 10^{-4}$	$1.9 \cdot 10^{-4}$	$4.2 \cdot 10^{-4}$	$1.3 \cdot 10^{-3}$	$3.8 \cdot 10^{-3}$	0.088	0.46

Table 4.6: 95% C.L. constraints on the combinations $|\alpha_{\rm Cu}\alpha_{\rm Cu}|$ as a function of $\lambda = 1/m_a$ set by the Irvine measurements [258].

4.5.4 Eöt-Wash (inverse-square law)

Apart from searches for WEP violations, some experiments look for deviations from the inverse-square law. The Eöt-Wash experiments accurately measured the force between an attractor, made of Mo and Ta, and a Pt or Mo test body as a function of the distance between them [259, 260]. The geometry of the experimental set-up cancels the attraction due to the gravitational potential, $\sim 1/r^2$, allowing one to constrain Yukawa forces. Although the attractor was made of several materials, we approximate the probed combinations by $|\alpha_{\rm Mo}\alpha_{\rm Mo}|$ and $|\alpha_{\rm Pt}\alpha_{\rm Mo}|$, the resulting constraints on which are listed in Table 4.7.

λ (mm)	0.01	0.025	0.05	0.1	0.25	0.5	1	2.5	5
$\lvert\alpha_{\rm Mo}\alpha_{\rm Mo}\rvert$	$4.1 \cdot 10^4$	43	1.4	0.1	$6.7 \cdot 10^{-3}$	$2.4 \cdot 10^{-3}$	$2.7 \cdot 10^{-3}$	$7.2 \cdot 10^{-3}$	$7.1 \cdot 10^{-3}$
$\lvert\alpha_{\rm Mo}\alpha_{\rm Pt}\rvert$	$3.1 \cdot 10^3$	6.4	0.42	0.077	0.029	0.025	0.019	0.013	0.012

Table 4.7: 95% C.L. constraints on the combinations $|\alpha_{\rm Mo}\alpha_{\rm Mo}|$ [259] and $|\alpha_{\rm Pt}\alpha_{\rm Mo}|$ [260] as a function of $\lambda = 1/m_a$ set by the Eöt-Wash experiment.

4.5.5 HUST

The HUST experiment [261–264] searches for inverse-square law violations caused by a fifth force between two plane masses made of tungsten (W) using a torsion

pendulum. The pendulum is suspended horizontally with a rectangular-shaped test mass of tungsten at each end. The test masses face a rotating attractor made of rectangular tungsten source masses and compensating masses designed to cancel out the torque due to Newtonian forces. This experiment is most sensitive in the range $\lambda = (40 - 350)\ \mu$m. The resulting constraints on $\alpha_I \alpha_J$ are collected in Table 4.8.

λ (mm)	0.025	0.05	0.1	0.25	0.5	1	2.5	5
$\lvert\alpha_{\rm W}\alpha_{\rm W}\rvert$	420	0.70	0.026	$3.8 \cdot 10^{-3}$	$3.6 \cdot 10^{-3}$	$1.4 \cdot 10^{-3}$	$1.0 \cdot 10^{-3}$	$2.2 \cdot 10^{-3}$

Table 4.8: 95% C.L. constraints on the combinations $|\alpha_{\rm W}\alpha_{\rm W}|$ as a function of $\lambda = 1/m_a$ set by the HUST experiment [261–264].

4.5.6 Stanford

The Stanford experiment [265] focused on axions in the range $\lambda \sim 5$ - 15 μm. A rectangular gold (Au) prism, located at the end of a cantilever, was used as a test mass. The force on the test mass was determined through its displacement. A source mass consisting of alternating gold and silicon (Si) bars was then moved horizontally below the test mass. In the presence of a fifth force, the test mass experiences different forces depending on whether an Au or Si bar is located directly below it, resulting in a different displacement of the cantilever. This would induce an oscillating force when the source mass is displaced horizontally. Note that the background due to Newtonian forces is negligible at this level of precision. The amplitude of the induced force is proportional to $\rho_I \alpha_I$, with ρ the mass density and $I =$ Au, Si. As $\rho_{\rm Au} \gg \rho_{\rm Si}$, we approximate the probed combination of axion charges by $\alpha_{\rm Au}^2$, the constraints on which are shown in Table 4.9.

λ (μm)	4	6	10	18	34	66
$\lvert\alpha_{\rm Au}\alpha_{\rm Au}\rvert$	$3.1 \cdot 10^{7}$	$4.6 \cdot 10^{5}$	$1.4 \cdot 10^{4}$	$1.1 \cdot 10^{3}$	$2.5 \cdot 10^{2}$	$1.5 \cdot 10^{2}$

Table 4.9: 95% C.L. constraints on the combinations $|\alpha_I \alpha_J|$ as a function of $\lambda = 1/m_a$ set by the Stanford experiment [265].

4.5.7 IUPUI

This experiment searches for fifth forces by measuring the differential force on masses separated by distances in the nm range [266], allowing it to probe axions in the range $\lambda \sim (40 - 8000)$ nm. The set-up involves a spherical test mass, made in large part of sapphire (S), located above a rotating disk which serves as a source mass. The latter involves several rings, each with a number of alternating

segments made of Au and Si. The source mass is rotated at a constant frequency so that a difference in force felt by the test mass due to Au and Si would show up as an oscillating signal. Such a difference would signify a fifth force, while the Newtonian force for this design is below the experimental sensitivity. As both the attractor and the sources masses involve several materials, we approximate the effectively probed combination of couplings by $\alpha_{\rm S}(\alpha_{\rm Au}-\alpha_{\rm Si})$, where $\alpha_{\rm S}$ is the effective axion charge of sapphire. The resulting constraints on $\alpha_I\alpha_J$ are collected in Table 4.10.

λ (mm)	$5\cdot10^{-5}$	$1\cdot10^{-4}$	$2.5\cdot10^{-4}$	$5\cdot10^{-4}$	$1\cdot10^{-3}$	$2.5\cdot10^{-3}$	$5\cdot10^{-3}$
$\lvert\alpha_{\rm S}(\alpha_{\rm Au}-\alpha_{\rm Si})\rvert$	$2.4\cdot10^{13}$	$1.0\cdot10^{11}$	$6.5\cdot10^{8}$	$4.3\cdot10^{7}$	$5.8\cdot10^{6}$	$6.3\cdot10^{5}$	$1.3\cdot10^{5}$

Table 4.10: 95% C.L. constraints on the combinations $|\alpha_{\rm W}\alpha_{\rm W}|$ as a function of $\lambda = 1/m_a$ set by the IUPUI experiment [266].

4.5.8 Asteroids and planets

It is possible to constrain a fifth force by measurements of the orbital trajectories of astronomical objects. In particular, Ref. [267] proposes to use the fifth-force-induced orbital precession of nine near-Earth asteroids, whose orbital trajectories are precisely tracked, to constrain a potential fifth force induced by the exchange of particles in the mass range $m_a \simeq 10^{-21} - 10^{-15}$eV. The analysis of Ref. [267] assumed that the new scalar particles coupled to the baryon charge, in which case the elemental composition of the Sun and the asteroids is not relevant. To constrain the axion couplings, we assume that the asteroids consist mainly of iron ($\alpha_{\rm asteroid} = \alpha_{\rm Fe}$). Since the orbits can only be affected by axions with $\lambda \gg R_\odot$, we model the Sun as a point particle, with

$$\alpha_\odot = (0.75\ \alpha_{\rm H} + 0.24\ \alpha_{\rm He})\,. \tag{4.57}$$

With these assumptions, we convert the estimated sensitivity of Ref. [267] to limits on axion-nucleon and axion-electron scalar couplings.

In a similar spirit, it is possible to constrain axion-induced fifth forces by measuring the perihelion procession of planetary orbits [268]. The most stringent limits arise from the perihelion procession of Mars and Mercury. The analysis of Ref. [268] assumed a model where hypothetical ultralight Z' bosons couple to electrons, which gives rise to a Yukawa potential similar to axions (but with opposite sign). We convert their limits by assuming Mars and Mercury have a similar composition to Earth with similar relative sizes of the mantle and core, which, for $\lambda \gg R_E$, gives $\alpha_{\rm planet} \simeq 0.33\alpha_{\rm Fe} + 0.67\alpha_{\rm SiO_2}$. The constraints on $\alpha_I\alpha_J$ from the asteroids and planets as a function of λ are collected in Table 4.11.

Black and gray lines in Figs 4.3 and 4.6 depict the resulting limits from the asteroid and planetary orbits, respectively.

λ (km)	$1 \cdot 10^6$	$5 \cdot 10^6$	$1 \cdot 10^7$	$5 \cdot 10^7$	$1 \cdot 10^8$	$5 \cdot 10^8$	$1 \cdot 10^9$
$\lvert\alpha_{\rm Fe}\alpha_\odot\rvert$	$2.5 \cdot 10^{-6}$	$9.8 \cdot 10^{-11}$	$3.5 \cdot 10^{-11}$	$7.5 \cdot 10^{-12}$	$1.1 \cdot 10^{-11}$	$1.1 \cdot 10^{-10}$	$4.2 \cdot 10^{-10}$
$\lvert\alpha_{\rm planet}\alpha_\odot\rvert$	–	$3.4 \cdot 10^{-9}$	$1.8 \cdot 10^{-10}$	$7.4 \cdot 10^{-12}$	$4.3 \cdot 10^{-12}$	$1.8 \cdot 10^{-11}$	$4.9 \cdot 10^{-11}$

Table 4.11: 95% C.L. projected constraints on the combination $|\alpha_{\rm Fe}\alpha_\odot|$ [267] and current limits on $|\alpha_{\rm planet}\alpha_\odot|$ [268] as a function of $\lambda = 1/m_a$. The constraints due to the planetary orbits are dominated by Mars for $\lambda > 2.6 \cdot 10^7$ km and Mercury for smaller values of λ.

4.5.9 Stellar Cooling

The stars can produce axions in the cores. If they escape, this provides a new source of stellar cooling, and we can search for the resulting distinct astronomical signatures. Here we briefly discuss the most stringent limits arising from these searches. A recent, more detailed discussion of these constraints can be found in Ref. [196].

The pseudoscalar axion-electron interaction can generate axions through Compton scattering $\gamma + e^- \to e^- + a$ and bremsstrahlung $e + Ze \to Ze + e + a$ [269,270]. These cooling processes allow heavier red giants as their cores now require more mass to reach the same temperature, thereby delaying helium ignition. The increase in mass then leads to a higher luminosity so that measurements of the brightness of red giants allow one to constrain the cooling processes induced by axions. The resulting limit is given by [271]

$$g_P^e \lesssim 1.6 \cdot 10^{-13} \,. \tag{4.58}$$

These cooling processes are suppressed for heavier axions, as they cannot be produced once the mass becomes significantly heavier than the temperature in the core. The limits in this section are valid for $m_a < 10$ keV.

The scalar axion-electron interaction can be constrained by using the fact that it causes the mixing of the axion with plasmons in stars [272]. This axion production is enhanced if the axion mass is below the plasmon frequency. The most stringent constraint comes from the resonant production in red giants [273]

$$g_S^e \lesssim 7.1 \cdot 10^{-16} \,. \tag{4.59}$$

The analogous resonant axion production in red giants, induced by scalar axion-nucleon interactions, gives the limit [273]

$$g_S^{(0)} \lesssim 1 \cdot 10^{-12} \,. \tag{4.60}$$

Finally, for the pseudoscalar coupling to neutrons, the most stringent limits arise from neutron stars. Young neutron stars that are formed from the collapsed star core after a supernova explosion can cool by emitting axions through bremsstrahlung, $n + n \to n + n + a$. Observation of a high surface temperature of neutron stars can then limit the amount of axion emission. The resulting

constraint is given by [274]

$$g_P^n \lesssim 2.8 \cdot 10^{-10} \,. \tag{4.61}$$

4.6 Searches for monopole-dipole interactions

In the previous section, we discussed constraints on the product of two scalar axion couplings. In the presence of both *CP*-even and *CP*-odd interactions, axion exchange also leads to a monopole-dipole potential of the form $V \sim (\boldsymbol{\sigma}\cdot\hat{r})e^{-m_a r}/r$, where $\boldsymbol{\sigma}$ is the spin of the particle with a *CP*-even axion coupling. Potentials of this form are searched for by various experiments, which we discuss in more detail below. Before doing so, we first introduce the *CP*-even axion interactions that make up the monopole-dipole potential. These *CP*-even couplings arise from the derivative terms $\sim c_{L,R}^f \frac{\partial_\mu a}{f_a} \bar{f}\gamma^\mu\gamma_5 f$ in Eq. (4.3). In addition, quark-axion interactions are generated by the axion-dependent part of the chiral rotation, A, which shifts the $\sim (c_R^q - c_L^q)\partial_\mu a$ terms contained in $r_\mu - l_\mu$ in Eq. (4.12). As a result, the quark interactions receive a model-independent contribution from the chiral rotation. At the same time, the lepton couplings only involve model-dependent terms since $c_{L,R}^f$ depend on the UV construction.

We write the final *CP*-conserving interactions as

$$\mathcal{L}_{aN} = \frac{\partial_\mu a}{2f_a}\left(C_P^p\,\bar{p}\,\gamma^\mu\gamma^5\,p + C_P^n\,\bar{n}\,\gamma^\mu\gamma^5\,n + C_P^e\,\bar{e}\,\gamma^\mu\gamma^5\,e\right) , \tag{4.62}$$

for couplings to protons, neutrons, and electrons, respectively. Within chiral EFT, these nucleon interactions result from the $\sim S_\mu$ terms in the first line of Eq. (4.17) as the above Lorentz structure reduces to $\gamma_\mu\gamma_5 \to 2S_\mu$ in the non-relativistic limit, see Eq. (2.64). For the axion-nucleon *CP*-even couplings, we apply recent results from next-to-next-to-leading-order chiral perturbation theory [275]

$$\begin{aligned} C_P^p &= -0.430(50) + 0.862(75)X_u - 0.417(66)X_d - 0.035(54)X_s \,, \\ C_P^n &= 0.007(46) - 0.417(66)X_u + 0.862(75)X_d - 0.035(54)X_s \,, \\ C_P^e &= X_e = \left(\frac{c_R^e - c_L^e}{2}\right)_{11} \,, \end{aligned} \tag{4.63}$$

with $X_q = \mathrm{Diag}(X_u, X_d, X_s) = \frac{1}{2}\mathrm{Diag}\,(c_R^q - c_L^q)$. These couplings are sometimes written in pseudoscalar form using the equations of motion for on-shell fermions $-g_P^f\, a\, \bar{f} i\gamma^5 f$ where $g_P^f = C_P^f m_f/f_a$ for $f = \{p, n, e\}$. Using Eq. (4.15) we write [196]

$$g_P^f = 1.7 \cdot 10^{-13}\, C_P^f \left(\frac{m_f}{1\,\mathrm{GeV}}\right)\left(\frac{m_a}{1\,\mu\mathrm{eV}}\right) . \tag{4.64}$$

Two of the most popular UV constructions (see Refs. [276,277] for more general constructions), which determine the $c_{L,R}^{(f)}$ couplings, are the KSVZ [278, 279] and

DFSZ [280, 281] models, see Ref. [185] for a recent review. In these scenarios, the couplings take the following values

$$\begin{aligned} \text{DFSZ}: \quad X_u &= \frac{1}{3}\sin^2\beta\,, \\ X_d &= X_s = X_e = \frac{1}{3}(1-\sin^2\beta)\,, \\ \text{KSVZ}: \quad X_q &= X_e = 0\,, \end{aligned} \tag{4.65}$$

where $\tan\beta = v_d/v_u$ is the ratio of vacuum expectation values of scalar fields in the DFSZ model. Assuming perturbativity of the Yukawa couplings appearing in the model, β lies in the range $\tan\beta \in [0.25, 170]$ [185, 282]. In our analysis, the exact values of the *CP*-even couplings are not our main concern (although they play a role in setting limits). For simplicity, we will consider the DFSZ model and set $\tan\beta \simeq 1$ and pick the central values of the matrix elements. That is, we take $C_P^p = -0.36$, $C_P^n = 0.08$, and $C_P^e = 0.17$. Using other values of $\tan\beta$ or the KSVZ couplings will not dramatically change our findings.

4.6.1 ARIADNE

The Axion Resonant InterAction Detection Experiment (ARIADNE) aims to probe axion masses up to 10^{-3} eV by using methods based on nuclear magnetic resonance (NMR) [283–285]. The experiment is sensitive to the axion-mediated monopole-dipole potential between two nuclei,

$$V_{SP} = \frac{g_P^N g_S^N}{8\pi m_N}\left(\frac{1}{r\lambda}+\frac{1}{r^2}\right)e^{-\frac{r}{\lambda}}(\boldsymbol{\sigma}\cdot\hat{r}) \equiv \boldsymbol{\mu}\cdot B_{\text{eff}}\,, \tag{4.66}$$

where $\boldsymbol{\mu} = \frac{1}{2}g_N\mu_B\boldsymbol{\sigma}$, with $\mu_B = \frac{e}{2m_p}$ and g_N the nuclear magneton and g factor, respectively. As implied by the second equality, we can interpret the effects of this potential as an effective magnetic field B_{eff}.

The setup consists of a source mass made of unpolarized tungsten in the form of a rotating cylinder with teeth-like structures pointing radially outwards. These teeth pass by an NMR sample of ^{3}He gas, thereby inducing an oscillating B_{eff} field. As the NMR sample resides in a conventional external magnetic field, the B_{eff} field will drive spin precession in the ^{3}He sample if it is chosen to oscillate at the nuclear Larmor frequency, determined by the external field. The resulting magnetization, proportional to $g_S^N g_P^N$, is precisely measured. These couplings can be written as $g_S^N = \frac{A-Z}{A}g_S^n + \frac{Z}{A}(g_S^p + g_S^{(e)})$ for the tungsten source mass and $g_P^N = 0.88g_P^n - 0.047g_P^p$ [76] for the ^{3}He sample. Ref. [283] considered the projected limits that would result from several setups. Table 4.12 shows the projected limits from their initial setup (with $T_2 = 1$ s) and those from a scaled-up version of the apparatus.

λ (cm)	0.003	0.01	0.03	0.1	0.3	1	3	10
$\lvert g_S^N g_P^N \text{(projected)}\rvert \cdot 10^{33}$	$6 \cdot 10^4$	500	60	10	6	4	4	4
$\lvert g_S^N g_P^N \text{(upgrade)}\rvert \cdot 10^{39}$	$7 \cdot 10^6$	$4 \cdot 10^5$	$2 \cdot 10^4$	$1 \cdot 10^3$	200	40	6	1

Table 4.12: The projected limits on the strength of the axion-mediated monopole-dipole interaction from the ARIADNE experiment using the initial and upgraded setups of Ref. [283].

4.6.2 QUAX

The QUest for AXions (QUAX-$g_P g_S$) experiment [286, 287] is similar in setup to the ARIADNE experiment, as it also makes use of the fictitious magnetic field induced by the combination of *CP*-even and *CP*-odd axion couplings. In this case, the source masses consist of lead, while the detector measures the magnetization of a sample of paramagnetic crystals that the axionic potential would induce. A key difference with the ARIADNE experiment is that the coupling induces the magnetization of electrons rather than nucleons. The probed couplings are therefore given by, $g_P = g_P^{(e)}$ and $g_S^N = \frac{A-Z}{A} g_S^n + \frac{Z}{A}(g_S^p + g_S^{(e)})$ for the case of lead. We show the current constraint [287] and projected limits [286] in Table 4.13.

λ (m)	0.003	0.01	0.03	0.1	0.3	1
$\lvert g_S^N g_P^{(e)} \text{(current)}\rvert \cdot 10^{30}$	–	530	17	5	4	4
$\lvert g_S^N g_P^{(e)} \text{(projected)}\rvert \cdot 10^{34}$	$14 \cdot 10^4$	120	15	8	6	6

Table 4.13: The current [287] and projected limits [286] on the strength of the axion-mediated monopole-dipole interaction from the QUAX.

4.7 Applications

4.7.1 Chromo-electric dipole moments

To illustrate the use of the EFT framework, we revisit a well-studied scenario where BSM *CP*-violation is dominated by the chromo-electric dipole moments (CEDMs) of first-generation quarks. We turn on the LEFT operators

$$\begin{aligned} \mathcal{L}_{CEDM} &= L_5^u\, \bar{u}_L\, T^A G^A_{\mu\nu} \sigma^{\mu\nu} u_R + L_5^d\, \bar{u}_L\, T^A G^A_{\mu\nu} \sigma^{\mu\nu} d_R + \text{h.c.} \\ &= \text{Re}\,(L_5^u)\, \bar{u}\, G \cdot \sigma\, u + \text{Im}\,(L_5^u)\, \bar{u}\, G \cdot \sigma i\gamma^5 u + (u \leftrightarrow d)\,, \end{aligned} \tag{4.67}$$

where we introduced $G \cdot \sigma = T^A G^A_{\mu\nu} \sigma^{\mu\nu}$in the second line. The terms proportional to the imaginary part of L_5^q are the *CP*-violating quark CEDMs. We read from Table 4.2 the induced isoscalar scalar axion-nucleon couplings

$$g_S^{(0)} = \frac{m_*}{f_a} \frac{1}{m_u} \text{Im}\,(L_5^u) \left(\frac{\partial}{\partial \text{Re}\,(L_5^u)} + \frac{2\bar{B}}{B} \frac{\partial}{\partial m_u} \right) \Delta m_N + (u \leftrightarrow d)\,. \tag{4.68}$$

We introduce the isoscalar and isovector combinations

$$L_5^0 = \frac{1}{2}(L_5^u + L_5^d)\,, \qquad L_5^3 = \frac{1}{2}(L_5^u - L_5^d)\,, \tag{4.69}$$

to rewrite

$$g_S^{(0)} = \frac{m_*}{f_a}\left(\frac{\mathrm{Im}\, L_5^u}{m_u} + \frac{\mathrm{Im}\, L_5^d}{m_d}\right)\left[\frac{1}{2}\frac{\partial}{\partial \mathrm{Re}\, L_5^0} + \frac{\bar{B}}{B}\frac{\partial}{\partial \bar{m}}\right]\Delta m_N \tag{4.70}$$

in agreement with Ref. [198].

Similarly, we can compute the *CP*-violating pion-nucleon couplings. We focus on the isovector coupling (the discussion for the isoscalar coupling goes along similar lines) and obtain

$$\bar{g}_1 = -2\frac{\mathrm{Im}\, L_5^3}{F_\pi}\left[\frac{1}{2}\frac{\partial}{\partial \mathrm{Re}\, L_5^0} + \frac{2\bar{B}}{B}\frac{\partial}{\partial \bar{m}}\right]\Delta m_N\,, \tag{4.71}$$

in agreement with Refs. [288, 289]. While the matrix elements appearing in Eqs. (4.70) and (4.71) are poorly known, we see that the matrix element drops out in the ratio

$$\frac{\bar{g}_1}{g_S^{(0)}} = -\left(\frac{f_a}{F_\pi}\right)\frac{1}{m_*}\frac{m_u m_d\,(\mathrm{Im}\, L_5^u - \mathrm{Im}\, L_5^d)}{m_d\,\mathrm{Im}\, L_5^u + m_u\,\mathrm{Im}\, L_5^d}\,. \tag{4.72}$$

This way, experiments looking for EDMs and *CP*-odd axion couplings can be directly compared for a given value of the axion mass $m_a \sim 1/f_a$.

To determine the absolute scale that various experiments are sensitive to, we do need to determine the matrix element

$$\tilde{\Delta} m_N \equiv \left[\frac{1}{2}\frac{\partial}{\partial \mathrm{Re}\, L_5^0} + \frac{\bar{B}}{B}\frac{\partial}{\partial \bar{m}}\right]\Delta m_N\,. \tag{4.73}$$

The two terms in square brackets correspond to direct and indirect contributions. The latter only depend on vacuum matrix elements and are relatively well known. The direct term depends on the nucleon matrix element of the chromomagnetic operator and is poorly understood. Recently, Seng [290] argued that while the direct term is not well known, it is subleading with respect to the indirect term. The argument is based on a connection between chromomagnetic nucleon matrix elements and higher-twist distributions that can be measured in deep inelastic scattering, finding only 10-20% corrections from the direct piece. This result is at odds with the QCD sum rule results of Ref. [288], where both terms are of similar size. Lattice-QCD might provide a resolution to this discrepancy [289]. For now we follow Ref. [290] and set $\bar{B}/B \simeq 0.4\,\mathrm{GeV}^2/g_s(2\,\mathrm{GeV})$ [290, 291], $g_s(2\,\mathrm{GeV}) \simeq 1.85$, and $\bar{m} = 3.4$ MeV [292] to obtain

$$\tilde{\Delta} m_N \simeq 3.7\,\mathrm{GeV}^2\,, \tag{4.74}$$

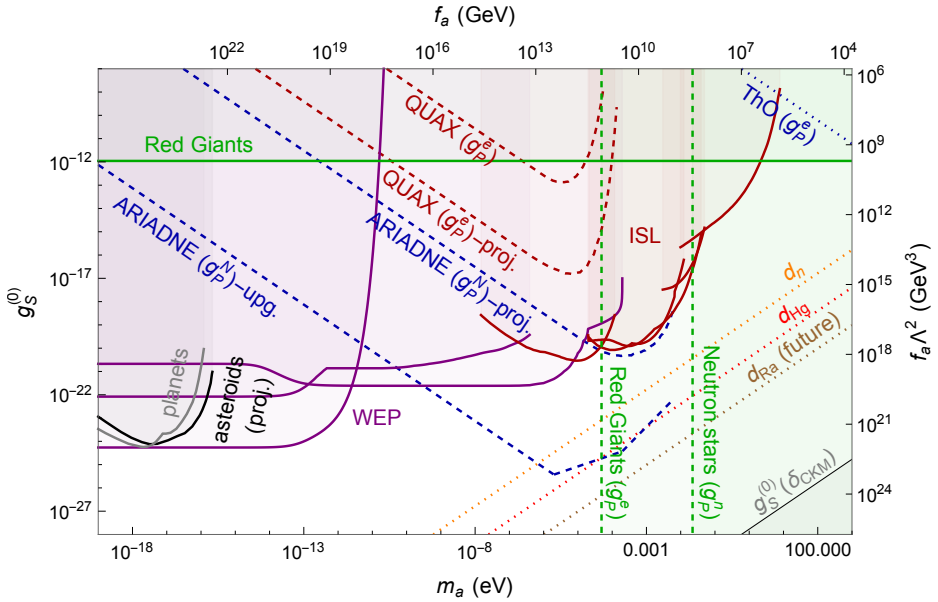

Figure 4.3: Constraints on the isoscalar scalar axion-nucleon coupling in case of a down-quark chromo-EDM. The *CP*-even axial axion-nucleon coupling is chosen as in the DFSZ model with $\tan\beta = 1$. The WEP experiment limits are shown in purple, from top to bottom on the low end of axion mass, the lines denote Eöt-Wash (2000) [256], Eöt-Wash (2008) [257], and the MICROSCOPE mission [255]. The inverse-square law (ISL) experiments limits are shown in red, from left to right the lines denote Irvine [258], HUST [261–264], Eöt-Wash [259,260], Stanford [265], and IUPUI [266]. The astronomical bounds from planets [268] are shown in gray, and the projected limits from asteroids [267] are shown in black. The stellar cooling bounds are shown in green for Red Giants [271,273] and neutron stars [274]. Note that the vertical line from Red Giants is a bound on g_P^e, which would be much weaker had we used the KSVZ model. The EDM limits are shown as dotted lines, where orange corresponds to the neutron [52], red to Hg [180], brown to Ra [243], and blue to ThO [246]. Red-dashed lines depict the current and projected limits from QUAX [287]. The ARIADNE limits are shown in blue-dashed for the initially envisioned setup (labeled 'proj.') and a upgraded version (labeled 'upg.') [283–285]. The estimated size of $g_S^{(0)}$ arising from the SM CKM phase is shown in gray at the bottom-right corner.

which is what we use in our analysis.

We can now compare the sensitivity of various experiments to the presence of the quark chromo-EDMs. For concreteness we turn on the down-quark chromo-EDM and assume $\mathrm{Im}\, L_5^d = \frac{m_d}{\Lambda^2}$. After the PQ mechanism is implemented, the presence of the *CP*-odd chromo-EDM leads to scalar axion-nucleon interactions, which fifth-force experiments can constrain. The isoscalar axion coupling is the

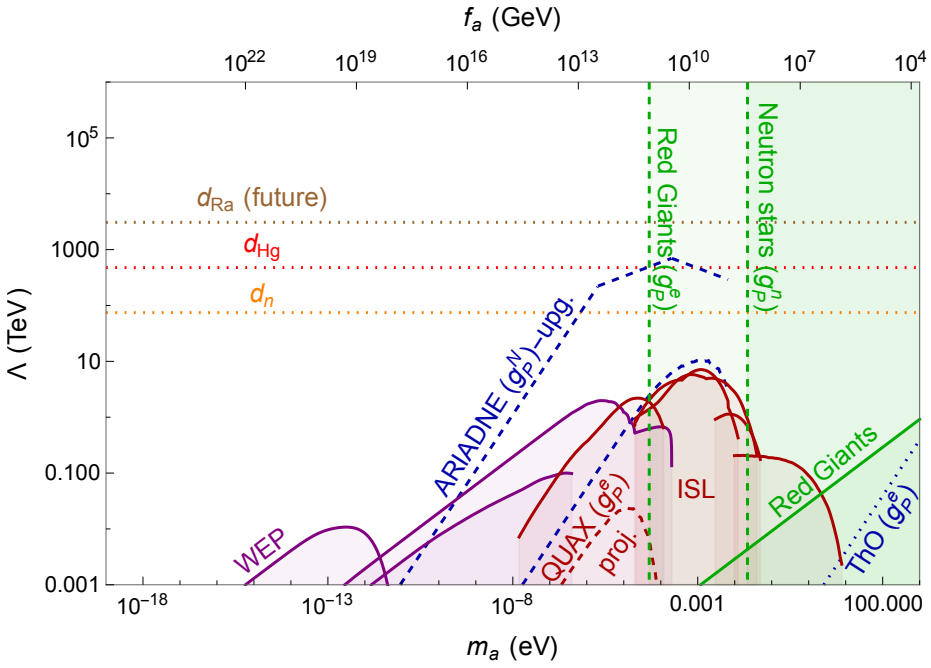

Figure 4.4: Constraints on Λ from various experiments discussed in Section 4.7. The labeling of the lines is explained in the caption of Fig. 4.3.

most relevant for the present discussion and scales as $g_S^{(0)} \sim 1/(f_a\Lambda^2)$. Fig. 4.3 shows the various constraints as a function of the axion mass (lower x-axis) or, equivalently, the axion decay constant (upper x-axis). For each observable, we compute the limit on the *CP*-odd Wilson coefficient, which we translate into a limit on $f_a\Lambda^2$ (shown on the right y-axis) and the corresponding value of $g_S^{(0)}$ (depicted on the left y-axis). Showing $g_S^{(0)}$ is a somewhat arbitrary choice, as different experiments are in principle sensitive to different combinations of $g_S^{(0,1)}$. However, once we assume a single Wilson coefficient, plotting $g_S^{(1)}$ instead would result in a rescaling of the (left) y-axis. The purple lines arise from searches for WEP violation, while the red lines are from tests of the inverse-square law. The constraints are most stringent for axion masses below 10^{-13} eV, reaching a sensitivity of $g_S^{(0)} \lesssim 10^{-24}$ which stems from the MICROSCOPE experiment. The limits are weaker for larger axion masses and disappear for $m_a > 1$ eV.

At the same time, the presence of a quark chromo-EDM can be looked for in EDM experiments. A down quark chromo-EDM induces the *CP*-odd pion-nucleon coupling $\bar{g}_1$ (among other *CP*-odd hadronic interactions), which leads to EDMs of nucleons and nuclei. In particular the limit on the EDM of the ^{199}Hg atom

sets a strong limit on $\bar{g}_1$ and thus $L_5^d \sim \Lambda^{-2}$. This limit can be converted into an indirect constraint on $g_S^{(0)}$ using Eq. (4.72). The corresponding constraints are depicted by dotted lines in Fig. 4.3. We observe that the indirect limits are at least several orders of magnitude stronger than the direct limits from fifth-force experiments, depending on m_a, in line with the conclusions of Ref. [198]. We also depict the constraint from a prospected ^{225}Ra EDM measurement at the level of 10^{-28} e cm [243]. This atom is particularly sensitive to $\bar{g}_1$ due to the octopole deformation of its nucleus. It would improve upon the current ^{199}Hg limit by one-to-two orders of magnitude at the projected sensitivity.

Perhaps a more promising way to detect *CP*-violating axion interactions than the current fifth-force measurements are monopole-dipole searches. Under the reasonable assumption that axions also have a *CP*-even axion-nucleon interaction of typical size, the proposed ARIADNE experiment could come very close to the EDM sensitivity for axions in the 10^{-5} - 10^{-1} eV mass range. The envisioned upgrade could even overtake the EDM limits in the same mass window. However, the CKM-induced *CP*-odd axion-nucleon couplings would still be too small by many orders of magnitude to be detected.

Finally, in Fig. 4.4, we show the same information slightly differently by putting the BSM scale Λ on the vertical axis. We observe that EDM limits reach scales of 10^2 to 10^3 TeV (note that this relies on the assumption $L_5^d = \frac{m_d}{\Lambda^2}$, while the quark chromo-EDMs are induced at one-loop order in many explicit BSM models), while fifth-force experiments only reach 10 TeV. The upgraded ARIADNE set-up could compete with EDM experiments in reaching a scale of around 10^3 TeV.

4.7.2 A leptoquark extension

Leptoquarks are hypothetical bosons that transform quarks into leptons and vice versa. They have become a popular model of BSM physics in light of various signals of lepton-flavor-universality violation, see e.g. [22, 23]. Leptoquarks generally have *CP*-violating interactions proportional to new, unconstrained phases. Unless these phases are chosen to be very small by hand, leptoquarks induce large radiative corrections to the QCD theta term and EDMs [238]. To illustrate this, we consider a simple scenario involving one scalar leptoquark. We pick the S_1 leptoquark that transforms as $(\bar{3}, 1, 1/3)$ under the SM gauge symmetries, $SU(3)_c \times SU(2) \times U(1)_Y$. These quantum numbers lead to four allowed dimension-four Yukawa-like interactions

$$\mathcal{L}_Y^{(S_1)} = S_1^\gamma \left[\bar{Q}_\gamma^{c,I} y_{LL} \epsilon_{IJ} L^J + \bar{u}_{R\,\gamma}^c y_{RR} e_R - \epsilon^{\alpha\beta\gamma} \bar{Q}_\alpha^I z_{LL}^\dagger \epsilon_{IJ} Q_\beta^{c,J} + \epsilon^{\alpha\beta\gamma} \bar{d}_{R\,\alpha} z_{RR}^\dagger u_{R\,\beta}^c \right] + \text{h.c.}\,. \tag{4.75}$$

Here α, β, γ are $SU(3)_c$ indices, $y_{LL,RR}$ and z_{RR} are generic 3×3 matrices in flavor space, while z_{LL} is a symmetric 3×3 matrix. $Q = (u_L\,, d_L)^T$ and $L = (\nu_L\,, e_L)^T$ denote the left-handed quark and lepton doublets in the weak eigenstate basis. We pick a basis in which the up-type quark and charged-lepton mass matrices are

diagonal so that the translation from weak to mass basis is given by $d_L^{\text{weak}} = V d_L$, where V is the CKM matrix. In principle, the interactions of S_1 lead to baryon-number-violating interactions, which can be avoided if either $y_{LL} = y_{RR} = 0$ or $z_{LL} = z_{RR} = 0$. These two cases lead to rather different conclusions regarding which EDM experiments are relevant and the type of axion interactions that are induced; we, therefore, consider both cases separately.

In the absence of an IR solution to the strong *CP* problem, the above LQ interactions can generate dangerously large contributions to $\bar{\theta}$. Similar to the R_2 leptoquark [293], the S_1 interactions induce the following threshold correction at the scale $\mu = m_{S_1}$ (in the $\overline{\text{MS}}$ scheme)

$$\begin{aligned}\delta\bar{\theta} \;\simeq\; & \frac{1}{(4\pi)^2}\left(\ln\left(\frac{m_{S_1}^2}{\mu^2}\right) - 1\right) \text{Im Tr}\left[Y_u^{-1} y_{LL}^* Y_e^* y_{RR}^T\right. \\ & \left. + 4 z_{LL}^\dagger \left(\left(Y_u^T\right)^{-1} z_{RR} Y_d^\dagger + Y_u^* z_{RR} Y_d^{-1}\right)\right] + \dots\,, \end{aligned} \tag{4.76}$$

where the SM Yukawa couplings are defined through $-\mathcal{L}_Y = \bar{Q} Y_u \tilde{H} u + \bar{Q} Y_d H d + \bar{L} Y_e H e + \text{h.c.}$ Furthermore, the ellipses are terms requiring two insertions of the SM Yukawa couplings. Any high-energy scale does not suppress the correction to $\bar{\theta}$. Thus, even when $\bar{\theta} = 0$ at the high scale, significant tuning of the LQ couplings is needed to ensure it remains small at low energies unless an IR solution of the strong *CP* problem, such as a PQ mechanism, is implemented. Therefore, we consider the above LQ interactions supplemented by a PQ mechanism.

Integrating out the leptoquarks at the tree-level leads to the following SMEFT operators

$$\begin{aligned}\mathcal{L}_{\psi^4} = {} & C_{lequ}^{(1)\,abcd} (\bar{L}_a^I e_{R_b}) \epsilon_{IJ} (\bar{Q}_c^J u_{R_d}) + C_{lequ}^{(3)\,abcd} (\bar{L}_a^I \sigma^{\mu\nu} e_{R_b}) \epsilon_{IJ} (\bar{Q}_c^J \sigma_{\mu\nu} u_{R_d}) \\ & + C_{quqd}^{(1)\,abcd} (\bar{Q}_a^I u_{R_b}) \epsilon_{IJ} (\bar{Q}_c^J d_{R_d}) + C_{quqd}^{(8)\,abcd} (\bar{Q}_a^I T^A u_{R_b}) \epsilon_{IJ} (\bar{Q}_c^J T^A d_{R_d}) + \text{h.c.}\,, \end{aligned} \tag{4.77}$$

with Wilson coefficients evaluated at the leptoquark threshold

$$\begin{aligned} C_{lequ}^{(1)\,abcd}(m_{S_1}) &= -4 C_{lequ}^{(3)\,abcd}(m_{S_1}) = \frac{1}{2} \frac{\left(y_{LL}^*\right)^{ca} \left(y_{RR}\right)^{db}}{m_{S_1}^2}\,, \\ C_{quqd}^{(1)\,abcd}(m_{S_1}) &= -\frac{1}{3} C_{quqd}^{(8)\,abcd}(m_{S_1}) = -\frac{2}{3} \frac{\left(z_{LL}^*\right)_{ac} \left(z_{RR}\right)_{bd}}{m_{S_1}^2}\,. \end{aligned} \tag{4.78}$$

The running of the induced SMEFT operators, as well as the subsequent matching onto the LEFT, is known as one-loop order [111–113, 211, 212], however, as we mainly aim to illustrate the connection between EDMs and probes of axion couplings, we neglect these effects in what follows. Since the same dimension-six operators generate *CP*-odd effects with and without axions, their renormalization

does not impact the comparison between the two types of experiments. However, the extraction of the bound on the BSM scale, $\Lambda \sim m_{S_1}$, can be affected by $\mathcal{O}(1)$ factors.

After electroweak symmetry breaking, these SMEFT coefficients generate the following LEFT interactions at tree level [9]

$$L^{S,RR}_{\substack{eu\\prst}} = -C^{(1)}_{\substack{lequ\\prst}}\,, \quad L^{S,RR}_{\substack{\nu edu\\prst}} = C^{(1)}_{\substack{lequ\\prvt}} V^*_{vs}\,, \quad L^{T,RR}_{\substack{eu\\prst}} = -C^{(3)}_{\substack{lequ\\prst}}\,, \quad L^{T,RR}_{\substack{\nu edu\\prst}} = C^{(3)}_{\substack{lequ\\prvt}} V^*_{vs}\,,$$
$$L^{S1,RR}_{\substack{ud\\prst}} = -L^{S1,RR}_{\substack{uddu\\prst}} = C^{(1)}_{\substack{quqd\\prvt}} V^*_{vs}\,, \qquad L^{S8,RR}_{\substack{ud\\prst}} = -L^{S8,RR}_{\substack{uddu\\prst}} = C^{(8)}_{\substack{quqd\\prvt}} V^*_{vs}\,. \tag{4.79}$$

Setting $V_{ud} \simeq 1$, these matching conditions then imply that $L^{2211}_{\mathbf{3}\times\mathbf{3}} = \frac{1}{2} C^{(1)}_{\substack{quqd\\1111}}$ while $L^{2211}_{\mathbf{6}\times\mathbf{6}} = 0$ and similar for couplings with $C^{(1)}_{quqd} \to C^{(8)}_{quqd}$ and $L_i \to \bar{L}_i$.

Semi-leptonic *CP*-violation. We begin by setting $z_{LL} = z_{RR} = 0$ such that only semi-leptonic operators are induced. For simplicity we consider couplings to first-generation fermions and set $a = b = c = d = 1$ in Eq. (4.78) resulting in *CP*-odd interactions between electrons and first-generation quarks. In particular, we obtain

$$C_S^{(0)} = -v_H^2 \frac{\sigma_{\pi N}}{m_u + m_d} \mathrm{Im}\, L^{S,RR}_{\substack{eu\\eeuu}}\,, \qquad C_S^{(1)} = -\frac{v_H^2}{2} \frac{\delta m_N}{m_d - m_u} \mathrm{Im}\, L^{S,RR}_{\substack{eu\\eeuu}}\,, \tag{4.80}$$

which contribute to *CP*-odd effects in ThO through Eq. (4.42). Here $C_S^{(1)}$ plays a marginal role and can be neglected for the present discussion. At the same time, the PQ mechanism leads to *CP*-odd axion-electron interactions. From Eq. (4.20) we read off

$$g_S^{(e)} = \frac{m_*}{2 f_a} \frac{m_\pi^2 F_\pi^2}{m_u + m_d} \frac{1}{m_u} \mathrm{Im}\, L^{S,RR}_{\substack{eu\\eeuu}}\,, \tag{4.81}$$

so that the ratio of these *CP*-odd interactions depends only on f_a (and thus the axion mass) and known QCD matrix elements

$$\frac{C_S^{(0)}}{g_S^{(e)}} = -2 \left(\frac{f_a}{F_\pi}\right) \frac{\sigma_{\pi N} v_H^2}{m_\pi^2 F_\pi} \frac{m_u + m_d}{m_d}\,, \tag{4.82}$$

in the limit $m_{u,d}/m_s \to 0$.

We compare the resulting constraints from EDM experiments and fifth-force searches in the $g_S^{(e)}$ versus m_a plane in the top panel of Fig. 4.5. Fifth-force experiments constrain $g_S^{(e)} \lesssim 10^{-24}$ for axion masses below 10^{-13} eV. The indirect constraints from EDM experiments are many orders of magnitude more stringent over the entire axion mass range. This gap is larger than was the case for the

[9] Here we moved to the mass basis of the quarks and charged leptons but left the neutrinos in the flavor eigenstates as they (and their masses) will not play a role in our analysis.

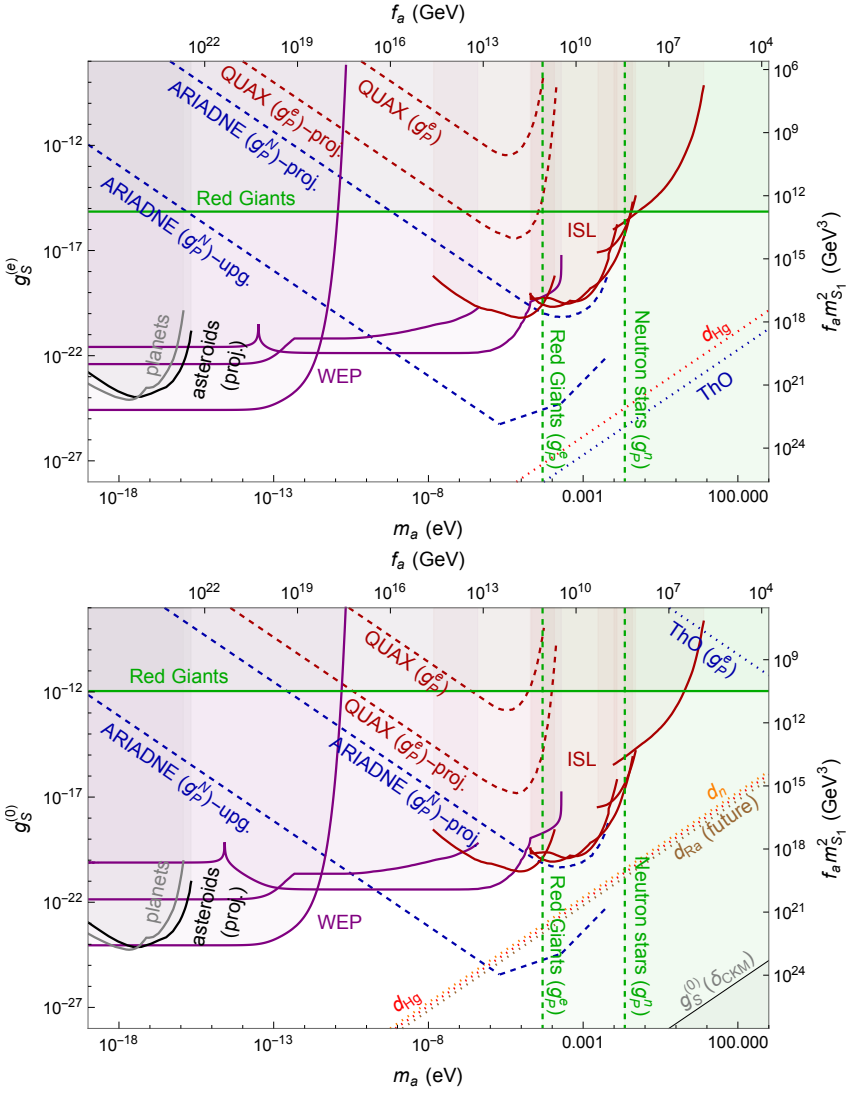

Figure 4.5: Constraints on the axion-electron and isoscalar axion-nucleon coupling in the leptoquark scenario discussed in Section 4.7.2. The top panel depicts the case in which semi-leptonic operators are induced by $y_{LL,RR} \neq 0$ while we set $z_{LL,RR} = 0$. The bottom panel shows the inverted scenario with $y_{LL,RR} = 0$ and $z_{LL,RR} \neq 0$, which leads to hadronic four-quark interactions. To obtain the mass scale, m_{S_1}, on right vertical axes we set the coupling constants to one, $\mathrm{Im}\,(y_{LL}^*)^{11}\, y_{RR}^{11} = 1$ and $\mathrm{Im}\,(z_{LL}^*)^{11}\, z_{RR}^{11} = 1$, for the upper and lower panels, respectively. The *CP*-even axial axion-fermion couplings are chosen as in the DFSZ model with $\tan\beta = 1$. For an explanation of the various lines, we refer to the caption of Fig. 4.3.

purely hadronic chromo-EDM operator because of the extremely tight limit from the ACME ThO experiment (Hg is slightly less constraining). The envisioned sensitivity of the ARIADNE experiment is no longer competitive with the EDM experiments in this case. Note that the SM contribution to $g_S^{(e)}$ is also harder to observe than the SM value of $g_S^{(0)}$, as can be seen from the fact that our estimate in Eq. (4.21) is too small to appear in Fig. 4.5.

Hadronic *CP*-violation. We now set $y_{LL} = y_{RR} = 0$ and focus on the resulting *CP*-odd four-quark interactions. In this case, we obtain *CP*-odd pion-nucleon couplings

$$\bar{g}_0 = -\frac{F_\pi \mathcal{A}_{\mathbf{3}\times\mathbf{3}}}{4B}\frac{\partial \delta m_N}{\partial(\bar{m}\epsilon)}\mathrm{Im}\left(C^{(1)}_{quqd}\right), \qquad \bar{g}_1 = \bar{g}_2 = 0\,, \tag{4.83}$$

and axion-nucleon interactions

$$\begin{aligned} g_S^{(0)} &= \frac{1}{2}\frac{m_*}{f_a}\frac{m_u+m_d}{m_u m_d}\mathrm{Im}\left(C^{(1)}_{quqd}\right)\left[\frac{1}{2}\frac{F_\pi^2\mathcal{A}_{\mathbf{3}\times\mathbf{3}}}{B}\frac{\partial}{\partial\bar{m}} + \frac{\partial}{\partial \mathrm{Re}\, L^{2211}_{\mathbf{3}\times\mathbf{3}}}\right]\Delta m_N\,, \\ g_S^{(1)} &= \frac{m_*}{8 f_a}\frac{m_d-m_u}{m_u m_d}\mathrm{Im}\left(C^{(1)}_{quqd}\right)\frac{F_\pi^2\mathcal{A}_{\mathbf{3}\times\mathbf{3}}}{B}\frac{\partial\delta m_N}{\partial(\bar{m}\epsilon)}\,, \end{aligned} \tag{4.84}$$

with similar contributions from color-octet operators, $C^{(1)}_{quqd} \to C^{(8)}_{quqd}$, $L_i \to \bar{L}_i$, $\mathcal{A}_{\mathbf{3}\times\mathbf{3}} \to \bar{\mathcal{A}}_{\mathbf{3}\times\mathbf{3}}$.

The ratios of these *CP*-odd interactions depend on the QCD matrix element $\partial\Delta m_N/\partial \mathrm{Re}\, L^{2211}_{\mathbf{3}\times\mathbf{3}}$ which is not known. For our analysis, we consider the indirect pieces only for which we do control the matrix elements. Under this assumption, we obtain

$$\begin{aligned} \frac{\bar{g}_0}{g_S^{(0)}} &= -\frac{1}{2}\frac{f_a}{F_\pi}\frac{m_u m_d}{m_*(m_u+m_d)}\frac{\partial\delta m_N}{\partial(\bar{m}\epsilon)}\left(\frac{\partial\Delta m_N}{\partial\bar{m}}\right)^{-1} \\ &\simeq -\frac{1}{2}\frac{f_a}{F_\pi}\frac{\partial\delta m_N}{\partial(\bar{m}\epsilon)}\left(\frac{\partial\Delta m_N}{\partial\bar{m}}\right)^{-1} + \mathcal{O}\left(\frac{m_{u,d}}{m_s}\right), \\ \frac{\bar{g}_0}{g_S^{(1)}} &= -2\frac{f_a}{F_\pi}\frac{m_u m_d}{m_*(m_d-m_u)} \simeq -2\frac{f_a}{F_\pi}\frac{m_u+m_d}{m_d-m_u} + \mathcal{O}\left(\frac{m_{u,d}}{m_s}\right), \end{aligned} \tag{4.85}$$

where the first ratio could be affected by $\mathcal{O}(1)$ factors due to unknown direct contribution.

In the bottom panel of Fig. 4.5 we compare limits from fifth-force experiments, EDM searches, and monopole-dipole experiments in the $g_S^{(0)} - m_a$ plane. Here the mass scale on the right vertical axis is obtained by setting $\mathrm{Im}\left(z^*_{LL}\right)^{11} z^{11}_{RR} = 1$ and using the color-singlet contributions as an estimate of the complete effect, with $\mathcal{A}_{\mathbf{3}\times\mathbf{3}} = \Lambda_\chi^2$, see Appendix C.1. As in Fig. 4.3, EDM experiments are more stringent than fifth-force searches. In this case, the projected ^{225}Ra measurement provides a smaller improvement on the ^{199}Hg limit than was the case for the

down-quark CEDM. This is because the generated four-quark operator, $L^{2211}_{\mathbf{3}\times\mathbf{3}}$, only induces $\bar{g}_0$ instead of $\bar{g}_1$, which comes with a smaller LEC (proportional to $\sim \delta m_N$ compared to $\sim \sigma_{\pi N}$). We again find that an upgraded version of ARIADNE could overtake the EDM limits in a small window of axion masses.

4.7.3 Left-right symmetric models

Left–right symmetric models are based on an extended gauge symmetry $SU(3)_c \times SU(2)_L \times SU(2)_R \times U(1)_{B-L}$ [17,18,190]. Minimal versions contain an enlarged scalar sector with one scalar bidoublet and two triplets whose vevs spontaneously break the extended gauge symmetry. Variants of the model with generalized parity forbid a QCD theta term at high scales where the discrete symmetry is exact. While this naively solves the strong *CP* problem, dangerous contributions to $\bar{\theta}$ are induced once the vevs spontaneously break the parity of the scalars. The leading correction arises from the phases in the quark mass matrices, which we can calculate explicitly [191]

$$\bar{\theta} \sim \text{Arg Det}\,(M_u M_d) \sim \frac{m_t}{m_b}\frac{\xi}{1-\xi^2}\sin\alpha\,, \tag{4.86}$$

where α is a phase related to *CP*-violation in the scalar sector, and ξ is related to the ratio of vacuum expectation values. This implies there is still a strong *CP* problem in the model: why $\bar{\theta}$ is much smaller than the naive $\mathcal{O}(1)$ expectation is then essentially translated to the question of why $\alpha \ll 1$ in the mLRSM.

If one extends the mLRSM with a PQ mechanism, the above contribution to $\bar{\theta}$ is relaxed to 0, but other contributions to $\langle\theta_a\rangle = \bar{\theta} + \frac{\langle a\rangle}{f_a}$ arise from *CP*-odd higher-dimensional operators that appear in the left-right model. In particular, integrating out the right-handed W boson leads to a dimension-six SMEFT operator [142]

$$\mathcal{L}_{6,\text{mLRSM}} \;=\; C^{ij}_{Hud} i\tilde{\varphi}^\dagger D_\mu \varphi\, \bar{u}^i_R \gamma^\mu d^j_R + \text{h.c.}\,, \tag{4.87}$$

where

$$C^{ij}_{Hud} \;=\; \frac{g_R^2}{m^2_{W_R}}\frac{\xi e^{i\alpha}}{1+\xi^2} V_{R,\,ij}\,, \tag{4.88}$$

in terms of the $SU(2)_R$ gauge coupling, $g_R = g$, and the mass of the right-handed gauge boson m_{W_R}. The matrix V_R is the right-handed version of the CKM matrix, and under a generalized parity symmetry we have $V_R = V$ in the limit $\xi \sin\alpha \to 0$ [296]. For more details, we refer to Ref. [295].

Again neglecting renormalization-group effects, we match to the LEFT operators below the electroweak scale

$$L^{V,LR}_{\substack{\nu edu\\ prst}} = -\delta_{pr}\left(C^{ts}_{Hud}\right)^*\,, \qquad L^{V1,LR}_{\substack{uddu\\ prst}} = -V_{pr}\left(C^{ts}_{Hud}\right)^*\,, \qquad L^{V8,LR}_{\substack{uddu\\ prst}} = 0\,. \tag{4.89}$$

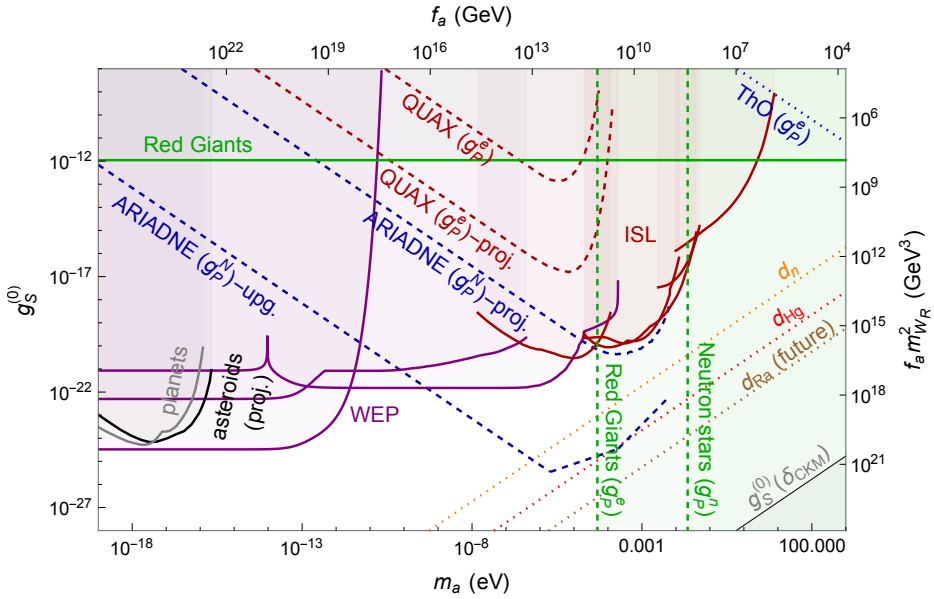

Figure 4.6: Constraints on the isoscalar axion-nucleon coupling in the left-right model discussed in Section 4.7.3. The *CP*-even axial axion-fermion couplings are chosen as in the DFSZ model with $\tan\beta = 1$. To obtain the mass scale, m_{W_R}, on the right vertical axis, we assumed $\frac{\xi \sin\alpha}{1+\xi^2} = m_b/m_t \sin\alpha$ (see Refs. [294, 295]) and pick $\sin\alpha = 1$. The labeling of the lines is explained in the caption of Fig. 4.3.

Focussing on the couplings to the first generation, we have $L^{1221}_{\mathbf{8}\times\mathbf{8}} = -V_{ud}\left(C^{ud}_{Hud}\right)^*$ and we read off the *CP*-odd pion-nucleon and axion-nucleon interactions

$$\begin{aligned} g_S^{(0)} &= \frac{m_*}{f_a}\frac{m_d - m_u}{m_u m_d}\mathrm{Im}\, L^{1221}_{\mathbf{8}\times\mathbf{8}}\left[\frac{\partial}{\partial \mathrm{Re}\, L^{1221}_{\mathbf{8}\times\mathbf{8}}} + \frac{1}{2}\frac{F_\pi^2 \mathcal{A}_{\mathbf{8}\times\mathbf{8}}}{2B}\frac{\partial}{\partial \bar{m}}\right]\Delta m_N\,, \\ g_S^{(1)} &= \frac{m_*}{f_a}\frac{m_d + m_u}{m_u m_d}\mathrm{Im}\, L^{1221}_{\mathbf{8}\times\mathbf{8}}\frac{F_\pi^2 \mathcal{A}_{\mathbf{8}\times\mathbf{8}}}{8B}\frac{\partial \delta m_N}{\partial(\bar{m}\epsilon)}\,. \end{aligned} \tag{4.90}$$

The *CP*-odd pion-nucleon couplings are

$$\bar{g}_0 = \bar{g}_2 = 0\,, \quad \bar{g}_1 = -\frac{2}{F_\pi}\mathrm{Im}\, L^{1221}_{\mathbf{8}\times\mathbf{8}}\left[\frac{\partial}{\partial \mathrm{Re}\, L^{1221}_{\mathbf{8}\times\mathbf{8}}} + \frac{1}{2}\frac{F_\pi^2 \mathcal{A}_{\mathbf{8}\times\mathbf{8}}}{2B}\frac{\partial}{\partial \bar{m}}\right]\Delta m_N\,. \tag{4.91}$$

While the matrix element $\partial \Delta m_N / \partial \mathrm{Re}\, L^{1221}_{\mathbf{8}\times\mathbf{8}}$ is not known, it drops out in the ratio of the isovector *CP*-odd pion-nucleon coupling to the isoscalar axion-nucleon coupling

$$\frac{\bar{g}_1}{g_S^{(0)}} = -2\frac{f_a}{F_\pi}\frac{m_u m_d}{(m_d - m_u)m_*}\,, \tag{4.92}$$

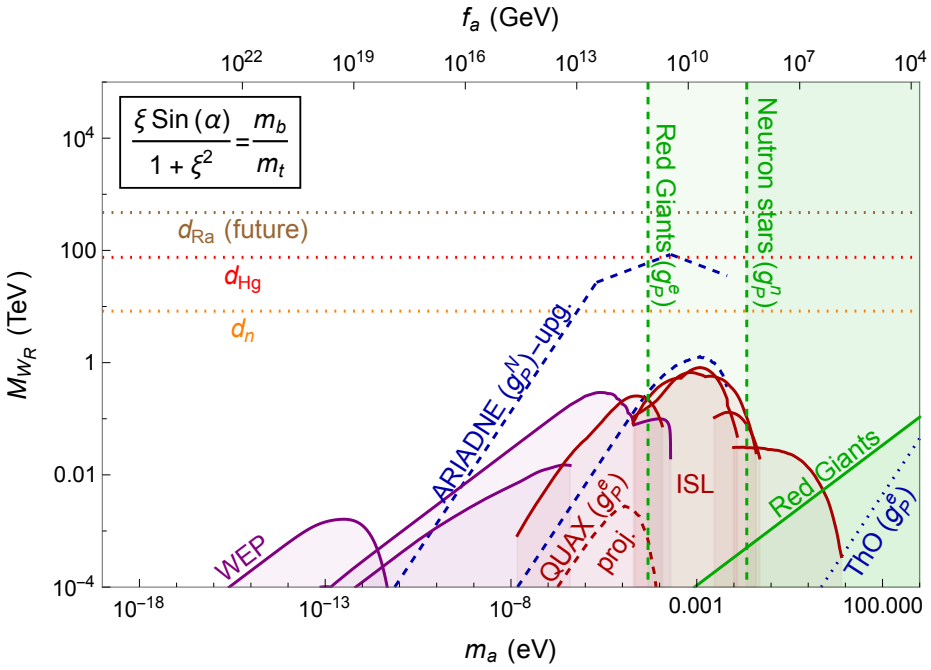

Figure 4.7: Limits on the mass of right-handed gauge bosons from various experiments discussed in Section 4.7. The labeling of the lines is explained in the caption of Fig. 4.3.

while the less relevant ratio $\bar{g}_1/g_S^{(s)}$ depends on the unknown matrix element. If we consider only the indirect pieces, we get a rough estimate

$$g_S^{(0)} \simeq 0.11\,\text{GeV}^2\,\frac{F_\pi}{f_a}\,\text{Im}\,L^{1221}_{\mathbf{8}\times\mathbf{8}}\,, \qquad \bar{g}_1 \simeq -0.62\,\text{GeV}^2\,\text{Im}\,L^{1221}_{\mathbf{8}\times\mathbf{8}}\,, \tag{4.93}$$

which we use to generate the lines in Fig. 4.6. In Fig. 4.7 we show the same information but now interpreted in terms of a limit on the mass of the right-handed gauge bosons M_{W_R}. EDM experiments set stringent limits on the *CP*-odd axion-nucleon coupling and on the mass of right-handed gauge bosons of around $M_{W_R} > 100$ TeV for reasonable choices of ξ and $\sin\alpha$. The neutron EDM limit was recently discussed in a similar LR scenario [201], with which we find general agreement. In addition, we observe that the Hg EDM sets an even more stringent constraint that can only be overtaken by the upgraded set-up of ARIADNE in a small window of axion masses around 10^{-4} eV. Note that the projected ^{225}Ra EDM measurement would provide a significant improvement on the current ^{199}Hg limits, as the generated four-quark operator, $L^{1221}_{\mathbf{8}\times\mathbf{8}}$, contributes to $\bar{g}_1$ in contrast to $L^{2211}_{\mathbf{3}\times\mathbf{3}}$ discussed in the previous section.

4.8 Conclusions

Axions provide a compelling solution to the strong *CP* problem that has led to a tremendous amount of theoretical and experimental effort toward their first detection. In the presence of *CP*-violating sources beyond the QCD $\bar{\theta}$-term, the axion develops interactions with SM fields that violate *CP* symmetry. Within the Standard Model, the CKM phase leads to small *CP*-odd axion-lepton and axion-hadron interactions that seem impossible to detect with foreseeable technology. However, in the presence of BSM sources of *CP*-violation, motivated, for instance, by the matter-antimatter asymmetry, *CP*-odd axion interactions can be much larger. Moreover, if such BSM sources emerge at energies well above the electroweak scale, they can be captured by local effective operators. In this part of the thesis, we have systematically studied the form and size of *CP*-violating axion interactions induced by *CP*-violating dimension-six interactions. We list here the main results of our analysis:

- We have implemented a Peccei-Quinn mechanism in the presence of a general set of *CP*-violating EFT operators built from elementary Standard Model fields. The *CP*-odd interactions involving quarks and gluons shift the minimum of the axion potential away from that of the pure QCD-axion case, leaving a remnant of *CP*-violation behind. In addition, hadronic *CP*-odd operators can cause a misalignment of the vacuum, allowing for meson-vacuum transitions. We determined the chiral rotations that are needed in order to align the vacuum in Section 4.2.2, with explicit expressions in Appendix C.5. The main consequence is that electric dipole moments and other *CP*-violating observables can be larger than the predictions from the CKM phase of the Standard Model and that axions can obtain *CP*-odd Lorentz-scalar interactions with nucleons and leptons in addition to the usual (derivative) axial-vector couplings.

- We have used chiral perturbation theory to derive *CP*-violating axion-lepton, axion-meson, and axion-baryon interactions, for dimension-five and -six *CP*-violating operators involving light quarks and gluons in LEFT. The axion-lepton interactions arise from *CP*-violating lepton-quark interactions that, for example, appear in leptoquark models. Because of spontaneous chiral symmetry breaking and the appearance of a nonzero quark condensate, these interactions allow the axion to couple to leptons. Hadronic *CP*-violation leads to couplings between axions and two pseudoscalar Goldstone bosons without derivatives. Axion couplings to pions lead to corrections to axion-nucleus interactions through loop diagrams and two-nucleon currents. Flavor-changing axion-meson-meson couplings can lead to rare decays such as $K \to \pi + a$.

  The most important hadronic interactions, however, are axion-nucleon couplings. We determined which low-energy constants, or QCD matrix elements, are required to calculate the coupling strengths. These axion-nucleon

couplings generally obtain indirect contributions from purely mesonic matrix elements after vacuum alignment. Most of these matrix elements are relatively well known, for instance, from lattice-QCD calculations for neutrinoless double beta decay [297] or the bag factors that enter $B - \bar{B}$ oscillations [298]. In addition, there are direct contributions in the same order involving baryonic matrix elements, about which much less is known. An advantage is that the same matrix elements appear in EDMs' study, which has led to large-scale efforts to determine them from lattice-QCD calculations; see Ref. [299] for a recent review.

- The *CP*-odd LEFT operators not only induce *CP*-odd couplings of the axion, but they also generate *CP*-violating nucleon-lepton and nucleon-pion couplings. Moreover, we show that these *CP*-odd couplings depend on the same QCD matrix elements that enter the expressions for the axion-lepton and axion-nucleon interactions. As a result, a clear relationship exists between the *CP*-odd couplings with and without axions.

- We have collected direct and indirect constraints on *CP*-odd axion-nucleon and axion-electron couplings from a broad range of experiments. Searches set the direct constraints for fifth-forces that are proportional to the product of two *CP*-odd couplings and by astrophysical processes. Indirect constraints arise from the product of a *CP*-even and *CP*-odd coupling. This leads to some model dependence as the *CP*-even couplings depend on the UV implementation of the Peccei-Quinn mechanism. Indirect constraints also arise from experiments probing beyond-the-Standard-Model *CP*-violation, in particular, electric dipole moment searches.

  For a given source of *CP*-violation and a given axion mass, a direct connection exists between *CP*-odd axion-nucleon and axion-electron couplings and electric dipole moments of nucleons, atoms, and molecules. In general, we find that EDMs set the most stringent constraints, but the prospects for the ARIADNE experiment are sufficiently strong to overtake EDM limits in a window of axion masses (10^{-5}-10^{-1} eV). This implies that if ARIADNE measures a nonzero signal, it will point to a specific range of axion masses. Similarly, if future fifth-force experiments find evidence for axions, it will point to a rather non-generic beyond-the-Standard-Model scenario. One option is that the dimension-six operators arose in a very specific combination, such that their contributions to EDMs are negligible while still generating sizable *CP*-odd axion couplings. The second possibility would be that the effective-field-theory framework set-up in this part of the thesis does not apply, implying the existence of additional light degrees of freedom.

4.9 Outlook

The framework we have constructed can be further developed in several directions.

- First of all, we have only computed the leading-order axion-nucleus interactions. In principle, the chiral Lagrangian leads to a richer structure at higher orders where, in addition to axion-nucleon effects, there also appear axion-nucleon-nucleon interactions (see Fig. 4.2). The power counting for nuclear currents is not fully understood as demonstrated in Chapter 3, and it would be interesting to study such contributions further, in analogy to similar studies for WIMP-nucleus scattering [100, 253, 254].

- Another direction would involve the study of EFT interactions with heavier leptons. We have focused on axion-electron couplings, probed by fifth-force searches and for which strong indirect constraints exist from EDM experiments. By turning on effective interactions between quarks and muons (motivated, for instance, by the muon $g-2$ discrepancy), CP-odd axion-muon interactions can appear which are not as stringently constrained directly and for which no indirect EDM constraints exist. Such axion-muon interactions can potentially be constrained by supernovae cooling rates in analogy to the analysis in Ref. [300] for CP-even axial vector couplings.

- This part of the thesis has mainly focused on flavor-conserving CP-violating LEFT operators involving light quarks and electrons. While we have briefly discussed more general couplings, for example the CP-odd $\Delta S = 1$ couplings that lead to $K \to \pi + a$ transitions or lepton-flavor-violating operators that could lead to $\mu + N \to e + N$, a more thorough analysis of such interactions would be very interesting. We have also not discussed operators involving bottom or charm quarks or SMEFT operators containing electroweak gauge and Higgs bosons, or top quarks, that are integrated out at the level of our LEFT analysis. It might be that CP-odd axion couplings to heavier fields could lead to interesting phenomenology at higher energies not discussed in this part of the thesis. Of course, the CP-odd operators are still stringently constrained by low-energy experiments such as EDMs or probes of lepton number violation. It remains to be seen how much room there is for axionic couplings.

- If axions form our Universe's dark matter, this will lead to additional tests. A popular axionic DM model is where axion acts like a coherently oscillating scalar field

$$a(t) = a_0 \cos(m_a t)\,, \tag{4.94}$$

  where $a_0 = \sqrt{2\rho_{\rm DM}}/m_a$ is the amplitude of axion oscillation, $\rho_{\rm DM}$ is the local DM density, and the frequency is given by the axion mass m_a. This axion DM creates a time oscillation of fundamental parameters. For example, by Eq. (4.20) we get time varying electron mass

$$\mathcal{L} = -m_e \bar{e} e + g_S^{(e)} a(t) \bar{e} = -\tilde{m}_e(t) \bar{e} e\,, \tag{4.95}$$

where

$$\tilde{m}_e(t) = m_e \left(1 - g_S^{(e)} \frac{\sqrt{\rho_{\rm DM}}}{m_a m_e} \cos m_a t\right) . \tag{4.96}$$

Similarly, we get the time-varying nucleon masses $\tilde{m}_p(t), \tilde{m}_n(t)$. The axion interaction to the electromagnetic tensor $\mathcal{L} = -\frac{\bar{g}_{a\gamma} a(t)}{4} F^{\mu\nu} F_{\mu\nu}$ leads to time-varying fine-structure constant $\alpha_{\rm em}(t)$. We are currently exploring whether these time-varying quantities lead to some resonance effects, which can be searched through atomic experiments. We are investigating whether these experiments provide competent constraints as the various experiments discussed in Sections 4.4, 4.5, and 4.6. The proposed atomic clock experiments exploit the DM axion-induced time oscillation of fine-structure constant to constrain the *CP*-violating axion couplings [301].

The $a(t)FF \sim a(t)(\mathbf{B}\cdot\mathbf{B} - \mathbf{E}\cdot\mathbf{E})$ interaction can lead to a coherently oscillating electric (magnetic) field for a static electric (magnetic) field background in ion trap experiments. This could result in a time-dependent potential for ions in a radiofrequecy trap. Furthermore, the micromotion induced by such potential could heat the ions by ion-atom collissions [302]. This could be a novel addition to axion searches. We are currently exploring the possibility of using ion traps and atomic clocks for setting constraints on *CP*-violating axion interactions.

Chapter 5

Dark Matter scattering off ^{4}He through scalar interactions

J. de Vries, C. Körber, A. Nogga, and S. Shain,
"Dark Matter scattering off ^{4}He through scalar interactions"
(to be submitted)

5.1 Introduction

There is an abundance of astrophysical and cosmological evidence for the existence of dark matter (DM) [9]. However, we have not yet observed any conclusive DM signal from any of the direct detection, indirect detection, or collider experiments (see Section 1.7). In the previous chapter, we explored axion as a possible DM candidate. In this part of the thesis, we consider the other famous class of DM candidates: weakly interacting massive particles (WIMPs). If the puzzle of DM has a particle solution, it must correspond to a massive, (semi-)stable particle that is not charged under QCD or quantum electrodynamics (technically it could be a milli-charged particle but we do not consider that there). While DM has to interact gravitationally we can only hope to detect it if it has some other interactions as well. In this chapter, we consider a specific well-motivated set of interactions and focus on DM direct detection using light nuclei.

Next-generation direct detection experiments aim to probe uncharted parameter space for a wide range of DM masses well beyond the 'traditional' WIMP regime of GeV-to-TeV DM masses. To interpret these direct detection searches in terms of the underlying DM models and to connect to cosmological aspects of DM, such as the relic density, it is essential to have well-controlled theoret-

ical predictions for WIMP cross-sections off atomic nuclei. These predictions are complicated due to widely separated energy scales associated with particle, hadronic, and nuclear processes. The last decade has seen the development of effective field theory (EFT) approaches to overcome this difficulty. For example, by assuming that DM fields are singlets under the Standard Model (SM) gauge symmetries, the DM interactions with SM fields can be captured by a series of effective operators which are dominated by the operators of the lowest dimension. After renormalization-group evolution to lower energies, these interactions can be matched to effective interactions between DM and hadrons and nuclei, which, in turn, can be used to compute DM-nucleus scattering rates.

The nuclear physics aspects of DM direct detection have also been discussed in different EFT frameworks [253, 303–307]. Ref. [304] described an EFT for DM-nucleon interactions by constructing all interactions up to a given order in momentum transfer. We take an approach that is grounded in QCD and includes the consequences of spontaneous chiral symmetry breaking. Assuming a given set of DM-SM interactions, the chiral-EFT approach allows for a systematic construction of DM-hadron interactions with a well-defined power counting. In chiral EFT, DM-nucleus scattering does not depend purely on DM-nucleon interactions but also from two- and more-nucleon currents that, for example, arise from DM-pion interactions [253, 305, 307, 308]. We will focus on scalar-mediated DM-SM interactions for several reasons. First of all, they appear in well-motivated scenarios such as Higgs portal DM [309]. Second, scalar current leads to spin-independent scattering rates that grow with A^2 where A is the atomic mass number of the target atoms. Third, for scalar currents, two-nucleon currents appear at the next-to-leading-order (NLO) in Weinberg's power counting. This last point is very interesting, NLO would imply $\mathcal{O}(30\%)$ corrections, and if they can be experimentally isolated, it might be possible to determine the type of DM-SM interactions (for instance, vector-mediated interactions also lead to spin-independent scattering rates but have much smaller two-body currents). Unfortunately, explicit computations of the two-body corrections are found to be inconclusive. While shell-model computations for ^{132}Xe found $\mathcal{O}(20\%)$ corrections [310], of the expected size, calculations on lighter nuclei found smaller effects [311].

More problematic is the observation that the two-body corrections in DM scattering off the deuteron, ^{3}H, and ^{3}He, strongly depend on the details of the applied wave function and thus on the applied nucleon-nucleon potential used to generate the wave functions [100]. Similar conclusions were drawn in Ref. [312], which applied phenomenological wave functions of various light nuclei and observed a large dependence on the applied regulator used in intermediate steps of the numerical calculations. These results are worrisome as they indicate a potential problem in the chiral EFT power counting and jeopardize the interpretation of large-scale WIMP-nucleus cross-section predictions. In Chapter 3, we have verified the failure Weinberg's power counting rule for *CP*-violating nuclear forces. Similar power-counting problems were recently identified in other nuclear probes of beyond-the-Standard Model physics, such as neutrinoless double beta decay [147]

and indicate the presence of additional short-range two-nucleon currents [179]. In this part of the thesis, we extend the calculations of Ref. [100] to scattering off ^{4}He nuclei in order to test the power counting.

We select ^{4}He because of two reasons. First of all, WIMP searches [313], see e.g. [314], have been proposed using a liquid ^{4}He detector [102]. The main motivation to use relatively light target nuclei is to get sensitivity to lighter WIMPs to which more conventional experiments, for instance, those involving Xe nuclei, have less sensitivity. Second, compared to $A = 2$ and $A = 3$ nuclei, the binding energy per nucleon is much larger and comparable to heavier isotopes. We are particularly interested in determining whether the conclusions of [100] regarding two-nucleon currents are related to specific spin-isospin properties and/or the diluteness of the deuteron, ^{3}H, and ^{3}He nuclei.

This chapter is organized as follows. In Section 5.2, we explain the computational framework in detail. This includes the chiral Lagrangian, scattering diagrams, LO and NLO DM currents, and the scattering cross sections. In Section 5.3, we outline the procedure we used to calculate the cross-section and briefly discuss the density matrix formalism. We present our results in Section 5.4 and conclude in Section 5.5.

5.2 Computational framework

We perform first-principle computations of DM scattering off ^{4}He isotopes. We apply chiral EFT to both generate the ^{4}He wave functions as well as the DM currents and systematically compute the resulting DM-^{4}He scattering rate. The scalar DM-SM interactions are given by

$$\mathcal{L}_\chi = \bar{\chi}\chi \left(c_u \, m_u \, \bar{u}u + c_d \, m_d \, \bar{d}d + c_s \, m_s \, \bar{s}s + c_G \, \alpha_s G^A_{\mu\nu} G^{\mu\nu\, A} \right) \ , \tag{5.1}$$

where χ denotes a spin-1/2 DM fermion (for other DM spins, the computations are almost identical). u, d, and s denote, respectively, quark fields with quark masses $m_{u,d,s}$, and $G^A_{\mu\nu}$ is the gluon field strength. We factored out one power of $\alpha_s = g_s^2/(4\pi)$. $c_{u,d,s,G}$ describe four unknown coupling constants of mass dimension (-3) that parametrize the couplings strengths of DM with quarks and gluons. They can be computed in specific DM models, for example, in Higgs portal models [309]. We consider the Lagrangian in Eq. (5.1) to be valid at relatively low energies ($\mu = 1$ GeV) where we match to hadronic DM interactions. Other interactions beyond those in Eq. (5.1) are certainly possible but tend to lead to suppressed two-body currents. See, for instance [307] for recent first-principle computations for spin-dependent cross sections. In what follows, we focus on the couplings to up and down quarks as only these lead to sizeable two-nucleon currents. For a discussion of the strange quark and gluonic interaction we refer to Ref. [100]. Since these interactions are dominated by one-body currents, they do not involve additional nuclear calculations from those performed here.

5.2.1 Chiral Lagrangian

By application of chiral perturbation theory, the interactions in Eq. (5.1) can be matched to interactions between DM and nucleons, pions, and heavier hadrons. We will use the $SU(2)$ χPT framework for simplicity. The relevant Lagrangian is

$$\mathcal{L} = \frac{F_\pi^2}{4}\mathrm{Tr}[U^\dagger\chi + U\chi^\dagger] + c_1\mathrm{Tr}(\chi_+)\bar{N}N + c_5\bar{N}\hat{\chi}_+N\,, \tag{5.2}$$

where [1]

$$U = u^2 = \exp\left(\frac{i\vec{\pi}\cdot\vec{\tau}}{F_\pi}\right), \qquad \chi = 2B(M_0 + s)\,, \tag{5.3}$$

$$M_0 = \begin{pmatrix} m_u & 0 \\ 0 & m_d \end{pmatrix}, \qquad \chi_+ = u^\dagger\chi u^\dagger + u\chi^\dagger u\,. \tag{5.4}$$

with $\hat{\chi}_+ = \chi - \frac{1}{2}\mathrm{Tr}\chi$. The DM interactions enter as the scalar current $s = \mathrm{Diag}(c_u m_u\bar{\chi}\chi, c_d m_d\bar{\chi}\chi)$ and the pion triplet and Pauli matrices are denoted by $\vec{\pi}$ and $\vec{\tau}$, respectively. $c_{1,5} \sim \mathcal{O}(1/\Lambda_\chi)$ are the LECs associated with the nucleon sigma term and the strong proton-neutron mass splitting.

The relevant DM-pion interactions from Eq. (5.2) are

$$\mathcal{L}_\pi = \frac{m_\pi^2}{2}\bar{c}_{q^{(\mathrm{is})}}\vec{\pi}\cdot\vec{\pi}\;\bar{\chi}\chi\,. \qquad c_q^\pi = \frac{m_\pi^2}{4}[c_u(1-\varepsilon) + c_d(1-\varepsilon)] \equiv \frac{m_\pi^2}{2}\bar{c}_{q^{(\mathrm{is})}}\,. \tag{5.5}$$

Effective isoscalar DM coupling is defined as

$$\bar{c}_{q^{(\mathrm{is})}} = \frac{1}{2}[c_u(1-\varepsilon) + c_d(1-\varepsilon)]\,, \tag{5.6}$$

with $\varepsilon = (m_d - m_u)/(m_d + m_u) = 0.36 \pm 0.03$ [53]. The relevant DM-nucleon interactions are

$$\mathcal{L}_N = -4m_\pi^2 c_1\bar{c}_{q^{(\mathrm{is})}}\bar{N}N\bar{\chi}\chi + B(m_d - m_u)c_5\bar{c}_{q^{(\mathrm{iv})}}\,, \tag{5.7}$$

where we defined the effective isovector DM coupling as

$$\bar{c}_{q^{(\mathrm{iv})}} = c_u(1-\varepsilon^{-1}) + c_d(1+\varepsilon^{-1})\,. \tag{5.8}$$

5.2.2 Power counting

The diagrams contributing to the DM-nucleon scattering are given in Fig. 5.1. The diagram 5.1a depicts the DM-nucleon contribution to the scattering, and diagrams 5.1b and 5.1c depict the DM-pion contributions to the scattering via one-nucleon and two-nucleon interactions, respectively. We use the χPT power counting rules, see Section 2.3.4, to determine the relative relevance of the DM-nucleon scattering

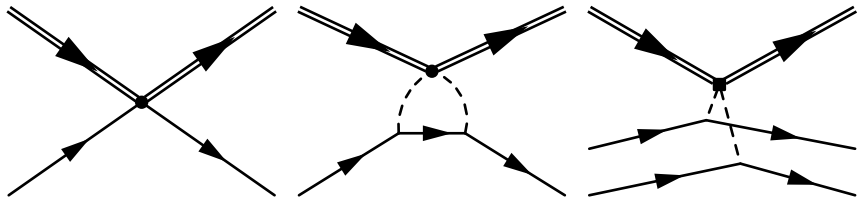

Figure 5.1: Diagrams contribution to DM-nucleus scattering. Solid lines correspond to nucleons, dashed lines to pions, and double-solid lines to DM.

diagrams in Fig. 5.1. Since we do not know the relative size of the scalar DM couplings, we treat the isoscalar and isovector interactions separately.

The power counting of diagram 5.1a gives

$$\mathcal{A}_a \sim m_\pi^2 c_1 \bar{c}_{q^{(\mathrm{is})}} \sim \bar{c}_{q^{(\mathrm{is})}} \frac{m_\pi^2}{\Lambda_\chi} \,. \tag{5.9}$$

Here we are including the overall normalization common to all diagrams. This diagram defines the LO contributions for DM scattering.

In comparison with the LO diagram, diagram 5.1b has an additional irreducible loop, one nucleon propagator, two pion propagators, and two pion-nucleon vertices. Thereby, the power counting gives

$$\mathcal{A}_b \sim m_\pi^2 \bar{c}_{q^{(\mathrm{is})}} \cdot \frac{p^4}{(4\pi)^2} \cdot \frac{1}{p} \cdot \left(\frac{1}{p}\right)^2 \cdot \left(\frac{g_A p}{F_\pi}\right)^2 \sim \bar{c}_{q^{(\mathrm{is})}} \frac{m_\pi^2}{\Lambda_\chi} \times \frac{p}{\Lambda_\chi} \,, \tag{5.10}$$

where we used $4\pi F_\pi = \Lambda_\chi$ and $g_A \sim 1$. This diagram contributes at the NLO since it has an additional factor of p/Λ_χ with respect to the LO diagram.

Once we compare the diagram 5.1c to the LO diagram, the former has an additional reducible loop, a nucleon propagator, two pion propagators, and two pion-nucleon vertices in comparison to the latter. The power counting rules gives

$$\mathcal{A}_c \sim m_\pi^2 \bar{c}_{q^{(\mathrm{is})}} \cdot \frac{p^5}{m_N (4\pi)^2} \cdot \frac{m_N}{p^2} \cdot \left(\frac{1}{p}\right)^2 \cdot \left(\frac{g_A p}{F_\pi}\right)^2 \sim \bar{c}_{q^{(\mathrm{is})}} \frac{m_\pi^2}{\Lambda_\chi} \times \frac{p}{\Lambda_\chi} \,. \tag{5.11}$$

Thereby, this diagram also contributes at the NLO.

Now we repeat the process for isovector interactions. Diagram 5.1a scales as $\sim \bar{c}_{q^{(\mathrm{iv})}} (\varepsilon m_\pi^2 / \Lambda_\chi)$ and contributes at LO. Naively, it seems that the isovector LO diagram is suppressed by a factor of ε relative to the isoscalar LO diagram. However, since we do not know the relative size of $\bar{c}_{q^{(\mathrm{is})}}$ and $\bar{c}_{q^{(\mathrm{iv})}}$, we can not make any such conclusions. Since there are no isospin-breaking DM-pion interactions in Eq. (5.5), the diagrams 5.1b and 5.1c do not contribute at NLO.

[1] χ is used to denote both DM and the chiral field. Since DM always appears as $\bar{\chi}\chi$ it is easy to distinguish it from the chiral field.

5.2.3 LO and NLO DM currents

The leading-order (LO) currents involve a single nucleon and are conveniently written as

$$J^{(\text{one-body})}(\boldsymbol{q}) = \left[\sigma_{\pi N} - \frac{9g_A^2\pi m_\pi^3}{4(4\pi F_\pi)^2} F\left(\frac{|\boldsymbol{q}|}{2m_\pi}\right)\right] \bar{c}_{q^{(\text{is})}} - \frac{\delta m_N}{4}\bar{c}_{q^{(\text{iv})}}\,\tau_i^3\,, \tag{5.12}$$

where $\boldsymbol{q}_i = \boldsymbol{p}_i' - \boldsymbol{p}_i$ is the difference between the outgoing and incoming momentum of nucleon i, and σ_i (τ_i) the spin (isospin) of nucleon i. The loop function associated to diagram 5.1b is

$$F(x) = \frac{-x + (1+2x^2)\arctan x}{3x}\,. \tag{5.13}$$

The various low-energy constants are given by [155]

$$\sigma_{\pi N} = (59.1 \pm 3.5)\,\text{MeV}\,, \qquad \delta m_N = (2.32 \pm 0.17)\,\text{MeV}\,, \tag{5.14}$$

where we used a Roy-Steiner extraction of the pion nucleon sigma term [225]. Lattice QCD tends to predict somewhat smaller values but might be plagued by excited-state contamination [315, 316]. dequation

In addition, diagram 5.1c induces a two-body current given by

$$J^{\text{two-body}}(\boldsymbol{q}) = -m_\pi^2\left(\frac{g_A}{2f_\pi}\right)^2 \frac{(\boldsymbol{\sigma}_1\cdot\boldsymbol{q}_1)(\boldsymbol{\sigma}_2\cdot\boldsymbol{q}_2)}{(\boldsymbol{q}_1^2+m_\pi^2)(\boldsymbol{q}_2^2+m_\pi^2)}\tau_1\cdot\tau_2\,\bar{c}_{q^{(\text{is})}}\,. \tag{5.15}$$

5.2.4 Scattering cross section

We investigate scattering processes $\chi(\boldsymbol{p}_\chi) + T(\boldsymbol{p}_T) \to \chi(\boldsymbol{p}_\chi') + T(\boldsymbol{p}_T')$, where T denotes the target nucleus consisting of A nucleons and has a mass m_T. The elastic unpolarized differential cross section is given by

$$\frac{\mathrm{d}\sigma}{\mathrm{d}\boldsymbol{q}^2} = \frac{1}{4\pi v_\chi^2}\frac{1}{2j+1}\sum_{m_j,m_j'=-j}^{j}\left|\left\langle\Psi_T, jm_j'\right|\hat{J}(\boldsymbol{q}^2)\left|\Psi_T, jm_j\right\rangle\right|^2\,, \tag{5.16}$$

where $\boldsymbol{q}$ is the momentum transfer from DM to the target nucleus, and v_χ the DM velocity. The wave function of the target nucleus $|\Psi_T, jm_j\rangle$ corresponds to a nucleus with total angular momentum j and polarization m_j.

It is convenient to factor out the isoscalar piece to discuss the various one- and two-body nuclear response functions. We follow the Ref. [100] and express the differential cross section in terms of response functions $\mathcal{F}_{i,a}^{(\nu)}(\boldsymbol{q}^2)$

$$\begin{aligned}\frac{\mathrm{d}\sigma}{\mathrm{d}\boldsymbol{q}^2} = \bar{c}_{q^{(\text{is})}}^2\frac{\sigma_{\pi N}^2 A^2}{4\pi v_\chi^2}\Big|&\left(\mathcal{F}_{\text{is}}^{(0)}(\boldsymbol{q}^2) + \mathcal{F}_{\text{is},2b}^{(1)}(\boldsymbol{q}^2) + \mathcal{F}_{\text{is},r}^{(1)}(\boldsymbol{q}^2) + \dots\right)\\ &+ \alpha_{\text{iv}}\left(\mathcal{F}_{\text{iv}}^{(0)}(\boldsymbol{q}^2) + \dots\right)\Big|^2\,,\end{aligned} \tag{5.17}$$

where we kept terms up to NLO in the chiral power counting. For response function $\mathcal{F}_{i,a}^{(\nu)}(\boldsymbol{q}^2)$, the superscript ν denotes the chiral order, the subscript $i = \{\text{is}, \text{iv}\}$ denote the types of DM couplings, and the subscript $a = \{r, 2b\}$ indicate the NLO radius and two-body corrections. We have defined

$$\alpha_{\text{iv}} = -\left(\frac{\delta m_N}{4\sigma_{\pi N}}\right)\frac{\bar{c}_{q^{(\text{iv})}}}{\bar{c}_{q^{(\text{is})}}}\,. \tag{5.18}$$

The above definitions imply a normalization $\mathcal{F}_{\text{is}}^{(0)}(0) = 1$. The radius correction $\mathcal{F}_{\text{is},\,r}^{(1)}\left(\boldsymbol{q}^2\right)$ involves the same nuclear information as $\mathcal{F}_{\text{is}}^{(0)}$ except for an additional overall dependence on $\boldsymbol{q}^2$. We therefore need to perform nuclear calculations of $\mathcal{F}_{\text{is}}^{(0)}(\boldsymbol{q}^2)$, $\mathcal{F}_{\text{iv}}^{(0)}(\boldsymbol{q}^2)$, and $\mathcal{F}_{\text{is},\,2b}^{(1)}\left(\boldsymbol{q}^2\right)$, which we will present below for various target nuclei.

5.3 Cross section calculation

To compute the necessary matrix elements, we require nuclear wave functions of various light isotopes. As our aim is to work fully in χPT, we want to derive wave functions and currents both from χPT Lagrangians. We refer to Chapter 3 for a discussion of χPT nucleon-nucleon potentials. We use the chiral interactions from Ref. [317] to calculate the chiral wave functions up to N^{4}LO chiral order. For ^{4}He, we also show results for wave functions which include N^{5}LO contact interactions in the F-waves; these are labeled N^{4}LO+. The main success of this approach is that it is able to describe various NN observables with high accuracy and that, once used in few-body calculations, can describe a large set of nuclear properties. The integral equations are divergent and are regulated using finite value cut-offs. In Chapter 3, we implemented a similar method to calculate the CP-violating observables for NN scattering process. Here, we use the regularization defined in the configuration space and use a short-distance scale R as a parameter. The previous works have shown that the $R > 0.8$ fm to capture the relevant physics, and the best results are obtained for $R = 0.9$ fm (R_2) [100]. Unfortunately, chiral potentials are only available for a mild range of cut-off variations up to $R \leq 1.2$ fm. For larger cut-offs, spurious bound states appear in the nuclear spectrum, which becomes harder and harder to subtract at higher orders in perturbation theory.

We use the momentum-space basis to calculate the wave function and matrix elements involving the DM interactions discussed above. ^{2}H, ^{3}He, and ^{4}He wave functions are evaluated by solving the non-relativistic Schrödinger equation in momentum-space. The wave function of deuteron (d) is easily evaluated by solving

$$|\psi_d\rangle = \frac{1}{E_d - T} V_{12}\,|\psi_d\rangle\ , \tag{5.19}$$

where E_d is the deuteron binding energy, T is the two-nucleon (NN) kinetic energy, and V_{12} is the NN potential. As we have discussed in Chapter 3, it is

convenient to use the partial wave basis $|p\alpha\rangle$. Then the partial waves contributing to the deuteron bound state is evaluated by solving the above equation with the constraint: the orbital angular momentum $l_{12} = 0, 2$, NN spin $s_{12} = 1$, and the total angular momentum $j_{12} = 1$. This calculation can be easily performed on a laptop.

Obtaining wave functions for larger systems is much more complicated. For instance, for ^{3}He we rewrite the Schrödinger equation into a Faddeev equation

$$|\psi_{12}\rangle = G_0\, t_{12}\, P\, |\psi_{12}\rangle + G_0\, (1 + t_{12} G_0)\, V_{123}^{(3)}\, (1 + P)\, |\psi_{12}\rangle\ , \tag{5.20}$$

in terms of Faddeev components $|\psi_{12}\rangle$. The various Faddeev components can be related to $|\psi_{12}\rangle$ using permutation operators due to the anti-symmetric nature of the wave functions. G_0 stands for the three-nucleon free-propagator. Nucleon-nucleon interactions enter via the T-matrices t_{12}, which we obtain by solving a Lippmann-Schwinger equation for the NN system embedded into a 3N system. Similar but larger equations are derived for the ^{4}He nucleus. These equations are then numerically solved on the supercomputer cluster of Forschungszentrum Jülich. These computations have been carried out by my collaborators Andreas Nogga and Christopher Körber.

5.3.1 Density matrix Formalism

In this section, we describe the theoretical framework for calculating matrix elements in Eq. (5.16). We can separate this calculation into two parts: the first part is the *interaction kernel*, which captures the one- and few-body currents, and the second part is the *structure*, which contains the accurate eigenstates of the Hamiltonian of the nucleus.

In the *traditional method*, we calculate the cross-section by integrating the interaction kernel directly with the wave function of the nucleus.

$$\langle \Psi' | O | \Psi \rangle_{\text{traditional}} = \int \{\mathrm{d}p_i\} \Psi'^{\dagger}(\{p_i\}) \Psi(\{p_i\}) O(\{p_i\})\,, \tag{5.21}$$

where $\{p_i\}$ are the momentum of the internal nucleons i, the quantum numbers of the nucleons are suppressed for simplicity.

Ref. [101] introduces a novel method using *transition density amplitudes* (referred to as *densities*).

$$\langle \Psi' | O | \Psi \rangle_{\text{density formalism}} = \sum_{\{n_i\}} \rho(\{n_i\}) \otimes O(\{n_i\})\,, \tag{5.22}$$

where $\{n_i\}$ are the quantum number of the internal nucleons i. This approach significantly improves the computational time; they have shown that for Compton scattering, the computation time gets reduced by a factor of ten [101]. We have used this method to calculate the matrix elements for this part of the thesis and

also found an order-of-magnitude speed-up. This works because the densities do not depend on the interaction probes (in our case, scalar dark matter interaction), and the nuclear-structure part of the calculation gets factorized from the interaction kernel part.

For any external-probe matrix element, we need to read these nuclear densities and do convolution with the appropriate interaction kernels that encode the one- and two-body current operators on the momentum-spin basis. The computational effort associated with this structured piece of the calculations increases significantly with A, but highly parallelized and optimized codes exist that solve the wave functions of light nuclei. Constructing densities from those wave functions is straightforward. In short, once we generate the nuclear densities using a supercomputer, all future matrix element calculations can be performed on personal computers by reading these densities. A detailed calculation of one- and two-body densities are given in Ref. [101]. In Appendix D, we provide a short version of this formalism for DM-nuclei scattering.

5.4 Results and discussions

We calculated the response functions $\mathcal{F}_{\rm is}^{(0,1)}(\boldsymbol{q}^2)$ for transfer momentum $q = (0 - 200)$ MeV, cut-off $\{R_2, R_3, R_4, R_5\} = \{0.9, 1.0, 1.1, 1.2\}$ fm. Before we discuss the wave function dependence and theoretical uncertainties of our computations, we first analyze the general features using a fixed wave function. As the response functions for ^{2}H and ^{3}He showed the fastest convergence for cut-off R_2 and the highest accuracy for N^{4}LO wave function, we chose this one. In Fig. 5.2, we present the response functions for ^{2}H, ^{3}He, and ^{4}He nuclei as function of the transferred momentum. The maximum momentum transfer is related to the DM and target mass and the DM velocity distribution. Using the standard distribution and the DM escape velocity $v_\chi^{\rm esc} \simeq 550$ km/s [318], and assuming $m_\chi \gg m_{^4{\rm He}}$ the maximum momentum transfer is about $|\boldsymbol{q}| \leq 3 \times A$ MeV, so about 12 MeV for ^{4}He [100]. We show results for larger momentum transfer as well to analyze the accuracy and cut-off dependence of our results and for non-standard DM velocity distributions.

At zero momentum transfer, the LO response function approaches unity. This is the direct result of the normalization condition. The LO response function with the NLO radius and two-body corrections is

$$|\mathcal{F}_{\rm is}^{(0+1)}(\boldsymbol{q}^2)|^2 \equiv |\mathcal{F}_{\rm is}^{(0)}(\boldsymbol{q}^2) + \mathcal{F}_{{\rm is},r}^{(1)}(\boldsymbol{q}^2) + \mathcal{F}_{{\rm is},2b}^{(1)}(\boldsymbol{q}^2)|^2 \,. \tag{5.23}$$

The results conclude that $\mathcal{F}_{\rm is}^{(0)}(\boldsymbol{q}^2)$ is a good approximation for the considered range of transfer momentum, as shown in Fig. 5.2. The NLO contributions only deviate LO results by a few percent even for ^{4}He. Our hopes that the correction would be larger for the much denser ^{4}He compared to the dilute ^{2}H and ^{3}He have been dashed. It is intriguing that much larger corrections, up to 20-30%, are

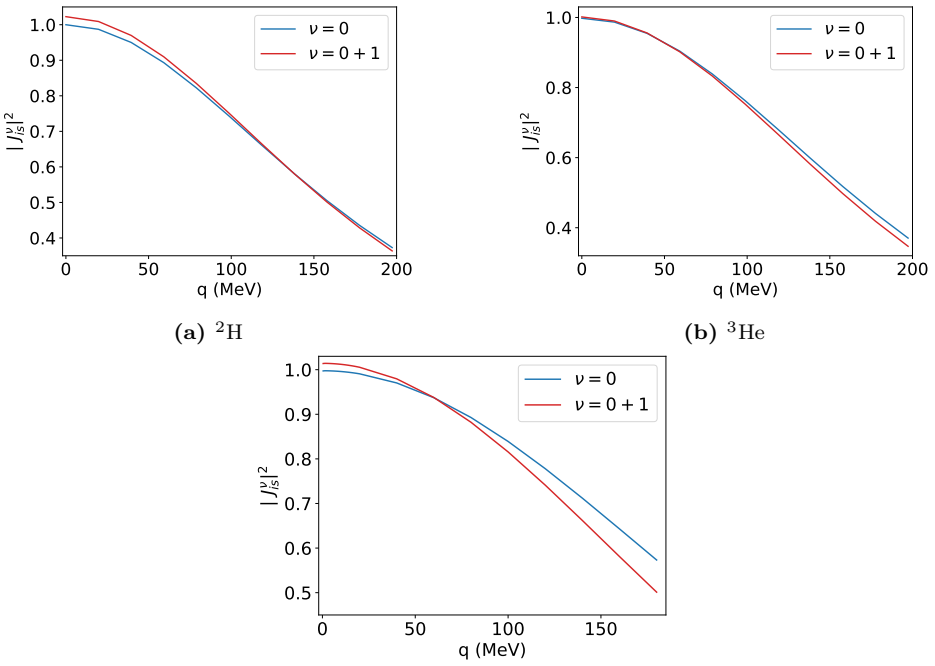

(a) ^{2}H **(b)** ^{3}He

(c) ^{4}He

Figure 5.2: Isoscalar structure functions of ^{2}H, ^{3}He, and ^{4}He as a function of transfer momentum q. We apply a fixed wave function corresponding to N^{4}LO wave functions with a fixed cut-off $R_2 = 0.9$ fm. The chiral order $\nu = 0$ $(0 + 1)$ is shown by the blue (red) line.

found for heavier systems [310]. For ^2H and ^{3}He the NLO corrections decrease for larger transfer momentum due to a cancellation between the radius and two-body NLO corrections. This is not true for ^{4}He where both terms have the same size, although, as discussed below, this does depend on the applied regulator.

To capture the details of NLO contribution, we introduce the relative radius and two-body corrections

$$\Delta^{(r)} = \frac{|\mathcal{F}_{\rm is}^{(0+1)}(\boldsymbol{q}^2)|^2 - |\mathcal{F}_{\rm is}^{(0)}(\boldsymbol{q}^2) + \mathcal{F}_{{\rm is},2b}^{(1)}(\boldsymbol{q}^2)|^2}{|\mathcal{F}_{\rm is}^{(0+1)}(\boldsymbol{q}^2)|^2},$$
$$\Delta^{(2b)} = \frac{|\mathcal{F}_{\rm is}^{(0+1)}(\boldsymbol{q}^2)|^2 - |\mathcal{F}_{\rm is}^{(0)}(\boldsymbol{q}^2) + \mathcal{F}_{{\rm is},r}^{(1)}(\boldsymbol{q}^2)|^2}{|\mathcal{F}_{\rm is}^{(0+1)}(\boldsymbol{q}^2)|^2}. \tag{5.24}$$

The radius contribution does not depend on the chiral order of the wave function

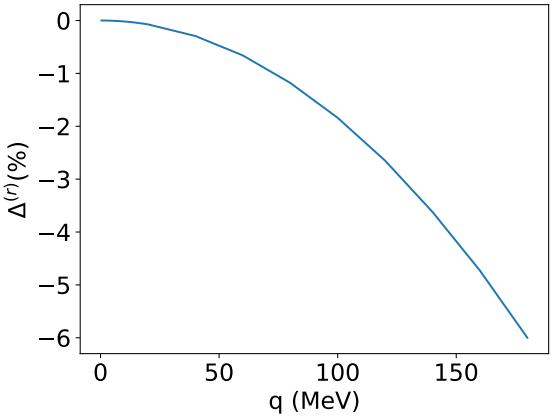

Figure 5.3: The percentage relative contribution of radius corrections of ^{4}He as a function of transfer momentum q for cut-off R_2 and N^{4}LO wave function.

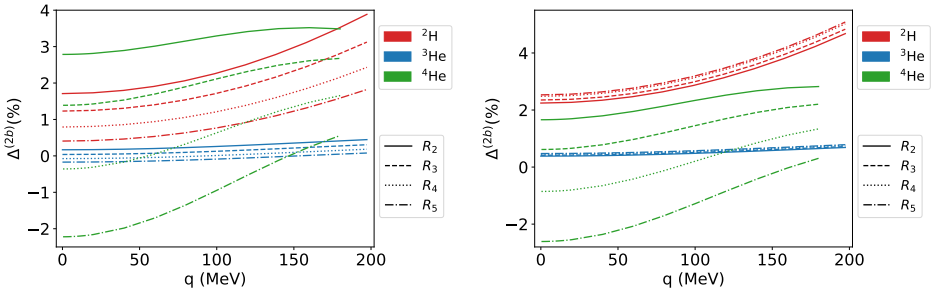

(a) **(b)**

Figure 5.4: The percentage relative contribution of two-body corrections of ^{2}H, ^{3}He, and ^{4}He as a function of transfer momentum q for various cut-offs for N^{2}LO (left panel) and N^{4}LO (right panel) chiral wave functions.

or the nuclear aspects. This can be seen by

$$\Delta^{(r)} \simeq \frac{2\mathcal{F}^{(1)}_{\mathrm{is},r}(\boldsymbol{q}^2)}{\mathcal{F}^{(0+1)}_{\mathrm{is}}(\boldsymbol{q}^2)} \simeq -\frac{2}{\sigma_{\pi N}} \frac{9g_A^2\pi m_\pi^2}{4(4\pi F_\pi)^2} F\left(\frac{|\boldsymbol{q}|}{2m_\pi}\right) \xrightarrow{|q|\ll 2m_\pi} -\frac{2}{\sigma_{\pi N}} \frac{5g_A^2\pi m_\pi^2}{4(4\pi F_\pi)^2} \frac{|\boldsymbol{q}|^2}{4m_\pi^2}\,. \tag{5.25}$$

From this, we can see that the radius contribution vanishes at lower momentum but becomes dominant at higher momentum, making the net NLO correction negative. Furthermore, all the nuclear effects drop out, and $\Delta^{(r)}$ shows identical momentum dependence for all nuclei; our results have verified this. In Fig. 5.3, we have shown momentum dependence of $\Delta^{(r)}$ for ^{4}He nucleus; we omitted other

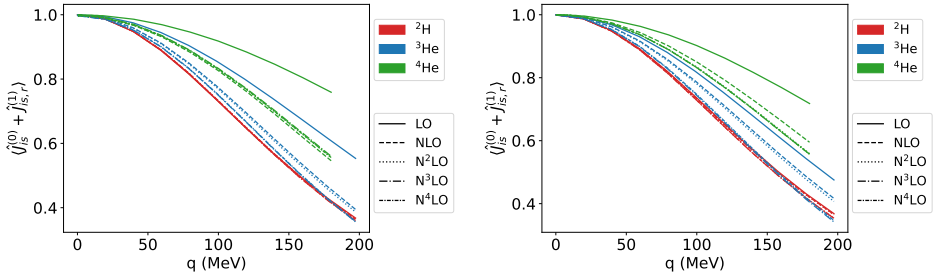

Figure 5.5: Isoscalar one-body structure functions as a function of transfer momentum q for LO to N^{4}LO chiral wave functions. The left (right) panel matrix elements are calculated using cut-off $R_2 = 0.9\,\text{fm}$ ($R_5 = 1.2\,\text{fm}$).

nuclei because of the identical behavior.

In Fig. 5.4, we present our results on $\Delta^{(2b)}$ for various nuclei. In the left panel, we apply N^{2}LO chiral wave functions and show results for the four applied regulators. The two-body corrections are small and lie well below power-counting estimates, as was found in Refs. [100, 312]. What is worrisome is that the regulator dependence is large, ranging from $\Delta^{(2b)}(^3\text{He}) = (-0.01 \pm 0.13)\%$ to $\Delta^{(2b)}(^4\text{He}) = (0.4 \pm 1.9)\%$ at $q^2 = 0$. Even the sign for ^{4}He is uncertain. One might hope this would improve once higher-order wave functions are applied, and the corresponding results are shown in the right panel. While the ^{2}H and ^{3}He results are now essentially regulator independent, confirming results found in Ref. [100], no such convergence is shown for ^{4}He. This can be seen in detail in Table 5.1. This is puzzling. The power counting indicates that at this order, only NLO currents are coming from one-body radius corrections and the pion-range two-body corrections. There are no free counter terms, so the calculations should show regulator-independent matrix elements. The fact that we do not observe this indicates a potential problem with Weinberg's power counting for scalar currents. In Fig. 5.5, we demonstrate that the power-counting issues only affect the two-body currents. The one-body corrections show good convergence for all nuclei, even for N^{2}LO wave functions.

The cut-off dependence of our results can be cast in a different light. In Fig. 5.6, we present an observed linear correlation between the two-body matrix element and the D-wave probability for ^{2}H, ^{3}He, and ^{4}He. The D-wave probability describes how much of the nuclear wave function involves $l = 2$ nucleon-nucleon states and is a consequence of $S - D$ mixing from the nuclear tensor force. It was pointed out by Friar [319] already that the D-wave probability is not an observable: it can be changed by unitary transformations of the nucleon-nucleon potential. However, suppose our computations are correct in principle. In that case, the two-nucleon scalar matrix elements can be measured in the laboratory (for instance,

NN interactions		$\langle \hat{J}_{(\mathrm{is}),2b} \rangle_{^2\mathrm{H}}$	$\langle \hat{J}_{(\mathrm{is}),2b} \rangle_{^3\mathrm{He}}$	$\langle \hat{J}_{(\mathrm{is}),2b} \rangle_{^4\mathrm{He}}$
AV18 + Urb 1XF		/	$2.62 \cdot 10^{-3}$	/
AV18		$1.58 \cdot 10^{-4}$	$2.83 \cdot 10^{-3}$	/
CD-Bonn + TM		/	$1.51 \cdot 10^{-3}$	/
CD-Bonn		$1.17 \cdot 10^{-4}$	$1.62 \cdot 10^{-3}$	/
NIJM		$1.57 \cdot 10^{-3}$	/	/
LO	(Q^0) R_1	$2.28 \cdot 10^{-3}$	$-1.45 \cdot 10^{-3}$	/
LO	(Q^0) R_2	$-5.95 \cdot 10^{-4}$	$-1.77 \cdot 10^{-3}$	$-8.45 \cdot 10^{-2}$
LO	(Q^0) R_3	$-2.66 \cdot 10^{-3}$	$-2.02 \cdot 10^{-3}$	$-9.18 \cdot 10^{-2}$
LO	(Q^0) R_4	$-4.12 \cdot 10^{-3}$	$-2.22 \cdot 10^{-3}$	$-9.17 \cdot 10^{-2}$
LO	(Q^0) R_5	$-5.13 \cdot 10^{-3}$	$-2.38 \cdot 10^{-3}$	$-8.55 \cdot 10^{-2}$
NLO	(Q^0) R_1	$1.17 \cdot 10^{-2}$	$1.62 \cdot 10^{-3}$	/
NLO	(Q^0) R_2	$8.80 \cdot 10^{-3}$	$8.18 \cdot 10^{-4}$	$-1.33 \cdot 10^{-3}$
NLO	(Q^0) R_3	$6.09 \cdot 10^{-3}$	$1.08 \cdot 10^{-4}$	$-8.78 \cdot 10^{-3}$
NLO	(Q^0) R_4	$3.70 \cdot 10^{-3}$	$-4.91 \cdot 10^{-4}$	$-1.83 \cdot 10^{-2}$
NLO	(Q^0) R_5	$1.65 \cdot 10^{-3}$	$-9.78 \cdot 10^{-4}$	$-3.01 \cdot 10^{-2}$
N^{2}LO	(Q^0) R_1	$1.1 \cdot 10^{-2}$	$1.51 \cdot 10^{-3}$	/
N^{2}LO	(Q^0) R_2	$8.59 \cdot 10^{-3}$	$8.39 \cdot 10^{-4}$	$1.39 \cdot 10^{-2}$
N^{2}LO	(Q^0) R_3	$6.17 \cdot 10^{-3}$	$1.93 \cdot 10^{-4}$	$6.93 \cdot 10^{-3}$
N^{2}LO	(Q^0) R_4	$3.97 \cdot 10^{-3}$	$-3.75 \cdot 10^{-4}$	$-1.80 \cdot 10^{-3}$
N^{2}LO	(Q^0) R_5	$2.04 \cdot 10^{-3}$	$-8.55 \cdot 10^{-4}$	$-1.12 \cdot 10^{-2}$
N^{3}LO	(Q^0) R_1	$7.31 \cdot 10^{-3}$	$8.61 \cdot 10^{-4}$	/
N^{3}LO	(Q^0) R_2	$1.09 \cdot 10^{-2}$	$1.81 \cdot 10^{-3}$	$6.37 \cdot 10^{-3}$
N^{3}LO	(Q^0) R_3	$1.29 \cdot 10^{-2}$	$2.38 \cdot 10^{-3}$	$2.69 \cdot 10^{-3}$
N^{3}LO	(Q^0) R_4	$1.37 \cdot 10^{-2}$	$2.62 \cdot 10^{-3}$	$-3.97 \cdot 10^{-3}$
N^{3}LO	(Q^0) R_5	$1.38 \cdot 10^{-2}$	$2.69 \cdot 10^{-3}$	$-1.23 \cdot 10^{-2}$
N^{4}LO	(Q^0) R_1	$1.06 \cdot 10^{-2}$	$1.77 \cdot 10^{-3}$	/
N^{4}LO	(Q^0) R_2	$1.13 \cdot 10^{-2}$	$1.92 \cdot 10^{-3}$	$8.27 \cdot 10^{-3}$
N^{4}LO	(Q^0) R_3	$1.18 \cdot 10^{-2}$	$2.07 \cdot 10^{-3}$	$3.08 \cdot 10^{-3}$
N^{4}LO	(Q^0) R_4	$1.25 \cdot 10^{-2}$	$2.27 \cdot 10^{-3}$	$-4.28 \cdot 10^{-3}$
N^{4}LO	(Q^0) R_5	$1.27 \cdot 10^{-2}$	$2.38 \cdot 10^{-3}$	$-1.31 \cdot 10^{-2}$
N^{4}LO$^+$	(Q^0) R_2	/	/	$1.03 \cdot 10^{-2}$
N^{4}LO$^+$	(Q^0) R_3	/	/	$4.76 \cdot 10^{-3}$
N^{4}LO$^+$	(Q^0) R_4	/	/	$-3.48 \cdot 10^{-3}$
N^{4}LO$^+$	(Q^0) R_5	/	/	$-1.27 \cdot 10^{-2}$

Table 5.1: $\langle \hat{J}_{(\mathrm{is}),2b} \rangle = (A|\sigma_{\pi N} \bar{c}_{q^{(\mathrm{is})}}|)^{-1} \left\langle \Psi_T, jm_j \right| \hat{J}_{\mathrm{is},2b}(\boldsymbol{q}^2) \left| \Psi_T, jm_j \right\rangle$ for chiral and phenomenological wave functions at zero transfer momentum $\boldsymbol{q} = 0$ for ^{2}H, ^{3}He, and ^{4}He nuclei. For ^{2}H and ^{3}He, we have used cut off $R_1 = 0.8\,\mathrm{fm}$ and phenomenological wave functions results from Ref. [100].

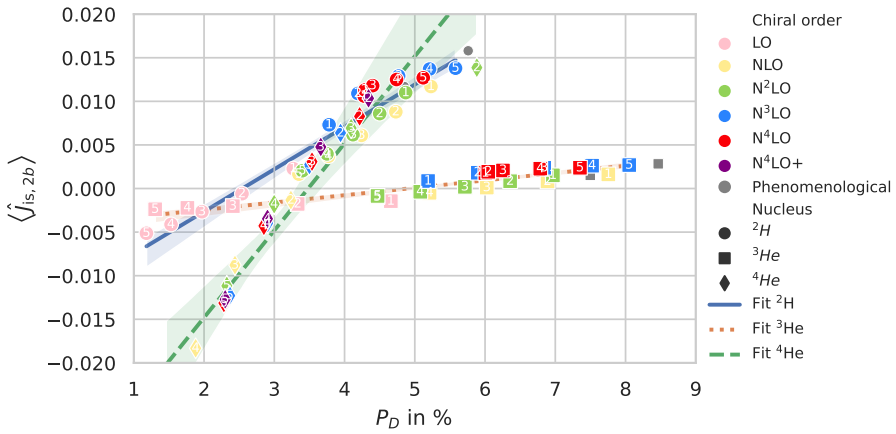

Figure 5.6: The plots show the correlation between the isoscalar structure functions and the D-wave probability for ^{2}H, ^{3}He, and ^{4}He represented by circle, square, and diamond data points. The data points are assigned different colors corresponding to the chiral order of the wave function. The cut-off R_i used for the calculation is indicated by label i on the data point. For ^{2}H and ^{3}He, we have used cut off $R_1 = 0.8\,\mathrm{fm}$ and phenomenological wave functions results from Ref. [100].

by comparing scalar currents on the deuteron and subtracting the single-nucleon contributions), and the D-wave admixture can then be experimentally extracted from the correlation in Fig. 5.6. This again highlights that something is missing in our computation.

Our findings indicate that something is wrong with Weinberg's power counting for scalar-induced currents. It might be that a short-distance contact term, describing DM-nucleon-nucleon scalar interactions, must be promoted to NLO to absorb the regulator dependence and, presumably, destroy the correlation with the D-wave probability. In Weinberg's power counting, such counter terms do appear but only at N^{3}LO in the scalar currents, see Ref. [320] for an explicit derivation. If true, this would impact the results for WIMP scattering of heavier nuclei as performed in the literature, where only pion-range currents are included. It would also impact our understanding of the quark mass dependence on nuclear binding energies through the nuclear sigma terms. Interestingly, given sufficiently accurate lattice QCD data on nuclear binding energies as a function of the quark mass, it should be possible to fit the scalar contact counter term to lattice data and determine whether indeed these terms must be promoted to leading order [311,321]. Finally, while it is tempting to argue that the missing counter term is not too relevant considering that the two-nucleon matrix elements are found to be only a few percent, this is somewhat dangerous as there is no guarantee that the finite part of the counter term is of the same size and could be a genuine $\mathcal{O}(30\%)$

correction. This has to be determined in the future.

5.5 Conclusions and outlook

We have investigated the DM scattering of light nuclei using the framework of χPT. Our main focus was on ^{4}He nucleus, but we also investigated ^{2}H and ^{3}He nuclei. The nuclear wave functions were calculated using the χPT, and we included up to N^{4}LO chiral order. The light nuclei allowed us to calculate bound-state and scattering equations directly, and with a high degree of accuracy. This allowed us to investigate the uncertainties and convergence of observables for different chiral orders of the wave functions with a higher degree of precision than any previous works.

We focused on the scalar interaction of DM and quarks. Using χPT, we calculated the ensuing scalar hadronic current up to NLO. The NLO current consists of radius and two-body corrections. For ^{2}H, ^{3}He, and ^{4}He, the NLO current modified the LO current by a few percent for the transfer momentum $q < 200\,\text{MeV}$. However, NLO currents could lead to more significant effects for heavier nuclei.

We observed that two-body contributions exhibit a regulator dependence for all three nuclei. Even though ^{2}H and ^{3}He recovers regulator independence when using higher order chiral wave functions, ^{4}He does not show any such features. Furthermore, in ^{4}He, the sign of the two-body contribution depends on the value of the regulator. Since there are no contact terms at NLO to absorb this regulator independence, we believe this is because the scalar currents are not properly renormalized. The LO current and NLO radius contributions do not show any such regulator dependence, indicating that all the regulator dependence arises from the two-body effects.

As an independent check of renormalization of two-body currents, we investigated the effects of D-wave probability on two-body currents for ^{2}H, ^{3}He, and ^{4}He. All three nuclei exhibited a linear correlation with ^{4}He showed the largest variation. This provides additional evidence that Weinberg's power counting fails for scalar currents. As we have seen in Chapter 3, the scalar can be renormalized by promoting a higher-order contact term to NLO to absorb the regular dependence. The first higher-order contact term for scalar currents occurs at N^{3}LO.

Even though we are promoting the contact term to NLO, we can not assume it can only contribute at few percent level to the two-nucleon matrix elements. The finite part of the contact term could have large contributions and lead to significant contribution to the calculations of WIMP DM scattering of heavy nuclei. Similarly, we need to revisit the quark mass dependence on nuclear binding energies in the presence of this contact term. Further studies are required to understand the effects of this promoted contact term.

In this part of the thesis, we only focused on the scalar interaction of DM with light quarks and gluons. One of our future goals is to perform similar studies for the axial-vector DM interactions with light quarks and gluons. The axial-

vector interactions lead to nuclear spin-dependent interactions. By analyzing the scattering result from different nuclei with different spins, we can understand the underlying axial-vector DM interactions with quark/gluons. Furthermore, we are looking forward to checking whether axial-vector currents exhibit a similar renormalization problem.

Since we have used the density matrix formalism, once we calculate the axial-vector operators, we can easily calculate the cross sections by reading the *density* of the light nuclei. We have already calculated the LO and NLO axial-vector DM-nucleon operators in a partial wave basis and used this result to analytically calculate the cross sections using a test nuclear wave functions.

Chapter 6

Conclusions and outlook

This thesis investigates the *CP*-violating interactions in the strong sector of the Standard Model and from hypothetical beyond-the-Standard-Model (BSM) sources. *CP* violation is closely connected to several intriguing puzzles of particle physics such as the strong *CP* problem, the related physics of axions, and the matter-antimatter asymmetry of the Universe. In this thesis, we have studied how strong *CP* violation arising from the QCD $\bar{\theta}$ term manifests at the hadronic and nuclear level, how BSM *CP* violation in the presence of a Peccei-Quinn mechanism leads to long-range axionic forces, and, somewhat off-topic, how dark matter (DM) particles scatter of atomic nuclei. Throughout the thesis, we have used a model-independent approach for BSM physics relying on the Standard Model effective field theory (SMEFT) framework, which is suitable as we focused on the description of low-energy precision experiments. We have gone beyond the SMEFT by introducing new fields, such as axions and DM fields, when necessary. Another crucial role in this thesis is played by chiral perturbation theory (χPT), which we have used to match quark-level interactions to hadronic interactions. This has allowed us to perform accurate computations for a large number of low-energy experiments that aim to further our understanding of the nature or constraints of BSM interactions.

Chapter 2 introduces the concept of EFTs and provides a detailed description of χPT. EFTs provide us with a means to approach a problem in a model-independent way. In some scenarios, EFT becomes the only viable solution. For example, QCD is the established theory of strong interactions. It could predict and describe various phenomena with a high degree of accuracy. However, because of the asymptotic freedom of QCD, it becomes non-perturbative in the energy scale of hadrons. Thereby making it impossible to use QCD to describe the nuclear physics phenomena. EFTs are extremely qualified to handle such situations. The χPT, a low-energy EFT of QCD, was able to describe these nuclear phenomena successfully and is the most popular QFT in this energy scale. This chapter briefly discusses other popular EFTs. We provide the key ingredients and the recipe to

construct any general EFT. We then use this prescription to construct χPT. We make use of these results in the later chapters.

In this thesis, we have emphasized the importance of *CP* violation in understanding the nature of the Universe. The current best model, the SM, can not describe the observed matter-antimatter asymmetry. This strongly indicates the existence of BSM *CP*-violating sources. One of the best probes for *CP* violation is EDMs. It has the added benefits of small backgrounds, requires relatively cheaper experimental setups, and is able to measure in different systems such as nuclear, atomic, and molecular EDMs. One of the key ingredients for calculating EDMs is the *CP*-violating nuclear force.

In Chapter 3, we investigated the renormalization of *CP*-violating nuclear forces. The most popular approach in calculating nuclear forces is using the χPT framework. Since it is an EFT, it should be renormalized at all orders in chiral expansion. It has been known that the power counting followed by χPT, Weinberg's power counting, fails for *CP*-even nuclear force and thereby fails to renormalize the nuclear force. However, there have been no such studies for *CP*-violating nuclear force. In this chapter, we checked the renormalization of *CP*-violating nuclear force by checking the dependence of various *CP*-even and *CP*-odd nucleon-nucleon scattering phase shifts and mixing angles on unphysical momentum cut-offs. If the nuclear force is properly renormalized, the observable should be cut-off independent. Our investigations revealed that $^1\mathrm{S}_0$-$^3\mathrm{P}_0$ is not properly renormalized. We demonstrated that the promotion of $\mathrm{N}^2\mathrm{LO}$ short-distance term to LO recovered the renormalization of this channel. However, the absence of *CP*-violating *NN* data make it impossible to calculate the LEC $\bar{C}_0$ associated with this short-distance term. We proposed a new strategy to calculate $\bar{C}_0$ indirectly using the available data on charge-symmetry-breaking in few-body systems. We hope our results motivate the community to calculate the $\bar{C}_0$ using LQCD or the proposed CSB data. Since current EDM calculations consider only the OPE term at the LO, these results are missing the $\mathcal{O}(1)$ effects caused by the promoted LO short-distance term.

In Chapter 4, we studied the *CP*-violating axion interactions in an EFT framework. Axions are the most popular solution to the problem of why the QCD $\bar{\theta}$ angle is vanishingly small, commonly known as the strong *CP* problem. The QCD $\bar{\theta}$ term is technically natural in the SM. That is, if $\bar{\theta}$ is chosen small at some specific energy scale then neither threshold corrections nor renormalization-group evolution induce a large $\bar{\theta}$ angle. This is no longer the case in BSM scenarios. A model with more *CP* violation than the SM, for instance, those motivated by the matter-antimatter asymmetry, generally renormalize $\bar{\theta}$ to unacceptably large values. This 'BSM *CP* problem' strongly motivates an infrared solution pointing towards the Peccei-Quinn mechanism and the existence of axions. We have investigated the impact of BSM sources of *CP* violation on axion interactions in the framework of the SMEFT and the LEFT. We start with dimension-six SMEFT operators in the presence of axions and 'integrate out' the top quark and massive W, Z bosons to get the low-energy effective field theory. Next, we list

out all possible dimension-six *CP*-violating LEFT operators and then use χPT to calculate the *CP*-violating axion interactions with baryons, mesons, leptons, and photons. We then collected the direct and indirect constraints on *CP*-odd observables from various experiments such as EDMs, fifth-force experiments, astrophysical experiments, and monopole-dipole experiments. We found that the EDMs set the strictest constrains among all these experiments. However, the upgraded ARIADNE setup could compete with EDM experiments in reaching a scale of around 10^3 TeV axion mass. Finally, we translated our EFT results to set constraints on parameters of some specific BSM models, such as leptoquarks and left-right symmetric models.

In Chapter 5, we studied DM scattering off light nuclei. We performed a first-principle calculation, i.e., we calculated the DM-nucleus cross-section starting with DM-quarks/gluon interactions. We focused on the light quarks (u, d, s) and restricted ourselves to the class of scalar interactions. We mainly focused on the ^{4}He nucleus, but we also considered ^{2}H and ^{3}He nuclei. We used the χPT framework to calculate DM-nucleon/pion interactions and the nuclear wave functions. The scattering cross section was calculated up to NLO order. Our results revealed a strong regulator dependence of the size of two-nucleon NLO corrections and a linear correction between the two-nucleon matrix element and the D-wave probability of the considered nucleus. These findings indicate a problem in the EFT framework: at this order, all results should have been regulator independent, and no correlation should exist between observables and unphysical wave function features such as the D-wave probability. We suspect that the χPT power counting for scalar nuclear currents needs to be modified, for instance, by promoting short-distance DM-nucleon-nucleon interaction to NLO. If so, this would directly impact the existing calculations for heavier nuclei. More work in this direction is needed.

Our work can be extended in various directions. Motivated by our results in Chapter 3, we plan to expand our work to calculate the EDM of ^{3}He. We expect to see the same renormalization problem for this EDM. We then plan to redo the calculation with the promoted LO short-distance term and hope to recover cut-off independence.

In Chapter 4, we considered the *CP*-violating axion interactions. If axions form the DM of our Universe, these interactions lead to interesting signals. Axion DM acts like a coherently oscillating scalar field $a(t) = a_0 \cos m_a t$. In this case, the *CP*-odd axion interactions lead to oscillating physical quantities such as electron mass $(m_e(t))$, proton mass $(m_p(t))$, neutron mass $(m_n(t))$, and the fine structure constant $(\alpha_{\rm em}(t))$. Various atomic physics experiments make use of the oscillating nature of these physical quantities to get constrains on axion couplings. We plan to check whether these experiments can provide better constraints than the axion searches we studied in Chapter 4. Furthermore, atomic physics experiments are showing tremendous advancements in a shorter time compared to EDM experiments, which could become an important avenue for future axion searches.

We studied the class of scalar interactions of DM with quarks and gluons in

Chapter 5. We plan to explore the class of axial-vector DM interactions of DM with quarks and gluons for our future work. The axial-vector interactions will lead to spin-dependent cross-sections. By comparing the results of DM-nucleus scattering with nuclei with different spins, we can identify the underlying nature of DM-quark/gluon interactions. Since we used density matrix formalism, we can reuse the nuclear wave functions we calculated and save considerable time for our calculations.

Appendix A

Spontaneous symmetry breaking

A.1 SO(3) $\to$ SO(2)

Let us first consider the following Lagrangian with three scalar fields $\mathbf{\Phi} = (\Phi_1, \Phi_2, \Phi_3)^T$

$$\mathcal{L} = \frac{1}{2}\partial_\mu \Phi_i \partial^\mu \Phi_i - \frac{m^2}{2}\Phi_i \cdot \Phi_i - \frac{\lambda}{4}(\Phi_i \cdot \Phi_i)^2 \,, \tag{A.1}$$

where $\lambda > 0$, and we are interested in the case where the potential has more than one minima ($m^2 < 0$). The Lagrangian is invariant under a global SO(3) symmetry,

$$g \in G = \mathrm{SO}(3) : \Phi_i \to \Phi_i' = \left(e^{-i\alpha_k T_k}\right)_{ij} \Phi_j \,. \tag{A.2}$$

The hermitian ($\Phi_i^\dagger = \Phi_i$) and orthogonality ($\mathbf{\Phi'}\cdot\mathbf{\Phi'} = \mathbf{\Phi}\cdot\mathbf{\Phi}$) condition ensures that T_k are purely imaginary and anti-symmetric, and they satisfy the so(3) Lie algebra $[T_i, T_k] = \epsilon_{ijk} T_k$. For this discussion, we use the representation $(T_i)_{jk} = -i\epsilon_{ijk}$. The minimum of the potential that is independent of x is

$$|\mathbf{\Phi}_{\min}| = \sqrt{\frac{-m^2}{\lambda}} \equiv v \,, \qquad\qquad |\mathbf{\Phi}| = \sqrt{\Phi_1^2 + \Phi_2^2 + \Phi_3^2} \,. \tag{A.3}$$

In general, $\mathbf{\Phi}_{\min}$ can point in any direction. This implies we have an infinite number of degenerate vacua. However, any infinitesimal external perturbation (spontaneous symmetry breaking) invariant under SO(3) could break this degeneracy and 'choose' one particular vacuum. Without loss of generality, let us assume this vacuum lies along $\hat{e}_3$

$$\mathbf{\Phi}_{\min} = \begin{pmatrix} 0 \\ 0 \\ v \end{pmatrix} \,, \tag{A.4}$$

and

$$T_1\mathbf{\Phi}_{\min} = \begin{pmatrix} 0 \\ -iv \\ 0 \end{pmatrix}, \qquad T_2\mathbf{\Phi}_{\min} = \begin{pmatrix} iv \\ 0 \\ 0 \end{pmatrix}, \qquad T_3\mathbf{\Phi}_{\min} = 0\,. \tag{A.5}$$

One observation from the above results is that the set of all transformations that leave the vacuum invariant form the SO(2)($\{e^{-i\theta T_3}\}$) subgroup of SO(3)

$$h \in H = \mathrm{SO}(2) : \mathbf{\Phi}_{\min} \to \mathbf{\Phi}'_{\min} = e^{-i\alpha_3 T_3}\mathbf{\Phi}_{\min} = \mathbf{\Phi}_{\min}\,. \tag{A.6}$$

The Lagrangian for scalar fields around the vacuum $\mathbf{\Phi} = (\Phi_1, \Phi_2, v + \eta)$ will give the potential

$$\mathcal{V} = \frac{\lambda}{4}v^4 + \frac{1}{2}(-2m^2)\eta^2 + \lambda v(\Phi_1^2 + \Phi_2^2 + \eta^2)\eta + \frac{\lambda}{4}(\Phi_1^2 + \Phi_2^2 + \eta^2)^2\,. \tag{A.7}$$

From this, one can obtain the masses of the scalar fields as

$$m^2_{\Phi_1} = m^2_{\Phi_2} = 0\,, \tag{A.8}$$

$$m^2_{\eta} = -2m^2\,. \tag{A.9}$$

From these observations, we can make the general remarks that for each generator that does not annihilate the vacuum, we obtain a *massless* Goldstone boson (see Eq. (A.5)).

A.2 $G \to H$

In this section, we will consider a multiplet of scalar (or pseudoscalar) fields $\mathbf{\Phi} = (\{\Phi_i\})^T$. We assume the Lagrangian takes the form

$$\mathcal{L} = \frac{1}{2}\partial_\mu\mathbf{\Phi}\partial^\mu\mathbf{\Phi} - \mathcal{V}(\mathbf{\Phi})\,, \tag{A.10}$$

and is invariant under the global compact Lie group G of the order n_G with generators T^a. Then an infinitesimal transformation of the fields is given by

$$g \in G : \Phi_i \to \Phi'_i = \Phi_i + \delta\Phi_i, \delta\Phi_i = -i\sum_{a=1}^{n_G}\epsilon_a(T^a)_{ij}\Phi_j\,. \tag{A.11}$$

The Hermitian condition ensures that T^a is anti-symmetric. Similar to the previous section, after spontaneous symmetry breaking, the ground state gets the vacuum expectation value (vev) $\mathbf{\Phi}_{\min} = \langle\mathbf{\Phi}\rangle$ which is invariant under the group H of order $n_H < n_G$. The potential near $\mathbf{\Phi}_{\min}$ is

$$\mathcal{V}(\mathbf{\Phi}) = \mathcal{V}(\mathbf{\Phi}_{\min}) + \frac{\partial\mathcal{V}(\mathbf{\Phi}_{\min})}{\partial\Phi_i}\eta_i + \frac{1}{2}\frac{\partial^2\mathcal{V}(\mathbf{\Phi}_{\min})}{\partial\Phi_i\partial\Phi_j}\eta_i\eta_j + \mathcal{O}(\eta_i^3) \tag{A.12}$$

where $|\mathbf{\Phi}_{\min}| = v, \mathbf{\Phi} = \mathbf{\Phi}_{\min} + \boldsymbol{\eta}$. By construction $\frac{\partial \mathcal{V}(\mathbf{\Phi}_{\min})}{\partial \Phi_i} = 0$ and we define the symmetric matrix $(M^2)_{ij} = m_{ij}^2 = \frac{\partial^2 \mathcal{V}(\mathbf{\Phi}_{\min})}{\partial \Phi_i \partial \Phi_j} = m_{ji}^2$. Then Eq. (A.12) becomes

$$\mathcal{V}(\mathbf{\Phi}) = \mathcal{V}(\mathbf{\Phi}_{\min}) + \frac{1}{2}\boldsymbol{\eta} \cdot M^2 \cdot \boldsymbol{\eta} + \mathcal{O}(\eta_i^3) \tag{A.13}$$

The invariance of $\mathcal{V}$ under G gives

$$\begin{aligned} \mathcal{V}(\mathbf{\Phi}_{\min}) &= \mathcal{V}(\mathbf{\Phi}_{\min} + \delta\mathbf{\Phi}_{\min}) \,, \\ &= \mathcal{V}(\mathbf{\Phi}_{\min}) + \frac{1}{2}\mathbf{\Phi}_{\min} \cdot M^2 \cdot \mathbf{\Phi}_{\min} + \mathcal{O}(\delta\Phi_{\min,\mathrm{i}}^3) \,. \end{aligned} \tag{A.14}$$

From this, we can conclude

$$\begin{aligned} \mathbf{\Phi}_{\min} \cdot M^2 \cdot \delta\mathbf{\Phi}_{\min} &= 0 \,, \\ \Rightarrow M^2 \delta\mathbf{\Phi}_{\min} &= 0 \,. \end{aligned} \tag{A.15}$$

By using Eq. (A.11) we have

$$M^2 T^a \mathbf{\Phi}_{\min} = 0 \,, \quad a = 1, 2, \ldots, n_G. \tag{A.16}$$

Let us assume $T^1, \ldots, T^{n_H}$ form the representation of the subgroup H. Since the vacuum is invariant under H,

$$\begin{aligned} \mathbf{\Phi}_{\min} &= \sum_{a=1}^{n_H} e^{-i\epsilon_a T^a} \mathbf{\Phi}_{\min} \\ &\simeq \mathbf{\Phi}_{\min} - i \sum_a \epsilon_a T^a \mathbf{\Phi}_{\min} \\ \Rightarrow T^a \mathbf{\Phi}_{\min} &= 0 \,, \quad a = 1, 2, \ldots, n_H \,. \end{aligned} \tag{A.17}$$

Since $T^a, a = n_H + 1, \ldots, n_G$ does not form the representation of H, $T^a \mathbf{\Phi}_{\min} \neq 0$. This result, along with Eq. (A.16) implies that $T^a \mathbf{\Phi}_{\min}$ are non-trivial eigenvectors of M^2 with eigenvalue 0. Moreover, they are also linearly independent

$$\begin{aligned} \sum_{a=n_H+1}^{n_G} c_a (T^a \mathbf{\Phi}_{\min}) &= \left(\sum_{a=n_H+1}^{n_G} c_a T^a \right) \mathbf{\Phi}_{\min} \,, \\ &= T \mathbf{\Phi}_{\min} \neq 0 \,, \end{aligned} \tag{A.18}$$

since T does not belong to the space of representation of the subgroup H. These $n_G - n_H$ linearly independent massless scalar (or psuedoscalars) corresponds to Goldstone bosons.

A.2.1 $SU(3)_L \times SU(3)_R \to SU(3)_V$

In the case of χPT, $SU(3)_L \times SU(3)_R (n_G = 8 + 8)$ is spontaneously broken to $SU(3)_V (n_H = 8)$ when the Universe cool down below $T_C = \Lambda_{\mathrm{QCD}} \sim 300\,\mathrm{MeV}$, which resulted in $n_G - n_H = 8$ Goldstone bosons. These Goldstone bosons are the meson octet $(\pi^{\pm,0}, K^{\pm,0}, \bar{K}^0, \eta)$.

Appendix B

Partial wave analysis

B.1 Scattering

We are considering the scattering between two nucleons. Since the nuclear potential only depends on the relative orientation of the nucleons, the potential is spherical $V(\boldsymbol{r}) = V(r)$, and only leads to elastic scattering. We will ignore the spin part of the wave function for this analysis.

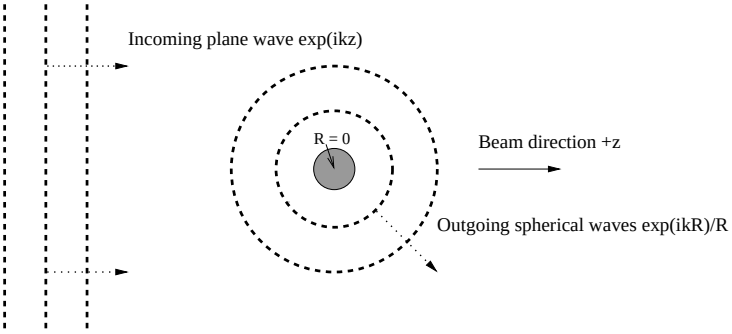

Figure B.1: The incoming plane waves in the +z direction is scattered off a spherical target [1]

The incoming plane wave is assumed to travel along the +z-axis. This will make the scattering symmetric around the z-axis and $\psi(r, \theta, \phi) = \psi(r, \theta)$. The

[1] The image is taken from the lecture notes on 'Scattering theory' by Prof. Filomena Nunes, available at https://www.asc.ohio-state.edu/physics/ntg/8805/refs/Filomena_Nunes_scattering-v3b.pdf.

Schrödinger equation for the relative motion of the nucleons is

$$\left(-\frac{1}{2\mu}\boldsymbol{\nabla}^2 + V(r) - E\right)\psi(r,\theta) = 0\,, \tag{B.1}$$

where μ is the reduced mass and $E = \frac{k^2}{2\mu}$ is the center of mass energy. Since the detectors are located outside the range of short-distance scattering potential, we are only interested in $\psi(r \to \infty, \theta) \equiv \Psi(r,\theta)$. The incident and scattered waves are

$$\Psi_{\text{inc}} = e^{ikz} = e^{ikr\cos\theta}\,, \tag{B.2}$$

$$\Psi_{\text{sct}} = e^{ikz} + f(\theta)\frac{e^{ikr}}{r}\,, \tag{B.3}$$

where $f(\theta)$ is the scattering amplitude and the differential cross section is $\frac{\mathrm{d}\sigma}{d\Omega} = |f(\theta,\phi)|^2 = |f(\theta)|^2$. From now on, unless explicitly stated $\psi/\Psi \equiv \psi_{\text{sct}}/\Psi_{\text{sct}}$.

We will expand the wave function in terms of partial waves. It is convenient to work with the partial wave because they are the eigenstates of angular momentum $\boldsymbol{L}^2$ and L_z with eigenvalues $l(l+1)$ and m_l (=0). The wave function in partial wave basis is given by

$$\psi(r,\theta) = \sum_{l=0}^{\infty} i^l(2l+1)P_l(\cos\theta)R_{kl}(r)\,. \tag{B.4}$$

where P_l are the Legendre polynomials and the $i^l(2l+1)$ factors are for later convenience. Each term in Eq. (B.4) is known as a *partial wave*. If we define $u_{kl}(r) \equiv rR_{kl}(r)$ and $\rho \equiv kr$, the radial part of the wave function satisfies

$$\left[\frac{\mathrm{d}^2}{\mathrm{d}\rho^2} - \frac{l(l+1)}{\rho^2} + 1\right]u_{kl}(\rho/k) = 0\,. \tag{B.5}$$

This is a particular case of the general 'Coulomb wave equation'

$$\left[\frac{\mathrm{d}^2}{\mathrm{d}\rho^2} - \frac{l(l+1)}{\rho^2} - \frac{2\eta}{\rho} + 1\right]w_l(\rho) = 0\,, \tag{B.6}$$

with $\eta = 0$. The general solution to the above equation are $F_l(\eta,\rho)$ and $G_l(\eta,\rho)$. In the asymptotic limit $\rho \gg l$ (or $r \to \infty$), these solutions becomes

$$F_l(0,\rho) \sim \sin(\rho - l\pi/2)\,, \tag{B.7}$$

$$G_l(0,\rho) \sim \cos(\rho - l\pi/2)\,. \tag{B.8}$$

Since the scattering wave function in Eq. (B.3) take the form $e^{\pm i\rho}$, it is more convenient to use the Coulomb Hankel solutions $H_l^{\pm}(\eta,\rho) = G_l(\eta,\rho) \pm iF_l(\eta,\rho)$, which takes the following form in the asymptotic limit

$$H_l^{\pm}(\eta,\rho) \sim e^{\pm(\rho - l\pi/2)} = i^{\mp l}e^{\pm\rho}\,. \tag{B.9}$$

Using these solutions, the partial wave decomposition of the incident wave is

$$\begin{aligned}\psi_{\text{inc}}(r,\theta) &= e^{ikz} = e^{ikr\cos\theta} \\ &= \sum_{l=0}^{\infty} i^l(2l+1)P_l(\cos\theta)\frac{1}{kr}F_l(0,kr) \\ &= \sum_{l=0}^{\infty} i^l(2l+1)P_l(\cos\theta)\frac{1}{kr}\frac{i}{2}[H_l^+(0,kr) - H_l^-(0,kr)]\,, \qquad \text{(B.10)}\end{aligned}$$

$$\Psi_{\text{inc}}(r,\theta) = \sum_{l=0}^{\infty} i^l(2l+1)P_l(\cos\theta)\frac{1}{kr}\frac{i}{2}[i^l e^{-ikr} - i^{-l}e^{ikr}]\,. \qquad \text{(B.11)}$$

From the above equations, it is easy to see that the incident wave has the same amplitude for the radially incoming wave H_l^- and radially outgoing wave H_l^+.

Outside the range of potential, $u_{kl}(r)$ should be given by some linear combination of $H_l^{\pm}(0,kr)$

$$u_{kl}(r) \xrightarrow{r\to\infty} A_l[H_l^+(0,kr) - S_l H_l^-(0,kr)]\,. \qquad \text{(B.12)}$$

The S_l is called the *partial wave S matrix element*. For the above equation to be proportional to Eq. (B.10) in the absence of potential, $S_l = 1$ for $V(r) = 0$. The scattering wave function for a general potential $V(r)$ is given by

$$\psi(r,\theta) = \sum_{l=0}^{\infty} i^l(2l+1)P_l(\cos\theta)\frac{1}{kr}A_l[H_l^+(0,kr) - S_l H_l^-(0,kr)]\,. \qquad \text{(B.13)}$$

For $r \to \infty$

$$\Psi(r,\theta) = \sum_{l=0}^{\infty} i^l(2l+1)P_l(\cos\theta)\frac{1}{kr}A_l[i^l e^{-ikr} - S_l i^{-l}e^{ikr}]\,. \qquad \text{(B.14)}$$

The A_l and S_l for a general potential $V(r)$ is determined by matching the above equation with Eq. (B.3)

$$\begin{aligned}&\sum_{l=0}^{\infty} i^l(2l+1)P_l(\cos\theta)\frac{1}{kr}A_l[i^l e^{-ikr} - S_l i^{-l}e^{ikr}] \\ &= \sum_{l=0}^{\infty} i^l(2l+1)P_l(\cos\theta)\frac{1}{kr}A_l[i^l e^{-ikr} - i^{-l}e^{ikr}] + f(\theta)\frac{e^{ikr}}{r}\,. \qquad \text{(B.15)}\end{aligned}$$

By matching the coefficients of the linearly independent functions $e^{\pm ikr}$ we get $A_l = \frac{i}{2}$ and

$$f(\theta) = \frac{1}{2ik}\sum_{l=0}^{\infty}(2l+1)P_l(\cos\theta)(S_l - 1)\,. \qquad \text{(B.16)}$$

An equivalent parameterization is to represent the S_l in terms of *phase shifts*

$$S_l = e^{2i\delta_l} \,. \tag{B.17}$$

Note that, for $r \to \infty$ the incident (Eq. (B.11) and scattered wave function (Eq. (B.14)) take the form

$$\Psi_{\text{inc}}(r,\theta) = \sum_{l=0}^{\infty} i^l (2l+1) P_l(\cos\theta) \frac{1}{kr} \sin(kr + l\pi/2) \,, \tag{B.18}$$

$$\Psi(r,\theta) = \sum_{l=0}^{\infty} i^l (2l+1) P_l(\cos\theta) \frac{1}{kr} e^{i\delta_l} \sin(kr + l\pi/2 + \delta_l) \,, \tag{B.19}$$

the latter is called the *distorted* plane wave. It differs from the incident plane wave by a *phase shift* δ_l. The δ_l are called the *phase shift of the* l^{th} *partial wave.*

We can express the scattered wave function as

$$\Psi(r,\theta) = \sum_{l=0}^{\infty} i^l (2l+1) P_l(\cos\theta) \frac{1}{kr} \left[F_l(0,kr) + T_l H_l^+(0,kr) \right] \,, \tag{B.20}$$

the $T_l = e^{i\delta_l} \sin\delta_l$ are called *partial wave T matrix element* and $S_l = 1 + i\pi T_l$. T_l is proportional to the amplitude of the outgoing scattered wave function.

The differential cross-section is given by

$$\begin{aligned}
\frac{\mathrm{d}\sigma}{\mathrm{d}\omega} &= |f(\theta)|^2 = \left| \sum_{l=0}^{\infty} f_l(\theta) \right|^2 \\
&= \left| \sum_{l=0}^{\infty} \frac{1}{2ik} (2l+1) P_l(\cos\theta)(S_l - 1) \right|^2 \\
&= \left| \sum_{l=0}^{\infty} \frac{1}{k} (2l+1) P_l(\cos\theta) e^{i\delta_l} \sin\delta_l \right|^2 \\
&= \frac{1}{2\mu E} \sum_{l=0}^{\infty} \sum_{l'=0}^{\infty} (2l+1)(2l'+1) P_l(\cos\theta) P_{l'}(\cos\theta) e^{i(\delta_l - \delta_{l'})} \sin\delta_l \sin\delta_{l'} \,.
\end{aligned} \tag{B.21}$$

B.1.1 Nucleon scattering

In this section, we will generalize the scattering results for nucleons with spin quantum numbers (s, m_s). The scattered wave function of the nucleon with spin quantum numbers (s, m_s) in the $r \to \infty$ is

$$\Psi = \left(e^{ikz} + f_{s\,m_s}(\theta,\phi) \frac{e^{ikr}}{r} \right) \chi_{s\,m_s} \,, \tag{B.22}$$

where $\chi_{s\,m_s}$ are the spin-state basis vectors. The scattering amplitude is given by [322]

$$f_{s\,m_s}(\theta,\phi) = \sum_{s',m'_s} M_{s\,m_s,s'\,m'_s}(\theta,\phi) a_{s'\,m'_s}\,, \tag{B.23}$$

where $a_{s\,m_s}$ are the amplitudes of various spin states in the incident plane wave. As we did in the previous section, we will expand the M matrix in the partial wave basis

$$\begin{aligned} M_{s\,m_s,s'\,m'_s}(\theta,\phi) &= \sum_{l,m_l} Y_{l\,m_l}(\theta,\phi) M(l\,m_l\ s\,m_s; l'\,m'_l) \\ &= \sum_{s',m'_s} Y_{l\,m_l}(\theta,\phi) M(l\,m_l\ s\,m_s; s'\,m'_s)\,, \end{aligned} \tag{B.24}$$

where $Y_{l\,m_l}$ are the spherical harmonics and

$$M(l\,m_l\ s\,m_s; l'\,m'_l) = \frac{1}{ik} i^{-l} \sum_{l'} i^{l'} \sqrt{\pi(2l'+1)} R(l\,m_l\ s\,m_s; l'\,0\ s'\,m'_s)\,, \tag{B.25}$$

where R is related to S matrix by $S = 1 + R$. Note that, in the absence of spin quantum numbers ($s = m_s = a_{s/,m_s} = 0$) and spherically symmetric potential, the angular momentum gets conserved, and we have $R(l\,m_l = 0\ s = 0\,m_s = 0; l'\,0\ s' = 0\,m'_s = 0) \equiv R_l \delta_{ll'} = \delta_{ll'}(S_l - 1)$. In this specific case, we recover the scattering amplitude from Eq. (B.16)

$$\begin{aligned} f_{0\,0}(\theta,0) &\equiv f(\theta) \\ &= \frac{1}{2ik} \sum_{l,l'} Y_{l\,0}(\theta,0) \sqrt{4\pi(2l'+1)} i^{l'-l} \delta_{ll'}(S_l - 1) \\ &= \frac{1}{2ik} \sum_{l=0}^{\infty} (2l+1) P_l(\cos\theta)(S_l - 1)\,. \end{aligned} \tag{B.26}$$

It is convenient to represent the scattering amplitude in terms of phase shifts related to $\alpha = (ls)j$ quantum number. We start with representing R matrix in the α basis

$$\begin{aligned} R(l\,m_l\ s\,m_s; l'\,m'_l\ s'\,m'_s) = \sum_{j,m_j} &\langle l\,m_l, s\,m_s | j\,m_j\rangle \langle l'\,m'_l, s'\,m'_s | j'\,m'_j\rangle \\ &\times R(l\,s\ jm_j; l'\,s'\ j'm'_j)\,. \end{aligned} \tag{B.27}$$

Since the total momentum and its z-components are conserved, we have $j' = j$ and $m'_j = m_j$. The parity conservation and wave function asymmetry conserve the spin of $p-p$ scattering, i.e., $s' = s$. The spin is also conserved for isospin-conserving interaction for $n-p$ scattering. Since we are interested in these types

of scattering, we will have $j' = j, m'_j = m_j$, and $s' = s$. This is the main advantage of the $(ls\ j)$ basis. Then, the only non-zero R matrix elements $R^{sj}_{ll'} \equiv R(l\,s\ jm_j; l'\,s'\ j'm'_j)$ are

- $s = 0, l' = l = j : R^{0j}_{jj} = S^{0j}_{jj} - 1$
- $s = 1, l' = l = j : R^{1j}_{lj} = S^{1j}_{lj} - 1$
- $s = 1, l = j \pm 1, l' = j \mp 1 : R^{1j}_{j\pm1\,j\mp1} = S^{1j}_{j\pm1\,j\mp1}$

The S matrix in terms of phase shifts for the uncoupled channels are

$$S^{0j}_{jj} = e^{2i\delta^{0j}_j}, \qquad S^{1j}_{jj} = e^{2i\delta^{1j}_j}, \tag{B.28}$$

and for coupled channels are

$$S = \begin{pmatrix} S^{1j}_{j-1\,j-1} & S^{1j}_{j-1\,j+1} \\ S^{1j}_{j-1\,j+1} & S^{1j}_{j+1\,j+1} \end{pmatrix} = \begin{pmatrix} \cos(2\epsilon)e^{2i\delta^{1j}_{j-1}} & i\sin(2\epsilon)e^{i(\delta^{1j}_{j-1}+\delta^{1j}_{j+1})} \\ i\sin(2\epsilon)e^{i(\delta^{1j}_{j-1}+\delta^{1j}_{j+1})} & \cos(2\epsilon)e^{2i\delta^{1j}_{j+1}} \end{pmatrix}, \tag{B.29}$$

this is the Stapp parametrization [322] and ϵ is called the *mixing angle*.

B.2 Partial wave decomposition

The *CP*-even OPE potential is given by

$$V_{\mathrm{str},\pi}(\boldsymbol{p}', \boldsymbol{p}) = -\frac{1}{(2\pi)^3}\left(\frac{g_A}{2F_\pi}\right)^2 \frac{(\boldsymbol{\sigma}_1\cdot\boldsymbol{q})(\boldsymbol{\sigma}_2\cdot\boldsymbol{q})}{\boldsymbol{q}^2 + m_\pi^2}\vec{\tau}_1\cdot\vec{\tau}_2\,, \tag{B.30}$$

with $\boldsymbol{q} = \boldsymbol{p} - \boldsymbol{p}'$. The partial wave decomposition of the potential is

$$V^{\alpha',\alpha}_{\mathrm{str},\pi}(p', p) = \langle p'(l's')j'm'_j; t'm'_t|V_{\mathrm{str},\pi}(\boldsymbol{p}', \boldsymbol{p})|p(ls)jm_j; tm_t\rangle\ . \tag{B.31}$$

We will follow the notations defined in Section B.2.1. The isospin part can be calculated separately

$$\langle t'm'_t|\vec{\tau}_1\cdot\vec{\tau}_2|tm_t\rangle = -\sqrt{3}\,\langle tm_t00|t'm'_t\rangle\,\langle t'\|\{\tau_1,\vec{\tau}_2\}^0\|t\rangle\ , \tag{B.32}$$

where we used the tensor representation of the scalar product $\boldsymbol{a}\cdot\boldsymbol{b} = -\sqrt{3}\{a,b\}^{00}$, and Wigner–Eckart theorem. Using Eq. (B.42) and Eq. (B.43) on the above equation we get

$$\langle t'm'_t|\vec{\tau}_1\cdot\vec{\tau}_2|tm_t\rangle = (2t(t+1) - 3)\delta^{t't}\delta^{m'_t m_t}\,. \tag{B.33}$$

The remaining part of the partial wave decomposition can be done by using the tensor representation of the scalar product and $\boldsymbol{q}$ vector in terms of spherical harmonics $\boldsymbol{q}_m = q\sqrt{\frac{4\pi}{3}}Y_{1m}(\hat{\boldsymbol{q}})$. Using the following relation

$$|(j_1,j_4)j_7,(j_2,j_5)j_8;j_9,m_{j_9}\rangle = \sum_{j_3,j_6}\sqrt{\hat{j}_3\,\hat{j}_6\,\hat{j}_7\,\hat{j}_8}\begin{Bmatrix} j_1 & j_4 & j_7\\ j_2 & j_5 & j_8\\ j_3 & j_6 & j_9\end{Bmatrix} \times |(j_1,j_2)j_3,(j_4,j_5)j_6;j_9,m_{j_9}\rangle\ , \tag{B.34}$$

and relations in Section B.2.1, we can separate the spin and angular momentum

$$\begin{aligned}\langle p'(l's')j'm'_j|\frac{(\boldsymbol{\sigma}_1\cdot\boldsymbol{q})(\boldsymbol{\sigma}_2\cdot\boldsymbol{q})}{\boldsymbol{q}^2+m_\pi^2}|p(ls)jm_j\rangle &= \delta^{j'j}\delta^{m'_jm_j}\sum_{f=0}^{2}3\sqrt{\frac{\hat{f}}{4\pi}}\begin{Bmatrix}1&1&0\\1&1&0\\f&f&0\end{Bmatrix}\\ &\times\langle 1010|f0\rangle\sqrt{\hat{l}'\hat{s}'\hat{j}}\begin{Bmatrix}l'&l&f\\s'&s&f\\j'&j&0\end{Bmatrix}\\ &\times\langle p'l'\|\frac{4\pi q^2}{q^2+m_\pi^2}Y_f(\hat{\boldsymbol{q}})\|pl\rangle\,\langle s'\|\{\sigma_1,\sigma_2\}^f\|s\rangle\ .\end{aligned} \tag{B.35}$$

The spin part calculations follow the same method as the isospin part, and we get

$$\langle s'\|\{\sigma_1,\sigma_2\}^f\|s\rangle = 6\sqrt{\hat{f}\hat{s}}\begin{Bmatrix}\frac{1}{2}&\frac{1}{2}&1\\\frac{1}{2}&\frac{1}{2}&1\\s'&s&f\end{Bmatrix}\ . \tag{B.36}$$

The orbital part using the spherical harmonics and other relations in Section B.2.1 is

$$\begin{aligned}\langle p'l'\|\frac{4\pi q^2}{q^2+m_\pi^2}Y_f(\hat{\boldsymbol{q}})\|pl\rangle = &\sum_{\substack{\lambda_1,\lambda_2\geq 0\\ \lambda_1+\lambda_2=f}}\sqrt{\frac{4\pi\hat{f}!}{\hat{\lambda}_1!\hat{\lambda}_2!}}p^{\lambda_1}(-p')^{\lambda_2}\sum_{k=0}^{\infty}g_k^f(p,p')\hat{k}\sqrt{\hat{f}\hat{\lambda}_1\hat{\lambda}_2}\\ &\times\begin{Bmatrix}k&k&0\\\lambda_1&\lambda_2&f\\l&l'&f\end{Bmatrix}\langle k0\lambda_10|l0\rangle\,\langle k0\lambda_20|l'0\rangle\,(-1)^l\sqrt{\frac{\hat{f}}{\hat{l}'}}\,,\end{aligned} \tag{B.37}$$

where $g_k^f(p,p') = \int_{-1}^{1}dxP_k(x)\frac{4\pi q(x)^{2-f}}{q(x)^2+m_\pi^2}$ with $q(x)=\sqrt{p^2+p'^2-2pp'x}$.

Combining all the above results, the partial wave decomposition of OPE *CP*-

even potential is

$$V^{\alpha',\alpha}_{\mathrm{str},\pi}(p',p) = \delta^{j'j}\delta^{m'_j m_j}\frac{-1}{(2\pi)^3}\left(\frac{g_A}{2F_\pi}\right)^2\sum_{f=0}^{2}3\sqrt{\frac{\hat{f}}{4\pi}}\begin{Bmatrix}1 & 1 & 0\\ 1 & 1 & 0\\ f & f & 0\end{Bmatrix}\langle 1010|f0\rangle$$
$$\times\sqrt{\hat{l}'\hat{s}'\hat{j}}\begin{Bmatrix}l' & l & f\\ s' & s & f\\ j' & j & 0\end{Bmatrix}\sum_{\substack{\lambda_1,\lambda_2\geq 0\\ \lambda_1+\lambda_2=f}}\sqrt{\frac{4\pi\hat{f}!}{\hat{\lambda}_1!\hat{\lambda}_2!}}p^{\lambda_1}(-p')^{\lambda_2}\sum_{k=0}^{\infty}(-1)^k\frac{\hat{k}}{2}\,g_k^f(p,p')$$
$$\times\hat{k}\sqrt{\hat{f}\hat{\lambda}_1\hat{\lambda}_2}\,\langle k0\lambda_1 0|l0\rangle\,\langle k0\lambda_2 0|l'0\rangle\begin{Bmatrix}k & k & 0\\ \lambda_1 & \lambda_2 & f\\ l & l' & f\end{Bmatrix}\begin{Bmatrix}\frac{1}{2} & \frac{1}{2} & 1\\ \frac{1}{2} & \frac{1}{2} & 1\\ s' & s & f\end{Bmatrix}$$
$$\times(-1)^l\sqrt{\frac{\hat{f}}{\hat{l}'}}6\sqrt{\hat{f}\hat{s}}(2t(t+1)-3)\delta^{t't}\delta^{m'_t m_t}\,. \tag{B.38}$$

The *CP*-odd OPE potential is

$$V_{\bar{g}_0} = -\frac{1}{(2\pi)^3}\frac{g_A\bar{g}_0}{2F_\pi}\frac{i(\boldsymbol{\sigma}_1-\boldsymbol{\sigma}_2)\cdot\boldsymbol{q}}{\boldsymbol{q}^2+m_\pi^2}\vec{\tau}_1\cdot\vec{\tau}_2\,. \tag{B.39}$$

The partial wave decomposition of the *CP*-odd OPE potential can be done by following the same calculations as the *CP*-even OPE potential, and the final result is

$$V^{\alpha',\alpha}_{\bar{g}_0,\pi}(p',p) = -\delta^{j'j}\delta^{m'_j m_j}\frac{1}{(2\pi)^3}\frac{ig_A\bar{g}_0}{2F_\pi}(-\sqrt{3})\sqrt{\hat{l}'\hat{s}'\hat{j}}\begin{Bmatrix}l' & l & 1\\ s' & s & 1\\ j' & j & 0\end{Bmatrix}$$
$$\times\sum_{\substack{\lambda_1,\lambda_2\geq 0\\ \lambda_1+\lambda_2=1}}\frac{p^{\lambda_1}(-p')^{\lambda_2}}{\sqrt{3}}\sum_{k=0}^{\infty}(-1)^k 2\pi\,\hat{k}\,g_k^{f=2}(p,p')\frac{\hat{k}\sqrt{3\hat{\lambda}_1\hat{\lambda}_2}}{4\pi}\,\langle k0\lambda_1 0|l0\rangle\,\langle k0\lambda_2 0|l'0\rangle$$
$$\times\begin{Bmatrix}k & k & 0\\ \lambda_1 & \lambda_2 & f\\ l & l' & 1\end{Bmatrix}(-1)^l\sqrt{\frac{3}{\hat{l}'}}6\sqrt{\hat{s}}(1-(-1)^{s+s'})\begin{Bmatrix}\frac{1}{2} & \frac{1}{2} & 1\\ \frac{1}{2} & \frac{1}{2} & 0\\ s' & s & 1\end{Bmatrix}$$
$$\times(2t(t+1)-3)\delta^{t't}\delta^{m'_t m_t}\,. \tag{B.40}$$

B.2.1 Notations and relations

By Wigner–Eckart theorem for tensor operator for the M-th of the spherical tensor operator $\mathcal{O}^L$ with rank L is

$$\langle j'm'_j|\mathcal{O}^{LM}|jm_j\rangle = \langle jm_jLM|j'm'_j\rangle\,\langle j'\|\mathcal{O}^L\|j\rangle\,, \tag{B.41}$$

where $\langle j' \| \mathcal{O}^L \| j \rangle$ is the reduced matrix element. The Clebsch–Gordan coefficient notation for spin j_1 and j_2 added to get j is $\langle j_1 m_{j_1} j_2 m_{j_2} | j m_j \rangle$.

Some common relations of reduced matrix elements are

$$\langle (j_1 j_2') j \| \{ T_{k_1}(j_1), T_{k_2}(j_2) \}^k \| (j_1 j_2) j \rangle = \sqrt{\hat{j}_1' \ \hat{j}_2' \ \hat{k} \ \hat{j}} \begin{Bmatrix} j_1' & j_1 & k_1 \\ j_2' & j_2 & k_2 \\ j' & j & k \end{Bmatrix} \times \langle j_1' \| T_{k_1}(j_1) \| j_1 \rangle \langle j_2' \| T_{k_2}(j_2) \| j_2 \rangle \ , \tag{B.42}$$

$$\langle \tfrac{1}{2} \| \sigma \| \tfrac{1}{2} \rangle = \sqrt{3} \, , \tag{B.43}$$

$$\langle l' \| Y_L \| l \rangle = (-1)^l \sqrt{\frac{\hat{L}\hat{l}}{4\pi}} \begin{Bmatrix} l' & L & l \\ 0 & 0 & 0 \end{Bmatrix} , \tag{B.44}$$

$$\langle l' \| \mathcal{Y}^f_{g_1 g_2}(\hat{\boldsymbol{p}}' \hat{\boldsymbol{p}}) \| l \rangle = (-1)^l \delta^{g_1 l'} \delta^{g_2 l} \sqrt{\frac{\hat{f}}{\hat{l}'}} \, , \tag{B.45}$$

where $\{ \dots \}$ are 9-j/3-j symbols, $\hat{x} = 2x+1$, and $\mathcal{Y}^f_{g_1 g_2}(\hat{\boldsymbol{p}}' \hat{\boldsymbol{p}}) \equiv \{ Y_{g_1}(\hat{\boldsymbol{p}}'), Y_{g_1}(\hat{\boldsymbol{p}}) \}^f$.

Some relations of spherical harmonics and Legendre polynomials (P_l) are

$$Y_{l,m}(\widehat{\boldsymbol{a} \pm \boldsymbol{b}}) = \sum_{\substack{l', l'', \\ l'+l''=l}} \sqrt{\frac{4\pi \hat{l}!}{\hat{l}'! \ \hat{l}''!}} \frac{a^{l'} (\pm b)^{l''}}{|\boldsymbol{a} + \boldsymbol{b}|^l} \mathcal{Y}^{l,m}_{l',l''}(\hat{\boldsymbol{a}}, \hat{\boldsymbol{b}}) \, , \tag{B.46}$$

$$\mathcal{Y}^{l,m}_{l',l''}(\hat{\boldsymbol{x}}, \hat{\boldsymbol{x}}) = \sqrt{\frac{\hat{l}' \ \hat{l}''}{4\pi \hat{l}}} \langle l', l''; 0, 0 \rangle \, l', l''; l, 0 Y_{l,m}(\hat{\boldsymbol{x}}) \, , \tag{B.47}$$

$$f(q = |\boldsymbol{p} - \boldsymbol{p}'|) = \sum_{k=0}^{\infty} 2\pi (-1)^k \sqrt{\hat{k}} \mathcal{Y}^{0,0}_k(\hat{\boldsymbol{p}}, \hat{\boldsymbol{p}}') \int_{-1}^{1} dx P_k(x) f[\sqrt{p^2 + p'^2 - 2pp'x}], \, . \tag{B.48}$$

Appendix C

LEFT operators

C.1 Notation and selection of operators

Here we clarify some of the notation related to the LEFT as well as the selection of the operators in Table 4.1.

As mentioned, the sum in Eq. (4.5) extends over all the operators in Table 4.1, as well as their hermitian conjugates, and flavor indices. For example, the Lagrangian due to $\mathcal{O}_{dd}^{\mathrm{S1,RR}}$ and its hermitian conjugate is written as $\mathcal{L} \supset \sum_{p,r,s,t} L^{\mathrm{S1,RR}}_{\substack{dd\\prst}} (\bar{q}_L^p q_R^r)\,(\bar{q}_L^s q_R^t) + \text{h.c.}$, where we explicitly sum over all possible flavor combinations. Note that this means that several different coefficients multiply the same operator since, e.g. $\mathcal{O}^{\mathrm{S1,RR}}_{\substack{dd\\prst}} = \mathcal{O}^{\mathrm{S1,RR}}_{\substack{dd\\stpr}}$. Without loss of generality this allows us to assume similar relations between the Wilson coefficients. The relevant cases for the operators of interest are

$$L^{\mathrm{S1,RR}}_{\substack{dd\\prst}} = L^{\mathrm{S1,RR}}_{\substack{dd\\stpr}}, \qquad L^{\mathrm{S8,RR}}_{\substack{dd\\prst}} = L^{\mathrm{S8,RR}}_{\substack{dd\\stpr}},$$
$$L^{\mathrm{V1,LR}}_{\substack{ud\\uust}} = \left(L^{\mathrm{V1,LR}}_{\substack{ud\\uuts}}\right)^*, \qquad L^{\mathrm{V1,LR}}_{\substack{du\\stuu}} = \left(L^{\mathrm{V1,LR}}_{\substack{du\\tsuu}}\right)^*, \qquad L^{\mathrm{V1,LR}}_{\substack{dd\\prst}} = \left(L^{\mathrm{V1,LR}}_{\substack{dd\\rpts}}\right)^*, \tag{C.1}$$

and similar for the $L^{\mathrm{V8,LR}}$ couplings.

As we focus on the dimension-five and -six operators that can be written as external sources or give rise to leading-order chiral interactions, it will be useful to write them in terms of the $SU(3)_L \times SU(3)_R$ representations they belong to. Below we consider the different classes of operators and the chiral representations they lead to. It turns out that all the operators in Table 4.1 only lead to a limited set of irreducible representations

- X^3
  This class only includes $SU(3)_L \times SU(3)_R$ singlets and the CP-odd term does not appear in the chiral Lagrangian at LO.

- $(\bar{L}R)X$
  This class contains the quark EM dipole moments that can be captured by the tensor sources, $t_R^{\mu\nu}$, described in Appendix C.2. In addition, there are the chromo-magnetic dipole moments which transform in the same way as the quark mass terms, $\bar{\mathbf{3}}_\mathbf{L} \times \mathbf{3}_\mathbf{R}$, leading to analogous interactions in the chiral Lagrangian. These cannot be captured by the external sources and are discussed in Appendix C.3.

- $(\bar{L}L)(\bar{L}L)$ and $(\bar{R}R)(\bar{R}R)$
  The semi-leptonic operators in these classes contribute to the external currents, l_μ and r_μ given in Appendix C.2. The four-quark interactions transform as $(\bar{\mathbf{3}} \times \mathbf{3} \times \bar{\mathbf{3}} \times \mathbf{3})_{\mathbf{L},\mathbf{R}}$, which lead to singlet terms that appear at LO but are CP even, or representations that can be CPV but require derivatives in the chiral Lagrangian. We thus only take into account the semi-leptonic terms.

- $(\bar{L}L)(\bar{R}R)$
  The semi-leptonic operators can again be captured by l_μ and r_μ discussed in Appendix C.2. The four-quark interactions now transform as $(\bar{\mathbf{3}} \times \mathbf{3})_\mathbf{L} \times (\bar{\mathbf{3}} \times \mathbf{3})_\mathbf{R}$. This again includes singlet terms that are CP even, as well as non-singlet pieces, $\sim \mathbf{1}_\mathbf{L} \times \mathbf{8}_\mathbf{R}$, that come with derivatives in the chiral Lagrangian. The remaining representation, $\mathbf{8}_\mathbf{L} \times \mathbf{8}_\mathbf{R}$, can lead to CPV terms that appear at LO in the chiral Lagrangian and is discussed further in Appendix C.3.

- $(\bar{L}R)(\bar{L}R)$
  The semi-leptonic operators in this class can be described by the scalar and tensor currents s, p, and $t_R^{\mu\nu}$. The four-quark operators now lead to two representations that can violate CP and appear at LO in the chiral Lagrangian, $(\bar{\mathbf{3}} \times \bar{\mathbf{3}})_\mathbf{L} \times (\mathbf{3} \times \mathbf{3})_\mathbf{R} \supset \mathbf{3}_\mathbf{L} \times \bar{\mathbf{3}}_\mathbf{R} \oplus \bar{\mathbf{6}}_\mathbf{L} \times \mathbf{6}_\mathbf{R}$.

- $(\bar{L}R)(\bar{R}L)$
  This class only involves semi-leptonic operators which are captured by the scalar currents s and p.

C.2 External sources

Here we list the explicit expressions of the external sources appearing in Eq. (4.7). The vector sources can be written as,

$$
\begin{aligned}
l_\mu =& -eQA_\mu + \frac{\partial_\mu a}{2f_a} c_L^q \\
&+ \bar{e}_L^p \gamma_\mu e_L^r \begin{pmatrix} L^{\mathrm{V,LL}}_{eu\,pruu} & 0 & 0 \\ 0 & L^{\mathrm{V,LL}}_{ed\,prdd} & L^{\mathrm{V,LL}}_{ed\,prds} \\ 0 & L^{\mathrm{V,LL}}_{ed\,prsd} & L^{\mathrm{V,LL}}_{ed\,prss} \end{pmatrix} + \bar{\nu}_L^p \gamma_\mu \nu_L^r \begin{pmatrix} L^{\mathrm{V,LL}}_{\nu u\,pruu} & 0 & 0 \\ 0 & L^{\mathrm{V,LL}}_{\nu d\,prdd} & L^{\mathrm{V,LL}}_{\nu d\,prds} \\ 0 & L^{\mathrm{V,LL}}_{\nu d\,prsd} & L^{\mathrm{V,LL}}_{\nu d\,prss} \end{pmatrix} \\
&+ \bar{e}_R^p \gamma_\mu e_R^r \begin{pmatrix} L^{\mathrm{V,LR}}_{ue\,uupr} & 0 & 0 \\ 0 & L^{\mathrm{V,LR}}_{de\,ddpr} & L^{\mathrm{V,LR}}_{de\,dspr} \\ 0 & L^{\mathrm{V,LR}}_{de\,sdpr} & L^{\mathrm{V,LR}}_{de\,sspr} \end{pmatrix} + \left[\bar{\nu}_L^p \gamma_\mu e_L^r \begin{pmatrix} 0 & 0 & 0 \\ L^{\mathrm{V,LL}}_{\nu edu\,prdu} & 0 & 0 \\ L^{\mathrm{V,LL}}_{\nu edu\,prsu} & 0 & 0 \end{pmatrix} + \mathrm{h.c.} \right],
\end{aligned}
\tag{C.2}
$$

$$
\begin{aligned}
r_\mu =& -eQA_\mu + \frac{\partial_\mu a}{2f_a} c_R^q \\
&+ \bar{e}_L^p \gamma_\mu e_L^r \begin{pmatrix} L^{\mathrm{V,LR}}_{eu\,pruu} & 0 & 0 \\ 0 & L^{\mathrm{V,LR}}_{ed\,prdd} & L^{\mathrm{V,LR}}_{ed\,prds} \\ 0 & L^{\mathrm{V,LR}}_{ed\,prsd} & L^{\mathrm{V,LR}}_{ed\,prss} \end{pmatrix} + \bar{\nu}_L^p \gamma_\mu \nu_L^r \begin{pmatrix} L^{\mathrm{V,LR}}_{\nu u\,pruu} & 0 & 0 \\ 0 & L^{\mathrm{V,LR}}_{\nu d\,prdd} & L^{\mathrm{V,LR}}_{\nu d\,prds} \\ 0 & L^{\mathrm{V,LR}}_{\nu d\,prsd} & L^{\mathrm{V,LR}}_{\nu d\,prss} \end{pmatrix} \\
&+ \bar{e}_R^p \gamma_\mu e_R^r \begin{pmatrix} L^{\mathrm{V,RR}}_{eu\,pruu} & 0 & 0 \\ 0 & L^{\mathrm{V,RR}}_{ed\,prdd} & L^{\mathrm{V,RR}}_{ed\,prds} \\ 0 & L^{\mathrm{V,RR}}_{ed\,prsd} & L^{\mathrm{V,RR}}_{ed\,prss} \end{pmatrix} + \left[\bar{\nu}_L^p \gamma_\mu e_L^r \begin{pmatrix} 0 & 0 & 0 \\ L^{\mathrm{V,LR}}_{\nu edu\,prdu} & 0 & 0 \\ L^{\mathrm{V,LR}}_{\nu esu\,prsu} & 0 & 0 \end{pmatrix} + \mathrm{h.c.} \right],
\end{aligned}
\tag{C.3}
$$

while the scalar, pseudoscalar, and tensor terms are given by

$$
\begin{aligned}
-(s+ip) =& \bar{e}_L^p e_R^r \begin{pmatrix} L^{\mathrm{S,RL}}_{eu\,pruu} & 0 & 0 \\ 0 & L^{\mathrm{S,RL}}_{ed\,prdd} & L^{\mathrm{S,RL}}_{ed\,prds} \\ 0 & L^{\mathrm{S,RL}}_{ed\,prsd} & L^{\mathrm{S,RL}}_{ed\,prss} \end{pmatrix} + \bar{e}_R^p e_L^r \begin{pmatrix} L^{\mathrm{S,RR}}_{eu\,rpuu} & 0 & 0 \\ 0 & L^{\mathrm{S,RR}}_{ed\,rpdd} & L^{\mathrm{S,RR}}_{ed\,rpsd} \\ 0 & L^{\mathrm{S,RR}}_{ed\,rpds} & L^{\mathrm{S,RR}}_{ed\,rpss} \end{pmatrix}^* \\
&+ \bar{\nu}_L^p e_R^r \begin{pmatrix} 0 & 0 & 0 \\ L^{\mathrm{S,RL}}_{\nu edu\,prdu} & 0 & 0 \\ L^{\mathrm{S,RL}}_{\nu edu\,prsu} & 0 & 0 \end{pmatrix} + \bar{e}_R^p \nu_L^r \begin{pmatrix} 0 & L^{\mathrm{S,RR}}_{\nu edu\,rpdu} & L^{\mathrm{S,RR}}_{\nu edu\,rpsu} \\ 0 & 0 & 0 \\ 0 & 0 & 0 \end{pmatrix}^*,
\end{aligned}
\tag{C.4}
$$

$$t_R^{\mu\nu} = F^{\mu\nu} \begin{pmatrix} L_{\substack{u\gamma \\ uu}} & 0 & 0 \\ 0 & L_{\substack{d\gamma \\ dd}} & L_{\substack{d\gamma \\ ds}} \\ 0 & L_{\substack{d\gamma \\ sd}} & L_{\substack{d\gamma \\ ss}} \end{pmatrix} + \bar{e}_L^p \sigma^{\mu\nu} e_R^r \begin{pmatrix} L^{\mathrm{T,RR}}_{\substack{eu \\ pruu}} & 0 & 0 \\ 0 & L^{\mathrm{T,RR}}_{\substack{ed \\ prdd}} & L^{\mathrm{T,RR}}_{\substack{ed \\ prds}} \\ 0 & L^{\mathrm{T,RR}}_{\substack{ed \\ prsd}} & L^{\mathrm{T,RR}}_{\substack{ed \\ prss}} \end{pmatrix}$$
$$+ \bar{\nu}_L^p \sigma^{\mu\nu} e_R^r \begin{pmatrix} 0 & 0 & 0 \\ L^{\mathrm{T,RR}}_{\substack{\nu edu \\ prdu}} & 0 & 0 \\ L^{\mathrm{T,RR}}_{\substack{\nu edu \\ prsu}} & 0 & 0 \end{pmatrix} . \tag{C.5}$$

C.3 Hadronic dimension-five and -six terms

The expressions for the couplings that are induced by the purely hadronic operators, appearing in Eq. (4.8) are given by

$$L_5 = \begin{pmatrix} L_{\substack{uG \\ uu}} & 0 & 0 \\ 0 & L_{\substack{dG \\ dd}} & L_{\substack{dG \\ ds}} \\ 0 & L_{\substack{dG \\ sd}} & L_{\substack{dG \\ ss}} \end{pmatrix} , \tag{C.6}$$

$$L^{ijkl}_{\mathbf{8}\times\mathbf{8}} = L^{ijkl}_{\mathrm{LLRR}} - \frac{\delta^{ij}}{3} L^{nnkl}_{\mathrm{LLRR}} - \frac{\delta^{kl}}{3} L^{ijnn}_{\mathrm{LLRR}} + \frac{\delta^{ij}\delta^{kl}}{9} L^{nnmm}_{\mathrm{LLRR}} , \tag{C.7}$$

where

$$\begin{aligned} L^{ijkl}_{\mathrm{LLRR}} =& L^{\mathrm{V1,LR}}_{\substack{ud \\ uuds}} \delta_1^i \delta_1^j \delta_2^k \delta_3^l + L^{\mathrm{V1,LR}}_{\substack{ud \\ uusd}} \delta_1^i \delta_1^j \delta_3^k \delta_2^l + L^{\mathrm{V1,LR}}_{\substack{du \\ dsuu}} \delta_1^k \delta_1^l \delta_2^i \delta_3^j + L^{\mathrm{V1,LR}}_{\substack{du \\ sduu}} \delta_1^k \delta_1^l \delta_3^i \delta_2^j \\ &+ L^{\mathrm{V1,LR}}_{\substack{dd \\ sddd}} \delta_3^i \delta_2^j \delta_2^k \delta_2^l + L^{\mathrm{V1,LR}}_{\substack{dd \\ dsdd}} \delta_2^i \delta_3^j \delta_2^k \delta_2^l + L^{\mathrm{V1,LR}}_{\substack{dd \\ ddsd}} \delta_2^i \delta_2^j \delta_3^k \delta_2^l + L^{\mathrm{V1,LR}}_{\substack{dd \\ ddds}} \delta_2^i \delta_2^j \delta_2^k \delta_3^l \\ &+ L^{\mathrm{V1,LR}}_{\substack{dd \\ dsss}} \delta_2^i \delta_3^j \delta_3^k \delta_3^l + L^{\mathrm{V1,LR}}_{\substack{dd \\ sdss}} \delta_3^i \delta_2^j \delta_3^k \delta_3^l + L^{\mathrm{V1,LR}}_{\substack{dd \\ ssds}} \delta_3^i \delta_3^j \delta_2^k \delta_3^l + L^{\mathrm{V1,LR}}_{\substack{dd \\ sssd}} \delta_3^i \delta_3^j \delta_3^k \delta_2^l \\ &+ L^{\mathrm{V1,LR}}_{\substack{dd \\ dssd}} \delta_2^i \delta_3^j \delta_3^k \delta_2^l + L^{\mathrm{V1,LR}}_{\substack{dd \\ sdds}} \delta_3^i \delta_2^j \delta_2^k \delta_3^l + L^{\mathrm{V1,LR}}_{\substack{dd \\ dsds}} \delta_2^i \delta_3^j \delta_2^k \delta_3^l + L^{\mathrm{V1,LR}}_{\substack{dd \\ sdsd}} \delta_3^i \delta_2^j \delta_3^k \delta_2^l \\ &+ L^{\mathrm{V1,LR}}_{\substack{uddu \\ uddu}} \delta_1^i \delta_2^j \delta_2^k \delta_1^l + L^{\mathrm{V1,LR}}_{\substack{uddu \\ usdu}} \delta_1^i \delta_3^j \delta_2^k \delta_1^l + L^{\mathrm{V1,LR}}_{\substack{uddu \\ udsu}} \delta_1^i \delta_2^j \delta_3^k \delta_1^l + L^{\mathrm{V1,LR}}_{\substack{uddu \\ ussu}} \delta_1^i \delta_3^j \delta_3^k \delta_1^l \\ &+ \left[L^{\mathrm{V1,LR}}_{\substack{uddu \\ uddu}} \delta_1^i \delta_2^j \delta_2^l \delta_1^k + L^{\mathrm{V1,LR}}_{\substack{uddu \\ usdu}} \delta_1^j \delta_3^i \delta_2^l \delta_1^k + L^{\mathrm{V1,LR}}_{\substack{uddu \\ udsu}} \delta_1^j \delta_2^i \delta_3^l \delta_1^k + L^{\mathrm{V1,LR}}_{\substack{uddu \\ ussu}} \delta_1^j \delta_3^i \delta_3^l \delta_1^k \right]^* , \end{aligned} \tag{C.8}$$

where we neglected CP even terms such as $L^{V1,LR}_{\substack{uu \\ uuuu}}$. $\bar{L}^{ijkl}_{\mathbf{8}\times\mathbf{8}}$ can be obtained from the expressions above by replacing, $L^{\mathrm{V1,LR}}_\alpha \to L^{\mathrm{V8,LR}}_\alpha$ in Eq. (C.8).

For the operators in the LRLR class, we can define

$$
\begin{aligned}
L^{ijkl}_{\mathrm{LRLR}} =& L^{\mathrm{S1,RR}}_{\substack{uu\\uuuu}}\delta^i_1\delta^j_1\delta^k_1\delta^l_1 + L^{\mathrm{S1,RR}}_{\substack{dd\\dddd}}\delta^i_2\delta^j_2\delta^k_2\delta^l_2 + L^{\mathrm{S1,RR}}_{\substack{dd\\ssss}}\delta^i_3\delta^j_3\delta^k_3\delta^l_3 \\
&+ L^{\mathrm{S1,RR}}_{\substack{dd\\ssdd}}\delta^i_3\delta^j_3\delta^k_2\delta^l_2 + L^{\mathrm{S1,RR}}_{\substack{dd\\sdsd}}\delta^i_3\delta^j_2\delta^k_3\delta^l_2 + L^{\mathrm{S1,RR}}_{\substack{dd\\sdds}}\delta^i_3\delta^j_2\delta^k_2\delta^l_3 \\
&+ L^{\mathrm{S1,RR}}_{\substack{dd\\dssd}}\delta^i_2\delta^j_3\delta^k_3\delta^l_2 + L^{\mathrm{S1,RR}}_{\substack{dd\\dsds}}\delta^i_2\delta^j_3\delta^k_2\delta^l_3 + L^{\mathrm{S1,RR}}_{\substack{dd\\ddss}}\delta^i_2\delta^j_2\delta^k_3\delta^l_3 \\
&+ L^{\mathrm{S1,RR}}_{\substack{dd\\sddd}}\delta^i_3\delta^j_2\delta^k_2\delta^l_2 + L^{\mathrm{S1,RR}}_{\substack{dd\\dsdd}}\delta^i_2\delta^j_3\delta^k_2\delta^l_2 + L^{\mathrm{S1,RR}}_{\substack{dd\\ddsd}}\delta^i_2\delta^j_2\delta^k_3\delta^l_2 + L^{\mathrm{S1,RR}}_{\substack{dd\\ddds}}\delta^i_2\delta^j_2\delta^k_2\delta^l_3 \\
&+ L^{\mathrm{S1,RR}}_{\substack{dd\\dsss}}\delta^i_2\delta^j_3\delta^k_3\delta^l_3 + L^{\mathrm{S1,RR}}_{\substack{dd\\sdss}}\delta^i_3\delta^j_2\delta^k_3\delta^l_3 + L^{\mathrm{S1,RR}}_{\substack{dd\\ssds}}\delta^i_3\delta^j_3\delta^k_2\delta^l_3 + L^{\mathrm{S1,RR}}_{\substack{dd\\sssd}}\delta^i_3\delta^j_3\delta^k_3\delta^l_2 \\
&+ L^{\mathrm{S1,RR}}_{\substack{ud\\uudd}}\delta^i_1\delta^j_1\delta^k_2\delta^l_2 + L^{\mathrm{S1,RR}}_{\substack{ud\\uuds}}\delta^i_1\delta^j_1\delta^k_2\delta^l_3 + L^{\mathrm{S1,RR}}_{\substack{ud\\uusd}}\delta^i_1\delta^j_1\delta^k_3\delta^l_2 + L^{\mathrm{S1,RR}}_{\substack{ud\\uuss}}\delta^i_1\delta^j_1\delta^k_3\delta^l_3 \\
&+ L^{\mathrm{S1,RR}}_{\substack{uddu\\uddu}}\delta^i_1\delta^j_2\delta^k_2\delta^l_1 + L^{\mathrm{S1,RR}}_{\substack{uddu\\udsu}}\delta^i_1\delta^j_2\delta^k_3\delta^l_1 + L^{\mathrm{S1,RR}}_{\substack{uddu\\usdu}}\delta^i_1\delta^j_3\delta^k_2\delta^l_1 + L^{\mathrm{S1,RR}}_{\substack{uddu\\ussu}}\delta^i_1\delta^j_3\delta^k_3\delta^l_1 \,,
\end{aligned}
\tag{C.9}
$$

so that

$$
\begin{aligned}
L^{ijkl}_{\mathbf{6\times6}} &= \frac{1}{4}\left[L^{ijkl}_{\mathrm{LRLR}} + L^{ilkj}_{\mathrm{LRLR}} + L^{kjil}_{\mathrm{LRLR}} + L^{klij}_{\mathrm{LRLR}}\right] , \\
L^{ijkl}_{\mathbf{3\times3}} &= \frac{1}{4}\left[L^{ijkl}_{\mathrm{LRLR}} - L^{ilkj}_{\mathrm{LRLR}} - L^{kjil}_{\mathrm{LRLR}} + L^{klij}_{\mathrm{LRLR}}\right] .
\end{aligned}
\tag{C.10}
$$

The couplings with different color structures, $\bar{L}_{\mathbf{6\times6}}$ and $\bar{L}_{\mathbf{3\times3}}$, can be obtained from the expressions for $L_{\mathbf{6\times6}}$ and $L_{\mathbf{3\times3}}$ with the replacement $L^{\mathrm{S1,RR}}_{\alpha} \to L^{\mathrm{S8,RR}}_{\alpha}$.

The four-quark operators in Eq. (4.6) then reproduce those in the original Lagrangian, Eq. (4.1), after one takes into account the relations

$$
L^{\mathrm{S1,RR}}_{\substack{dd\\prst}} = L^{\mathrm{S1,RR}}_{\substack{dd\\stpr}} , \qquad L^{\mathrm{S8,RR}}_{\substack{dd\\prst}} = L^{\mathrm{S8,RR}}_{\substack{dd\\stpr}} .
\tag{C.11}
$$

C.4 Hadronic dimension-five and -six terms

The matrix elements that enter in the rotation angles α_i discussed in Section 4.2.2 and their relations to the LECs discussed in Section 4.3, can be written as

$$
\begin{aligned}
&\langle 0|\bar{q}_p q_r|0\rangle = -F_0^2 B\delta_{pr} , \qquad \langle 0|\bar{q}_p\sigma^{\mu\nu}G^A_{\mu\nu}t^A q_r|0\rangle = -2F_0^2\bar{B}\delta_{pr} , \\
&\langle 0|(\bar{q}_{L\,p}\gamma_\mu q_{L\,r})\,(\bar{q}_{R\,s}\gamma^\mu q_{R\,t})_{\mathbf{8_L\times8_R}}|0\rangle = -\frac{F_0^4}{4}\mathcal{A}_{\mathbf{8\times8}}\left(\delta_{pt}\delta_{rs} - \frac{1}{3}\delta_{pr}\delta_{st}\right) , \\
&\langle 0|(\bar{q}_{L\,p}\gamma_\mu t^A q_{L\,r})\,(\bar{q}_{R\,s}\gamma^\mu t^A q_{R\,t})_{\mathbf{8_L\times8_R}}|0\rangle = -\frac{F_0^4}{4}\bar{\mathcal{A}}_{\mathbf{8\times8}}\left(\delta_{pt}\delta_{rs} - \frac{1}{3}\delta_{pr}\delta_{st}\right) , \\
&\langle 0|(\bar{q}_{L\,p}q_{R\,r})\,(\bar{q}_{L\,s}q_{R\,t})_{\mathbf{3\times3}}|0\rangle = -\frac{F_0^4}{4}\mathcal{A}_{\mathbf{3\times3}}\frac{\delta_{pr}\delta_{st} - \delta_{pt}\delta_{rs}}{2} , \\
&\langle 0|(\bar{q}_{L\,p}q_{R\,r})\,(\bar{q}_{L\,s}q_{R\,t})_{\mathbf{6\times6}}|0\rangle = -\frac{F_0^4}{4}\mathcal{A}_{\mathbf{6\times6}}\frac{\delta_{pr}\delta_{st} + \delta_{pt}\delta_{rs}}{2} ,
\end{aligned}
$$

$$\langle 0|(\bar{q}_{L\,p}t^A q_{R\,r})\,(\bar{q}_{L\,s}t^A q_{R\,t})_{\mathbf{3}\times\mathbf{3}}|0\rangle = -\frac{F_0^4}{4}\bar{\mathcal{A}}_{\mathbf{3}\times\mathbf{3}}\frac{\delta_{pr}\delta_{st}-\delta_{pt}\delta_{rs}}{2}\,,$$
$$\langle 0|(\bar{q}_{L\,p}t^A q_{R\,r})\,(\bar{q}_{L\,s}t^A q_{R\,t})_{\mathbf{6}\times\mathbf{6}}|0\rangle = -\frac{F_0^4}{4}\bar{\mathcal{A}}_{\mathbf{6}\times\mathbf{6}}\frac{\delta_{pr}\delta_{st}+\delta_{pt}\delta_{rs}}{2}\,. \tag{C.12}$$

These relations hold after performing the basis transformation in Eq. (4.9) has been performed. Here B, $\bar{B}$, $\mathcal{A}_i$, and $\bar{\mathcal{A}}_i$ are low-energy constants which appear in the chiral Lagrangian. Comparing with [295, 323] we have,

$$\bar{B} = -\tilde{B}/g_s\,,$$
$$\mathcal{A}_{\mathbf{8}\times\mathbf{8}} = \mathcal{A}_{1\,LR} = -g_4^{\pi\pi}\,,\quad \bar{\mathcal{A}}_{\mathbf{8}\times\mathbf{8}} = \frac{1}{2}\mathcal{A}_{2\,LR} - \frac{1}{2N_c}\mathcal{A}_{1\,LR} = -\left[\frac{1}{2}g_5^{\pi\pi} - \frac{1}{2N_c}g_4^{\pi\pi}\right]\,,$$
$$\mathcal{A}_{\mathbf{6}\times\mathbf{6}} = -g_2^{\pi\pi}\,,\qquad \bar{\mathcal{A}}_{\mathbf{6}\times\mathbf{6}} = -\left[\frac{1}{2}g_3^{\pi\pi} - \frac{1}{2N_c}g_2^{\pi\pi}\right]\,. \tag{C.13}$$

The LECs of these four-quark operators can be determined from matrix elements of the form $\langle(\pi\pi)_{I=0,2}|O_i|K^0\rangle$ which have been computed on the lattice [234, 324, 325]. Using chiral symmetry, the same LECs can be related to matrix elements that play a role in neutrinoless double beta decay [297] or to the bag factors appearing in $K-\bar{K}$ oscillations [298], up to $SU(3)$ corrections [326]. Using the results of Ref. [297] , we have

$$\begin{aligned} g_2^{\pi\pi} &= 2.0(0.2)\text{GeV}^2\,, & g_3^{\pi\pi} &= -0.62(0.06)\text{GeV}^2\,,\\ g_4^{\pi\pi} &= -1.9(0.2)\text{GeV}^2\,, & g_5^{\pi\pi} &= -8.0(0.6)\text{GeV}^2\,, \end{aligned} \tag{C.14}$$

while $\mathcal{A}_{\mathbf{3}\times\mathbf{3}}$ and $\bar{\mathcal{A}}_{\mathbf{3}\times\mathbf{3}}$ have not been computed. They are expected to be $\mathcal{O}(\Lambda_\chi^2)$ by naive dimensional analysis [127, 223] and we use the estimate $\mathcal{A}_{\mathbf{3}\times\mathbf{3}} = \bar{\mathcal{A}}_{\mathbf{3}\times\mathbf{3}} \simeq 1\,\text{GeV}^2$ in numerical evaluations.

C.5 Chiral rotations

Here we give explicit expressions for the rotations discussed in Section 4.2.2. Starting with the vev of the axion, we have $a = \langle a\rangle + a_{\text{ph}}$ with

$$\begin{aligned} \frac{\langle a\rangle}{f_a} = &-\frac{\bar{B}}{B}\langle iL_5 M_0^{-1} + \text{h.c.}\rangle + \frac{F_0^2\mathcal{A}_{\mathbf{8}\times\mathbf{8}}}{2B}\sum_{i>j}\left(\frac{1}{m_i}-\frac{1}{m_j}\right)\mathcal{A}_{\mathbf{8}\times\mathbf{8}}\,\text{Im}\,L_{\mathbf{8}\times\mathbf{8}}^{ijji} + \begin{pmatrix} L_\alpha \to \bar{L}_\alpha \\ \mathcal{A}_\alpha \to \bar{\mathcal{A}}_\alpha \end{pmatrix}\\ &+ \frac{F_0^2}{B}\sum_{i\geq j}(1-\frac{1}{2}\delta_{ij})\left(\frac{1}{m_i}+\frac{1}{m_j}\right)\left(\mathcal{A}_{\mathbf{3}\times\mathbf{3}}\,\text{Im}\,L_{\mathbf{3}\times\mathbf{3}}^{iijj} + \mathcal{A}_{\mathbf{6}\times\mathbf{6}}\,\text{Im}\,L_{\mathbf{6}\times\mathbf{6}}^{iijj}\right)\,. \end{aligned} \tag{C.15}$$

The axion-independent parts of the rotation angles needed to align the vacuum are given by

$$\begin{aligned}
\alpha_3 =& \frac{m_* F_0^2}{2Bm_u m_d m_s}\Bigg\{ \mathcal{A}_{\mathbf{3}\times\mathbf{3}}\mathrm{Im}\left[(m_d-m_u)L^{2211}_{\mathbf{3}\times\mathbf{3}}+(2m_s+m_u)L^{3311}_{\mathbf{3}\times\mathbf{3}}-(2m_s+m_d)L^{3322}_{\mathbf{3}\times\mathbf{3}}\right] \\
&+\mathcal{A}_{\mathbf{6}\times\mathbf{6}}\mathrm{Im}\Big[(2m_s+m_d)L^{1111}_{\mathbf{6}\times\mathbf{6}}-(2m_s+m_u)L^{2222}_{\mathbf{6}\times\mathbf{6}}+(m_u-m_d)L^{3333}_{\mathbf{6}\times\mathbf{6}} \\
&+(m_d-m_u)L^{2211}_{\mathbf{6}\times\mathbf{6}}+(2m_s+m_u)L^{3311}_{\mathbf{6}\times\mathbf{6}}-(2m_s+m_d)L^{3322}_{\mathbf{6}\times\mathbf{6}}\Big] \\
&+\frac{1}{2}\mathcal{A}_{\mathbf{8}\times\mathbf{8}}\mathrm{Im}\Big[(2m_s+2m_u-m_d)L^{3223}_{\mathbf{8}\times\mathbf{8}}-(4m_s+m_d+m_u)L^{2112}_{\mathbf{8}\times\mathbf{8}} \\
&-(2m_s-m_u+2m_d)L^{3113}_{\mathbf{8}\times\mathbf{8}}\Big]+\frac{2\bar{B}}{F_0^2}\mathrm{Im}\Big[(2m_s+m_d)L_5^{11}-(2m_s+m_u)L_5^{22} \\
&+(m_u-m_d)L_5^{33}\Big]\Bigg\}+\dots\,, \\
\alpha_7+i\alpha_6 =& \frac{F_0^2}{B(m_d+m_s)}\Bigg\{\sum_i\Big[\mathcal{A}_{\mathbf{3}\times\mathbf{3}}\left(L^{23ii}_{\mathbf{3}\times\mathbf{3}}-\left(L^{32ii}_{\mathbf{3}\times\mathbf{3}}\right)^*\right)+\mathcal{A}_{\mathbf{6}\times\mathbf{6}}\left(L^{23ii}_{\mathbf{6}\times\mathbf{6}}-\left(L^{32ii}_{\mathbf{6}\times\mathbf{6}}\right)^*\right)\Big] \\
&+\frac{\mathcal{A}_{\mathbf{8}\times\mathbf{8}}}{2}\sum_i\left(L^{2ii3}_{\mathbf{8}\times\mathbf{8}}-\left(L^{3ii2}_{\mathbf{8}\times\mathbf{8}}\right)^*\right)+\frac{2\bar{B}}{F_0^2}\left[L_5^{23}-\left(L_5^{32}\right)^*\right]\Bigg\}+\dots\,, \\
\alpha_8 =& \frac{\sqrt{3}m_* F_0^2}{2Bm_u m_d m_s}\Bigg\{ \mathcal{A}_{\mathbf{3}\times\mathbf{3}}\mathrm{Im}\left[(m_d+m_u)L^{2211}_{\mathbf{3}\times\mathbf{3}}-m_u L^{3311}_{\mathbf{3}\times\mathbf{3}}-m_d L^{3322}_{\mathbf{3}\times\mathbf{3}}\right] \\
&+\mathcal{A}_{\mathbf{6}\times\mathbf{6}}\mathrm{Im}\Big[m_d L^{1111}_{\mathbf{6}\times\mathbf{6}}+m_u L^{2222}_{\mathbf{6}\times\mathbf{6}}-(m_u+m_d)L^{3333}_{\mathbf{6}\times\mathbf{6}} \\
&+(m_d+m_u)L^{2211}_{\mathbf{6}\times\mathbf{6}}-m_u L^{3311}_{\mathbf{6}\times\mathbf{6}}-m_d L^{3322}_{\mathbf{6}\times\mathbf{6}}\Big] \\
&+\frac{1}{2}\mathcal{A}_{\mathbf{8}\times\mathbf{8}}\mathrm{Im}\Big[(m_u-m_d)L^{2112}_{\mathbf{8}\times\mathbf{8}}-(2m_u+m_d)L^{3223}_{\mathbf{8}\times\mathbf{8}}-(2m_d+m_u)L^{3113}_{\mathbf{8}\times\mathbf{8}}\Big] \\
&+\frac{2\bar{B}}{F_0^2}\mathrm{Im}\Big[m_d L_5^{11}+m_u L_5^{22}-(m_u+m_d)L_5^{33}\Big]\Bigg\}+\dots\,,
\end{aligned} \tag{C.16}$$

where the dots stand for analogous terms for the color-octet operators, with $L_\alpha \to \bar{L}_\alpha$, $\mathcal{A}_\alpha \to \bar{\mathcal{A}}_\alpha$, as well as axion-dependent contributions and higher-order terms in $1/\Lambda$. The remaining angles vanish, $\alpha_{1,2,4,5}=0$.

C.6 Meson-meson-axion couplings

As discussed in Section 4.3.4, the hadronic LEFT operators can induce CP-odd interactions between the axions and mesons through the chiral Lagrangian of Eq. (4.14). These interactions can arise both from the terms in Eq. (4.14) involving the LEFT Wilson coefficients, as well as from those involving $\sim \chi$. The former arise after performing the $U(1)_A$ rotation that removes the $aG\tilde{G}$ term from the Lagrangian, while the latter are induced once the α_i rotations, needed for vacuum alignment, have been performed as well. Although the general expressions

are fairly lengthy, the axion-meson interactions can be related to the somewhat simpler contributions to the meson masses. These contributions to the meson masses can be written as,

$$\begin{aligned}\mathcal{L}_m =& F_0^2\Bigg\{(t\cdot\pi)_{ij}(t\cdot\pi)_{kl}\Bigg[\left(\mathcal{A}_{\mathbf{3}\times\mathbf{3}}\frac{L^{jilk}_{\mathbf{3}\times\mathbf{3}}-L^{lijk}_{\mathbf{3}\times\mathbf{3}}}{2}+\mathcal{A}_{\mathbf{6}\times\mathbf{6}}\frac{L^{jilk}_{\mathbf{6}\times\mathbf{6}}+L^{lijk}_{\mathbf{3}\times\mathbf{3}}}{2}+\text{h.c.}\right)\\ &-\mathcal{A}_{\mathbf{8}\times\mathbf{8}}L^{lijk}_{\mathbf{8}\times\mathbf{8}}\Bigg]+(t\cdot\pi\, t\cdot\pi)_{ij}\Bigg[\left(\mathcal{A}_{\mathbf{3}\times\mathbf{3}}\frac{L^{aaji}_{\mathbf{3}\times\mathbf{3}}-L^{jaai}_{\mathbf{3}\times\mathbf{3}}}{2}+\mathcal{A}_{\mathbf{6}\times\mathbf{6}}\frac{L^{aaji}_{\mathbf{6}\times\mathbf{6}}+L^{jaai}_{\mathbf{3}\times\mathbf{3}}}{2}+\text{h.c.}\right)\\ &+\frac{\mathcal{A}_{\mathbf{8}\times\mathbf{8}}}{2}\left(L^{aija}_{\mathbf{8}\times\mathbf{8}}+L^{jaai}_{\mathbf{8}\times\mathbf{8}}\right)+\frac{1}{F_0^2}\left(-B\left(M_q+M_q^\dagger\right)+2\bar{B}\left(L_5+L_5^\dagger\right)\right)_{ji}\Bigg]\Bigg\},\end{aligned} \tag{C.17}$$

with analogous terms for the $\bar{L}_{\mathbf{3}\times\mathbf{3},\mathbf{6}\times\mathbf{6},\mathbf{8}\times\mathbf{8}}$ Wilson coefficients. Using the fact that

$$\pi\cdot t=\frac{1}{\sqrt{2}}\begin{pmatrix}\frac{\pi_3}{\sqrt{2}}+\frac{\pi_8}{\sqrt{6}} & \pi^+ & K^+\\ \pi^- & -\frac{\pi_3}{\sqrt{2}}+\frac{\pi_8}{\sqrt{6}} & K^0\\ K^- & \overline{K}^0 & -2\frac{\pi_8}{\sqrt{6}}\end{pmatrix}, \tag{C.18}$$

the contributions from a specific a given Wilson coefficient can then be read off. These mass terms also allow one to obtain the axion-meson-meson interactions after making the following replacements

$$\begin{aligned}\mathcal{L}_{a\pi^2} &= \frac{m_*}{2}\frac{a}{f_a}\mathcal{L}_m\left(M_q\to\tilde{M}_q\,, L_\alpha\to\tilde{L}_\alpha\right),\\ \left(\tilde{M}_q\right)_{ij} &= i\frac{m_i^2+6m_im_j+m_j^2}{m_im_j(m_i+m_j)}\left[\frac{\bar{B}}{B}L_5^{ij}+\frac{F_0^2\mathcal{A}_{\mathbf{3}\times\mathbf{3}}}{2B}L^{aaij}_{\mathbf{3}\times\mathbf{3}}+\frac{F_0^2\mathcal{A}_{\mathbf{6}\times\mathbf{6}}}{2B}L^{aaij}_{\mathbf{6}\times\mathbf{6}}+\frac{F_0^2\mathcal{A}_{\mathbf{8}\times\mathbf{8}}}{4B}L^{iaaj}_{\mathbf{8}\times\mathbf{8}}\right],\\ \tilde{L}_5^{ij} &= i\left(\frac{1}{m_i}+\frac{1}{m_j}\right)L_5^{ij},\\ \tilde{L}^{ijkl}_{\substack{\mathbf{3}\times\mathbf{3}\\ \mathbf{6}\times\mathbf{6}}} &= i\left(\frac{1}{m_i}+\frac{1}{m_j}+\frac{1}{m_k}+\frac{1}{m_l}\right)L^{ijkl}_{\substack{\mathbf{3}\times\mathbf{3}\\ \mathbf{6}\times\mathbf{6}}},\\ \tilde{L}^{ijkl}_{\mathbf{8}\times\mathbf{8}} &= i\left(\frac{1}{m_i}-\frac{1}{m_j}-\frac{1}{m_k}+\frac{1}{m_l}\right)L^{ijkl}_{\mathbf{8}\times\mathbf{8}}.\end{aligned} \tag{C.19}$$

Note that these replacements do not change the flavor structure, so that the contribution from a specific Wilson coefficient to the $\pi^2 a$ interactions is determined purely from its contribution to the meson masses and $\tilde{M}_q$.

Appendix D

Density matrix formalism

D.1 Kinematics and partial-wave decomposition

We assume the nucleus has A nucleons, which in the initial state have total angular momentum J, spin-projection M onto the z-axis, and isospin-projection M_T, several isospins T may contribute in general. As an example, for ^{3}He one has $A = 3, J = \frac{1}{2}, M_T = \frac{1}{2}$, the dominant contribution comes from $T = \frac{1}{2}$, but isospin breaking introduces small $T = \frac{3}{2}$ contribution to the ^{3}He wave function.

Additionally, we also assume that the scattering happens in the center of mass frame of the nucleus-DM system. We denote the momentum of the incoming (outgoing) nucleon as $-\boldsymbol{k}$ ($-\boldsymbol{k}'$), and the incoming (outgoing) DM will have the opposite momentum. The momentum of incoming DM chosen to lie along the z-axis $\boldsymbol{k} = k\vec{e}_z$, which also the quantization axis for the spin-projections, and we also assume the scattering is happening in x-z plane.The elastic scattering ensures $|\boldsymbol{k}| = |\boldsymbol{k}'|$, and the transfer momentum into nucleus is $\boldsymbol{q}$.

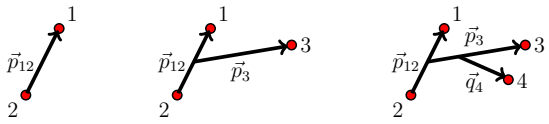

Figure D.1: Jacobi coordinates of the two-, three- and four-nucleon systems. The relative momenta of the constituent nucleon is denoted by $\boldsymbol{p}$ and $\boldsymbol{q}$. This figure is taken from Ref. [101]

.

The most efficient Jacobi momentum coordinate to represent the few-body wave function ($A \geq 4$) are the hierarchical framework shown in Fig. D.1. We always choose the (12) subsystem for the two-body operators and the last nucleon (A^{th}) nucleon for the one-body operators. We label the momentum of the

individual nucleons as $\boldsymbol{k}_1, \boldsymbol{k}_2, \ldots$, which satisfies $\sum_i \boldsymbol{k}_i = -\boldsymbol{k}$ from conservation of momentum.

For one-body densities, we define the momentum of the A^{th} nucleon as,

$$\boldsymbol{p}_A = \frac{A-1}{A}\boldsymbol{k}_A - \frac{1}{A}\sum_{i=1}^{A-1}\boldsymbol{k}_i, \tag{D.1}$$

for ^{3}He (A=3) nucleus,

$$\boldsymbol{p}_3 = \frac{2}{3}\boldsymbol{k}_3 - \frac{1}{3}(\boldsymbol{k}_1 + \boldsymbol{k}_2) = \boldsymbol{k}_3 + \frac{1}{3}\boldsymbol{k}. \tag{D.2}$$

The relative and total pair momenta of the (12) nucleon system is,

$$\boldsymbol{p}_{12} = \frac{1}{2}(\boldsymbol{k}_1 - \boldsymbol{k}_2), \qquad \boldsymbol{k}_{12} = \boldsymbol{k}_1 + \boldsymbol{k}_2. \tag{D.3}$$

We will be focusing on ^{3}He for the remaining discussions. We denote the spin-projection state of ^{3}He as $|M\rangle$, where we suppress the labels of JM_T and bound-state energy. This state is the eigenstate for the nucleus at rest, total angular momentum, and its z-component. We can define the wave function as,

$$\psi_\alpha(p_{12}p_3) = \langle p_{12}p_3\alpha|M\rangle\,, \tag{D.4}$$

where α represent the labels of orbital angular momentum (l) and spin (s) (combined to give j), and isospin quantum numbers (t) of our Jacobi-momentum basis,

$$|\alpha\rangle = |[(l_{12}s_{12})j_{12}(l_3s_3)j_3]JM, (t_{12}t_3)TM_T\rangle\,. \tag{D.5}$$

The labels of outgoing particles are primed. The states $|M\rangle$ must be multiplied by an eigenstate of the nuclear cm momentum operator to conserve the momentum. In the non-relativistic case, this will result in the $\delta^{(3)}(\boldsymbol{k}-\boldsymbol{k}'-\boldsymbol{q})$. These momentum delta functions are not included in the following calculations for convenience.

D.2 One-body density

The relevant matrix element for one-body operator is,

$$\begin{aligned}&\langle \boldsymbol{k}'_3|\,\langle l'_3 m_3^{l\prime}|\,\langle s'_3 m_3^{s\prime}|\,\langle t'_3 m_3^{t\prime}|\,\hat{O}_3(\boldsymbol{k},\boldsymbol{q})\,|t_3 m_3^t\rangle\,|s_3 m_3^s\rangle\,|l_3 m_3^l\rangle\,|\boldsymbol{k}_3\rangle \\ &= \delta_{m_3^{t\prime},m_3^t}\delta^{(3)}(\boldsymbol{k}'_3 - \boldsymbol{k}_3 - \boldsymbol{q})O_3(m_3^{s'} m_3^s m_3^t; \boldsymbol{k}_3; \boldsymbol{k}, \boldsymbol{q}).\end{aligned} \tag{D.6}$$

Here m^t is conserved because the DM interaction does not change the charge of the struck nucleon. Now we do a multipole expansion of the $\boldsymbol{k}_3$ dependence of

the spin-isospin matrix elements in spherical coordinates up to the multipolarity $K_{\max}$,

$$O_3(m_3^{s\prime}m_3^s m_3^t;\boldsymbol{k}_3;\boldsymbol{k},\boldsymbol{q}) \equiv \sum_{K=0}^{K_{\max}}\sum_{\kappa=-K}^{K}\sqrt{\frac{4\pi}{2K+1}}(k_3)^K Y_{K\kappa}(\hat{k}_3)\tilde{O}_3(m_3^{s\prime}m_3^s m_3^t;K\kappa;\boldsymbol{k},\boldsymbol{q}), \tag{D.7}$$

where $\hat{k}_3$ is the unit vector of $\boldsymbol{k}_3$.

Now let us look at matrix element of $\hat{O}_3$ that we want to calculate

$$\begin{aligned}\langle M'|\,\hat{O}_3(\boldsymbol{k},\boldsymbol{q})\,|M\rangle = &\sum_{\alpha\alpha'}\int \mathrm{d}p_{12}\; p_{12}^2\;\mathrm{d}p_3\; p_3^2\;\mathrm{d}p'_{12}\; p'^2_{12}\;\mathrm{d}p'_3\; p'^2_3\;\psi^\dagger_{\alpha'}(p'_{12}p'_3)\psi_\alpha(p_{12}p_3)\\ &\times\langle p'_{12}p'_3,[l'_{12}s'_{12}]j'_{12}(l'_3s'_3)j'_3]J'M',(t'_{12}t'_3)T'M'_T|\,\hat{O}_3(\boldsymbol{k},\boldsymbol{q})\\ &\quad|p_{12}p_3,[l_{12}s_{12}]j_{12}(l_3)j_3]JM,(t_{12}t_3)TM_T\rangle\,.\end{aligned} \tag{D.8}$$

Using Clebsch-Gordan coefficients $\langle j_1\,m_1,j_2\,m_2|j\,m\rangle$ we can explicitly decompose α so as to separate the spin-isospin quantum numbers of the pair from those of the third nucleon:

$$\langle M'|\,\hat{O}_3(\boldsymbol{k},\boldsymbol{q})\,|M\rangle = \tag{D.9}$$

$$\begin{aligned}&\sum_{\alpha\alpha'}\int \mathrm{d}p_{12}\; p_{12}^2\;\mathrm{d}p_3\; p_3^2\;\mathrm{d}p'_{12}\; p'^2_{12}\;\mathrm{d}p'_3\; p'^2_3\;\psi^\dagger_{\alpha'}(p'_{12}p'_3)\psi_\alpha(p_{12}p_3)\\ &\times\sum_{m'_3}\langle j'_{12}\,(M'-m'_3),j'_3\,m'_3|J'\,M'\rangle\sum_{m_3^{t\prime}}\langle t'_{12}\,(M'_T-m_3^{t\prime}),t'_3\,m_3^{t\prime}|T'\,M'_T\rangle\\ &\times\sum_{m_3}\langle j_{12}\,(M-m_3),j_3\,m_3|J\,M\rangle\sum_{m_3^t}\langle t_{12}\,(M_T-m_3^t),t_3\,m_3^t|T\,M_T\rangle\\ &\times\langle p'_{12},(l'_{12}s'_{12})j'_{12}(M'-m'_3),t'_{12}(M'_T-m_3^{t\prime})|p_{12},(l_{12}s_{12})j_{12}(M-m_3),t_{12}(M_T-m_3^t)\rangle\\ &\times\langle p'_3,(l'_3s'_3)j'_3m'_3,t'_3m_3^{t\prime}|\hat{O}_3(\boldsymbol{k},\boldsymbol{q})|p_3,(l_3)j_3m_3,t_3m_3^t\rangle\end{aligned} \tag{D.10}$$

Here we used identities from the spin projections: $M = m_3 + m_{12}, M_T = m_3^t + m_{12}^t, \ldots$. Now we expand the last term in the above equation using Eq. (D.6), the momentum conserving delta function can be rewritten using Eq. (D.2) as

$$\delta^{(3)}(\boldsymbol{k}'_3-\boldsymbol{k}_3-\boldsymbol{q}) = \delta^{(3)}(\boldsymbol{p}'_3-\boldsymbol{p}_3-\frac{2}{3}\boldsymbol{q}) \tag{D.11}$$

We further expand the last line of Eq. (D.10) by inserting the solid angles $\hat{p}_3, \hat{p}'_3$ of the third particles' momentum. Then we use the result in Eq. (D.7), and perform the integrations and summations corresponding to the appropriate delta functions to arrive at the final form

$$\begin{aligned}&\langle M'|\,\hat{O}_3(\boldsymbol{k},\boldsymbol{q})\,|M\rangle\\ &=\sum_{K=0}^{K_{\max}}\sum_{\kappa=-K}^{K}\sum_{\substack{m_3^{s\prime}m_3^s\\ m_3^t}}\tilde{O}_3(m_3^{s\prime}m_3^s m_3^t;K\kappa;\boldsymbol{k},\boldsymbol{q})\rho^{K\kappa;m_3^tM_T,M'M}_{m_3^{s\prime}m_3^s}(\boldsymbol{k},\boldsymbol{q})\end{aligned} \tag{D.12}$$

where we define the one-body (transition) density by summing over those quantum numbers that are not involved in the interaction:

$$
\begin{aligned}
&\rho^{K\kappa;m_3^t M_T,M'M}_{m_3^{s\prime}m_3^s}(\boldsymbol{k},\boldsymbol{q}) \\
&:= \sum_{\alpha}\int \mathrm{d}p_{12}p_{12}^2\int \mathrm{d}p_3 p_3^2 \sum_{\alpha'}\ \delta_{l'_{12}l_{12}}\,\delta_{s'_{12}s_{12}}\,\delta_{j'_{12}j_{12}}\,\delta_{t'_{12}t_{12}}\,\delta_{M'_T M_T} \\
&\times \sum_{m_3}\langle j_{12}\,(M-m_3), j'_3\,(M'-M+m_3)|J'\,M'\rangle\,\langle t'_{12}\,(M'_T-m_3^{t\prime}), t'_3\,m_3^{t\prime}|T'\,M'_T\rangle \\
&\times \langle j_{12}\,(M-m_3), j_3\,m_3|J\,M\rangle\,\langle t_{12}\,(M_T-m_3^t), t_3\,m_3^t|T\,M_T\rangle \\
&\times \langle l'_3\,(M'-M+m_3-m_3^{s\prime}), s'_3\,m_3^{s\prime}|j'_3\,(M'-M+m_3)\rangle\,\langle l_3\,(m_3-m_3^s), s_3\,m_3^s|j_3\,m_3\rangle \\
&\times \int \mathrm{d}\hat{p}_3 Y^{\dagger}_{l'_3(M'-M+m_3-m_3^{s\prime})}(\widehat{\boldsymbol{p}_3+\tfrac{2}{3}\boldsymbol{q}})Y_{l'_3(m_3-m_3^s)}(\hat{\boldsymbol{p}}_3) \\
&\times \sum_{K=0}^{K_{\max}}\sum_{\kappa=-K}^{K}\sqrt{\frac{4\pi}{2K+1}}(k_3)^K Y_{K\kappa}(\hat{k}_3)\psi^{\dagger}_{\alpha'}(p_{12}|\boldsymbol{p}_3+\tfrac{2}{3}\boldsymbol{q}|)\psi_{\alpha}(p_{12}p_3).
\end{aligned}
\tag{D.13}
$$

D.3 Two-body density

Now we will focus on the two-nucleon currents where DM interacts with the nucleon pair (12). The relevant matrix operator is given by,

$$
\begin{aligned}
&\langle \boldsymbol{p}'_{12}\boldsymbol{k}'_{12}|\,\langle s'_{12}m_{12}^{s\prime}|\,\langle t'_{12}m_{12}^{t\prime}|\,\hat{O}_{12}(\boldsymbol{k},\boldsymbol{q})\,|t_{12}m_{12}^t\rangle\,|s_{12}m_{12}^s\rangle\,|\boldsymbol{p}_{12}\boldsymbol{k}_{12}\rangle \\
&= \delta^{(3)}(\boldsymbol{k}'_{12}-\boldsymbol{k}_{12}-\boldsymbol{q})\delta_{m_{12}^{t\prime}m_{12}^t}O_{12}(s'_{12}t'_{12}m_{12}^{s\prime}s_{12}t_{12}m_{12}^t;\boldsymbol{p}'_{12},\boldsymbol{p}_{12};\boldsymbol{q}).
\end{aligned}
\tag{D.14}
$$

The two-nucleon operator is usually represented in terms of partial-wave states, which can be written as,

$$
\begin{aligned}
&\langle \alpha'_{12}\boldsymbol{p}'_{12}\boldsymbol{k}'_{12}|\hat{O}_{12}|\alpha_{12}\boldsymbol{p}_{12}\boldsymbol{k}_{12}\rangle = \delta_{m_{12}^{t\prime}m_{12}^t}\delta^{(3)}(\boldsymbol{k}'_{12}-\boldsymbol{k}_{12}-\boldsymbol{q}) \\
&\times \sum_{m_{12}^{s\prime}m_{12}^s}\langle l_{12}\,(m_{12}-m_{12}^s), s_{12}\,m_{12}^s|j_{12}\,m_{12}\rangle\,\langle l'_{12}\,(m'_{12}-m_{12}^{s\prime}), s'_{12}\,m_{12}^{s\prime}|j'_{12}\,m'_{12}\rangle \\
&\times \int \mathrm{d}\hat{p}'_{12}\mathrm{d}\hat{p}_{12}Y^{\dagger}_{l'_{12}(m'_{12}-m_{12}^{s\prime})}(\hat{p}'_{12})Y_{l_{12}(m_{12}-m_{12}^s)}(\hat{p}_{12}) \\
&\times O_{12}(s'_{12}t'_{12}m_{12}^{s\prime}s_{12}t_{12}m_{12}^s m_{12}^t;\boldsymbol{p}'_{12},\boldsymbol{p}_{12};\boldsymbol{k}\boldsymbol{q}) \\
&\equiv \delta_{m_{12}^{t\prime}m_{12}^t}\delta^{(3)}(\boldsymbol{k}'_{12}-\boldsymbol{k}_{12}-\boldsymbol{q})O_{12}^{\alpha'_{12}\alpha_{12}}(p'_{12},p_{12}).
\end{aligned}
\tag{D.15}
$$

Using Eq. (D.2) and Eq. (D.3) along with $\sum_i \boldsymbol{k}_i = -\boldsymbol{k}$, we can rewrite the delta function as,

$$
\delta^{(3)}(\boldsymbol{k}'_{12}-\boldsymbol{k}_{12}-\boldsymbol{q}) = \delta^{(3)}(\boldsymbol{p}_3-\boldsymbol{p}'_3-\frac{1}{3}\boldsymbol{q}),
\tag{D.16}
$$

we can use this delta function to integrate $\boldsymbol{p}_3$ while calculating the matrix element. Now we can write the two-body matrix element following the same procedure as

one-body matrix element and we get the factorization,

$$\langle M'|\,\hat{O}_{12}(\boldsymbol{q})\,|M\rangle \equiv \sum_{\alpha'_{12}\alpha_{12}} \int \mathrm{d}p_{12}p_{12}^2\mathrm{d}p'_{12}\mathrm{d}p_{12}^{'2} O_{12}^{\alpha'_{12}\alpha_{12}}(p'_{12},p_{12})\rho_{\alpha'_{12}\alpha_{12}}^{M_T,M',M}(p'_{12},p_{12};\boldsymbol{q}) \tag{D.17}$$

where we define the two-body (transition) density as:

$$\begin{aligned}
&\rho_{\alpha'_{12}\alpha_{12}}^{M_T,M',M} \\
&= \sum_{\alpha'(\alpha'_{12})\alpha(\alpha_{12})} \langle j_{12}\, m_{12}, j_3\,(M-m_{12})|J\,M\rangle\,\langle j'_{12}\, m'_{12}, j'_3\,(M'-m'_{12})|J'\,M'\rangle \\
&\times \langle t_{12}\, m^t_{12}, t_3\,(M_T-m^t_{12})|T\,M_T\rangle\,\langle t'_{12}\, m^t_{12}, t'_3\,(M_T-m^t_{12})|T'\,M'_T\rangle \\
&\times \int \mathrm{d}p'_3 p_3^{'2} \int \mathrm{d}\hat{p}'_3 \psi^\dagger_{\alpha'}(p'_{12}p'_3)\psi_\alpha(p_{12}|\boldsymbol{p}_3+\tfrac{1}{3}\boldsymbol{q}|) \\
&\times \sum_{m^s_3} Y^\dagger_{l'_3(M'-m'_{12}-m^s_3)}(\hat{p}'_3) Y_{l_3(M-m_{12}-m^s_3)}(\widehat{\boldsymbol{p}_3+\tfrac{1}{3}\boldsymbol{q}}) \\
&\times \langle l_3\,(M-m_{12}-m^s_3), s_3\, m^s_3|j_3\,(M-m_{12})\rangle\,\langle l'_3\,(M'-m'_{12}-m^s_3), s_3\, m^s_3|j'_3\,(M'-m'_{12})\rangle\,.
\end{aligned} \tag{D.18}$$

Summary

In this thesis, we have traveled a few new paths in search of the true nature of the Universe. However, unless you are already deep in the broad highway of high-energy physics, it isn't easy to follow all the details. This summary provides an easy-to-understand version of the reasons for the paths I chose and the results I discovered during my journey during my Ph.D.

Particle Physics

Particle physics is one of the current frontiers in the journey undertaken to fulfill human curiosity in finding the fundamental nature of our Universe. We took the first step in this endeavor around 3000 BCE when ancient civilizations got mesmerized by the night sky. These civilizations had a basic knowledge of the Moon, Sun and other stars. They both marveled at these heavenly bodies, and their desire to understand these heavenly bodies led to the branch of Astronomy. Human curiosity to understand the world we live in led to the independent development of science around the globe. By 13^{th} century, scientists started to gather at universities to share their observations and findings. By the 17^{th} century, this developed into modern science and the scientific method: make observations, analyze them, formulate a mathematical theory to explain the observations, and predict future observations. If the predictions fail, repeat the process by accounting for the failure. We can broadly separate two branches of modern physics: *theory* and *experiments*. Theorists often come up with new ideas and theories and various ways to test them. Experimentalists test these ideas/theories in the lab and provide evidence to support or disprove the theoretical models. If they support the theory, then theorists make more predictions to test at the lab, and if the theory is successful in all these tests, then we are one step closer to unraveling the true nature of the Universe. If the experiments disprove the theory, then theorists work on a new model with the added knowledge of the previous model's failure to develop a better theoretical model. This interplay between these two branches is key in advancing this far in our quest to understand the true nature of the Universe. This thesis falls into the theory category and combines various experimental results to arrive at the results.

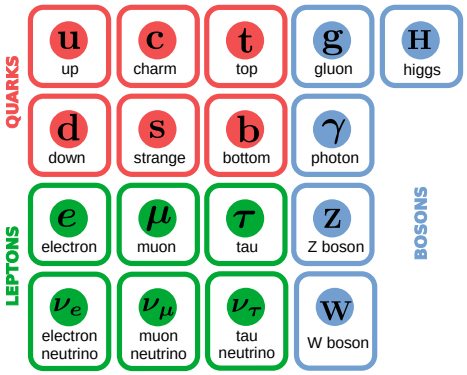

Figure 2: The constituents of Standard Model of particle physics. The gluons, W and Z bosons, and photons mediate the strong, weak, and electromagnetic interactions. The Higgs boson gives mass to the elementary particles.

Another approach to learning about the Universe is by figuring out the fundamental building blocks of matter. We believed atoms were the fundamental particles. However, more precise measurements indicated that atoms are made up of a positively charged nucleus, which, in turn, is made up of protons and neutrons and surrounded by a cloud of electrons. Moreover, *common sense* did not seem to work at this length/energy scale and led to the invention of quantum mechanics. By colliding atoms at higher energies, we were able to *see* smaller length scales (or higher energy scales) and found hundreds of particles called hadrons. It turned out that these particles themselves are made up of more fundamental particles called quarks. For example, protons and neutrons are members of baryons, which are hadrons composed of three quarks. Particle physics is the branch of physics that studies the nature of all these subatomic particles. By analyzing various subatomic phenomena, we came up with the Standard Model (SM) of particle physics. The constituents of the SM are given in Fig. 2. The Standard Model successfully explains the electromagnetic, weak and strong interactions, and essentially all subatomic phenomena to a high degree of accuracy.

Beyond the Standard Model

We now know that SM is not the final destination in our search for the fundamental building blocks of nature. It fails to explain gravity, which is best described by Einstein's general theory of relativity. It also fails to explain the matter-antimatter asymmetry, the nature of dark matter, and the masses of the neutrinos. All this indicates the existence of new physics that lies beyond the Standard Model (BSM). Antimatter is similar to matter but with opposite charge. When matter and antimatter particles interact, they destroy one another, releas-

ing a significant quantity of energy. The bulk of the Universe's mass is made up of dark matter, a mystery element. It makes up around 85% of the Universe's total matter, whereas regular matter, like stars and planets, only accounts for 15%. Dark matter is not visible to telescopes and other devices because it does not emit, absorb, or reflect any light or other types of electromagnetic radiation, unlike regular matter that humans can see and interact with, such as stars and galaxies.

There are two main approaches on the theoretical front to address BSM physics. These are the *model-dependent* approach and *model-independent* approach. In the model-dependent approach, we start with a theoretical model with a handful of parameters (or constants). For example, Newton's law of gravitation has the parameter G, the gravitational constant. This approach has the benefit of making predictions and providing a unique signature that can be tested in experiments. However, the primary limitations come from the assumptions of the model, which can be wrong and thereby overlook the underlying physics. A successful example of this approach is Kepler's laws, verified by the experimental data.

On the other hand, the model-independent approach focuses on directly measuring and analyzing experimental data and extracts the underlying physics. The main advantage is that any biased assumptions do not limit this approach, and the comprehensive view of the data could lead to a comprehensive understanding of the new physics. However, this approach needs a large set of parameters, which makes interpreting data difficult and slows down progress. Therefore, this method is best used when the underlying physics is poorly understood. An example of this approach is using the observations of galaxy rotations and their velocities to determine the mass of the galaxy without relying on any specific model. In this thesis, I adopt the model-independent approach to study dark matter, and a proposed BSM particle called the axion.

Quantum field theories (QFTs) form an important tool in the manufacturing process of fundamental theories. From a theoretical point of view, particles are the quantum excitation of the quantum fields. This makes quantum fields more fundamental than particles. A key feature of all fundamental theories are they are constrained by a set of local and global symmetries. These symmetries manifest in nature as conservation laws. For example, the conservation of electric charge is the consequence of local symmetry. The main obstacle in making BSM models is that we do not yet know the new physics's symmetries or conservation laws. If CP was a good symmetry of nature, then there would have been an equal number of matter and antimatter particles. Similar to having an equal number of positively and negatively charged particles, making the electric charge a conserved quantity. However, nature chooses to prefer matter over antimatter. This matter-antimatter asymmetry implies that the CP symmetry is violated in theory. The CP symmetry is the combination of charge conjugation (C) and parity (P) symmetry. If the former is true, then nature would not get affected if we replace particles with their antiparticles. If the latter is true, then nature has the same preference for physical processes and their mirror image processes.

The *CP* symmetry states that the physical laws should remain unchanged if a particle's charge is reversed and its spatial coordinates are inverted (i.e. left becomes right and vice versa). It means that if we swap the positions of all particles with the opposite charge and the opposite handedness, everything will look the same as before. If it is still hard to visualize, consider a toy with blue color on one side and red color on the other side. If you flip the top over, it *looks* the same to nature given *CP* is a good symmetry.

Even though SM contains *CP* violation, it can not account for all the observed matter-antimatter asymmetry. This is clear evidence that new physics has *CP* violating sources. The only source of *CP* violation in the strong sector of SM is the $\bar{\theta}$ term. The experimental evidence indicates that the strength of this term is 10^{10} times smaller than we expected. Even though nothing is wrong with this, it could be a consequence of BSM physics that we are yet to discover. This is called the strong *CP* problem. A popular solution to this problem is the existence of a BSM particle called the axion, even though we have yet to obtain any direct evidence. In this thesis, I investigate the effects of *CP* violating BSM sources on nuclear forces and axions.

Effective field theories

Do we need to know what happens at the fundamental level to describe the physical phenomena around us? The answer is not really. However, the microscopic effects do have macroscopic consequences. For example, the energy of water molecules determines whether the water exists in a solid, liquid, or gaseous state. Once we determine the macroscopic laws based on the macroscopic observations, we no longer need to care about the microscopic laws. This is because of a feature of nature called *decoupling*. It states that physics at a given energy (length) scale has almost no influence over physics at a different energy (length) scale. This is why engineers do not consider atomic theory or particle physics when designing and constructing bridges and houses. Effective field theories (EFTs) are based on this feature of nature.

The search for BSM physics happens in mainly three frontiers. The first one is the high energy frontier, where we collide protons/neutrons traveling almost at the speed of light. Next, the high-precision frontier includes high-precision atomic and nuclear experiments, and finally, the cosmological and astrophysical frontier covers galaxies and the aftereffects of the big bang. It became inconvenient to use a theory tailor-made in one energy scale to describe the phenomena happening at a wide range of energies. For example, chemists do not need to know about the existence of quarks for their work.

EFTs are powerful theoretical tools to describe phenomena at a given energy scale in a model-independent way. We choose an energy scale and a problem we want to study, then follow the general recipe to make the EFT. This recipe is outlined with an example in Chapter 2. The trade-off for model independence is

that we have to deal with many constants, called low energy constants (LECs), which must be determined from the data. However, EFTs come with a built-in mechanism to handle this. This mechanism comprises expansion parameters and a power counting rule. We can think of an EFT calculation similar to a power series expansion for easier visualization. Consider $e^x = 1 + x + \frac{x^2}{2!} + \frac{x^3}{3!} + \mathcal{O}(x^4)$, in this context x is analogous to the expansion parameter, $\frac{1}{n!}$ corresponds to the LECs. Power counting rules determine how many operators come in $\mathcal{O}(x^n)$. The results are commonly denoted as the leading order (LO), next-to-the-leading order (NLO), next-to-the-next-to-the leading order ($\mathrm{N^2LO}$), and so on as we go higher in the power of expansion parameters and thereby higher in accuracy.

In this thesis, I chose high-precision frontier experiments involving nucleons, atoms, or light particles like pions (pions are members of mesons, which are hadrons composed of one quark and one anti-quark). Since nucleons originate from the strong interaction of quarks, I used an EFT based on quantum chromo dynamics (QCD), which describes the strong interaction, commonly known as chiral perturbation theory (χPT). χPT is based on the chiral symmetry of the QCD, which states that the laws of physics are the same for objects that are mirror images of each other, but the objects themselves cannot be superimposed onto each other. For example, consider left and right gloves. Both are mirror images of each other but cannot be worn in the wrong hand. In QCD, this symmetry is violated by the masses of quarks. However, chiral symmetry is a good approximation for light quarks, and χPT can describe the interactions of particles composed of light quarks to a good approximation. χPT provides a systematic, low-energy approximation to the underlying theory (QCD) that describes the interactions of subatomic particles like nucleons and pions.

Results

In Chapter 3, we investigated the renormalization of the *CP*-violating nuclear force using χPT. In QFT, we consider particles as point-like objects, leading to infinities in the calculation. Regularization is a mathematical procedure used to remove these infinities by introducing a cut-off, which regulates the behavior of infinite quantities. This makes the observables finite values, and this arbitrary cut-off is removed in the final step of the calculation. This process is called renormalization. Renormalization is a necessary condition for all QFTs describing physical phenomena. In an EFT, renormalization is achieved in every order in the expansion parameter. If the theory is renormalized and the regulator is above the relevant energy scale, then the observables should be regulator independent.

Our results revealed that the *CP*-violating observable ϵ^0_{SP} displays an oscillatory behavior and even changes sign as a function of regulator, thereby confirming that *CP*-violating nuclear force is not properly renormalized. This indicates a missing contact term (or counter term) at the LO to absorb the infinities. Since the power counting rule of an EFT determines the terms for any given order,

our results point to the failure of the power counting rule. Therefore, we *fixed* the power counting rule by promoting a higher order contact term to the LO. We confirmed that this added term restores the regulator independence of $\epsilon^0_{\rm SP}$. However, given the absence of experimental data, there is no direct way to obtain the low energy constant (LEC) associated with this counter term. Therefore, we proposed a novel solution to calculate the LEC indirectly. Our results will impact the current calculations of electric dipole moment (EDM) and other searches for *CP*-violating BSM physics, which neglect this LO term. We plan to expand on this project by calculating ^{3}He EDM with the counter term and checking its cut-off dependence.

In Chapter 4, we studied the *CP*-violating axion interaction in effective field theory. We start with the most general *CP*-violating sources in the low energy effective field theory framework (LEFT) up to two orders in expansion parameter. This popular EFT in particle physics describes physics below the electroweak symmetry-breaking scale. Then we used χPT to calculate *CP*-violating axion-baryons, -mesons, and -leptons interactions. For easier interpretation of experimental results, we narrowed our focus to *CP*-violating interaction between axion and nucleons, pions, and electrons. Next, we studied a wide range of experiments searching for *CP*-violating axion interactions and summarized the constraints imposed by these experiments on the *CP*-violating BSM parameters. The EDM experiments set the most stringent constraints, and the projected Axion Resonant InterAction Detection Experiment could compete with EDM experiments in a limited range of parameter space. Finally, we translated our EFT results to a few BSM models, such as leptoquarks and the left-right symmetric model.

In the future, we plan to use our results to study the flavor violating *CP*-violating processes like kaon to pion decay, muon to electron conversions, and so on. Since axions satisfy the criteria for a dark matter (DM) candidate, we plan to study the implications of our results for DM axion. We found that the *CP*-violating interactions of DM axion lead to time-varying oscillations in the fine structure constant and the masses of nucleons and electrons. The oscillation of the fine structure constant leads to oscillations of energy levels of atoms, which can be searched in atomic clock experiments. The DM axion-photon can induce a time-varying potential for ions in ion-trap experiments, providing a novel addition to axion searches.

In Chapter 5, we studied the dark matter scattering off ^{4}He through scalar interactions. Scalar interactions are interesting because it does not depend on the spin of the nuclei and scales as the number of nucleons in the nuclei. We focused on ^{4}He because of the proposed ^{4}He DM detectors and ^{4}He have binding energy comparable to heavier isotopes used in other DM detectors. We started with a scalar DM-quark and -gluon interactions and translated it to scalar DM-nucleon and -pion interactions using χPT. We calculated DM-nucleon scattering amplitudes for ^{2}H, ^{3}He, and ^{4}He nuclei up to NLO. The NLO contributions can be divided into two parts: the radius (or one-body) correction, which involves scattering with one nucleon, and two-body corrections, which involves scattering

with two nucleons. We included up to N^5LO nuclear wave functions to check the convergence of our results with increasing order in the wave function. We found that the NLO contributions only change the LO results by a few percent. The most interesting results were the NLO two-body corrections displayed a significant cut-off dependence. We strongly suspect this points to the failure of the power counting rule at the NLO level. The linear correlation between two-body currents and the D-wave probability of the wave functions provides further evidence for this hypothesis since D-wave probability is not a physical observable. We suspect that promoting a higher-order contact term to NLO could restore the renormalization. However, further studies are required to confirm this hypothesis. We plan to study spin-dependent DM-nuclei scattering in the future.

Nederlandse samenvatting

In dit proefschrift hebben we een aantal nieuwe wegen bewandeld op zoek naar de ware aard van het heelal. Tenzij je al diep in de brede snelweg van hogeenergiefysica zit, is het niet eenvoudig om alle details te volgen. Deze samenvatting is een gemakkelijk te begrijpen versie van de redenen voor de paden die ik heb gekozen en de resultaten die ik ontdekte tijdens mijn reis tijdens mijn Ph.D.

Deeltjesfysica

Deeltjesfysica is een van de huidige grenzen in de reis die wordt ondernomen om de menselijke nieuwsgierigheid naar het vinden van de fundamentele aard van ons universum te bevredigen. Men zette de eerste stap in dit streven rond 3000 v.Chr. toen oude beschavingen betoverd raakten door de nachtelijke hemel. Deze beschavingen hadden een basiskennis van de maan, de zon en andere sterren. Ze verwonderden zich beiden over deze hemellichamen en hun verlangen om deze hemellichamen te begrijpen, leidde tot de wetenschap van de astronomie. Menselijke nieuwsgierigheid om de wereld waarin we leven te begrijpen, heeft geleid tot de onafhankelijke ontwikkeling van wetenschap over de hele wereld. Rond de 13^{e} eeuw kwamen wetenschappers bijeen op universiteiten om hun observaties en bevindingen te delen. Tegen de 17^{e} eeuw ontwikkelde dit zich tot moderne wetenschap en de wetenschappelijke methode: voer waarnemingen uit, analyseer ze, formuleer een wiskundige theorie om de waarnemingen te verklaren en voorspel toekomstige waarnemingen. Als de voorspellingen mislukken, herhaalt u het proces door rekening te houden met de mislukking. We kunnen grofweg twee takken van de moderne natuurkunde scheiden: *theorie* en *experimenten*. Theoretici bedenken vaak nieuwe ideeën en theorieën en verschillende manieren om ze te testen. Experimentalisten testen deze ideeën/theorieën in het laboratorium en leveren bewijs om de theoretische modellen te ondersteunen of te weerleggen. Als ze de theorie ondersteunen, doen theoretici meer voorspellingen om in het lab te testen, en als de theorie in al deze tests slaagt, zijn we een stap dichter bij het ontrafelen van de ware aard van het heelal. Als de experimenten de theorie weerleggen, werken theoretici aan een nieuw model met de toegevoegde kennis van het falen van het vorige model om een beter theoretisch model te ontwikkelen. Dit

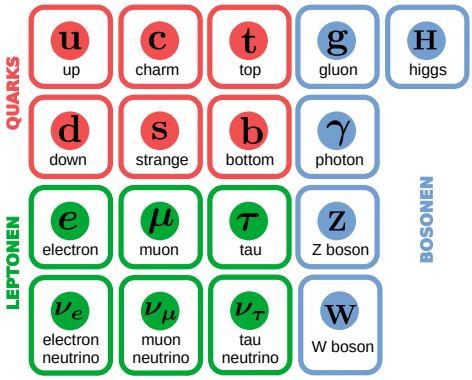

Figure 3: De bestanddelen van het Standaard Model van deeltjesfysica. De gluonen, W en Z bosonen en fotonen bemiddelen de sterke, zwakke en elektromagnetische interacties. Het Higgs-deeltje geeft massa aan de elementaire deeltjes.

samenspel tussen deze twee wetenschappelijke takken is de sleutel om zo ver te komen in onze zoektocht om de ware aard van het universum te begrijpen. Dit proefschrift valt in de categorie theorie en combineert verschillende experimentele resultaten om tot de resultaten te komen.

Een andere benadering om meer te weten te komen over het heelal, is door de fundamentele bouwstenen van de materie nader te onderzoeken. Men geloofde dat atomen de fundamentele deeltjes waren. Nauwkeurigere metingen gaven echter aan dat atomen zijn opgebouwd uit een positief geladen kern, die op zijn beurt is opgebouwd uit protonen en neutronen en is omgeven door een wolk van elektronen. Bovendien leek *gezond verstand* niet te werken op deze lengte-/energieschaal en leidde dit tot de uitvinding van de kwantummechanica. Door atomen met hogere energieën te laten botsen, konden we kleinere lengteschalen (of hogere energieschalen) *zien* en vonden we honderden deeltjes die hadronen worden genoemd. Het bleek dat deze deeltjes zelf zijn opgebouwd uit meer fundamentele deeltjes die quarks worden genoemd. Protonen en neutronen zijn bijvoorbeeld leden van baryonen, dit zijn hadronen die zijn samengesteld uit drie quarks. Deeltjesfysica is de tak van de natuurkunde die de aard van al deze subatomaire deeltjes bestudeert. Door verschillende subatomaire fenomenen te analyseren, kwamen we tot het Standaard Model (SM) van de deeltjesfysica. De bestanddelen van het SM worden gegeven in Fig. 3. Het standaardmodel verklaart met succes de elektromagnetische, zwakke en sterke interacties, en in wezen alle subatomaire verschijnselen met een hoge mate van nauwkeurigheid.

Voorbij het standaardmodel

We weten nu dat het SM niet de eindbestemming is in onze zoektocht naar de fundamentele bouwstenen van de natuur. Het verklaart de zwaartekracht niet, die het best beschreven kan worden door de algemene relativiteitstheorie van Einstein. Het kan ook de asymmetrie tussen materie en antimaterie, de aard van donkere materie en de massa's van de neutrino's niet verklaren. Dit alles duidt op het bestaan van nieuwe fysica die buiten het Standaard Model (BSM) ligt. Antimaterie lijkt op materie, maar heeft een tegenovergestelde lading. Wanneer materie en antimaterie met elkaar in aanraking komen, vernietigen ze elkaar, waarbij een significante hoeveelheid energie vrijkomt. Het merendeel van de massa in het universum bestaat uit donkere materie, een geheimzinnig onderdeel. Het is verantwoordelijk voor 85% van alle materie in het universum, terwijl normale materie, zoals sterren en planeten, slechts voor 15% bijdragen. Donkere materie is niet zichtbaar voor telescopen en andere meetapparatuur, omdat het geen licht, of enkele andere vorm van elektromagnetische straling, uitzendt, absorbeert of reflecteert. Dit geldt niet voor normale materie die mensen wel kunnen waarnemen, zoals de sterren en sterrenstelsels.

Er zijn twee hoofdbenaderingen op het theoretische front om BSM-fysica aan te pakken. Dit zijn de *modelafhankelijke* benadering en *modelonafhankelijke* benadering. Bij de modelafhankelijke benadering vertrekken we van een theoretisch model met een handvol parameters (of constanten). De zwaartekrachtwet van Newton heeft bijvoorbeeld de parameter G, de zwaartekrachtconstante. Deze benadering heeft het voordeel dat er voorspellingen worden gedaan en dat er een unieke signatuur ontstaat die in experimenten kan worden getest. De primaire beperkingen komen echter voort uit de aannames van het model, die verkeerd kunnen zijn en daardoor de onderliggende fysica over het hoofd zien. Een succesvol voorbeeld van deze benadering zijn de wetten van Kepler, geverifieerd door de experimentele gegevens.

Aan de andere kant richt de modelonafhankelijke benadering zich op het direct meten en analyseren van experimentele gegevens en extraheert de onderliggende fysica. Het belangrijkste voordeel is dat vooringenomen aannames deze benadering niet beperken, en het uitgebreide overzicht van de gegevens kan leiden tot een alomvattend begrip van de nieuwe fysica. Deze aanpak vereist echter een groot aantal parameters, wat het interpreteren van gegevens bemoeilijkt en de voortgang vertraagt. Daarom kan deze methode het beste worden gebruikt wanneer de onderliggende fysica slecht wordt begrepen. Een voorbeeld van deze benadering is het gebruik van de waarnemingen van de rotaties van sterrenstelsels en hun snelheden om de massa van de melkweg te bepalen zonder te vertrouwen op een specifiek model. In dit proefschrift pas ik de modelonafhankelijke benadering toe om donkere materie te bestuderen, en een voorgesteld BSM-deeltje genaamd het axion.

Kwantumveldentheorieën (QFT's) vormen een belangrijk hulpmiddel in het fabricageproces van fundamentele theorieën. Vanuit theoretisch oogpunt zijn

deeltjes de kwantumexcitatie van de kwantumvelden. Dit maakt kwantumvelden fundamenteler dan deeltjes. Een belangrijk kenmerk van alle fundamentele theorieën is dat ze worden beperkt door een reeks lokale en globale symmetrieën. Deze symmetrieën manifesteren zich in de natuur als behoudswetten. Het behoud van elektrische lading is bijvoorbeeld het gevolg van een lokale symmetrie. Het belangrijkste obstakel bij het maken van BSM-modellen is dat we de symmetrieën of behoudswetten van de nieuwe natuurkunde nog niet kennen. Als *CP* een geldige symmetrie was geweest in de natuur, dan zou er een gelijk aantal materie- en antimateriedeeltjes zijn geweest. Net zoals een gelijk aantal positieve en negatieve geladen deeltjes het ladingsgetal behouden maakt. Deze materie-antimaterie asymmetrie houdt in dat de *CP* symmetrie in theorie geschonden wordt. De *CP* symmetrie is de combinatie van ladingsconjugatie (C) en pariteitssymmetrie (P). Als het eerst genoemde waar is, dan zou de natuur niet worden aangetast als we deeltjes vervangen door hun antideeltjes. Als het laatst genoemde waar is, dan eeft de natuur dezelfde voorkeur voor fysische processen en hun spiegelbeeld processen.

De *CP* symmetrie stelt dat de fysische wetten onveranderd moeten blijven als de lading van een deeltje wordt omgekeerd en de ruimtelijke coördinaten worden omgekeerd (d.w.z. links wordt rechts en vice versa). Het betekent dat als we de posities van alle deeltjes met de tegenovergestelde lading en de tegenovergestelde handigheid verwisselen, alles er hetzelfde uit zal zien als voorheen. Als het nog steeds moeilijk te visualiseren is, overweeg dan speelgoed met een blauwe kleur aan de ene kant en een rode kleur aan de andere kant. Als je de bovenkant omdraait, *lijkt* hetzelfde voor de natuur, gegeven dat *CP* een goede symmetrie is.

Ook al bevat het SM *CP*-symmetry schending, het kan niet alle waargenomen materie-antimaterie asymmetrie verklaren. Dit is een duidelijk bewijs dat nieuwe fysica bronnen heeft die *CP* schenden. De enige bron van *CP* schending in de sterke sector van het SM is de $\bar{\theta}$ term. Het experimentele bewijs geeft aan dat de kracht van deze term 10^{10} keer kleiner is dan we hadden verwacht. Ook al is hier niets mis mee, het zou een gevolg kunnen zijn van BSM-fysica die we nog moeten ontdekken. Dit wordt het sterke *CP*-probleem genoemd. Een populaire oplossing voor dit probleem is het bestaan van een BSM-deeltje, het axion genaamd, hoewel we nog geen direct bewijs hebben. In dit proefschrift onderzoek ik de effecten van *CP* schendende BSM-bronnen op nucleaire krachten en axions.

Effectieve veldentheorieën

Moeten we weten wat er op het fundamentele niveau gebeurt om de fysieke verschijnselen om ons heen te beschrijven? Het antwoord is niet echt. De microscopische effecten hebben echter wel macroscopische gevolgen. De energie van watermoleculen bepaalt bijvoorbeeld of het water in een vaste, vloeibare of gasvormige toestand bestaat. Zodra we de macroscopische wetten hebben bepaald op basis van de macroscopische waarnemingen, hoeven we ons niet langer druk te

maken om de microscopische wetten. Dit komt door een eigenschap van de natuur genaamd *ontkoppeling*. Het stelt dat fysica op een gegeven energie(lengte)schaal bijna geen invloed heeft op fysica op een andere energie(lengte)schaal. Daarom houden ingenieurs geen rekening met atoomtheorie of deeltjesfysica bij het ontwerpen en bouwen van bruggen en huizen. Effectieve veldtheorieën (EFT's) zijn gebaseerd op dit kenmerk van de natuur.

De zoektocht naar BSM-fysica gebeurt op voornamelijk drie fronten. De eerste is het hoge-energie front, waar we protonen/neutronen laten botsen die bijna met de snelheid van het licht reizen. Vervolgens omvat het hoge-precisie front de uiterst nauwkeurige atoom- en kernexperimenten, en tot slot omvatten de kosmologische en astrofysische fronten sterrenstelsels en de nawerkingen van de oerknal. Het werd onhandig om een op maat gemaakte theorie in één energieschaal te gebruiken om de verschijnselen te beschrijven die plaatsvinden bij een breed scala aan energieën. Zo hoeven scheikundigen voor hun werk niets af te weten van het bestaan van quarks.

EFT's zijn krachtige theoretische hulpmiddelen om fenomenen op een bepaalde energieschaal op een modelonafhankelijke manier te beschrijven. We kiezen een energieschaal en een probleem dat we willen bestuderen, en volgen dan het algemene recept om de EFT te maken. Dit recept wordt geschetst met een voorbeeld in Hoofdstuk 2. De afweging voor modelonafhankelijkheid is dat we te maken hebben met veel constanten, lage-energieconstanten (LEC's) genoemd, die uit de gegevens moeten worden bepaald. EFT's hebben echter een ingebouwd mechanisme om hiermee om te gaan. Dit mechanisme omvat uitbreidingsparameters en een regel voor het tellen van machten in macht-reeksen. We kunnen denken aan een EFT-berekening die vergelijkbaar is met een machtreeksuitbreiding voor eenvoudigere visualisatie. Beschouw $e^x = 1 + x + \frac{x^2}{2!} + \frac{x^3}{3!} + \mathcal{O}(x^4)$, in deze context is x analoog aan de uitbreidingsparameter, $\frac{1}{n!}$ komt overeen met de LEC's. Macht-reeks regels bepalen hoeveel operatoren er in $\mathcal{O}(x^n)$ voorkomen. De resultaten worden gewoonlijk aangeduid als de leidende volgorde (LO), volgende-aan-de-leidende volgorde (NLO), volgende-aan-de-volgende-aan-de-leidende volgorde ($\mathrm{N^2LO}$), enzovoort als we hoger gaan in de kracht van uitbreidingsparameters en daardoor hoger in nauwkeurigheid.

In dit proefschrift heb ik gekozen voor hoge-precisie front grensexperimenten met nucleonen, atomen of lichtdeeltjes zoals pionen (pionen zijn leden van mesonen, dit zijn hadronen die zijn samengesteld uit één quark en één antiquark). Omdat nucleonen voortkomen uit de sterke interactie van quarks, heb ik een EFT gebruikt op basis van kwantumchromodynamica (QCD), die de sterke interactie beschrijft, algemeen bekend als de chirale perturbatietheorie (χPT). χPT is gebaseerd op de chirale symmetrie van de QCD, die stelt dat de wetten van de fysica hetzelfde zijn voor objecten die elkaars spiegelbeeld zijn, maar dat de objecten zelf niet op elkaar kunnen worden gelegd. Denk bijvoorbeeld aan linker- en rechterhandschoenen. Beide zijn spiegelbeelden van elkaar maar kunnen niet in de verkeerde hand gedragen worden. In QCD wordt deze symmetrie geschonden

door de massa's van de quarks. Chirale symmetrie is echter een goede benadering voor lichte quarks, en χPT kan de interacties beschrijven van deeltjes die zijn samengesteld uit lichte quarks tot een goede benadering. χPT biedt een systematische, lage-energie benadering van de onderliggende theorie (QCD) die de interacties van subatomaire deeltjes zoals nucleonen en pionen beschrijft.

Resultaten

In Hoofdstuk 3, onderzochten we de renormalisatie van de *CP*-symmetrie-schendend - kernkracht met behulp van χPT. In QFT beschouwen we deeltjes als puntachtige objecten, wat leidt tot oneindigheden in de berekening. Regularisatie is een wiskundige procedure die wordt gebruikt om deze oneindigheden te verwijderen door een grens te introduceren, die het gedrag van oneindige hoeveelheden regelt. Dit maakt de waarneembare waarden eindig en deze willekeurige grens wordt verwijderd in de laatste stap van de berekening. Dit proces wordt renormalisatie genoemd. Renormalisatie is een noodzakelijke voorwaarde voor alle QFT's die fysieke verschijnselen beschrijven. Bij een EFT wordt renormalisatie bereikt in elke orde in de uitbreidingsparameter. Als de theorie opnieuw is genormaliseerd en de regulator boven de relevante energieschaal ligt, dan zouden de waarneembare gegevens regulatoronafhankelijk moeten zijn.

Onze resultaten onthulden dat de *CP*-symmetrie-schendend observabele $\epsilon^0_{\rm SP}$ een oscillerend gedrag vertoont en zelfs van teken verandert als functie van de regulator, waarmee wordt bevestigd dat *CP*-symmetrie-schendend - kernkracht niet correct is gerenormaliseerd. Dit duidt op een ontbrekende contactterm (of tegenterm) bij de LO om de oneindigheden op te vangen. Aangezien de machttel-regel van een EFT de termen voor een bepaalde orde bepaalt, wijzen onze resultaten op het falen van de machttel-regel. Daarom *fixeerden* we de machttel-regel door een contactterm van hogere orde te promoten bij de LO. We hebben bevestigd dat deze toegevoegde term de regulator-onafhankelijkheid van $\epsilon^0_{\rm SP}$ herstelt. Gezien de afwezigheid van experimentele gegevens, is er echter geen directe manier om de lage energieconstante (LEC) te verkrijgen die bij deze tegenterm hoort. Daarom hebben we een nieuwe oplossing voorgesteld om de LEC indirect te berekenen. Onze resultaten zullen van invloed zijn op de huidige berekeningen van het elektrisch dipoolmoment (EDM) en andere zoektochten voor *CP*-symmetrie-schendend BSM-fysica, die deze LO-term verwaarlozen. We zijn van plan dit project uit te breiden door ^{3}He EDM te berekenen met de tegenterm en de grensafhankelijkheid ervan te controleren.

In Hoofdstuk 4, bestudeerden we de *CP*-symmetrie-schendend axion-interactie in effectieve veldtheorie. We beginnen met de meest algemene *CP*-symmetrie-schendend-bronnen in het lage energie effectieve veldentheorie framework (LEFT) tot twee orden in uitbreidingsparameter. Deze populaire EFT in de deeltjesfysica beschrijft de fysica onder de elektrozwakke symmetrie-brekingsschaal. Daarna gebruikten we χPT om *CP*-symmetrie-schendend axion-baryonen, -mesonen en

-leptonen interacties te berekenen. Om de experimentele resultaten gemakkelijker te kunnen interpreteren, hebben we onze focus beperkt tot *CP*-symmetrie-schendend - interactie tussen axion en nucleonen, pionen en elektronen. Vervolgens bestudeerden we een breed scala aan experimenten op zoek naar *CP*-symmetrie-schendend axion-interacties en vatten we de beperkingen samen die deze experimenten oplegden aan de *CP*-symmetrie-schendend BSM-parameters. De EDM-experimenten stelden de strengste beperkingen en het geprojecteerde Axion Resonant InterAction Detection Experiment zou kunnen concurreren met EDM-experimenten in een beperkt bereik van parameterruimte. Ten slotte hebben we onze EFT-resultaten vertaald naar enkele BSM-modellen, zoals leptoquarks en het links-rechts symmetrische model.

In de toekomst zijn we van plan om onze resultaten te gebruiken om de smaak-schendende *CP*-symmetrie-schendend - processen te bestuderen, zoals kaon naar pion-verval, muon naar elektron-conversies, enzovoort. Aangezien axions voldoen aan de criteria voor een kandidaat voor donkere materie (DM), zijn we van plan de implicaties van onze resultaten voor DM-axion te bestuderen. We ontdekten dat de *CP*-symmetrie-schendend - interacties van DM-axion leiden tot in de tijd variërende oscillaties in de fijne structuurconstante en de massa's van nucleonen en elektronen. De oscillatie van de fijne structuurconstante leidt tot oscillaties van energieniveaus van atomen, die kunnen worden doorzocht in atoomklokexperimenten. Het DM-axion-foton kan een in de tijd variërend potentiaal voor ionen in ion-trap-experimenten induceren, wat een nieuwe toevoeging vormt aan axion-zoektochten.

In Hoofdstuk 5, bestudeerden we de verstrooiing van donkere materie tegen ^{4}He door middel van scalaire interacties. Scalaire interacties zijn interessant omdat het niet afhankelijk is van de spin van de kernen en schalen als het aantal nucleonen in de kernen. We hebben ons gericht op ^{4}He vanwege de voorgestelde ^{4}He DM-detectoren en ^{4}He heeft een bindingsenergie die vergelijkbaar is met zwaardere isotopen die in andere DM-detectoren worden gebruikt. We zijn begonnen met een scalaire DM-quark- en -gluon-interacties en hebben dit vertaald naar scalaire DM-nucleon- en -pion-interacties met behulp van χPT. We berekenden DM-nucleonverstrooiingsamplitudes voor ^{2}H, ^{3}He en ^{4}He kernen tot aan NLO. De NLO-bijdragen kunnen in twee delen worden verdeeld: de radiuscorrectie (of eenlichaamscorrectie), waarbij verstrooiing met één nucleon plaatsvindt, en tweelichaamscorrecties, waarbij verstrooiing met twee nucleonen plaatsvindt. We hebben maximaal N^{5}LO nucleaire golffuncties opgenomen om de convergentie van onze resultaten met toenemende orde in de golffunctie te controleren. We hebben geconstateerd dat de NLO-bijdragen de LO-uitkomsten slechts met enkele procenten veranderen. De meest interessante resultaten waren dat de NLO tweelichaamscorrecties correcties een significante afkapafhankelijkheid lieten zien. We hebben sterk het vermoeden dat dit wijst op het falen van de machttel-regel op NLO-niveau. De lineaire correlatie tussen tweelichaamsstromen en de D-golfkans van de golffuncties levert verder bewijs voor deze hypothese, aangezien de D-golfkans niet fysiek waarneembaar is. We vermoeden dat het promoten van een

contactterm van hogere orde voor NLO de renormalisatie zou kunnen herstellen. Verdere studies zijn echter nodig om deze hypothese te bevestigen. We zijn van plan om in de toekomst spin-afhankelijke DM-kernverstrooiing te bestuderen.

Acknowledgements

First of all, I would like to thank my thesis supervisor Dr. Jordy de Vries for providing me with the opportunity to complete my Ph.D. Even though this was his first time mentoring graduate students, he did an excellent job, and I am delighted to be his student. His passion for research, friendly jokes, and academic guidance made my Ph.D. journey fulfilling and memorable. He was always available for meetings and was only a slack message or email away from answering any questions I had. I am grateful for his immense help with writing papers, presentations, and this thesis.

I am also thankful to my research collaborators Wouter, Andreas, and Christopher, for the productive discussions and advice when I got stuck during the projects. I have learned a lot in those zoom meetings. Even though I could not meet all of you because of COVID-19, I hope to meet you all in the near future.

I would like to thank my doctoral committee members for spending time reading this long thesis and for their feedback, which helped me to make this thesis better.

I started my Ph.D. journey almost seven years back in the master-Ph.D. program at the University of Massachusetts Amherst (UMass), USA. It was my first time living outside my own country, India, and it was almost on the other side of the globe. However, it quickly became my second home because of my friends at UMass. I would like to thank Vahini, Sumon, Ashlin, Arjun, Devadyouti, Devin, Adithya, Pavithra, Abhiram, Suman, and all my other friends at UMass for the road trips and for making my time there fun and memorable. In addition, I have special thanks to Sumon for making the cover page of this thesis. I would like to mention my thanks to Sandeep *chettan* and Varsha *chechi* for all the advice and for helping me settle in the USA. I enjoyed visiting both of you and Gauri in Boston.

I also want to mention my appreciation to the faculty and staff at the Department of Physics, UMass, for all the career and academic advisements and for organizing all the events that made my Ph.D. more enjoyable. I am incredibly thankful to Heath and Andrea for their advice on life after Ph.D.

I finished the last year of my Ph.D. at the University of Amsterdam (UvA). However, I spend almost all my time at the Nikhef theory group, The Netherlands.

It was a great workplace because of its friendly and stimulating environment. I enjoyed the discussions, table tennis matches, coffee breaks, and lunch with the theory group. I would like to thank Avanish, Vaisakh, Andrea, Coenraad, Jaco, Guanghui and my other friends from the theory group for making the last year of my Ph.D. delightful and unforgettable. I like to give my special thanks to my paranymphs Avanish and Jaco for all their help during the final stages of my Ph.D. I appreciate the advice and discussions from Wouter, Eric, Jordy, and other staff, which helped me learn more and improve myself.

I am especially thankful to my family for their continued support during my Ph.D. The video chats with my father, mother, and brother made me feel connected and at home.

Finally, I thank my friends from IISER Bhopal, India. I am especially thankful to Ritwika, Shikha, Geo, Arunraj, Nikhil, Vipin, Shibu, and Anto. Their continued support and encouragement helped me overcome my short-term panic attacks during my Ph.D.

Bibliography

[1] S. L. Glashow, "Partial Symmetries of Weak Interactions," *Nucl. Phys.* **22** (1961) 579–588.

[2] S. Weinberg, "A Model of Leptons," *Phys. Rev. Lett.* **19** (1967) 1264–1266.

[3] A. Salam and J. C. Ward, "Weak and electromagnetic interactions," *Nuovo Cim.* **11** (1959) 568–577.

[4] D. J. Gross and F. Wilczek, "Ultraviolet Behavior of Nonabelian Gauge Theories," *Phys. Rev. Lett.* **30** (1973) 1343–1346.

[5] H. D. Politzer, "Reliable Perturbative Results for Strong Interactions?," *Phys. Rev. Lett.* **30** (1973) 1346–1349.

[6] G. 't Hooft and M. J. G. Veltman, "Regularization and Renormalization of Gauge Fields," *Nucl. Phys. B* **44** (1972) 189–213.

[7] **ATLAS** Collaboration, G. Aad *et al.*, "Observation of a new particle in the search for the Standard Model Higgs boson with the ATLAS detector at the LHC," *Phys. Lett. B* **716** (2012) 1–29, [arXiv:1207.7214].

[8] **CMS** Collaboration, S. Chatrchyan *et al.*, "Observation of a New Boson at a Mass of 125 GeV with the CMS Experiment at the LHC," *Phys. Lett. B* **716** (2012) 30–61, [arXiv:1207.7235].

[9] G. Bertone and D. Hooper, "History of dark matter," *Rev. Mod. Phys.* **90** no. 4, (2018) 045002, [arXiv:1605.04909].

[10] V. D. Shiltsev, "High energy particle colliders: past 20 years, next 20 years and beyond," *Phys. Usp.* **55** (2012) 965–976, [arXiv:1205.3087].

[11] V. Shiltsev and F. Zimmermann, "Modern and Future Colliders," *Rev. Mod. Phys.* **93** (2021) 015006, [arXiv:2003.09084].

[12] A. D. Dolgov, "Cosmology and new physics," *Phys. Atom. Nucl.* **71** (2008) 651–670, [hep-ph/0606230].

[13] V. Cirigliano and M. J. Ramsey-Musolf, "Low Energy Probes of Physics Beyond the Standard Model," *Prog. Part. Nucl. Phys.* **71** (2013) 2–20, [arXiv:1304.0017].

[14] **Muon g-2** Collaboration, B. Abi *et al.*, "Measurement of the Positive Muon Anomalous Magnetic Moment to 0.46 ppm," *Phys. Rev. Lett.* **126** no. 14, (2021) 141801, [arXiv:2104.03281].

[15] S. Borsanyi *et al.*, "Leading hadronic contribution to the muon magnetic moment from lattice QCD," *Nature* **593** no. 7857, (2021) 51–55, [arXiv:2002.12347].

[16] A. Gérardin, "Muon g−2 from the lattice," *Nucl. Part. Phys. Proc.* **318-323** (2022) 187–193.

[17] J. C. Pati and A. Salam, "Lepton Number as the Fourth Color," *Phys. Rev. D* **10** (1974) 275–289. [Erratum: Phys.Rev.D 11, 703–703 (1975)].

[18] R. N. Mohapatra and J. C. Pati, "Left-Right Gauge Symmetry and an Isoconjugate Model of CP Violation," *Phys. Rev. D* **11** (1975) 566–571.

[19] G. Senjanovic and R. N. Mohapatra, "Exact Left-Right Symmetry and Spontaneous Violation of Parity," *Phys. Rev. D* **12** (1975) 1502.

[20] G. Senjanovic, "Spontaneous Breakdown of Parity in a Class of Gauge Theories," *Nucl. Phys. B* **153** (1979) 334–364.

[21] N. G. Deshpande, J. F. Gunion, B. Kayser, and F. I. Olness, "Left-right symmetric electroweak models with triplet Higgs," *Phys. Rev. D* **44** (1991) 837–858.

[22] S. Fajfer, J. F. Kamenik, I. Nisandzic, and J. Zupan, "Implications of Lepton Flavor Universality Violations in B Decays," *Phys. Rev. Lett.* **109** (2012) 161801, [arXiv:1206.1872].

[23] D. Buttazzo, A. Greljo, G. Isidori, and D. Marzocca, "B-physics anomalies: a guide to combined explanations," *JHEP* **11** (2017) 044, [arXiv:1706.07808].

[24] D. B. Kaplan and H. Georgi, "SU(2) x U(1) Breaking by Vacuum Misalignment," *Phys. Lett. B* **136** (1984) 183–186.

[25] M. J. Dugan, H. Georgi, and D. B. Kaplan, "Anatomy of a Composite Higgs Model," *Nucl. Phys. B* **254** (1985) 299–326.

[26] W. Buchmuller and D. Wyler, "Effective Lagrangian Analysis of New Interactions and Flavor Conservation," *Nucl. Phys. B* **268** (1986) 621–653.

[27] B. Grzadkowski, M. Iskrzynski, M. Misiak, and J. Rosiek, "Dimension-Six Terms in the Standard Model Lagrangian," *JHEP* **10** (2010) 085, [arXiv:1008.4884].

[28] I. Brivio and M. Trott, "The Standard Model as an Effective Field Theory," *Phys. Rept.* **793** (2019) 1–98, [arXiv:1706.08945].

[29] E. E. Jenkins, A. V. Manohar, and P. Stoffer, "Low-Energy Effective Field Theory below the Electroweak Scale: Operators and Matching," *JHEP* **03** (2018) 016, [arXiv:1709.04486].

[30] S. Scherer, "Introduction to chiral perturbation theory," *Adv. Nucl. Phys.* **27** (2003) 277, [hep-ph/0210398].

[31] B. C. Tiburzi, "Chiral Perturbation Theory," *Lect. Notes Phys.* **889** (2015) 107–152.

[32] P. F. Bedaque and U. van Kolck, "Effective field theory for few nucleon systems," *Ann. Rev. Nucl. Part. Sci.* **52** (2002) 339–396, [nucl-th/0203055].

[33] H. W. Hammer, S. König, and U. van Kolck, "Nuclear effective field theory: status and perspectives," *Rev. Mod. Phys.* **92** no. 2, (2020) 025004, [arXiv:1906.12122].

[34] A. Pich, "Effective field theory: Course," in *Les Houches Summer School in Theoretical Physics, Session 68: Probing the Standard Model of Particle Interactions*, pp. 949–1049. 6, 1998. hep-ph/9806303.

[35] D. B. Kaplan, "Effective field theories," in *7th Summer School in Nuclear Physics Symmetries*. 6, 1995. nucl-th/9506035.

[36] K. G. Wilson, "Quantum Chromodynamics on a Lattice," in *Cargese Summer Institute: New Developments in Quantum Field Theory and Statistical Mechanics*. 1, 1977.

[37] N. Ishii, S. Aoki, and T. Hatsuda, "The Nuclear Force from Lattice QCD," *Phys. Rev. Lett.* **99** (2007) 022001, [nucl-th/0611096].

[38] H. B. Meyer, "Lattice QCD: A Brief Introduction," *Lect. Notes Phys.* **889** (2015) 1–34.

[39] E. Noether, "Invariant Variation Problems," *Gott. Nachr.* **1918** (1918) 235–257, [physics/0503066].

[40] C. S. Wu, E. Ambler, R. W. Hayward, D. D. Hoppes, and R. P. Hudson, "Experimental Test of Parity Conservation in β Decay," *Phys. Rev.* **105** (1957) 1413–1414.

[41] A. D. Sakharov, "Violation of CP Invariance, C asymmetry, and baryon asymmetry of the universe," *Pisma Zh. Eksp. Teor. Fiz.* **5** (1967) 32–35.

[42] N. Cabibbo, "Unitary Symmetry and Leptonic Decays," *Phys. Rev. Lett.* **10** (1963) 531–533.

[43] M. Kobayashi and T. Maskawa, "CP Violation in the Renormalizable Theory of Weak Interaction," *Prog. Theor. Phys.* **49** (1973) 652–657.

[44] S. Weinberg, "The U(1) Problem," *Phys. Rev. D* **11** (1975) 3583–3593.

[45] K. Fujikawa, "Path Integral Measure for Gauge Invariant Fermion Theories," *Phys. Rev. Lett.* **42** (1979) 1195–1198.

[46] K. Fujikawa, "Path Integral for Gauge Theories with Fermions," *Phys. Rev. D* **21** (1980) 2848. [Erratum: Phys.Rev.D 22, 1499 (1980)].

[47] G. 't Hooft, "Symmetry Breaking Through Bell-Jackiw Anomalies," *Phys. Rev. Lett.* **37** (1976) 8–11.

[48] G. 't Hooft, "How Instantons Solve the U(1) Problem," *Phys. Rept.* **142** (1986) 357–387.

[49] J. Dragos, T. Luu, A. Shindler, J. de Vries, and A. Yousif, "Confirming the Existence of the strong CP Problem in Lattice QCD with the Gradient Flow," *Phys. Rev. C* **103** no. 1, (2021) 015202, [arXiv:1902.03254].

[50] A. Wirzba, J. Bsaisou, and A. Nogga, *Permanent electric dipole moments of single-, two- and three-nucleon systems: Memorial Volume Dedicated to Gerald E Brown*, pp. 471–488. World Scientific, Singapore, May, 2017.

[51] C.-Y. Seng, "Reexamination of The Standard Model Nucleon Electric Dipole Moment," *Phys. Rev. C* **91** no. 2, (2015) 025502, [arXiv:1411.1476].

[52] C. Abel *et al.*, "Measurement of the Permanent Electric Dipole Moment of the Neutron," *Phys. Rev. Lett.* **124** no. 8, (2020) 081803, [arXiv:2001.11966].

[53] **Particle Data Group** Collaboration, R. L. Workman *et al.*, "Review of Particle Physics," *PTEP* **2022** (2022) 083C01.

[54] A. G. Cohen, D. B. Kaplan, and A. E. Nelson, "Testing m(u)=0 on the lattice," *JHEP* **11** (1999) 027, [hep-lat/9909091].

[55] M. Dine, P. Draper, and G. Festuccia, "Instanton Effects in Three Flavor QCD," *Phys. Rev. D* **92** no. 5, (2015) 054004, [arXiv:1410.8505].

[56] C. Alexandrou, J. Finkenrath, L. Funcke, K. Jansen, B. Kostrzewa, F. Pittler, and C. Urbach, "Ruling Out the Massless Up-Quark Solution to the Strong ***CP*** Problem by Computing the Topological Mass Contribution with Lattice QCD," *Phys. Rev. Lett.* **125** no. 23, (2020) 232001, [arXiv:2002.07802].

[57] J. R. Ellis and M. K. Gaillard, "Strong and Weak CP Violation," *Nucl. Phys. B* **150** (1979) 141–162.

[58] M. A. B. Beg and H. S. Tsao, "Strong P, T Noninvariances in a Superweak Theory," *Phys. Rev. Lett.* **41** (1978) 278.

[59] H. Georgi, "A Model of Soft CP Violation," *Hadronic J.* **1** (1978) 155.

[60] A. E. Nelson, "Naturally Weak CP Violation," *Phys. Lett. B* **136** (1984) 387–391.

[61] S. M. Barr, "Solving the Strong CP Problem Without the Peccei-Quinn Symmetry," *Phys. Rev. Lett.* **53** (1984) 329.

[62] R. D. Peccei and H. R. Quinn, "CP Conservation in the Presence of Instantons," *Phys. Rev. Lett.* **38** (1977) 1440–1443.

[63] R. D. Peccei and H. R. Quinn, "Constraints Imposed by CP Conservation in the Presence of Instantons," *Phys. Rev. D* **16** (1977) 1791–1797.

[64] S. Weinberg, "A New Light Boson?," *Phys. Rev. Lett.* **40** (1978) 223–226.

[65] F. Wilczek, "Problem of Strong P and T Invariance in the Presence of Instantons," *Phys. Rev. Lett.* **40** (1978) 279–282.

[66] D. d'Enterria and P. Z. Skands, eds., *Proceedings, High-Precision α_s Measurements from LHC to FCC-ee: Geneva, Switzerland, October 2-13, 2015*. CERN, Geneva, 12, 2015. arXiv:1512.05194.

[67] D. R. Entem and R. Machleidt, "Accurate charge dependent nucleon nucleon potential at fourth order of chiral perturbation theory," *Phys. Rev. C* **68** (2003) 041001, [nucl-th/0304018].

[68] E. Epelbaum, W. Glockle, and U.-G. Meissner, "The Two-nucleon system at next-to-next-to-next-to-leading order," *Nucl. Phys. A* **747** (2005) 362–424, [nucl-th/0405048].

[69] R. Machleidt, "Nuclear forces from chiral effective field theory," in *Workshop on Physics and Astrophysics of Hadrons and Hadronic Matter*. 4, 2007. arXiv:0704.0807.

[70] T. Bhattacharya, V. Cirigliano, R. Gupta, H.-W. Lin, and B. Yoon, "Neutron Electric Dipole Moment and Tensor Charges from Lattice QCD," *Phys. Rev. Lett.* **115** no. 21, (2015) 212002, [arXiv:1506.04196].

[71] M. Abramczyk, S. Aoki, T. Blum, T. Izubuchi, H. Ohki, and S. Syritsyn, "Lattice calculation of electric dipole moments and form factors of the nucleon," *Phys. Rev. D* **96** no. 1, (2017) 014501, [arXiv:1701.07792].

[72] E. Mereghetti, W. H. Hockings, and U. van Kolck, "The Effective Chiral Lagrangian From the Theta Term," *Annals Phys.* **325** (2010) 2363–2409, [arXiv:1002.2391].

[73] J. de Vries, E. Mereghetti, R. G. E. Timmermans, and U. van Kolck, "The Effective Chiral Lagrangian From Dimension-Six Parity and Time-Reversal Violation," *Annals Phys.* **338** (2013) 50–96, [arXiv:1212.0990].

[74] J. Bsaisou, U.-G. Meißner, A. Nogga, and A. Wirzba, "P- and T-Violating Lagrangians in Chiral Effective Field Theory and Nuclear Electric Dipole Moments," *Annals Phys.* **359** (2015) 317–370, [arXiv:1412.5471].

[75] S. Ban, J. Dobaczewski, J. Engel, and A. Shukla, "Fully self-consistent calculations of nuclear Schiff moments," *Phys. Rev. C* **82** (2010) 015501, [arXiv:1003.2598].

[76] J. de Vries, R. Higa, C. P. Liu, E. Mereghetti, I. Stetcu, R. G. E. Timmermans, and U. van Kolck, "Electric Dipole Moments of Light Nuclei From Chiral Effective Field Theory," *Phys. Rev. C* **84** (2011) 065501, [arXiv:1109.3604].

[77] J. Bsaisou, J. de Vries, C. Hanhart, S. Liebig, U.-G. Meissner, D. Minossi, A. Nogga, and A. Wirzba, "Nuclear Electric Dipole Moments in Chiral Effective Field Theory," *JHEP* **03** (2015) 104, [arXiv:1411.5804]. [Erratum: JHEP 05, 083 (2015)].

[78] J. Dobaczewski, J. Engel, M. Kortelainen, and P. Becker, "Correlating Schiff moments in the light actinides with octupole moments," *Phys. Rev. Lett.* **121** no. 23, (2018) 232501, [arXiv:1807.09581].

[79] A. Gnech and M. Viviani, "Time Reversal Violation in Light Nuclei," *Phys. Rev. C* **101** no. 2, (2020) 024004, [arXiv:1906.09021].

[80] D. J. Fixsen, E. S. Cheng, J. M. Gales, J. C. Mather, R. A. Shafer, and E. L. Wright, "The Cosmic Microwave Background spectrum from the full COBE FIRAS data set," *Astrophys. J.* **473** (1996) 576, [astro-ph/9605054].

[81] C. L. Reichardt *et al.*, "High resolution CMB power spectrum from the complete ACBAR data set," *Astrophys. J.* **694** (2009) 1200–1219, [arXiv:0801.1491].

[82] **QUaD** Collaboration, S. Gupta *et al.*, "Parameter Estimation from Improved Measurements of the CMB from QUaD," *Astrophys. J.* **716** (2010) 1040–1046, [arXiv:0909.1621].

[83] **WMAP** Collaboration, G. Hinshaw *et al.*, "Nine-Year Wilkinson Microwave Anisotropy Probe (WMAP) Observations: Cosmological Parameter Results," *Astrophys. J. Suppl.* **208** (2013) 19, [arXiv:1212.5226].

[84] J. D. Lewin and P. F. Smith, "Review of mathematics, numerical factors, and corrections for dark matter experiments based on elastic nuclear recoil," *Astropart. Phys.* **6** (1996) 87–112.

[85] M. W. Goodman and E. Witten, "Detectability of Certain Dark Matter Candidates," *Phys. Rev. D* **31** (1985) 3059.

[86] **DAMIC** Collaboration, J. R. T. de Mello Neto *et al.*, "The DAMIC dark matter experiment," *PoS* **ICRC2015** (2016) 1221, [arXiv:1510.02126].

[87] J. Schieck *et al.*, "Direct Dark Matter Search with the CRESST II Experiment," *PoS* **ICHEP2016** (2016) 217, [arXiv:1611.02113].

[88] **EDELWEISS** Collaboration, J. Gascon *et al.*, "Low-mass Dark Matter searches with EDELWEISS," in *19th International Workshop on Low Temperature Detectors*. 12, 2021. arXiv:2112.05467.

[89] **SuperCDMS** Collaboration, M. F. Albakry *et al.*, "A Strategy for Low-Mass Dark Matter Searches with Cryogenic Detectors in the SuperCDMS SNOLAB Facility," in *2022 Snowmass Summer Study*. 3, 2022. arXiv:2203.08463.

[90] **LZ** Collaboration, J. Aalbers *et al.*, "First Dark Matter Search Results from the LUX-ZEPLIN (LZ) Experiment," arXiv:2207.03764.

[91] **XENON100** Collaboration, S. E. A. Orrigo, "Direct Dark Matter Search with XENON100," *EPJ Web Conf.* **121** (2016) 06006, [arXiv:1501.03492].

[92] N. Marcelli *et al.*, "Helium Fluxes Measured by the PAMELA Experiment from the Minimum to the Maximum Solar Activity for Solar Cycle 24," *Astrophys. J. Lett.* **925** no. 2, (2022) L24, [arXiv:2201.01045].

[93] F. Calore, M. Cirelli, L. Derome, Y. Genolini, D. Maurin, P. Salati, and P. D. Serpico, "AMS-02 antiprotons and dark matter: Trimmed hints and robust bounds," *SciPost Phys.* **12** no. 5, (2022) 163, [arXiv:2202.03076].

[94] **Fermi-LAT, DES** Collaboration, A. Albert *et al.*, "Searching for Dark Matter Annihilation in Recently Discovered Milky Way Satellites with Fermi-LAT," *Astrophys. J.* **834** no. 2, (2017) 110, [arXiv:1611.03184].

[95] **H.E.S.S.** Collaboration, L. Rinchiuso, "Latest results on dark matter searches with H.E.S.S," *EPJ Web Conf.* **209** (2019) 01023, [arXiv:1901.05299].

[96] **MAGIC** Collaboration, M. Doro, "A review of the past and present MAGIC dark matter search program and a glimpse at the future," in *25th European Cosmic Ray Symposium*. 1, 2017. arXiv:1701.05702.

[97] **ATLAS** Collaboration, G. Aad *et al.*, "Search for dark matter in events with a Z boson and missing transverse momentum in pp collisions at $\sqrt{s}$=8 TeV with the ATLAS detector," *Phys. Rev. D* **90** no. 1, (2014) 012004, [arXiv:1404.0051].

[98] **ATLAS** Collaboration, G. Aad *et al.*, "Search for dark matter candidates and large extra dimensions in events with a jet and missing transverse momentum with the ATLAS detector," *JHEP* **04** (2013) 075, [arXiv:1210.4491].

[99] **CMS** Collaboration, S. Chatrchyan *et al.*, "Search for Dark Matter and Large Extra Dimensions in Monojet Events in pp Collisions at $\sqrt{s} = 7$ TeV," *JHEP* **09** (2012) 094, [arXiv:1206.5663].

[100] C. Körber, A. Nogga, and J. de Vries, "First-principle calculations of Dark Matter scattering off light nuclei," *Phys. Rev. C* **96** no. 3, (2017) 035805, [arXiv:1704.01150].

[101] H. W. Grießhammer, J. A. McGovern, A. Nogga, and D. R. Phillips, "Scattering Observables from One- and Two-Body Densities: Formalism and Application to $\gamma\,^3$He Scattering," *Few Body Syst.* **61** no. 4, (2020) 48, [arXiv:2005.12207].

[102] S. A. Hertel, A. Biekert, J. Lin, V. Velan, and D. N. McKinsey, "Direct detection of sub-GeV dark matter using a superfluid ^{4}He target," *Phys. Rev. D* **100** no. 9, (2019) 092007, [arXiv:1810.06283].

[103] S. Weinberg, "Phenomenological Lagrangians," *Physica A* **96** no. 1-2, (1979) 327–340.

[104] H. Leutwyler, "On the foundations of chiral perturbation theory," *Annals Phys.* **235** (1994) 165–203, [hep-ph/9311274].

[105] S. Rivat, "Drawing Scales Apart: The Origins of Wilson's Conception of Effective Field Theories," arXiv:2111.03148.

[106] M. Neubert, "Renormalization Theory and Effective Field Theories," arXiv:1901.06573.

[107] A. V. Manohar, "Introduction to Effective Field Theories," arXiv:1804.05863.

[108] E. Fermi, "Tentativo di una teoria dell'emissione dei raggi beta," *Ric. Sci.* **4** (1933) 491–495.

[109] T. D. Lee and C.-N. Yang, "Question of Parity Conservation in Weak Interactions," *Phys. Rev.* **104** (1956) 254–258.

[110] S. Weinberg, "Baryon and Lepton Nonconserving Processes," *Phys. Rev. Lett.* **43** (1979) 1566–1570.

[111] E. E. Jenkins, A. V. Manohar, and M. Trott, "Renormalization Group Evolution of the Standard Model Dimension Six Operators I: Formalism and lambda Dependence," *JHEP* **10** (2013) 087, [arXiv:1308.2627].

[112] E. E. Jenkins, A. V. Manohar, and M. Trott, "Renormalization Group Evolution of the Standard Model Dimension Six Operators II: Yukawa Dependence," *JHEP* **01** (2014) 035, [arXiv:1310.4838].

[113] R. Alonso, E. E. Jenkins, A. V. Manohar, and M. Trott, "Renormalization Group Evolution of the Standard Model Dimension Six Operators III: Gauge Coupling Dependence and Phenomenology," *JHEP* **04** (2014) 159, [arXiv:1312.2014].

[114] L. Lehman, "Extending the Standard Model Effective Field Theory with the Complete Set of Dimension-7 Operators," *Phys. Rev. D* **90** no. 12, (2014) 125023, [arXiv:1410.4193].

[115] Y. Liao and X.-D. Ma, "Renormalization Group Evolution of Dimension-seven Baryon- and Lepton-number-violating Operators," *JHEP* **11** (2016) 043, [arXiv:1607.07309].

[116] H.-L. Li, Z. Ren, J. Shu, M.-L. Xiao, J.-H. Yu, and Y.-H. Zheng, "Complete set of dimension-eight operators in the standard model effective field theory," *Phys. Rev. D* **104** no. 1, (2021) 015026, [arXiv:2005.00008].

[117] J. Gasser and H. Leutwyler, "Chiral Perturbation Theory to One Loop," *Annals Phys.* **158** (1984) 142.

[118] M. Gell-Mann and Y. Ne'eman, "The Eightfold way: a review with a collection of reprints,".

[119] S. R. Coleman, J. Wess, and B. Zumino, "Structure of phenomenological Lagrangians. 1.," *Phys. Rev.* **177** (1969) 2239–2247.

[120] N. Fettes, U.-G. Meissner, M. Mojzis, and S. Steininger, "The Chiral effective pion nucleon Lagrangian of order p**4," *Annals Phys.* **283** (2000) 273–302, [hep-ph/0001308]. [Erratum: Annals Phys. 288, 249–250 (2001)].

[121] R. Machleidt and D. R. Entem, "Chiral effective field theory and nuclear forces," *Phys. Rept.* **503** (2011) 1–75, [arXiv:1105.2919].

[122] E. E. Jenkins and A. V. Manohar, "Chiral corrections to the baryon axial currents," *Phys. Lett. B* **259** (1991) 353–358.

[123] H. Georgi, "An Effective Field Theory for Heavy Quarks at Low-energies," *Phys. Lett. B* **240** (1990) 447–450.

[124] S. Weinberg, "Nuclear forces from chiral Lagrangians," *Phys. Lett. B* **251** (1990) 288–292.

[125] S. Weinberg, "Effective chiral Lagrangians for nucleon - pion interactions and nuclear forces," *Nucl. Phys. B* **363** (1991) 3–18.

[126] S. Weinberg, "Three body interactions among nucleons and pions," *Phys. Lett. B* **295** (1992) 114–121, [hep-ph/9209257].

[127] A. Manohar and H. Georgi, "Chiral Quarks and the Nonrelativistic Quark Model," *Nucl. Phys. B* **234** (1984) 189–212.

[128] S. Weinberg, "Larger Higgs Exchange Terms in the Neutron Electric Dipole Moment," *Phys. Rev. Lett.* **63** (1989) 2333.

[129] N. Kaiser, R. Brockmann, and W. Weise, "Peripheral nucleon-nucleon phase shifts and chiral symmetry," *Nucl. Phys. A* **625** (1997) 758–788, [nucl-th/9706045].

[130] N. Yamanaka, B. K. Sahoo, N. Yoshinaga, T. Sato, K. Asahi, and B. P. Das, "Probing exotic phenomena at the interface of nuclear and particle physics with the electric dipole moments of diamagnetic atoms: A unique window to hadronic and semi-leptonic CP violation," *Eur. Phys. J. A* **53** no. 3, (2017) 54, [arXiv:1703.01570].

[131] T. Chupp, P. Fierlinger, M. Ramsey-Musolf, and J. Singh, "Electric dipole moments of atoms, molecules, nuclei, and particles," *Rev. Mod. Phys.* **91** no. 1, (2019) 015001, [arXiv:1710.02504].

[132] Y. Yamaguchi and N. Yamanaka, "Large long-distance contributions to the electric dipole moments of charged leptons in the standard model," *Phys. Rev. Lett.* **125** (2020) 241802, [arXiv:2003.08195].

[133] C. Abel *et al.*, "The n2EDM experiment at the Paul Scherrer Institute," *EPJ Web Conf.* **219** (2019) 02002, [arXiv:1811.02340].

[134] D. E. Morrissey and M. J. Ramsey-Musolf, "Electroweak baryogenesis," *New J. Phys.* **14** (2012) 125003, [arXiv:1206.2942].

[135] V. Cirigliano, W. Dekens, J. de Vries, and E. Mereghetti, "Constraining the top-Higgs sector of the Standard Model Effective Field Theory," *Phys. Rev. D* **94** no. 3, (2016) 034031, [arXiv:1605.04311].

[136] K. Kirch and B. Lauss, "Ultracold Neutrons," arXiv:2006.04568.

[137] R. J. Crewther, P. Di Vecchia, G. Veneziano, and E. Witten, "Chiral Estimate of the Electric Dipole Moment of the Neutron in Quantum Chromodynamics," *Phys. Lett. B* **88** (1979) 123. [Erratum: Phys.Lett.B 91, 487 (1980)].

[138] E. Mereghetti, J. de Vries, W. H. Hockings, C. M. Maekawa, and U. van Kolck, "The Electric Dipole Form Factor of the Nucleon in Chiral Perturbation Theory to Sub-leading Order," *Phys. Lett. B* **696** (2011) 97–102, [arXiv:1010.4078].

[139] F.-K. Guo and U.-G. Meissner, "Baryon electric dipole moments from strong CP violation," *JHEP* **12** (2012) 097, [arXiv:1210.5887].

[140] C.-Y. Seng, J. de Vries, E. Mereghetti, H. H. Patel, and M. Ramsey-Musolf, "Nucleon electric dipole moments and the isovector parity- and time-reversal-odd pion–nucleon coupling," *Phys. Lett. B* **736** (2014) 147–153, [arXiv:1401.5366].

[141] C. M. Maekawa, E. Mereghetti, J. de Vries, and U. van Kolck, "The Time-Reversal- and Parity-Violating Nuclear Potential in Chiral Effective Theory," *Nucl. Phys. A* **872** (2011) 117–160, [arXiv:1106.6119].

[142] W. Dekens, J. de Vries, J. Bsaisou, W. Bernreuther, C. Hanhart, U.-G. Meißner, A. Nogga, and A. Wirzba, "Unraveling models of CP violation through electric dipole moments of light nuclei," *JHEP* **07** (2014) 069, [arXiv:1404.6082].

[143] D. B. Kaplan, M. J. Savage, and M. B. Wise, "Nucleon - nucleon scattering from effective field theory," *Nucl. Phys. B* **478** (1996) 629–659, [nucl-th/9605002].

[144] U. van Kolck, "The Problem of Renormalization of Chiral Nuclear Forces," *Front. in Phys.* **8** (2020) 79, [arXiv:2003.06721].

[145] A. Nogga, R. G. E. Timmermans, and U. van Kolck, "Renormalization of one-pion exchange and power counting," *Phys. Rev. C* **72** (2005) 054006, [nucl-th/0506005].

[146] M. Pavón Valderrama and D. R. Phillips, "Power Counting of Contact-Range Currents in Effective Field Theory," *Phys. Rev. Lett.* **114** no. 8, (2015) 082502, [arXiv:1407.0437].

[147] V. Cirigliano, W. Dekens, J. De Vries, M. L. Graesser, E. Mereghetti, S. Pastore, and U. Van Kolck, "New Leading Contribution to Neutrinoless Double-β Decay," *Phys. Rev. Lett.* **120** no. 20, (2018) 202001, [arXiv:1802.10097].

[148] C. Abel *et al.*, "Search for Axionlike Dark Matter through Nuclear Spin Precession in Electric and Magnetic Fields," *Phys. Rev. X* **7** no. 4, (2017) 041034, [arXiv:1708.06367].

[149] D. Budker, P. W. Graham, M. Ledbetter, S. Rajendran, and A. Sushkov, "Proposal for a Cosmic Axion Spin Precession Experiment (CASPEr)," *Phys. Rev. X* **4** no. 2, (2014) 021030, [arXiv:1306.6089].

[150] Y. V. Stadnik and V. V. Flambaum, "Axion-induced effects in atoms, molecules, and nuclei: Parity nonconservation, anapole moments, electric dipole moments, and spin-gravity and spin-axion momentum couplings," *Phys. Rev. D* **89** no. 4, (2014) 043522, [arXiv:1312.6667].

[151] G. 't Hooft, "Computation of the Quantum Effects Due to a Four-Dimensional Pseudoparticle," *Phys. Rev. D* **14** (1976) 3432–3450. [Erratum: Phys.Rev.D 18, 2199 (1978)].

[152] V. Baluni, "CP Violating Effects in QCD," *Phys. Rev. D* **19** (1979) 2227–2230.

[153] V. Bernard, N. Kaiser, and U.-G. Meissner, "Chiral dynamics in nucleons and nuclei," *Int. J. Mod. Phys. E* **4** (1995) 193–346, [hep-ph/9501384].

[154] J. de Vries, E. Mereghetti, and A. Walker-Loud, "Baryon mass splittings and strong CP violation in SU(3) Chiral Perturbation Theory," *Phys. Rev. C* **92** no. 4, (2015) 045201, [arXiv:1506.06247].

[155] D. A. Brantley, B. Joo, E. V. Mastropas, E. Mereghetti, H. Monge-Camacho, B. C. Tiburzi, and A. Walker-Loud, "Strong isospin violation and chiral logarithms in the baryon spectrum," arXiv:1612.07733.

[156] C. P. Liu and R. G. E. Timmermans, "Time-reversal violation in threshold vector-n vector-p scattering," *Phys. Lett. B* **634** (2006) 488–492, [nucl-th/0602010].

[157] P. Fadeev and V. V. Flambaum, "Time reversal invariance violation in neutron-nucleus scattering," *Phys. Rev. C* **100** no. 1, (2019) 015504, [arXiv:1903.08937].

[158] D. C. Schaper *et al.*, "A modular apparatus for use in high-precision measurements of parity violation in polarized eV neutron transmission," *Nucl. Instrum. Meth. A* **969** (2020) 163961, [arXiv:2001.03432].

[159] V. G. J. Stoks, R. A. M. Klomp, M. C. M. Rentmeester, and J. J. de Swart, "Partial wave analysis of all nucleon-nucleon scattering data below 350-MeV," *Phys. Rev. C* **48** (1993) 792–815.

[160] Y.-H. Song, R. Lazauskas, and U. van Kolck, "Triton binding energy and neutron-deuteron scattering up to next-to-leading order in chiral effective field theory," *Phys. Rev. C* **96** no. 2, (2017) 024002, [arXiv:1612.09090]. [Erratum: Phys.Rev.C 100, 019901 (2019)].

[161] P. Reinert, H. Krebs, and E. Epelbaum, "Semilocal momentum-space regularized chiral two-nucleon potentials up to fifth order," *Eur. Phys. J. A* **54** no. 5, (2018) 86, [arXiv:1711.08821].

[162] M. Lüscher, "Properties and uses of the Wilson flow in lattice QCD," *JHEP* **08** (2010) 071, [arXiv:1006.4518]. [Erratum: JHEP 03, 092 (2014)].

[163] K. Orginos, A. Parreno, M. J. Savage, S. R. Beane, E. Chang, and W. Detmold, "Two nucleon systems at $m_\pi \sim 450$ MeV from lattice QCD," *Phys. Rev. D* **92** no. 11, (2015) 114512, [arXiv:1508.07583]. [Erratum: Phys.Rev.D 102, 039903 (2020)].

[164] U. van Kolck, J. A. Niskanen, and G. A. Miller, "Charge symmetry violation in p n —> d pi0 as a test of chiral effective field theory," *Phys. Lett. B* **493** (2000) 65–72, [nucl-th/0006042].

[165] A. Gardestig, C. J. Horowitz, A. Nogga, A. C. Fonseca, C. Hanhart, G. A. Miller, J. A. Niskanen, and U. van Kolck, "Survey of charge symmetry breaking operators for dd —> alpha pi0," *Phys. Rev. C* **69** (2004) 044606, [nucl-th/0402021].

[166] A. Nogga, A. C. Fonseca, A. Gardestig, C. Hanhart, C. J. Horowitz, G. A. Miller, J. A. Niskanen, and U. van Kolck, "Realistic few-body physics in the dd —> alpha pi0 reaction," *Phys. Lett. B* **639** (2006) 465–470, [nucl-th/0602003].

[167] V. Baru, C. Hanhart, and F. Myhrer, "Effective field theory calculations of $NN \to NN\pi$," *Int. J. Mod. Phys. E* **23** no. 4, (2014) 1430004, [arXiv:1310.3505].

[168] **WASA-at-COSY** Collaboration, P. Adlarson *et al.*, "Charge symmetry breaking in dd$\to{}^4$Heπ^0 with WASA-at-COSY," *Phys. Lett. B* **739** (2014) 44–49, [arXiv:1407.2756].

[169] M. Pospelov and A. Ritz, "Electric dipole moments as probes of new physics," *Annals Phys.* **318** (2005) 119–169, [hep-ph/0504231].

[170] I. B. Khriplovich and R. A. Korkin, "P and T odd electromagnetic moments of deuteron in chiral limit," *Nucl. Phys. A* **665** (2000) 365–373, [nucl-th/9904081].

[171] **CPEDM** Collaboration, F. Abusaif *et al.*, *Storage ring to search for electricdipole moments of charged particles: Feasibility study*. CERN, Geneva, 6, 2021. arXiv:1912.07881.

[172] V. A. Dzuba, V. V. Flambaum, and S. G. Porsev, "Calculation of P,T-odd electric dipole moments for diamagnetic atoms Xe-129, Yb-171, Hg-199, Rn-211, and Ra-225," *Phys. Rev. A* **80** (2009) 032120, [arXiv:0906.5437].

[173] K. Yanase and N. Shimizu, "Large-scale shell-model calculations of nuclear Schiff moments of ^{129}Xe and ^{199}Hg," *Phys. Rev. C* **102** no. 6, (2020) 065502, [arXiv:2006.15142].

[174] W. C. Haxton and B. R. Holstein, "Hadronic Parity Violation," *Prog. Part. Nucl. Phys.* **71** (2013) 185–203, [arXiv:1303.4132].

[175] D. B. Kaplan and M. J. Savage, "An Analysis of parity violating pion - nucleon couplings," *Nucl. Phys. A* **556** (1993) 653–671. [Erratum: Nucl.Phys.A 570, 833–833 (1994), Erratum: Nucl.Phys.A 580, 679–679 (1994)].

[176] S.-L. Zhu, C. M. Maekawa, B. R. Holstein, M. J. Ramsey-Musolf, and U. van Kolck, "Nuclear parity-violation in effective field theory," *Nucl. Phys. A* **748** (2005) 435–498, [nucl-th/0407087].

[177] J. de Vries, E. Epelbaum, L. Girlanda, A. Gnech, E. Mereghetti, and M. Viviani, "Parity- and Time-Reversal-Violating Nuclear Forces," *Front. in Phys.* **8** (2020) 218, [arXiv:2001.09050].

[178] **NPDGamma** Collaboration, D. Blyth *et al.*, "First Observation of P-odd γ Asymmetry in Polarized Neutron Capture on Hydrogen," *Phys. Rev. Lett.* **121** no. 24, (2018) 242002, [arXiv:1807.10192].

[179] V. Cirigliano, W. Dekens, J. De Vries, M. L. Graesser, E. Mereghetti, S. Pastore, M. Piarulli, U. Van Kolck, and R. B. Wiringa, "Renormalized approach to neutrinoless double- β decay," *Phys. Rev. C* **100** no. 5, (2019) 055504, [arXiv:1907.11254].

[180] B. Graner, Y. Chen, E. G. Lindahl, and B. R. Heckel, "Reduced Limit on the Permanent Electric Dipole Moment of Hg199," *Phys. Rev. Lett.* **116** no. 16, (2016) 161601, [arXiv:1601.04339]. [Erratum: Phys.Rev.Lett. 119, 119901 (2017)].

[181] L. F. Abbott and P. Sikivie, "A Cosmological Bound on the Invisible Axion," *Phys. Lett. B* **120** (1983) 133–136.

[182] M. Dine and W. Fischler, "The Not So Harmless Axion," *Phys. Lett. B* **120** (1983) 137–141.

[183] D. J. E. Marsh, "Axion Cosmology," *Phys. Rept.* **643** (2016) 1–79, [arXiv:1510.07633].

[184] P. Sikivie, "Invisible Axion Search Methods," *Rev. Mod. Phys.* **93** no. 1, (2021) 015004, [arXiv:2003.02206].

[185] L. Di Luzio, M. Giannotti, E. Nardi, and L. Visinelli, "The landscape of QCD axion models," *Phys. Rept.* **870** (2020) 1–117, [arXiv:2003.01100].

[186] Q. Bonnefoy, E. Gendy, C. Grojean, and J. T. Ruderman, "Beyond Jarlskog: 699 invariants for CP violation in SMEFT," arXiv:2112.03889.

[187] B. Yu and S. Zhou, "Spelling out leptonic <math display="inline"><mi>C</mi><mi>P</mi></math> violation in the language of invariant theory," *Phys. Rev. D* **106** no. 5, (2022) L051701, [arXiv:2203.00574].

[188] B. Yu and S. Zhou, "CP violation and flavor invariants in the seesaw effective field theory," *JHEP* **08** (2022) 017, [arXiv:2203.10121].

[189] M. Dine and P. Draper, "Challenges for the Nelson-Barr Mechanism," *JHEP* **08** (2015) 132, [arXiv:1506.05433].

[190] G. Senjanović and R. N. Mohapatra, "Exact Left-Right Symmetry and Spontaneous Violation of Parity," *Phys. Rev. D* **12** (1975) 1502.

[191] A. Maiezza and M. Nemevšek, "Strong P invariance, neutron electric dipole moment, and minimal left-right parity at LHC," *Phys. Rev. D* **90** no. 9, (2014) 095002, [arXiv:1407.3678].

[192] K. S. Babu and R. N. Mohapatra, "A Solution to the Strong CP Problem Without an Axion," *Phys. Rev. D* **41** (1990) 1286.

[193] J. de Vries, P. Draper, and H. H. Patel, "Do Minimal Parity Solutions to the Strong CP Problem Work?," arXiv:2109.01630.

[194] J. de Vries, P. Draper, K. Fuyuto, J. Kozaczuk, and D. Sutherland, "Indirect Signs of the Peccei-Quinn Mechanism," *Phys. Rev. D* **99** no. 1, (2019) 015042, [arXiv:1809.10143].

[195] J. E. Moody and F. Wilczek, "NEW MACROSCOPIC FORCES?," *Phys. Rev. D* **30** (1984) 130.

[196] C. A. J. O'Hare and E. Vitagliano, "Cornering the axion with CP-violating interactions," *Phys. Rev. D* **102** no. 11, (2020) 115026, [arXiv:2010.03889].

[197] I. G. Irastorza and J. Redondo, "New experimental approaches in the search for axion-like particles," *Prog. Part. Nucl. Phys.* **102** (2018) 89–159, [arXiv:1801.08127].

[198] M. Pospelov, "CP odd interaction of axion with matter," *Phys. Rev. D* **58** (1998) 097703, [hep-ph/9707431].

[199] S. Okawa, M. Pospelov, and A. Ritz, "Long-range axion forces and hadronic CP violation," *Phys. Rev. D* **105** no. 7, (2022) 075003, [arXiv:2111.08040].

[200] F. Bigazzi, A. L. Cotrone, M. Järvinen, and E. Kiritsis, "Non-derivative Axionic Couplings to Nucleons at large and small N," *JHEP* **01** (2020) 100, [arXiv:1906.12132].

[201] S. Bertolini, L. Di Luzio, and F. Nesti, "Axion-mediated forces, CP violation and left-right interactions," *Phys. Rev. Lett.* **126** no. 8, (2021) 081801, [arXiv:2006.12508].

[202] L. Di Luzio, "CP-violating axions," *PoS* **EPS-HEP2021** (2022) 513, [arXiv:2108.09071].

[203] P. W. Graham and S. Rajendran, "Axion Dark Matter Detection with Cold Molecules," *Phys. Rev. D* **84** (2011) 055013, [arXiv:1101.2691].

[204] P. W. Graham and S. Rajendran, "New Observables for Direct Detection of Axion Dark Matter," *Phys. Rev. D* **88** (2013) 035023, [arXiv:1306.6088].

[205] V. V. Flambaum, H. B. Tran Tan, D. Budker, and A. Wickenbrock, "Atomic and molecular transitions induced by axions via oscillating nuclear moments," *Phys. Rev. D* **101** no. 7, (2020) 073004, [arXiv:1910.07705].

[206] R. Janish and H. Ramani, "Muon g-2 and EDM experiments as muonic dark matter detectors," *Phys. Rev. D* **102** (2020) 115018, [arXiv:2006.10069].

[207] Y. K. Semertzidis and S. Youn, "Axion dark matter: How to see it?," *Sci. Adv.* **8** no. 8, (2022) abm9928, [arXiv:2104.14831].

[208] D. F. Jackson Kimball *et al.*, "Overview of the Cosmic Axion Spin Precession Experiment (CASPEr)," *Springer Proc. Phys.* **245** (2020) 105–121, [arXiv:1711.08999].

[209] A. Mitridate, T. Trickle, Z. Zhang, and K. M. Zurek, "Detectability of Axion Dark Matter with Phonon Polaritons and Magnons," *Phys. Rev. D* **102** no. 9, (2020) 095005, [arXiv:2005.10256].

[210] P. W. Graham, S. Hacıömeroğlu, D. E. Kaplan, Z. Omarov, S. Rajendran, and Y. K. Semertzidis, "Storage ring probes of dark matter and dark energy," *Phys. Rev. D* **103** no. 5, (2021) 055010, [arXiv:2005.11867].

[211] W. Dekens and P. Stoffer, "Low-energy effective field theory below the electroweak scale: matching at one loop," *JHEP* **10** (2019) 197, [arXiv:1908.05295].

[212] E. E. Jenkins, A. V. Manohar, and P. Stoffer, "Low-Energy Effective Field Theory below the Electroweak Scale: Anomalous Dimensions," *JHEP* **01** (2018) 084, [arXiv:1711.05270].

[213] M. Bauer, M. Neubert, S. Renner, M. Schnubel, and A. Thamm, "The Low-Energy Effective Theory of Axions and ALPs," *JHEP* **04** (2021) 063, [arXiv:2012.12272].

[214] M. Chala, G. Guedes, M. Ramos, and J. Santiago, "Running in the ALPs," *Eur. Phys. J. C* **81** no. 2, (2021) 181, [arXiv:2012.09017].

[215] A. M. Galda, M. Neubert, and S. Renner, "ALP — SMEFT interference," *JHEP* **06** (2021) 135, [arXiv:2105.01078].

[216] F. del Aguila, S. Bar-Shalom, A. Soni, and J. Wudka, "Heavy Majorana Neutrinos in the Effective Lagrangian Description: Application to Hadron Colliders," *Phys. Lett.* **B670** (2009) 399–402, [arXiv:0806.0876].

[217] Y. Liao and X.-D. Ma, "Operators up to Dimension Seven in Standard Model Effective Field Theory Extended with Sterile Neutrinos," *Phys. Rev.* **D96** no. 1, (2017) 015012, [arXiv:1612.04527].

[218] **Muon (g-2)** Collaboration, G. W. Bennett *et al.*, "An Improved Limit on the Muon Electric Dipole Moment," *Phys. Rev. D* **80** (2009) 052008, [arXiv:0811.1207].

[219] **Belle** Collaboration, K. Inami *et al.*, "Search for the electric dipole moment of the tau lepton," *Phys. Lett. B* **551** (2003) 16–26, [hep-ex/0210066].

[220] V. Cirigliano, R. Kitano, Y. Okada, and P. Tuzon, "On the model discriminating power of mu —> e conversion in nuclei," *Phys. Rev. D* **80** (2009) 013002, [arXiv:0904.0957].

[221] A. Crivellin, S. Davidson, G. M. Pruna, and A. Signer, "Renormalisation-group improved analysis of $\mu \to e$ processes in a systematic effective-field-theory approach," *JHEP* **05** (2017) 117, [arXiv:1702.03020].

[222] C. Jarlskog, "Commutator of the Quark Mass Matrices in the Standard Electroweak Model and a Measure of Maximal CP Violation," *Phys. Rev. Lett.* **55** (1985) 1039.

[223] B. M. Gavela, E. E. Jenkins, A. V. Manohar, and L. Merlo, "Analysis of General Power Counting Rules in Effective Field Theory," *Eur. Phys. J. C* **76** no. 9, (2016) 485, [arXiv:1601.07551].

[224] **HERMES** Collaboration, A. Airapetian *et al.*, "Precise determination of the spin structure function g(1) of the proton, deuteron and neutron," *Phys. Rev.* **D75** (2007) 012007, [hep-ex/0609039].

[225] M. Hoferichter, J. Ruiz de Elvira, B. Kubis, and U.-G. Meißner, "High-Precision Determination of the Pion-Nucleon sigma Term from Roy-Steiner Equations," *Phys. Rev. Lett.* **115** (2015) 092301, [arXiv:1506.04142].

[226] **ETM** Collaboration, A. Abdel-Rehim, C. Alexandrou, M. Constantinou, K. Hadjiyiannakou, K. Jansen, C. Kallidonis, G. Koutsou, and A. Vaquero Aviles-Casco, "Direct Evaluation of the Quark Content of Nucleons from Lattice QCD at the Physical Point," *Phys. Rev. Lett.* **116** no. 25, (2016) 252001, [arXiv:1601.01624].

[227] S. Borsanyi *et al.*, "Ab initio calculation of the neutron-proton mass difference," *Science* **347** (2015) 1452–1455, [arXiv:1406.4088].

[228] **NA62** Collaboration, E. Cortina Gil *et al.*, "Measurement of the very rare $K^+ \to \pi^+ \nu\bar{\nu}$ decay," *JHEP* **06** (2021) 093, [arXiv:2103.15389].

[229] **NA62** Collaboration, E. Cortina Gil *et al.*, "First search for $K^+ \to \pi^+ \nu\bar{\nu}$ using the decay-in-flight technique," *Phys. Lett. B* **791** (2019) 156–166, [arXiv:1811.08508].

[230] **NA62** Collaboration, E. Cortina Gil *et al.*, "An investigation of the very rare $K^+ \to \pi^+ \nu\bar{\nu}$ decay," *JHEP* **11** (2020) 042, [arXiv:2007.08218].

[231] J. Aebischer, C. Bobeth, A. J. Buras, and J. Kumar, "BSM master formula for ε'/ε in the WET basis at NLO in QCD," *JHEP* **12** (2021) 043, [arXiv:2107.12391].

[232] A. Pich, "CP violation," *ICTP Ser. Theor. Phys.* **10** (1994) 14–42, [hep-ph/9312297].

[233] J. Aebischer, C. Bobeth, and A. J. Buras, "ε'/ε in the Standard Model at the Dawn of the 2020s," *Eur. Phys. J. C* **80** no. 8, (2020) 705, [arXiv:2005.05978].

[234] **RBC, UKQCD** Collaboration, R. Abbott *et al.*, "Direct CP violation and the $\Delta I = 1/2$ rule in $K \to \pi\pi$ decay from the standard model," *Phys. Rev. D* **102** no. 5, (2020) 054509, [arXiv:2004.09440].

[235] V. Cirigliano, H. Gisbert, A. Pich, and A. Rodríguez-Sánchez, "Isospin-violating contributions to ϵ'/ϵ," *JHEP* **02** (2020) 032, [arXiv:1911.01359].

[236] **Particle Data Group** Collaboration, P. A. Zyla *et al.*, "Review of Particle Physics," *PTEP* **2020** no. 8, (2020) 083C01.

[237] H. Georgi and L. Randall, "Flavor Conserving CP Violation in Invisible Axion Models," *Nucl. Phys. B* **276** (1986) 241–252.

[238] W. Dekens, J. de Vries, M. Jung, and K. K. Vos, "The phenomenology of electric dipole moments in models of scalar leptoquarks," *JHEP* **01** (2019) 069, [arXiv:1809.09114].

[239] M. Denis and T. Fleig, "In search of discrete symmetry violations beyond the standard model: Thorium monoxide reloaded," *The Journal of Chemical Physics* **145** no. 21, (2016) 214307. https://doi.org/10.1063/1.4968597.

[240] T. Fleig, "$\mathcal{P}, \mathcal{T}$-odd and magnetic hyperfine-interaction constants and excited-state lifetime for HfF^+," *Phys. Rev. A* **96** no. 4, (2017) 040502, [arXiv:1706.02893].

[241] A. Sunaga, M. Abe, M. Hada, and B. P. Das, "Relativistic coupled-cluster calculation of the electron-nucleus scalar-pseudoscalar interaction constant W_s in ybf," *Phys. Rev. A* **93** (Apr, 2016) 042507. https://link.aps.org/doi/10.1103/PhysRevA.93.042507.

[242] Y. V. Stadnik, V. A. Dzuba, and V. V. Flambaum, "Improved Limits on Axionlike-Particle-Mediated P , T -Violating Interactions between Electrons and Nucleons from Electric Dipole Moments of Atoms and Molecules," *Phys. Rev. Lett.* **120** no. 1, (2018) 013202, [arXiv:1708.00486].

[243] M. Bishof *et al.*, "Improved limit on the ^{225}Ra electric dipole moment," *Phys. Rev. C* **94** no. 2, (2016) 025501, [arXiv:1606.04931].

[244] J. J. Hudson, D. M. Kara, I. J. Smallman, B. E. Sauer, M. R. Tarbutt, and E. A. Hinds, "Improved measurement of the shape of the electron," *Nature* **473** (2011) 493–496.

[245] W. B. Cairncross, D. N. Gresh, M. Grau, K. C. Cossel, T. S. Roussy, Y. Ni, Y. Zhou, J. Ye, and E. A. Cornell, "Precision Measurement of the Electron's Electric Dipole Moment Using Trapped Molecular Ions," *Phys. Rev. Lett.* **119** no. 15, (2017) 153001, [arXiv:1704.07928].

[246] **ACME** Collaboration, V. Andreev *et al.*, "Improved limit on the electric dipole moment of the electron," *Nature* **562** no. 7727, (2018) 355–360.

[247] J. Engel, M. J. Ramsey-Musolf, and U. van Kolck, "Electric Dipole Moments of Nucleons, Nuclei, and Atoms: The Standard Model and Beyond," *Prog. Part. Nucl. Phys.* **71** (2013) 21–74, [arXiv:1303.2371].

[248] T. Fleig and M. Jung, "Model-independent determinations of the electron EDM and the role of diamagnetic atoms," *JHEP* **07** (2018) 012, [arXiv:1802.02171].

[249] K. V. P. Latha, D. Angom, B. P. Das, and D. Mukherjee, "Probing CP violation with the electric dipole moment of atomic mercury," *Phys. Rev. Lett.* **103** (2009) 083001, [arXiv:0902.4790]. [Erratum: Phys. Rev. Lett.115,no.5,059902(2015)].

[250] V. F. Dmitriev and R. A. Sen'kov, "Schiff moment of the mercury nucleus and the proton dipole moment," *Phys. Rev. Lett.* **91** (2003) 212303, [nucl-th/0306050].

[251] K. Yanase, N. Yoshinaga, K. Higashiyama, and N. Yamanaka, "Electric dipole moment of ^{199}Hg atom from P, CP-odd electron-nucleon interaction," *Phys. Rev. D* **99** no. 7, (2019) 075021, [arXiv:1805.00419].

[252] T. Damour and J. F. Donoghue, "Equivalence Principle Violations and Couplings of a Light Dilaton," *Phys. Rev. D* **82** (2010) 084033, [arXiv:1007.2792].

[253] V. Cirigliano, M. L. Graesser, and G. Ovanesyan, "WIMP-nucleus scattering in chiral effective theory," *JHEP* **10** (2012) 025, [arXiv:1205.2695].

[254] M. Hoferichter, P. Klos, J. Menéndez, and A. Schwenk, "Nuclear structure factors for general spin-independent WIMP-nucleus scattering," *Phys. Rev. D* **99** no. 5, (2019) 055031, [arXiv:1812.05617].

[255] J. Bergé, P. Brax, G. Métris, M. Pernot-Borràs, P. Touboul, and J.-P. Uzan, "MICROSCOPE Mission: First Constraints on the Violation of the Weak Equivalence Principle by a Light Scalar Dilaton," *Phys. Rev. Lett.* **120** no. 14, (2018) 141101, [arXiv:1712.00483].

[256] G. L. Smith, C. D. Hoyle, J. H. Gundlach, E. G. Adelberger, B. R. Heckel, and H. E. Swanson, "Short range tests of the equivalence principle," *Phys. Rev. D* **61** (2000) 022001.

[257] S. Schlamminger, K. Y. Choi, T. A. Wagner, J. H. Gundlach, and E. G. Adelberger, "Test of the equivalence principle using a rotating torsion balance," *Phys. Rev. Lett.* **100** (2008) 041101, [arXiv:0712.0607].

[258] J. K. Hoskins, R. D. Newman, R. Spero, and J. Schultz, "Experimental tests of the gravitational inverse square law for mass separations from 2-cm to 105-cm," *Phys. Rev. D* **32** (1985) 3084–3095.

[259] D. J. Kapner, T. S. Cook, E. G. Adelberger, J. H. Gundlach, B. R. Heckel, C. D. Hoyle, and H. E. Swanson, "Tests of the gravitational inverse-square law below the dark-energy length scale," *Phys. Rev. Lett.* **98** (2007) 021101, [hep-ph/0611184].

[260] J. G. Lee, E. G. Adelberger, T. S. Cook, S. M. Fleischer, and B. R. Heckel, "New Test of the Gravitational $1/r^2$ Law at Separations down to 52 μm," *Phys. Rev. Lett.* **124** no. 10, (2020) 101101, [arXiv:2002.11761].

[261] W.-H. Tan *et al.*, "Improvement for Testing the Gravitational Inverse-Square Law at the Submillimeter Range," *Phys. Rev. Lett.* **124** no. 5, (2020) 051301.

[262] W.-H. Tan, S.-Q. Yang, C.-G. Shao, J. Li, A.-B. Du, B.-F. Zhan, Q.-L. Wang, P.-S. Luo, L.-C. Tu, and J. Luo, "New Test of the Gravitational Inverse-Square Law at the Submillimeter Range with Dual Modulation and Compensation," *Phys. Rev. Lett.* **116** no. 13, (2016) 131101.

[263] S.-Q. Yang, B.-F. Zhan, Q.-L. Wang, C.-G. Shao, L.-C. Tu, W.-H. Tan, and J. Luo, "Test of the Gravitational Inverse Square Law at Millimeter Ranges," *Phys. Rev. Lett.* **108** (2012) 081101.

[264] L.-C. Tu, S.-G. Guan, J. Luo, C.-G. Shao, and L.-X. Liu, "Null Test of Newtonian Inverse-Square Law at Submillimeter Range with a Dual-Modulation Torsion Pendulum," *Phys. Rev. Lett.* **98** (2007) 201101.

[265] A. A. Geraci, S. J. Smullin, D. M. Weld, J. Chiaverini, and A. Kapitulnik, "Improved constraints on non-Newtonian forces at 10 microns," *Phys. Rev. D* **78** (2008) 022002, [arXiv:0802.2350].

[266] Y. J. Chen, W. K. Tham, D. E. Krause, D. Lopez, E. Fischbach, and R. S. Decca, "Stronger Limits on Hypothetical Yukawa Interactions in the 30–8000 nm Range," *Phys. Rev. Lett.* **116** no. 22, (2016) 221102, [arXiv:1410.7267].

[267] Y.-D. Tsai, Y. Wu, S. Vagnozzi, and L. Visinelli, "Asteroid astrometry as a fifth-force and ultralight dark sector probe," arXiv:2107.04038.

[268] T. Kumar Poddar, S. Mohanty, and S. Jana, "Constraints on long range force from perihelion precession of planets in a gauged $L_e - L_{\mu,\tau}$ scenario," *Eur. Phys. J. C* **81** no. 4, (2021) 286, [arXiv:2002.02935].

[269] G. G. Raffelt, "Particle physics from stars," *Ann. Rev. Nucl. Part. Sci.* **49** (1999) 163–216, [hep-ph/9903472].

[270] G. G. Raffelt, "Astrophysical axion bounds," *Lect. Notes Phys.* **741** (2008) 51–71, [hep-ph/0611350].

[271] F. Capozzi and G. Raffelt, "Axion and neutrino bounds improved with new calibrations of the tip of the red-giant branch using geometric distance determinations," *Phys. Rev. D* **102** no. 8, (2020) 083007, [arXiv:2007.03694].

[272] G. G. Raffelt, *Stars as laboratories for fundamental physics: The astrophysics of neutrinos, axions, and other weakly interacting particles.* the University of Chicago Press, May, 1996.

[273] E. Hardy and R. Lasenby, "Stellar cooling bounds on new light particles: plasma mixing effects," *JHEP* **02** (2017) 033, [arXiv:1611.05852].

[274] M. V. Beznogov, E. Rrapaj, D. Page, and S. Reddy, "Constraints on Axion-like Particles and Nucleon Pairing in Dense Matter from the Hot Neutron Star in HESS J1731-347," *Phys. Rev. C* **98** no. 3, (2018) 035802, [arXiv:1806.07991].

[275] T. Vonk, F.-K. Guo, and U.-G. Meißner, "Precision calculation of the axion-nucleon coupling in chiral perturbation theory," *JHEP* **03** (2020) 138, [arXiv:2001.05327].

[276] L. Di Luzio, F. Mescia, and E. Nardi, "Redefining the Axion Window," *Phys. Rev. Lett.* **118** no. 3, (2017) 031801, [arXiv:1610.07593].

[277] V. Plakkot and S. Hoof, "Anomaly ratio distributions of hadronic axion models with multiple heavy quarks," *Phys. Rev. D* **104** no. 7, (2021) 075017, [arXiv:2107.12378].

[278] J. E. Kim, "Weak Interaction Singlet and Strong CP Invariance," *Phys. Rev. Lett.* **43** (1979) 103.

[279] M. A. Shifman, A. I. Vainshtein, and V. I. Zakharov, "Can Confinement Ensure Natural CP Invariance of Strong Interactions?," *Nucl. Phys. B* **166** (1980) 493–506.

[280] A. R. Zhitnitsky, "On Possible Suppression of the Axion Hadron Interactions. (In Russian)," *Sov. J. Nucl. Phys.* **31** (1980) 260.

[281] M. Dine, W. Fischler, and M. Srednicki, "A Simple Solution to the Strong CP Problem with a Harmless Axion," *Phys. Lett. B* **104** (1981) 199–202.

[282] F. Björkeroth, L. Di Luzio, F. Mescia, E. Nardi, P. Panci, and R. Ziegler, "Axion-electron decoupling in nucleophobic axion models," *Phys. Rev. D* **101** no. 3, (2020) 035027, [arXiv:1907.06575].

[283] A. Arvanitaki and A. A. Geraci, "Resonantly Detecting Axion-Mediated Forces with Nuclear Magnetic Resonance," *Phys. Rev. Lett.* **113** no. 16, (2014) 161801, [arXiv:1403.1290].

[284] **ARIADNE** Collaboration, A. A. Geraci *et al.*, "Progress on the ARIADNE axion experiment," *Springer Proc. Phys.* **211** (2018) 151–161, [arXiv:1710.05413].

[285] **ARIADNE** Collaboration, C. Lohmeyer *et al.*, "Source Mass Characterization in the ARIADNE Axion Experiment," *Springer Proc. Phys.* **245** (2020) 71–81, [arXiv:2011.10141].

[286] N. Crescini, C. Braggio, G. Carugno, P. Falferi, A. Ortolan, and G. Ruoso, "The QUAX-g_p g_s experiment to search for monopole-dipole Axion interaction," *Nucl. Instrum. Meth. A* **842** (2017) 109–113, [arXiv:1606.04751].

[287] N. Crescini, C. Braggio, G. Carugno, P. Falferi, A. Ortolan, and G. Ruoso, "Improved constraints on monopole-dipole interaction mediated by pseudo-scalar bosons," *Phys. Lett. B* **773** (2017) 677–680, [arXiv:1705.06044].

[288] M. Pospelov, "Best values for the CP odd meson nucleon couplings from supersymmetry," *Phys. Lett. B* **530** (2002) 123–128, [hep-ph/0109044].

[289] J. de Vries, E. Mereghetti, C.-Y. Seng, and A. Walker-Loud, "Lattice QCD spectroscopy for hadronic CP violation," *Phys. Lett. B* **766** (2017) 254–262, [arXiv:1612.01567].

[290] C.-Y. Seng, "Relating hadronic CP-violation to higher-twist distributions," *Phys. Rev. Lett.* **122** no. 7, (2019) 072001, [arXiv:1809.00307].

[291] V. M. Belyaev and B. L. Ioffe, "Determination of Baryon and Baryonic Resonance Masses from QCD Sum Rules. 1. Nonstrange Baryons," *Sov. Phys. JETP* **56** (1982) 493–501.

[292] Y. Aoki *et al.*, "FLAG Review 2021," arXiv:2111.09849.

[293] J. de Vries, P. Draper, K. Fuyuto, J. Kozaczuk, and B. Lillard, "Uncovering an axion mechanism with the EDM portfolio," *Phys. Rev. D* **104** no. 5, (2021) 055039, [arXiv:2107.04046].

[294] G. Senjanović and V. Tello, "Restoration of Parity and the Right-Handed Analog of the CKM Matrix," *Phys. Rev. D* **94** no. 9, (2016) 095023, [arXiv:1502.05704].

[295] W. Dekens, L. Andreoli, J. de Vries, E. Mereghetti, and F. Oosterhof, "A low-energy perspective on the minimal left-right symmetric model," *JHEP* **11** (2021) 127, [arXiv:2107.10852].

[296] G. Senjanović and V. Tello, "Right Handed Quark Mixing in Left-Right Symmetric Theory," *Phys. Rev. Lett.* **114** no. 7, (2015) 071801.

[297] A. Nicholson *et al.*, "Heavy physics contributions to neutrinoless double beta decay from QCD," *Phys. Rev. Lett.* **121** no. 17, (2018) 172501, [arXiv:1805.02634].

[298] **Flavour Lattice Averaging Group** Collaboration, S. Aoki *et al.*, "FLAG Review 2019: Flavour Lattice Averaging Group (FLAG)," *Eur. Phys. J. C* **80** no. 2, (2020) 113, [arXiv:1902.08191].

[299] A. Shindler, "Flavor-diagonal CP violation: the electric dipole moment," *Eur. Phys. J. A* **57** no. 4, (2021) 128.

[300] R. Bollig, W. DeRocco, P. W. Graham, and H.-T. Janka, "Muons in Supernovae: Implications for the Axion-Muon Coupling," *Phys. Rev. Lett.* **125** no. 5, (2020) 051104, [arXiv:2005.07141]. [Erratum: Phys.Rev.Lett. 126, 189901 (2021)].

[301] A. Arvanitaki, J. Huang, and K. Van Tilburg, "Searching for dilaton dark matter with atomic clocks," *Phys. Rev. D* **91** no. 1, (2015) 015015, [arXiv:1405.2925].

[302] E. Trimby, H. Hirzler, H. Fürst, A. Safavi-Naini, R. Gerritsma, and R. S. Lous, "Buffer gas cooling of ions in time-dependent traps using ultracold atoms," arXiv:2109.15195.

[303] J. Fan, M. Reece, and L.-T. Wang, "Non-relativistic effective theory of dark matter direct detection," *JCAP* **11** (2010) 042, [arXiv:1008.1591].

[304] A. L. Fitzpatrick, W. Haxton, E. Katz, N. Lubbers, and Y. Xu, "The Effective Field Theory of Dark Matter Direct Detection," *JCAP* **02** (2013) 004, [arXiv:1203.3542].

[305] P. Klos, J. Menéndez, D. Gazit, and A. Schwenk, "Large-scale nuclear structure calculations for spin-dependent WIMP scattering with chiral effective field theory currents," *Phys. Rev. D* **88** no. 8, (2013) 083516, [arXiv:1304.7684]. [Erratum: Phys.Rev.D 89, 029901 (2014)].

[306] R. J. Hill and M. P. Solon, "Standard Model anatomy of WIMP dark matter direct detection II: QCD analysis and hadronic matrix elements," *Phys. Rev. D* **91** (2015) 043505, [arXiv:1409.8290].

[307] M. Hoferichter, P. Klos, and A. Schwenk, "Chiral power counting of one- and two-body currents in direct detection of dark matter," *Phys. Lett. B* **746** (2015) 410–416, [arXiv:1503.04811].

[308] G. Prezeau, A. Kurylov, M. Kamionkowski, and P. Vogel, "New contribution to wimp-nucleus scattering," *Phys. Rev. Lett.* **91** (2003) 231301, [astro-ph/0309115].

[309] G. Arcadi, A. Djouadi, and M. Raidal, "Dark Matter through the Higgs portal," *Phys. Rept.* **842** (2020) 1–180, [arXiv:1903.03616].

[310] M. Hoferichter, P. Klos, J. Menéndez, and A. Schwenk, "Analysis strategies for general spin-independent WIMP-nucleus scattering," *Phys. Rev. D* **94** no. 6, (2016) 063505, [arXiv:1605.08043].

[311] S. R. Beane, S. D. Cohen, W. Detmold, H. W. Lin, and M. J. Savage, "Nuclear σ terms and scalar-isoscalar WIMP-nucleus interactions from lattice QCD," *Phys. Rev. D* **89** (2014) 074505, [arXiv:1306.6939].

[312] L. Andreoli, V. Cirigliano, S. Gandolfi, and F. Pederiva, "Quantum Monte Carlo calculations of dark matter scattering off light nuclei," *Phys. Rev. C* **99** no. 2, (2019) 025501, [arXiv:1811.01843].

[313] W. Guo and D. N. McKinsey, "Concept for a dark matter detector using liquid helium-4," *Phys. Rev. D* **87** no. 11, (2013) 115001, [arXiv:1302.0534].

[314] **SPICE/HeRALD** Collaboration, A. Biekert *et al.*, "Scintillation yield from electronic and nuclear recoils in superfluid He4," *Phys. Rev. D* **105** no. 9, (2022) 092005, [arXiv:2108.02176].

[315] S. Borsanyi, Z. Fodor, C. Hoelbling, L. Lellouch, K. K. Szabo, C. Torrero, and L. Varnhorst, "Ab-initio calculation of the proton and the neutron's scalar couplings for new physics searches," arXiv:2007.03319.

[316] R. Gupta, T. Bhattacharya, M. Hoferichter, E. Mereghetti, S. Park, and B. Yoon, "The pion-nucleon sigma term from Lattice QCD," in *10th International workshop on Chiral Dynamics*. 3, 2022. arXiv:2203.13862.

[317] E. Epelbaum, H. Krebs, and U. G. Meißner, "Precision nucleon-nucleon potential at fifth order in the chiral expansion," *Phys. Rev. Lett.* **115** no. 12, (2015) 122301, [arXiv:1412.4623].

[318] M. C. Smith *et al.*, "The RAVE Survey: Constraining the Local Galactic Escape Speed," *Mon. Not. Roy. Astron. Soc.* **379** (2007) 755–772, [astro-ph/0611671].

[319] J. L. Friar, "Measurability of the deuteron D state probability," *Phys. Rev. C* **20** (1979) 325–330.

[320] H. Krebs, E. Epelbaum, and U.-G. Meißner, "Subleading contributions to the nuclear scalar isoscalar current," *Eur. Phys. J. A* **56** no. 9, (2020) 240, [arXiv:2005.07433].

[321] **NPLQCD** Collaboration, E. Chang, Z. Davoudi, W. Detmold, A. S. Gambhir, K. Orginos, M. J. Savage, P. E. Shanahan, M. L. Wagman, and F. Winter, "Scalar, Axial, and Tensor Interactions of Light Nuclei from Lattice QCD," *Phys. Rev. Lett.* **120** no. 15, (2018) 152002, [arXiv:1712.03221].

[322] H. P. Stapp, T. J. Ypsilantis, and N. Metropolis, "Phase shift analysis of 310-MeV proton proton scattering experiments," *Phys. Rev.* **105** (1957) 302–310.

[323] V. Cirigliano, W. Dekens, J. de Vries, M. L. Graesser, and E. Mereghetti, "A neutrinoless double beta decay master formula from effective field theory," *JHEP* **12** (2018) 097, [arXiv:1806.02780].

[324] **RBC, UKQCD** Collaboration, Z. Bai *et al.*, "Standard Model Prediction for Direct CP Violation in K→ππ Decay," *Phys. Rev. Lett.* **115** no. 21, (2015) 212001, [arXiv:1505.07863].

[325] T. Blum *et al.*, "Lattice determination of the $K \to (\pi\pi)_{I=2}$ Decay Amplitude A_2," *Phys. Rev. D* **86** (2012) 074513, [arXiv:1206.5142].

[326] V. Cirigliano, W. Dekens, M. Graesser, and E. Mereghetti, "Neutrinoless double beta decay and chiral $SU(3)$," *Phys. Lett. B* **769** (2017) 460–464, [arXiv:1701.01443].